8-2014

Phenotypic Modulation of Smooth Muscle Cells on Biodegradable Elastomeric Substrates

Xifeng Liu
University of Tennessee - Knoxville, xliu41@vols.utk.edu

To the Graduate Council:

I am submitting herewith a dissertation written by Xifeng Liu entitled "Phenotypic Modulation of Smooth Muscle Cells on Biodegradable Elastomeric Substrates." I have examined the final electronic copy of this dissertation for form and content and recommend that it be accepted in partial fulfillment of the requirements for the degree of Doctor of Philosophy, with a major in Materials Science and Engineering.

Shanfeng Wang, Major Professor

We have read this dissertation and recommend its acceptance:

Roberto S Benson, Gajanan S. Bhat, Meizhen Cui

Accepted for the Council:

Carolyn R. Hodges

Vice Provost and Dean of the Graduate School

(Original signatures are on file with official student records.)

Phenotypic Modulation of Smooth Muscle Cells on Biodegradable Elastomeric Substrates

A Dissertation Presented for the

Doctor of Philosophy

Degree

The University of Tennessee, Knoxville

Xifeng Liu

August 2014

ACKNOWLEDGEMENTS

Firstly, I would like to express special appreciation and thanks to my advisor, Professor Shanfeng Wang, for supporting me during my four years' study here. He is professional, knowledgeable as both a researcher and mentor, and one of the smartest people I know. I would like to thank Dr. Wang for encouraging me and spending tremendous time in guiding me how to do research well, from designing scientific projects to preparing qualified manuscripts. Dr. Wang also provided me with precious instructions to help me developing a research career. His advices on both my research in these years as well as on my future career have been invaluable.

I would like to thank my committee members, Dr. Benson, Dr. Bhat, and Dr. Cui for reviewing my dissertation and serving on my defense. I gained wide knowledge about polymers from Dr. Benson, who has taught me Polymer Chemistry, Thermo-Dynamics in Polymer Solutions, and Dr. Bhat, who has taught me High Performance Fiber course. In addition, I learned intensive biomedical knowledge from Dr. Cui, an expert in biomedical studies from the department of Biomedical and Diagnostic Sciences. My committee members have been very helpful and supportive whenever I have questions or need help. I also thank all the other professors and teachers who taught me in the engineering field, including Dr. Kevin M. Kit, Dr. Jayne Wu, Dr. Bin Hu, Dr. Matthew M. Mench, Dr. Mingjun Zhang and Dr. David C. Joy.

I would like to express my sincere gratitude to my colleagues and coworkers: Dr. Kan Wang, Dr. Lei Cai, Dr. Xiaohui Wu, Jinbo Dou, Qingya Zeng, Charles H. Sprague, Michael Henry, Timothy Mickens and Katherine E. Ray for their collaboration, discussion and assistance. I am grateful to our collaborators Dr. Jingyan Dong and Dr. Li Zhang at North Carolina State University, Dr. Jennifer L. Morrell-Falvey, Dr. Scott Retterer and Sarah J. Melton at Oak Ridge National Lab, Dr. Feng Hao from the department of Biomedical and Diagnostic Sciences at UT.

I would also like to thank Dr. Bin Zhao in the Chemistry Department at UT for using contact angle goniometer, Dr. John Dunlap of Microscopy Facility at UT for confocal microscopy observation, and Gregory Jones of MSE at UT for scanning electronic microscopy operation. I appreciate staff of MSE department at UT, e.g., Carla, Susan, Martha, Frank, Randy, Sandy, Doug Fielden, Stephen Stiner and Carolyn Nelson for their valuable help.

Finally, I appreciate my family members for their support during these years.

ABSTRACT

Cardiovascular disease is the number one killer in the U.S. Cardiovascular tissue engineering holds enormous potential by providing synthetic materials as vessel replacements. This dissertation focused on the development of novel biodegradable and photo-crosslinkable polymers with controlled surface chemistry, stiffness, and topographical features in regulating smooth muscle cell (SMC) adhesion, proliferation and phenotypic conversion for cardiovascular tissue engineering applications. Chapter II presents a facile synthesis route to obtain a series of photocrosslinkable poly(epsilon-caprolactone) triacrylates (PCLTA) with varied mechanical properties and further demonstrated tunable cell responses using these polymer system. Chapter III demonstrates a model polymer network from PCLTA that can gradually stiffen in 24 h through impeded crystallization at body temperature (37 ℃) and distinct SMC attachment, proliferation and spreading are found. Chapter IV presents the fabrication of a series of PCLTA networks with defined gradients in stiffness for regulation of SMCs behaviors. Chapter V fabricates cylindrical pillars with three different heights of 3.4, 7.4, and 15.1 micrometers by photo-crosslinking PCLTA in silicon molds with predesigned micropatterns. Chapter VI prepared photo-crosslinked PCLTA nanowire arrays with diameters of 20, 100 and 200 nanometers using inorganic nanoporous aluminum oxide (AAO) templates. Chapter VII reports a series of novel poly(L-lactic acid) triacrylates (PLLATAs) networks with same chemical composition but different crystallinity and surface roughness achieved by increasing the annealing time from 0 to 5, 7, 10, and 20 h at 70 ℃. Chapter VIII presents a method for tuning surface chemistry by grafting hydrophilic photocrosslinkable mPEGA chains into the hydrophobic PCLTA at various compositions and reports the smooth muscle cell responses. Chapter IX incorporates poly(L-lysine) (PLL) dangling chains into PCLTA networks at different PLL compositions of 0.5%, 1.0%, 1.5%, and 3%. The surface morphology, hydrophilicity and serum protein adsorption of all these polymer networks were characterized. Primary rat SMCs were cultured on these polymer networks and their attachment, spreading, proliferation, focal adhesions, expression of four contractile gene markers (SM-MHC, smoothlin, transgelin, and calponin) and contractile proteins were characterized systematically. Chapter X makes a summary of these separate investigations and draws general conclusions from the results obtained in these studies.

TABLE OF CONTENTS

LIST OF TABLES

LIST OF FIGURES

Chapter I. Introduction

1.1 Background

According to the American Heart Association, cardiovascular diseases are the biggest cause of death in the U.S. and they accounted for 32.3% or one third of all 2.4 million deaths and an estimated cost of $312.6 billion in 2009 [1]. The number of inpatient cardiovascular operations and procedures is still increasing, with the data of from 5.9 million in 2000 to 7.5 million in 2010. The current applicable treatments are either transplanting a donor heart or using assisting devices. Unfortunately, donor hearts are limited or may not be available timely at the moment when severe heart attack happens. Assisting devices, on the other hand, are not affordable for most patients [2]. Thus the high demands from patients suffering from cardiovascular diseases push the searching of other promising approaches.

Cardiovascular tissue engineering is a complex approach that combines multi-disciplinary efforts in engineering, material science, life science, and medical technologies. The ultimate goal of this approach is to create new autologous living substitutes with structures and functions similar to those of native human organs. Cardiovascular tissue-engineering techniques include injectable biomaterials, cell therapies, and artificial organ fabrication by *in vitro* culturing cells with supporting scaffolds [3,4]. The underlying substrates made from biomaterials affect cell adhesion, spreading, proliferation, migration, phenotype, and gene/protein expression. A variety of cell types and polymeric biomaterials have been studied to understand cell-material interactions with the goal of improving materials design strategies for different clinical purposes.

Materials for cardiovascular tissue-engineering applications need to satisfy the following requirements: good biocompatibility, suitable mechanical properties, good processability, and biodegradability [5,6]. Compared with metals and ceramics, polymers have advantages such as tailorability in chemical structures and physical properties. Because the stabilities of different chemical bonds, e.g., ester bonds, glycosidic bonds, and peptide bonds, are different, polymers composed of these bonds have adjustable degradation kinetics. Polymers can also be readily molded into desirable shapes and structures. Biodegradable polymers widely used in cardiovascular tissue-engineering applications include poly(glycolic acid) (PGA), poly(lactic acid) (PLA), poly(ε-caprolactone) (PCL), poly(ethylene glycol) (PEG), polyhydroxyalkanoate

(PHA), and their copolymers[6].

Here I supply an overview of recent progress in investigating cellular responses to biodegradable polymers for cardiovascular tissue-engineering applications. The review is presented in terms of different cell types related to the diseases, different polymers, and different surface characteristics in regulating cellular behavior.

1.2 Cell-material interface in cardiovascular tissue engineering

1.2.1 Components at the interface and cellular sensors

To create neo-tissue, e.g., blood vessel or heart valve, materials are required to contact the surrounding biological elements in implantation. After a material is immersed in body fluid or culture medium, protein adhesion occurs first and then cells start adhering to the surface, followed by a series of external sensing or internal signal transductions.

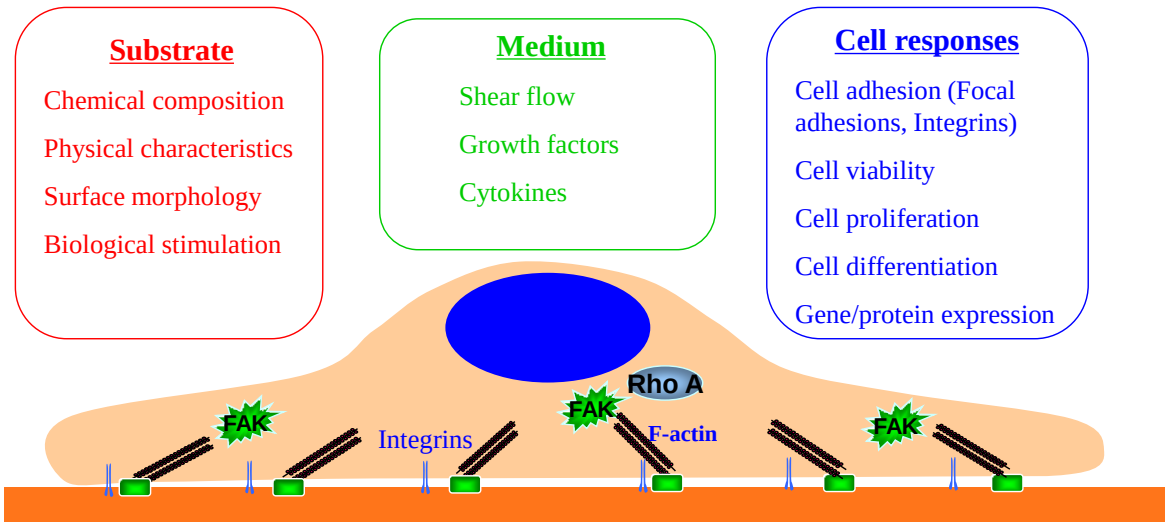

Figure 1.1 Scheme of the factors involved at the cell-material interface.

Many components are involved at the cell-material interface, including cells, underlying materials, and surrounding culture media (Fig. 1.1). Cell types used in the fundamental studies of cardiovascular tissue engineering include SMCs, endothelial cells (ECs), myocytes, skeletal myoblasts, and stem cells. All these cell types are anchorage-dependent, with their growth and function closely related to the underlying matrix. Cells have an extraordinary capacity in

responding to multiple environmental signals [7]. Transmembrane focal adhesions (FAs) tightly connect the cells with the underlying substrate and are critical in cellular recognition processes. FAs are dynamic protein complexes consisting of a wide range of proteins with functional diversity through which the internal cytoskeleton anchors the extra-cellular matrix (ECM).

Integrins are a large family of receptors across through the cell membrane and link cytoskeleton with ECM proteins. Integrins play primary roles at the early stage of cell sensing of the external environment [8]. Integrins are heterodimers composed of an α subunit and a β subunit, and they can link to adapter proteins such as talin, α-actinin, filamin and vinculin [9,10]. The complex of integrin-adapter protein-cytoskeleton is the basis of an FA. Integrin engagement at the cell-material interface passes signals to the cell through signaling enzymes and adaptors, e.g., focal adhesion kinase (FAK). FAK is an FA-associated protein kinase that can be phosphorylated in response to integrin engagement. The phosphorylation of FAK further induces stronger stress fibers and activates GTPase proteins like Ras homolog gene family member A (RhoA), and affects cell proliferation, motility, and differentiation [11-14].

1.2.2 Crosstalk between cells and the underlying substrate

Cellular responses to the underlying substrate can be regulated by the surface characteristics of the substrate. Cells can sense the substrate through a combination of biochemical and biophysical signals given by the substrate material with different mechanical, chemical, topographical and biological properties [15,16]. These surface cues sensed by the cells also affect cell fate collectively [17,18]. The changes in cell behavior are caused by triggering specific membrane molecular recognitions such as FAs, integrins, and other cellular sensors at the cell-material interface [19,20]. Different cues may have similar effects on cellular behavior while distinct cellular responses can be induced by one cue [21-23].

Despite the efforts in the past decades, the understanding on cell-material interactions is still far from satisfactory as the studies were limited by modest signal strength, rough spatial arrangement, and short time scale [22]. With the growing advancements in nanotechnology, biotechnology, and materials science, new findings have been reported by exerting new defined signals or unprecedented signal strengths [19]. In particular, dynamic mechanical cues, nanoscale topographies, and sophisticated chemical/biological molecules have been developed

for studying cell-material interactions [15]. Polymers used as substrates in these studies are summarized and discussed in the following section.

1.3 Biodegradable polymers for regulating cell behavior in cardiovascular tissue engineering

1.3.1 Natural polymers

Biodegradable natural polymers exist in plants and animals, and the cost of using them is affordable. These polymers normally have a large number of repeating units with functional groups along the backbone, which serve as sites for further modification. Excellent candidates in this category are polysaccharides, proteins, and bacterial polyesters. These natural polymers are discussed below and listed in Table 1.1 with their chemical structures and the results for regulating cells.

1.3.1.1 Polysaccharides

The typical examples of natural polysaccharides include cellulose, starch, alginic acid, hyaluronic acid, and chitosan. These polysaccharides have high molecular weights.

Cellulose. Natural cellulose is an excellent candidate material for making vascular grafts because of its unique characteristics such as high mechanical modulus, low hydrophobicity, and good cellular guidance from its nanofibril structures [24]. The mechanical modulus of the cellulose obtained from bacteria is similar to that of carotid artery in human body and cellulose nanofibers support human SMC adhesion and guide SMC migration [25]. α,β-unsaturated aldehydes from cigarette smoke can reduce the viability, adhesion, and proliferation of human umbilical vein endothelial cells (HUVECs) on cellulose, suggesting the risk of applying cellulose grafts to cigarette-smoking cardiovascular disease patients [26]. Cellulose modified with adhesive peptide Arg-Gly-Asp (RGD) or Gly-Arg-Gly-Asp-Tyr (GRGDY) significantly increases the attachment of human microvascular ECs (HMECs) [27]. Cellulose modified using nitrogen plasma enhances HMEC adhesion because of increased porosity and concentration of functional groups [28].

Hyaluronic acid (HA). Natural HA is a polysaccharide found in connective tissues and synovial fluids. The repeating structure of HA is composed of D-glucuronic acid and 2-acetamido-2-deoxy-D-glucose monosaccharide unit. HA and its derivatives are mostly water soluble and can be shaped into membranes, sponges, and microspheres [29,30]. In cell-biomaterial interface studies, HA is often used as an additive to other polymers to improve cell attachment and proliferation. For example, rat aortic ECs are stimulated to proliferate better by HA-oligomer additives, and platelet adhesion and activation on the EC layer are attenuated by HA additives [31]. Doping HA to conductive polypyrrole (PPy) increases rabbit vascular SMC proliferation and promote the expression of contractile phenotype proteins (smooth muscle α-actin and smooth muscle myosin heavy chain) [32]. Synthetic tunable HA hydrogels with modified adhesion and degradation parameters can enable human endothelial colony-forming cells to form efficient vascular networks [33].

Chitosan. Natural chitosan is an odorless, semi-crystalline polysaccharide consisting of β-1,4-linked 2-amino-2-deoxy-D-glucopyranose residues and randomly distributed *N*-acetyl glucosamine groups in the linear backbone [34,35]. The solubility of chitosan is highly related to the pH value of the solution: it is insoluble at 7.0 and above while soluble at 6.0 and lower [34,35]. Chitosan undergoes *in vivo* biodegradation to nontoxic products through enzymatic hydrolysis. For tissue-engineering applications, chitosan and its derivatives are often grafted or coated onto substrate surfaces for enhancing cytocompatibility and cell recognition [35]. For example, immobilization of *O*-carboxymethyl chitosan on the surface of poly(ethylene terephthalate) (PET) film can improve the biocompatibility of PET and enhance proliferation of rat SMCs [36]. Photo-initiated grafting of *N*-maleic acyl-chitosan to PLA was also reported to improve hemocompatibility by enhancing HUVEC adhesion, proliferation, and function [37]. Chemical modification of chitosan is also an effective way to enhance biocompatibility and cell proliferation. A phosphorylcholine-modified chitosan can increase survival, differentiation, and amplification of endothelial progenitor cells (EPCs) [38]. Phthalization of chitosan also enhances mouse fibroblast compatibility, processibility, and antithrombogenic properties, and it may have a potential application in small-diameter vascular engineering because it can be readily fabricated into selective permeable tubular constructs of varying sizes, morphology, and

properties [39]. Neutralization of chitosan surface in NaOH solutions and ethanol affect the surface chemistry, nanotopography, and mechanical properties as the treated films enhance the spreading, adhesion and proliferation of HMECs, with retention of the endothelial phenotype and function [40].

1.3.1.2 Proteins

Proteins are a category of high-molecular-weight polymers that have one or more chains of amino acid residues. Proteins are abundant in nature and have excellent compatibility with cells and tissue environment, thus they have been extensively studied for many applications such as sutures, haemostatic agents, and tissue-engineering scaffolds.

Collagen. Collagen is one of the most familiar natural proteins used in cardiovascular tissue engineering. The basic unit of collagen is a polypeptide with glycine, proline, and hydroxyproline as the basic repeating sequence and this polypeptide combines with 12 others to form a left-handed triple helix structure [41]. At least 22 collagen types were discovered from human tissues such as skin, cartilage, and blood vessels, among which types I, II, III, and IV are the most frequently studied ones [41]. Soluble collagen is a cell-adhesive protein that can influence cell motility, proliferation, state of differentiation, and predisposition to apoptosis [42]. In studying cell-material interactions, collagen is used to enhance vascular cell compatibility and proliferation on materials [43-45]. The amount and structure of collagen adsorbed on a polymer substrate are determined by the surface chemistry. In one study, collagen is adsorbed onto surfaces with varied chemical functional groups, and only the one on hydrophobic surfaces collagen films has structure and morphology similar to those of fibrillar collagen gels [46]. Collagen can be stable and sustainable when it is covalently immobilized to polymer surfaces. For example, collagen is immobilized onto PLA with a density gradient to regulate human umbilical cord vein EC motilities toward specific directions, providing implication for controlling angiogenesis of implantable constructs through surface chemical stimuli [47]. Covalently immobilized collagen onto PCL via surface-initiated atom transfer radical polymerization significantly improves HUVEC affinity and growth [48].

Collagen can be crosslinked with carbodiimide as cardiovascular tissue-engineering substrates [49]. Crosslinked collagen films are stiffer and smoother but the crosslinking process reduces the available mouse myoblast cell binding sites and consequently the capacity to support cell activity is lower [49]. On fully hydrated collagen fibrils, rat aortic SMCs have poor spreading and non-proliferative phenotypes [50]. Dehydrated thin films of collagen fibrils have a topology similar to that of the fully hydrated collagen fibrils, but they are stiffer and can allow rat aortic vascular SMCs to exert more mechanical tension on the matrix and consequently to exhibit proliferative phenotypes [51]. Collagen-incorporated polyacrylamide (PAAm) gel polymerized in microfluidic devices via photo-initiation produces a substrate with a modulus gradient of 1-4 kPa/100 μm and absolute moduli of 1-80 kPa [52]. Bovine aortic vascular SMC spreading, polarization, and motility are all higher on the stiffer side of the gel; moreover, both cell durotaxis (the tactic index for a biased persistent random walk) and cell orientation with respect to the stiffer side increase with increasing magnitude of stiffness gradient [52].

Gelatin. After denaturation, collagen can be further developed into gelatin, which is another peptide consisting of a limited number of amino acids. Like collagen, gelatin exhibits a haemostatic effect and is widely studied for applications such as biological glue and hydrogel. After it is blended into a hydrogel or bonded onto a surface, gelatin enhances the adhesion, spreading, and proliferation of bovine arterial ECs and human umbilical artery SMCs [53,54]. For example, protein adsorption and bovine arterial EC proliferation are improved on polyvinyl alcohol (PVA) hydrogels blended with gelatin [53]. Dextran hydrogel bonded with gelatin has a higher compressive modulus of 51.9 ±0.1 kPa than the original value of 15.4 ± 3.0 kPa and promotes human vascular EC adhesion and vascular SMC spreading and proliferation [54]. Crosslinked gelatin/PAAm gels with varied mechanical properties are used as substrates to study the morphologies of HUVECs and the less rigid ones support more cells to switch to a tube-like pattern, suggesting that a reduced tension between HUVECs and the ECM can trigger an intracellular signaling cascade leading to tubulogenesis, which is an event that mimics one of the last steps of angiogenesis [55].

1.3.1.3 Bacterial polyesters

In nature, microorganisms produce non-toxic and biodegradable bacterial polyesters [56]. These polyesters with varied mechanical and physical properties can be used as biodegradable adhesives and elastomers in tissue engineering [56]. As one group of this kind, PHAs are synthesized by various bacteria and have a common β-hydroxy fatty acid unit, as shown in Table 1.1 [57]. Most PHAs in nature have a very high molecular weight and are highly crystalline and insoluble in water [57]. PHAs have high structural diversity because of the variance in *R* group in the alkyl side chain -[*R*CHCH2COOH]$_n$- shown in Table 1.1. As one of PHAs, poly(3-hydroxy butyrate) (PHB, *R* = CH3) is the most investigated bacterial polyester [57]. Electrospun fiber mesh made of PHB and its copolymer poly(3-hydroxybutyrate-*co*-3-hydroxyvalerate) (PHB-HV) promotes the human adipose tissue-derived stem cell differentiation into the endothelial lineage, thus it is a potential material in improving vascularization in cardiovascular tissue engineering [58]. Vascular-related cellular affinity and HUVEC proliferation can be enhanced through surface modification using ammonia plasma and fibronectin coating of 3-hydroxybutyrate and 3-hydroxyhexanoate copolyester PHBHHx; however, rabbit aorta SMC proliferation is not improved [59]. Binding PHAs with PHA repressor protein (PhaR) and Lys-Gln-Ala-Gly-Asp-Val (KQAGDV) oligopeptide (PhaR-KQAGDV) enhances human vascular SMC adhesion and proliferation [60].

Table 1.1 Natural polymers in the cell-material interface studies for cardiovascular tissue engineering.

Material	Chemical structure	Substrate characteristics	Cell types	Effects on cellular behavior	References
Cellulose	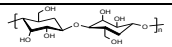	Nanofibrils and desirable mechanical properties; α,β-unsaturated aldehyde; Functionalized with RGD; Porous surface after nitrogen plasma treatment.	Human SMC; HUVEC; HMEC.	Good SMC adhesion, proliferation, and migration; Aldehyde treatment reduces HUVEC adhesion, viability, and growth; RGD and nitrogen plasma treatment enhance HMEC adhesion.	[25-28]
HA	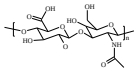	Culture with HA-oligomers; Doping HAs to conducting PPy; HA hydrogels with tunable adhesion and degradation parameters.	Rat aortic EC; Rabbit vascular SMC; Human endothelial colony-forming cells.	HA-oligomers stimulate better EC proliferation and tube formation; Doping with HA increases SMC proliferation and promotes contractile phenotype protein expression; Tunable HA hydrogels enable ECs to form efficient vascular networks.	[31-33]
Chitosan		Immobilize chitosan and *O*-carboxymethyl chitosan onto PET; Graft chitosan to PLA surface; Phosphorylcholine-modified chitosan; Chemical phthalization of chitosan; Neutralization of chitosan surfaces.	Rat thoracic aortic SMC; HUVEC; Mouse EPC derived from bone marrow; Mouse NIH3T3 fibroblasts; HMEC.	Chitosan modified PET improves SMC proliferation; Grafting chitosan improves hemocompatibility potential of PLA; Phosphorylcholine-modified chitosan supports ECs survival/differentiation; Phthalized chitosan has better anti-thrombogenic properties; Neutralizing solution-treated chitosan surfaces have better adhesion and proliferation of HMECs.	[36-40]
Collagen		Immobilize collagen onto PDLLA with a density gradient; Covalently immobilize collagen onto PCL; Crosslinked collagen with different stiffnesses; Dehydrate collagen films with higher rigidities; Collagen-incorporated PAAm gel with a stiffness gradient.	HUVEC; Mouse myoblast; Rat aortic vascular SMCs; Bovine aortic vascular SMCs.	HUVEC motility is regulated by the collagen gradient; HUVEC affinity and growth are significantly better on collagen-immobilized PCL substrates; Crosslinking reduces capacity to support cell activity and limit the effectiveness of collagen scaffolds; Dehydrate collagen fibrils increase its nanoscale rigidity and lead rat vascular SMCs to exhibit proliferative phenotypes; Increasing stiffness gradient increased cell orientation to the stiffer side.	[47-52]
Gelatin		Blend gelatin with PVA hydrogels; Gelatin-bonded dextran hydrogel; Crosslink gelatin with PAAm gels of varied mechanical properties.	Bovine arterial EC; Human umbilical artery SMC and EC; HUVEC.	Gelatin enhances EC proliferation on the hydrogels; Gelatin gel promotes EC 2D adhesion and SMC 3D spreading/proliferation; Less rigid gelatin-PAAm gels support more ECs to switch to a tube-like pattern.	[53-55]

Table 1.1 Natural polymers in the cell-material interface studies for cardiovascular tissue engineering. Continued.

Material	Chemical structure	Substrate characteristics	Cell types	Effects on cellular behavior	References
PHA	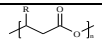	PHB/PHB-HV electrospun fiber mesh; Ammonia plasma-treated and fibronectin-coated surface of PHBHHx; Bind a fusion protein of PhaR and KQAGDV to PHA.	Human adipose tissue-derived stem cell; HUVEC; Rabbit aorta SMC; Human vascular SMC.	Fiber mesh promotes stem cell differentiation into the endothelial lineage; Plasma-treated surface stimulates HUVEC proliferation, but not for SMCs; Oligopeptide enhances SMC adhesion and proliferation.	[58-60]

1.3.2 Synthetic polymers

Natural polymers have limited availability in structures and physicochemical properties for applications in cardiovascular tissue engineering. Synthetic biodegradable polymers provide tailorability in molecular weight, chemical structures, functional groups, mechanical properties, and degradation kinetics for different applications. In addition, synthetic biodegradable polymers are normally easier to be dissolved in common solvents and fabricated into structures with pre-designed topographical features for supporting cell functions and tissue in-growth. Typical synthetic polymers are discussed below and listed in Table 1.2 with their chemical structures and the results for regulating cells.

1.3.2.1 Polyesters

Polyesters can be synthesized via ring-opening polymerization (ROP) of cyclic diesters, glycolides, lactides and lactones, polycondensation of diacids and diols, or self polycondensation of hydroxyacids. The most widely used monomers for polyester synthesis in cardiovascular tissue-engineering applications include glycolide, lactide, and ε-caprolactone.

PGA. PGA is one of the earliest biodegradable synthetic polyesters for tissue-engineering applications. High-molecular-weight PGA can be synthesized through ROP of glycolide or polycondensation of glycolic acid [61]. The melting point of PGA is higher than 200 °C and the glass transition temperature is higher than 30 °C [62]. Therefore, PGA is stiff at room or body temperature and it is hard to be dissolved in organic solvents. PGA degrades through hydrolysis of the ester bonds into non-toxic glycolic acids, which are further metabolized by enzymes into water and carbon dioxide. Thus PGA is not sustainable *in vivo* as it loses strength and completely disappears several months after implantation. PGA is normally used as temporary support substrates or scaffolds in cardiovascular tissue engineering. Surface hydrolysis of PGA in NaOH solution can transform surface ester groups into carboxylic acid and hydroxyl groups to improve bovine thoracic aorta SMC attachment [63]. Introduction of chemically synthesized hetero-bifunctional peptide linkers to PGA surface can enhance interactions between PGA and HUVEC integrin receptors and thus promote binding and spreading of these ECs [64].

Table 1.2 Synthetic polymers in the cell-material interface studies for cardiovascular tissue engineering.

Material	Chemical structure	Substrate Characteristics	Cell types	Effects on cellular behavior	References
PGA	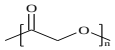	Surface hydrolysis by NaOH; Introducing hetero-bifunctional peptide linkers to PGA surface.	Bovine thoracic aorta SMC; HUVEC.	Surface hydrolysis improves SMC attachment; Peptide linkers promote EC binding and spreading.	[63,64]
PLGA	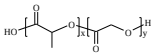	PLGA surface treated with NaOH ; PS nanospheres with various diameters on PLGA surface; Surface Immobilization of sulfated silk fibroin.	Rat aortic SMC; Rat aortic EC; Ovine bladder SMC; Porcine thoracic aorta EC.	NaOH treatment enhances SMC adhesion and proliferation but inhibits EC adhesion/proliferation; Surface nanostructure promotes SMC and EC adhesion; Surface fibroin reduces platelet adhesion and accelerates EC endothelialization.	[66-69]
PLLA	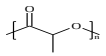	PLLA nanofiber mesh scaffold; Aligned PLLA nanofibrous scaffolds; P(LLA-CL) nanofibrous scaffolds; Aligned P(LLA-CL) nanofibrous structure; Blending lecithin with PLLA; PLLA/PVP microfibrous scaffolds; PVAA deposition or fibronectin conjugation to PLLA surface.	Bovine aortic EC; Rabbit outgrowth EC; Human aortic SMC; Human coronary artery EC; Human coronary artery SMC; Rat thoracic aorta SMC; MSC isolated from rat bone marrow; Vascular SMC; Pig aorta EC.	PLLA nanofibers increase EC adherence and proliferation. Lecithin significantly enhances the proliferation and viability of SMCs and MSCs; PVAA deposition enhances EC endothelialization on PLLA; Aligned PLLA fibers promote proliferation of ECs; Both ECs and SMCs show good adhesion and proliferation on P(LLA-CL) fibers; SMCs adhere with cytoskeleton parallel to nanofibers, migrate along aligned nanofibers with a higher proliferation rate on nanofibers; Porous nanofibrous PLLA preferentially supports contractile phenotype of SMCs.	[71,73,74, 76-81]

Table 1.2 Synthetic polymers in the cell-material interface studies for cardiovascular tissue engineering. Continued.

Material	Chemical structure	Substrate Characteristics	Cell types	Effects on cellular behavior	References
PCL	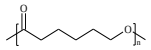	Surface functionalized with RGD; PCL-heparin conjugate loaded with FGF2; PCL-heparin conjugate loaded with VEGF; Immobilization of ASA and VEGF; Deposition of chitosan/heparin multilayer; Immobilization of anti-CD31 antibody; Nanometer roughness through etching; Blend and photo-crosslink with PPF.	Human EC; Mouse fibroblast; HUVEC; Ovine bladder SMCs; Rat aortic SMC.	Grafting RGD or deposition of chitosan/heparin improves hemocompatibility; Heparin and FGF2 improve vascular cell density and morphology; ASA and VEGF enhance the biofunctionalization; Angiogenic response of PCL can be tuned by modulating the dose of VEGF; Nanometer range surface features enhance SMC adhesion; SMC responses are distinct in the presence or absence of crosslinks and stiffer substrates support better SMC adhesion and proliferation.	[83-90,96]
PEG	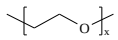	Conjugate ephrinA1; Immobilize RGDS and VEGF; Incorporation of VGVAPG; Porous PEG hydrogel modified with VEGF and RGD; Incorporate PEG-GRGDS into photo-crosslinked elastomers; RGD-modified heparin-releasing PEGDA gel; Incorporate RGD, fibronectin, and laminin; Positive charges from agmatine; Copolymerize with ethylene glycol; Incorporate PEG-GRGDSP into PAAm gels to make substrates with tunable mechanics.	HUVEC; Bovine aortic EC; Human coronary artery SMC; Human aortic SMC.	PEG-ephrinA1 induces robust vascular response and higher vessel density; RGDS-modification increases EC motility on PEG hydrogels. VEGF modified porous hydrogel has superior angiogenic potential in stimulating new vessel formation; GRGDS incorporation enhances SMC proliferation; Heparin on PEG hydrogel upregulates expression of contractile phenotype markers in SMCs; SMCs cultured on PEG hydrogels with immobilized RGD, fibronectin and laminin can redifferentiate to the contractile phenotype; Agmatine improves the adsorption of serum components onto PPF-PEG hydrogel and enhances SMC adhesion. Copolymerize with PEG changes hydrophobicity of PPF and enhances SMC adhesion; PEG-GRGDSP in stiffer PAAm gels enhances SMC proliferation.	[103-113]

Table 1.2 Synthetic polymers in the cell-material interface studies for cardiovascular tissue engineering. Continued.

Material	Chemical structure	Substrate Characteristics	Cell types	Effects on cellular behavior	References
PU	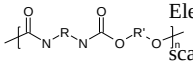	PU grafted with electrospun PLGA fibers treated with argon plasma; Conjugation of fibronectin onto porous PCU scaffolds; Surface crosslinking of ELP4; Modification with GRGDSP peptide; Electrospun PEGMA/PU crosslinked hybrid scaffolds; Porous 3D PU scaffolds, compared with 2D topography; Polar hydrophobic ionic PU porous scaffolds; Porous 3D waterborne PU scaffolds with controllable pore size and porosity.	HUVEC; Human coronary artery SMC; HUV-SMC; SMC derived from thoracic aorta of embryonic rats.	Plasma treatment increases EC attachment and proliferation; Fibronectin improves SMC attachment and infiltration depth into PCU scaffolds; ELP4 enhances SMC adhesion, density, and contractile phenotype marker expression; GRGDSP enhances EC adhesion and proliferation on 3D PU scaffolds; Crosslinking PU with PEGMA triggers better EC morphology and proliferation on the scaffolds; PU scaffolds with 3D porous topography induce the synthetic phenotype of SMC and their ability to produce elastin; Polar hydrophobic ionic polyurethane porous scaffolds support good adhesion and growth of SMCs; HUVEC adhesion and proliferation are better in 3D waterborne PU scaffolds with smaller pores and a lower porosity.	[115-122]

Poly(lactic-*co*-glycolic acid) (PLGA). PLGA with various compositions can be synthesized via ring-opening copolymerization of lactide and glycolide. Because of its tunable degradation rate and mechanical properties, biocompatibility and solubility in common organic solvents, PLGA is widely used to fabricate tissue-engineering scaffolds and drug delivery carriers [65]. PLGA is also well studied for understanding cell-material interactions in cardiovascular tissue engineering. Surface treatment of PLGA using NaOH solutions can improve rat aortic SMC adhesion and proliferation but cannot for rat aortic ECs [66]. In another study, NaOH-etched PLGA has nanoscale topographical features to enhance ovine bladder SMC adhesion [67]. Polystyrene (PS) spheres with diameters of 500, 200, or 100 nm are used as templates to fabricate PLGA films with spherical features to enhance adhesion for both rat aortic SMCs and ECs because they promote fibronectin spreading [68]. Covalently grafting sulfated silk fibroin on the surface of PLGA scaffolds using γ irradiation can reduce platelet adhesion, prolong porcine EC adhesion time, and upregulate protein expression of EC-specific markers [69].

PLA. PLA is synthesized through ROP of lactide. PLA has a backbone similar to that of PGA but with one extra methyl group. Because of this methyl group, PLA is much more hydrophobic and has a lower degradation rate than PGA [70]. Because lactide exists in two different forms, D-lactide and L-lactide, PLA has three isomeric forms, poly(D-lactic acid) (PDLA), poly(L-lactic acid) (PLLA), and poly(D,L-lactic acid) (PDLLA), among which PLLA is most studied in cardiovascular tissue-engineering applications. Scaffolds made of air-spun PLLA nanofibers enable bovine aortic ECs to proliferate in a monolayer at a high rate [71,72]. Aligned PLLA nanofibers are compatible with outgrowth ECs originally isolated from rabbit peripheral blood, and can promote and guide their sustained proliferation [73]. PLLA scaffolds modified using porous nanofibers on the surface can preferentially support the contractile phenotype of human aortic SMCs, as evidenced by upregulated expression of contractile gene markers of myocardin, smoothelin, and smooth muscle myosin heavy chain [74]. All these results support that vascular cells are influenced by topographical features of the underlying substrates in addition to chemical cues. Synthetic nanostructures are very important in dictating vascular cell adhesion, proliferation, migration, and gene expression [75].

In addition to PLLA, PLLA-related copolymers are also used to fabricate vascular tissue scaffolds with topographical patterns, for example, electrospun poly(L-lactide-*co*-caprolactone) (PLLA-CL, 75:25) nanofibers with diameters of 0.5-1.5 μm for supporting good adhesion and proliferation of human coronary artery ECs and SMCs [76]. Aligned electrospun P(LLA-CL) nanofibers with a diameter of ~0.5 μm are used to mimic the topography of circumferentially oriented cells and fibrils in the medial layer of a native artery [77]. Human coronary artery SMCs on these aligned fibers adhere with cytoskeleton parallel to direction of nanofibers and migrate along the axis of the aligned nanofibers, with significantly faster proliferation and better functional contractile phenotype compared with the synthetic phenotype with fewer myofilaments on the flat polymer films [77].

One limitation of PLLA to be used in cardiovascular tissue engineering is its relatively low cytocompatibility. Blending PLLA with lecithin (3-7 wt%), a mixture of phospholipids and neutral lipids that can serve as a linker between cell membrane and ECM, remarkably improves the cytocompatibility of PLLA as the proliferation and viability of both rat aorta vascular SMC and mesenchymal stem cells (MSCs) isolated from rat bone marrow are significantly enhanced [78,79]. Blending PLLA with polyvinyl pyrrolidone (PVP) can also induce better morphology and proliferation of vascular SMCs [80]. Other surface modification to PLLA using poly(vinylacetic acid) (PVAA) deposition, fibronectin conjugation, and surface delivery of vascular endothelial growth factor can also enhance pig aorta EC endothelialization [81].

PCL. As one of the most widely used biodegradable polymer in cardiovascular tissue engineering, PCL is synthesized via ROP of cyclic ε-caprolactone in the presence of an initiator such as alcohol and a catalyst such as stannous octoate [82]. PCL has excellent elasticity and toughness, and relatively long degradation time of 2-3 years [6]. To improve the interactions between cells and PCL, the surface of PCL can be functionalized with chemicals that favor cell adhesion [83-86]. For example, RGD peptide, heparin, fibroblast growth factor 2 (FGF2), acetylsalicylic acid (ASA), and vascular endothelial growth factor (VEGF) can be immobilized onto PCL surface to improve its hemocompatibility and induce better vascular cell adhesion, density, and morphology [83-86]. *In vivo* VEGF-mediated angiogenesis on PCL is enhanced after heparin is crosslinked onto the surface [87]. Layer-by-layer deposition of chitosan/heparin

onto PCL surface is effective in improving hemocompatibility [88]. Immobilization of anti-cellular transmembrane adhesion molecules, e.g., anti-CD31 antibody, on PCL surface, significantly enhances the specific adhesion of mouse embryonic vascular NIH3T3 cells [89]. PCL treated with 0.1 M NaOH can reduce the polymer surface features from conventional microns to biologically inspired nanometer dimensions, which enhance ovine bladder SMC adhesion [90].

Poly(propylene fumarate) (PPF) is crosslinkable, biodegradable polyester synthesized via polycondensation of diethyl fumarate and propylene glycol [91,92]. Because of the carbon-carbon double bonds in the backbone, PPF can be cured into a network with a stable shape and a high mechanical strength [93]. Enzymatic degradation of PPF results in two non-toxic monomers, which are fumaric acid, a naturally existing substance in human body, and 1,2-propane diol, a commonly used diluent solvent [94,95]. In our research group, PCL is blended with PPF as substrates for SMCs and cell behavior is distinct when PPF is photo-crosslinked or uncrosslinked as the result of the differences in physicochemical characteristics, in particular, stiffness [96].

I have also developed a series of photo-crosslinked PCL triacrylate substrates with controllable stiffness by varying the crosslinking density and crystallinity [97]. SMCs cultured on stiffer semi-crystalline PCLTA networks have stronger FAs, better spreading, faster growth and motility, and better conversion from the synthetic phenotype to the more functional contractile phenotype [97]. The high hydrophobicity of PCLTA networks can be relieved by photo-crosslinking with hydrophilic methoxy PEG monoacrylate (mPEGA) [98]. After grafting a small amount (5 wt%) of mPEGA chains to the PCLTA network, it becomes less hydrophobic and can result in better SMC attachment, spreading, proliferation, and contractile gene/protein expression [98].

1.3.2.2 Biodegradable polyethers

Polyethers are synthesized by polymerizing monomers through ether links, with typical examples as PEG, polyetherketoneketone, polypropylene glycol, polyoxymethylene, polyphenyl ether, and polytetrahydrofuran. Not all the polyethers are biodegradable, and only some of them are being used as tissue-engineering biomaterials. For cardiovascular studies, the

most studied polyethers are PEG and its derivatives. PEG is a liquid at low molecular weights and waxy at high molecular weights. PEG has a low surface free energy with water and is inert to protein adsorption and cell adhesion because of its high chain mobility and repulsion. Because of this unique property, PEG chains have been introduced to hydrophobic polymer surfaces through blending, copolymerizing, or covalent linking to improve surface hydrophilicity [98-101]. Good endothelialization without platelet adhesion is crucial for blood-contacting implants. For this purpose, PEG has been applied to modify other polymers to prevent platelet adhesion and immunogenic activities. For example, introducing a peptide-PEG segment into polyurethane (PU) significantly enhances bovine aortic EC adhesion, spreading, and migration while prohibits platelet adhesion [102].

PEG-based hydrogels have been studied for cardiovascular tissue-engineering applications, especially when they are modified by incorporating peptides such as RGD, heparin, growth factors, fibronectin, and laminin [103-107]. Arg-Gly-Asp-Ser (RGDS) increases HUVEC motility while VEGF increases the tubulogenesis of ECs [103]. A peptide containing the Gly-Arg-Gly-Asp-Ser (GRGDS) sequence enhances proliferation of bovine coronary artery SMCs [104]. Human coronary artery SMCs cultured on PEG hydrogels modified with RGD, fibronectin, and laminin can redifferentiate to the contractile phenotype [105]. Heparin upregulates the expression of contractile gene markers in human coronary artery SMCs [106]. Porous PEG hydrogels with VEGF releasing ability have better angiogenic potential in stimulating new vessel formation from HUVECs [107]. Incorporation of elastin mimetic peptide that contains Val-Gly-Val-Ala-Pro-Gly (VGVAPG) sequence supports stronger human aortic SMC adhesion and elastin deposition on the PEG hydrogels [108]. EphrinA1, a factor expressed in ECs, is of interest for promoting vascularization on vascular grafts and conjugation of ephrinA1 to PEG hydrogels can induce a more robust vascular response [109].

PPF-*co*-PEG synthesized through copolymerization of PPF and PEG can be used to prepare hydrogels to relieve the strong hydropobicity of crosslinked PPF and enhance human aortic SMC adhesion [110]. Further introduction of positive charges from agmatine into PPF-*co*-PEG hydrogels promotes the surface adsorption of serum components and then benefits human aortic SMC adhesion [111,112]. Incorporating PEG-Gly-Arg-Gly-Asp-Ser-Pro (GRGDSP) into PAAm gels produces substrates with tunable mechanical properties for exploring the effect of

tissue stiffness on Platelet Derived Growth Factor (PDGF) signaling in primary bovine vascular SMCs [113]. Substrate stiffness significantly enhances PDGF receptor activity and vascular SMC proliferation, implying that stiffening of the vessel wall can increase vascular SMC growth and survival by enhancing PDGF receptor signaling and thus facilitate pathogenesis of vascular diseases [113].

1.3.2.3 Biodegradable polyurethanes

PUs are series of synthetic polymers containing carbamate (urethane) links formed by reaction between isocyanate and polyol. PUs normally have good mechanical strength, excellent biocompatibility, and relatively long durability, thus they can be used to fabricate long-term implants such as vascular grafts. Biodegradable PUs can also be synthesized for fabricating temporary tissue-engineering scaffolds and grafts by incorporating degradable chemical linkages [114]. Current modification methods for improving the cellular interactions with PUs include plasma treatment, conjugation of cell-adhesive proteins such as fibronectin, recombinant elastin-like polypeptide-4 (ELP4), and GRGDSP peptide, and fabrication of 3D porous structures [115-122]. HUVECs and SMCs are used to study their interactions with biodegradable PUs [115-122]. Surface treatment using microwave-induced argon plasma increases HUVEC adhesion and growth on PUs grafted with electrospun PLGA fiber [115]. Introducing fibronectin into a highly porous 3D poly(carbonate urethane) (PCU) scaffold improves human coronary artery SMC adherence and infiltration into the scaffold [116]. ELP4 crosslinked on PCU surface enhances human umbilical vein SMC (HUV-SMC) attachment, growth, and contractile phenotypic conversion [117]. Surface grafting of GRGDSP peptide improves HUVEC adhesion and proliferation on non-toxic biodegradable waterborne PU scaffolds [118]. Photo-crosslinking PEG methacrylate (PEGMA) into PU electrospun nanofibrous scaffolds with average fiber diameters of 622 ± 110 and 547 ± 77 nm not only improves the mechanical properties and fiber morphology, but also enhances HUVEC adhesion, viability, and proliferation [119]. PCU scaffolds with 3D porous topography induce the synthetic phenotype of human coronary artery SMCs and enable these cells to produce elastin, compared with 2D topography [120]. Degradable hydrophobic ionic PU porous scaffolds containing a lysine-based polycarbonate divinyl oligomer support good adhesion and growth

of SMCs that are derived from thoracic aorta of embryonic rats [121]. Among a series of 3D interconnected porous scaffolds with various pore diameters (3-229 μm) and porosities (80-92%) fabricated by freeze-drying with waterborne PU emulsions, HUVEC adhesion and proliferation are better when the pores are smaller and the porosity is lower [122].

1.4 Conclusions and Perspectives

As reviewed above, numerous biodegradable polymers that include both natural and synthetic ones have been used to regulate cells that are related to cardiovascular tissue-engineering applications. Chemical modification is the major means to improve the cytocompatibility of these polymers. The results in these studies offer valuable information to improve the material design strategies for the clinical goals. Incorporation of different surface characteristics such as stiffness, topography, and structural features with the intrinsic polymer chemical properties is critical in development of novel advanced biomaterials.

References

1. Go AS, Mozaffarian D, Roger VL, Benjamin EJ, Berry JD, Borden WB, Bravata DM, Dai S, Ford ES, Fox CS; Franco S; Fullerton HJ, Gillespie C, Hailpern SM, Heit JA, Howard VJ, Huffman MD, Kissela BM, Kittner SJ, Lackland DT, Lichtman JH, Lisabeth LD, Magid D, Marcus GM, Marelli A, Matchar DB, McGuire DK, Mohler ER, Moy CS, Mussolino ME, Nichol G, Paynter NP, Schreiner PJ, Sorlie PD, Stein J, Turan TN, Virani SS, Wong ND, Woo D, Turner MB, American Heart Association Statistics Committee and Stroke Statistics Subcommittee. Heart disease and stroke statistics--2013;update: a report from the American Heart Association. Circulation 2013;127(1):e6-e245
2. Prabhakaran MP, Venugopal J, Kai D, Ramakrishna S. Biomimetic material strategies for cardiac tissue engineering. Mater Sci Eng C 2011;31(3):503-13
3. Tee R, Lokmic Z, Morrison WA, Dilley RJ. Strategies in cardiac tissue engineering. ANZ J Surg 2010;80(10):683-93
4. Ye KY, Black LD. Strategies for tissue engineering cardiac constructs to affect functional repair following myocardial infarction. J Cardiovasc Transl Res 2011;4(5):575-91
5. Hutmacher DW. Scaffold design and fabrication technologies for engineering tissues--state of the art and future perspectives. J Biomater Sci Polym Ed 2001;12(1):107-24
6. Gunatillake PA, Adhikari R. Biodegradable synthetic polymers for tissue engineering. Eur Cell Mater 2003;5;1-16;
7. Geiger B, Spatz JP, Bershadsky AD. Environmental sensing through focal adhesions. Nat Rev Mol Cell Biol 2009;10(1):21-33
8. Miranti CK, Brugge JS. Sensing the environment: a historical perspective on integrin signal transduction. Nat Cell Biol 2002;4(4):E83-90
9. Critchley DR. Cytoskeletal proteins talin and vinculin in integrin-mediated adhesion. Biochem Soc Trans 2004;32:831-6
10. Lee SE, Kamm RD, Mofrad MR. Force-induced activation of talin and its possible role in focal adhesion mechanotransduction. J Biomech 2007;40(9):2096-106
11. Peyton SR, Putnam AJ. Extracellular matrix rigidity governs smooth muscle cell motility

in a biphasic fashion. J Cell Physiol 2005;204(1):198-209

12. Jin L, Hastings NE, Blackman BR, Somlyo AV. Mechanical properties of the extracellular matrix alter expression of smooth muscle protein LPP and its partner palladin; relationship to early atherosclerosis and vascular injury. J Muscle Res Cell Motil 2009;30(1-2):41-55
13. Andrae J, Gallini R, Betsholtz C. Role of platelet-derived growth factors in physiology and medicine. Genes Dev 2008;22(10):1276-312
14. Peyton SR, Ghajar CM, Khatiwala CB, Putnam AJ. The emergence of ECM mechanics and cytoskeletal tension as important regulators of cell function. Cell Biochem Biophys 2007;47(2):300-20
15. Ventre M, Causa F, Netti PA. Determinants of cell-material crosstalk at the interface: towards engineering of cell instructive materials. J R Soc Interface 2012;9(74):2017-32
16. Charest JL. Topographic and Chemical Patterning of Cell-surface Interfaces to Influence; ProQuest LLC: Ann Arbor MI 2008
17. Charest JL, Eliason MT, Garc á AJ, King WP. Combined microscale mechanical topography and chemical patterns on polymer cell culture substrates. Biomaterials 2006;27(11):2487-94
18. Craighead HG, James CD, Turner AMP. Chemical and topographical patterning for directed cell attachment. Curr Opin Solid State Mater Sci 2001;5(2-3):177-84
19. Zhao W, Schafer S, Choi J, Yamanaka YJ, Lombardi ML, Bose S, Carlson AL, Phillips JA, Teo W, Droujinine IA, Cui CH, Jain RK, Lammerding J, Love JC, Lin CP, Sarkar D, Karnik R, Karp JM. Cell-surface sensors for real-time probing of cellular environments. Nat Nanotechnol 20116(8):524-31
20. Garc á AJ. Interfaces to control cell-biomaterial adhesive interactions. Adv Polym Sci 2006;203:171-90
21. Wong JY, Leach JB, Brown XQ. Balance of chemistry topography and mechanics at the cell-biomaterial interface: issues and challenges for assessing the role of substrate mechanics on cell response. Surf Sci 2004;570(1-2):119-33
22. Nemir S, West JL. Synthetic materials in the study of cell response to substrate rigidity. Ann Biomed Eng 2010;38(1):2-20
23. Discher DE, Janmey P, Wang YL. Tissue cells feel and respond to the stiffness of their

substrate. Science 2005;310(5751):1139-43

24. Wang JP, Zhu YZ, Du J. Bacterial cellulose: a natural nanomaterial for biomedical applications. J Mech Med Biol 2011;11(02):285-306

25. Backdahl H, Helenius G, Bodin A, Nannmark U, Johansson BR, Risberg B, Gatenholm P. Mechanical properties of bacterial cellulose and interactions with smooth muscle cells. Biomaterials 2006;27(9):2141-9

26. Jeong S, Lee SE, Yang H, Park CS, Jin YH, Park YS. Effect of αβ-unsaturated aldehydes on endothelial cell growth in bacterial cellulose for vascular tissue engineering. Mol Cell Toxicol 2012;8(2):119-26

27. Andrade FK, Costa R, Domingues L, Soares R, Gama M. Improving bacterial cellulose for blood vessel replacement: Functionalization with a chimeric protein containing a cellulose-binding module and an adhesion peptide. Acta Biomater 2010;6(10):4034-41

28. Pertilea RAN, Andradea FK, Alves CJr, Gama M. Surface modification of bacterial cellulose by nitrogen-containing plasma for improved interaction with cells. Carbohyd Polym 2010;82(3):692-8

29. Pandis L, Zavan B, Bassetto F, Ferroni L, Iacobellis L, Abatangelo G, Lepidi S, Cortivo R, Vindigni V. Hyaluronic acid biodegradable material for reconstruction of vascular wall: a preliminary study in rats. Microsurgery 2011;31(2):138-45

30. Svensson Holm AC, Bengtsson T, Greneg ård M, Lindstr öm EG. Hyaluronic acid influence on platelet-induced airway smooth muscle cell proliferation. Exp Cell Res 2012;318(5):632-40

31. Ibrahim S, Ramamurthi A. Hyaluronic acid cues for functional endothelialization of vascular constructs. J Tissue Eng Regen Med 2008;2(1):22-32

32. Rowlands AS, Cooper-White JJ. Directing phenotype of vascular smooth muscle cells using electrically stimulated conducting polymer. Biomaterials 2008;29(34):4510-20

33. Hanjaya-Putra D, Bose V, Shen YI, Yee J, Khetan S, Fox-Talbot K, Steenbergen C, Burdick JA, Gerecht S. Controlled activation of morphogenesis to generate a functional human microvasculature in a synthetic matrix. Blood 2011;118(3):804-15

34. Khor E, Lim LY. Implantable applications of chitin and chitosan. Biomaterials 2003;24(13):2339-49

35. Deng C, Li F, Griffith M, Ruel M, Suuronen EJ. Application of chitosan-based biomaterials for blood vessel regeneration. Macromol Symp 2010;297(1):138-46

36. Zhu AP, Zhao F, Fang N. Regulation of vascular smooth muscle cells on poly(ethylene terephthalate):film by *O*-carboxymethylchitosan surface immobilization. J Biomed Mater Res A 2008;86(2):467-76

37. Zhu A, Zhao F, Ma T. Photo-initiated grafting of gelatin/*N*-maleic acyl-chitosan to enhance endothelial cell adhesion proliferation and function on PLA surface. Acta Biomater 2009;5(6):2033-44

38. Tardif K, Cloutier I, Miao Z, Lemieux C, St-Denis C, Winnik FM, Tanguay JF. A phosphorylcholine-modified chitosan polymer as an endothelial progenitor cell supporting matrix. Biomaterials 2011;32(22):5046-55

39. Qiu Y, Zhang N, Kang Q, An Y, Wen X. Fabrication of permeable tubular constructs from chemically modified chitosan with enhanced antithrombogenic property. J Biomed Mater Res B Appl Biomater 2009;90(2):668-78

40. He Q, Ao Q, Gong Y, Zhang X. Preparation of chitosan films using different neutralizing solutions to improve endothelial cell compatibility. J Mater Sci Mater Med 2011;22(12):2791-802

41. Nair LS, Laurencin CT. Polymers as biomaterials for tissue engineering and controlled drug delivery. Adv Biochem Eng Biotechnol 2006;102:47-90

42. Bornstein P, Sage EH. Matricellular proteins: extracellular modulators of cell function. Curr Opin Cell Biol 2002;14(5):608-16

43. Zhu Y, Chan-Park MB. Density quantification of collagen grafted on biodegradable polyester: its application to esophageal smooth muscle cell. Anal Biochem 2007;363(1):119-27

44. He X, Zhai Z, Wang Y, Wu G, Zheng Z, Wang Q, Liu Y. New method for coupling collagen on biodegradable polyurethane for biomedical application. J Appl Polym Sci 2012;126(S1):E354-61

45. Elliott JT, Woodward JT, Langenbach KJ, Tona A, Jones PL, Plant AL. Vascular smooth muscle cell response on thin films of collagen. Matrix Biol 2005;24(7):489-502

46. Elliott JT, Woodward JT, Umarji A, Mei Y, Tona A. The effect of surface chemistry on the

formation of thin films of native fibrillar collagen. Biomaterials 2007;28(4):576-85

47. Cai K, Kong T, Wang L, Liu P, Yang W, Chen C. Regulation of endothelial cells migration on poly(DL-lactic acid):films immobilized with collagen gradients. Colloids Surf B Biointerfaces 2010;79(1):291-7

48. Yuan SJ, Xiong GD, Wang XY, Zhang S, Choong C. Surface modification of polycaprolactone substrates using collagen-conjugated poly(methacrylic acid):brushes for the regulation of cell proliferation and endothelialisation. J Mater Chem 2012;22:13039-49

49. Grover CN, Gwynne JH, Pugh N, Hamaia S, Farndale RW, Best SM, Cameron RE. Crosslinking and composition influence the surface properties mechanical stiffness and cell reactivity of collagen-based films. Acta Biomater 2012;8(8):3080-90

50. Elliott JT, Tona A, Woodward JT, Jones PL, Plant AL. Thin films of collagen affect smooth muscle cell morphology. Langmuir 2003;19(5):1506-14

51. McDaniel DP, Shaw GA, Elliott JT, Bhadriraju K, Meuse C, Chung KH, Plant AL. The stiffness of collagen fibrils influences vascular smooth muscle cell phenotype. Biophys J 2007;92(5):1759-69

52. Isenberg BC, Dimilla PA, Walker M, Kim S, Wong JY. Vascular smooth muscle cell durotaxis depends on substrate stiffness gradient strength. Biophys J 2009;97(5):1313-22

53. Liu Y, Vrana NE, Cahill PA, McGuinness GB. Physically crosslinked composite hydrogels of PVA with natural macromolecules: structure mechanical properties and endothelial cell compatibility. J Biomed Mater Res B Appl Biomater 2009;90(2):492-502

54. Liu YX, Chan-Park MB. Hydrogel based on interpenetrating polymer networks of dextran and gelatin for vascular tissue engineering. Biomaterials 2009;30(2):196-207

55. Deroanne CF, Lapiere CM, Nusgens BV. In vitro tubulogenesis of endothelial cells by relaxation of the coupling extracellular matrix-cytoskeleton. Cardiovasc Res 2001;49(3):647-58

56. Lenz RW, Marchessault RH. Bacterial polyesters: biosynthesis biodegradable plastics and biotechnology. Biomacromolecules 2005;6(1):1-8

57. Hazer B, Steinbüchel A. Increased diversification of polyhydroxyalkanoates by modification reactions for industrial and medical applications. Appl Microbiol Biotechnol 2007;74(1):1-12

58. Zonari A, Novikoff S, Electo NR, Breyner NM, Gomes DA, Martins A, Neves NM, Reis RL, Goes AM. Endothelial differentiation of human stem cells seeded onto electrospun polyhydroxybutyrate/polyhydroxybutyrate-*co*-hydroxyvalerate fiber mesh. PLoS One 2012;7(4):e35422

59. Qu XH, Wu Q, Liang J, Qu X, Wang SG, Chen GQ. Enhanced vascular-related cellular affinity on surface modified copolyesters of 3-hydroxybutyrate and 3-hydroxyhexanoate (PHBHHx). Biomaterials 2005;26(34):6991-7001

60. Dong CL, Li SY, Wang Y, Dong Y, Tang JZ, Chen JC, Chen GQ. The cytocompatability of polyhydroxyalkanoates coated with a fusion protein of PHA repressor protein (PhaR):and Lys-Gln-Ala-Gly-Asp-Val (KQAGDV):polypeptide. Biomaterials 2012;33(9):2593-9

61. Takahashi K, Taniguchi I, Miyamoto M, Kimura Y. Melt/solid polycondensation of glycolic acid to obtain highmolecular-weight poly(glycolic acid). Polymer 2000;41(24):8725-8

62. Singh V, Tiwari M. Structure-processing-property relationship of poly(glycolic acid):for drug delivery systems 1: synthesis and catalysis. Int J Polym Sci 2010;2010;1-23

63. Gao J, Niklason L, Langer R. Surface hydrolysis of poly(glycolic acid):meshes increases the seeding density of vascular smooth muscle cells. J Biomed Mater Res 1998;42(3):417-24

64. Huang X, Zauscher S, Klitzman B, Truskey GA, Reichert WM, Kenan DJ, Grinstaff MW. Peptide interfacial biomaterials improve endothelial cell adhesion and spreading on synthetic polyglycolic acid materials. Ann Biomed Eng 2010;38(6):1965-76

65. Pan Z, Ding J. Poly(lactide-*co*-glycolide):porous scaffolds for tissue engineering and regenerative medicine. Interface Focus 2012;2(3):366-77

66. Miller DC, Thapa A, Haberstroh KM, Webster TJ. Endothelial and vascular smooth muscle cell function on poly(lactic-*co*-glycolic acid):with nano-structured surface features. Biomaterials 2004;25(1):53-61

67. Thapa A, Miller DC, Webster TJ, Haberstroh KM. Nano-structured polymers enhance bladder smooth muscle cell function. Biomaterials 2003;24(17):2915-26

68. Miller DC, Haberstroh KM, Webster TJ. PLGA nanometer surface features manipulate fibronectin interactions for improved vascular cell adhesion. J Biomed Mater Res A 2007;81(3):678-84

69. Liu H, Li X, Niu X, Zhou G, Li P, Fan Y. Improved hemocompatibility and endothelialization of vascular grafts by covalent immobilization of sulfated silk fibroin on poly(lactic-co-glycolic acid):scaffolds. Biomacromolecules 2011;12(8):2914-24

70. Kannan RY, Salacinski HJ, Butler PE, Hamilton G, Seifalian AM. Current status of prosthetic bypass grafts: a review. J Biomed Mater Res B Appl Biomater 2005;74(1):570-81

71. Francois S, Chakfe N, Durand B, Laroche G. A poly(L-lactic acid):nanofibre mesh scaffold for endothelial cells on vascular prostheses. Acta Biomater 2009;5(7):2418-28

72. Francois S, Sarra-Bournet C, Jaffre A, Chakf é N, Durand B, Laroche G. Characterization of an air-spun poly(L-lactic acid):nanofiber mesh. J Biomed Mater Res B Appl Biomater 2010;93(2):531-43

73. Lu H, Feng Z, Gu Z, Liu C. Growth of outgrowth endothelial cells on aligned PLLA nanofibrous scaffolds. J Mater Sci Mater Med 2009;20(9):1937-44

74. Hu J, Sun X, Ma H, Xie C, Chen YE, Ma PX. Porous nanofibrous PLLA scaffolds for vascular tissue engineering. Biomaterials 2010;31(31):7971-7

75. Yim EK, Leong KW. Significance of synthetic nanostructures in dictating cellular response. Nanomedicine 2005;1(1):10-21

76. Mo XM, Xu CY, Kotaki M, Ramakrishna S. Electrospun P(LLA-CL):nanofiber: a biomimetic extracellular matrix for smooth muscle cell and endothelial cell proliferation. Biomaterials 2004;25(10):1883-90

77. Xu CY, Inai R, Kotaki M, Ramakrishna S. Aligned biodegradable nanofibrous structure: a potential scaffold for blood vessel engineering. Biomaterials 2004;25(5):877-86

78. Zhu N, Cui FZ, Hu K, Zhu L. Biomedical modification of poly(L-lactide):by blending with lecithin. J Biomed Mater Res A 2007;82(2):455-61

79. Xu ZH, Wu QY. Effect of lecithin content blend with poly(L-lactic acid):on viability and proliferation of mesenchymal stem cells. Mater Sci Eng C 2009;29(5):1593-8

80. Xu F, Cui FZ, Jiao YP, Meng QY, Wang XP, Cui XY. Improvement of cytocompatibility of electrospinning PLLA microfibers by blending PVP. J Mater Sci Mater Med 2009;20(6):1331-8

81. Xu H, Deshmukh R, Timmons R, Nguyen KT. Enhanced endothelialization on surface

modified poly(L-lactic acid):substrates. Tissue Eng Part A 2011;17(5-6):865-76

82. Cai L, Wang S. Poly(ε-caprolactone):acrylates synthesized using a facile method for fabricating networks to achieve controllable physicochemical properties and tunable cell responses. Polymer 2010;51(1):164-177

83. Zheng W, Wang Z, Song L, Zhao Q, Zhang J, Li D, Wang S, Han J, Zheng XL, Yang Z, Kong D. Endothelialization and patency of RGD-functionalized vascular grafts in a rabbit carotid artery model. Biomaterials 2012;33(10):2880-91

84. Ye L, Wu X, Mu Q, Chen B, Duan Y, Geng X, Gu Y, Zhang A, Zhang J, Feng ZG. Heparin-conjugated PCL scaffolds fabricated by electrospinning and loaded with fibroblast growth factor 2. J Biomater Sci Polym Ed 2011;22(1-3):389-406

85. Ye L, Wu X, Duan HY, Geng X, Chen B, Gu YQ, Zhang AY, Zhang J, Feng ZG. The in vitro and in vivo biocompatibility evaluation of heparin-poly(ε-caprolactone):conjugate for vascular tissue engineering scaffolds. J Biomed Mater Res A 2012;100(12):3251-8

86. Wulf K, Teske M, Löbler M, Luderer F, Schmitz KP, Sternberg K. Surface functionalization of poly(ε-caprolactone):improves its biocompatibility as scaffold material for bioartificial vessel prostheses. J Biomed Mater Res B Appl Biomater 201198(1):89-100

87. Singh S, Wu BM, Dunn JC. The enhancement of VEGF-mediated angiogenesis by polycaprolactone scaffolds with surface cross-linked heparin. Biomaterials 2011;32(8):2059-69

88. Liu L, Guo S, Chang J, Ning C, Dong C, Yan D. Surface modification of polycaprolactone membrane via layer-by-layer deposition for promoting blood compatibility. J Biomed Mater Res B Appl Biomater 2008;87(1):244-50

89. Zhang M, Wang Z, Wang Z, Feng S, Xu H, Zhao Q, Wang S, Fang J, Qiao M; Kong D. Immobilization of anti-CD31 antibody on electrospun poly(ε-caprolactone):scaffolds through hydrophobins for specific adhesion of endothelial cells. Colloids Surf B Biointerfaces 2011;85(1):32-9

90. Thapa A, Webster TJ, Haberstroh KM. Polymers with nano-dimensional surface features enhance bladder smooth muscle cell adhesion. J Biomed Mater Res A 2003;67(4):1374-83

91. Wang S, Lu L, Gruetzmacher JA, Currier BL, Yaszemski MJ. A biodegradable and cross-linkable multiblock copolymer consisting of poly(propylene fumarate):and poly(ε-

caprolactone): synthesis characterization and physical properties. Macromolecules 2005;38 (17):7358-70

92. Wang S, Lu L, Yaszemski MJ. Bone-tissue-engineering material poly(propylene fumarate): correlation between molecular weight chain dimensions and physical properties. Biomacromolecules 2006;7(6):1976-82

93. Temenoff JS, Kasper FK, Mikos AG. Fumarate-based macromers as scaffolds for tissue engineering applications. In Topics in Tissue Engineering; Ashammakhi N Reis RL Chiellini E Eds, Expertissues E-book University of Oulu Oulu Finland 2007; Vol 3 61-616

94. Sabir MI, Xu X, Li L. A review on biodegradable polymeric materials for bone tissue engineering applications. J Mater Sci 2009;44(21):5713-24

95. He S, Timmer MD, Yaszemski MJ, Yasko AW, Engel PS, Mikos AG. Synthesis of biodegradable poly(propylene fumarate):networks with poly(propylene fumarate)-diacrylate macromers as crosslinking agents and characterization of their degradation products. Polymer 2001;42 1251-60

96. Wang K, Cai L, Hao F, Xu X, Cui M, Wang S. Distinct cell responses to substrates consisting of poly(ε-caprolactone):and poly(propylene fumarate):in the presence or absence of cross-links. Biomacromolecules 2010;11(10):2748-59

97. Liu X, Cai L, Hao F, Cui M, Wang S. Biodegradable elastomeric substrates with controllable stiffness for regulating smooth muscle cell behavior. 242nd ACS National Meeting Denver Colorado USA August 28-September 1 2011

98. Liu X, Cai L, Wang S. Smooth muscle cell behavior on poly(ε-caprolactone):triacrylate networks grafted with poly(ethylene glycol). 243rd ACS National Meeting & Exposition San Diego California USA March 25-29 2012

99. Chawla K, Lee S, Lee BP, Dalsin JL, Messersmith PB, Spencer ND. A novel low-friction surface for biomedical applications: modification of poly(dimethylsiloxane):(PDMS):with polyethylene glycol(PEG)-DOPA-lysine. J Biomed Mater Res A 2009;90(3):742-9

100. Zhao H, Feng Y, Guo J. Grafting of poly(ethylene glycol):monoacrylate onto polycarbonateurethane surfaces by ultraviolet radiation grafting polymerization to control hydrophilicity. J Appl Polym Sci 2011;119 3717-27

101. Ko YG, Kim YH, Park KD, Lee HJ, Lee WK, Park HD, Kim SH, Lee GS, Ahn DJ.

Immobilization of poly(ethylene glycol):or its sulfonate onto polymer surfaces by ozone oxidation. Biomaterials 2001;22(15):2115-23

102. Jun HW, West JL. Modification of polyurethaneurea with PEG and YIGSR peptide to enhance endothelialization without platelet adhesion. J Biomed Mater Res Part B: Appl Biomater 2005;72B 131-9

103. Leslie-Barbick JE, Moon JJ, West JL. Covalently-immobilized vascular endothelial growth factor promotes endothelial cell tubulogenesis in poly(ethylene glycol):diacrylate hydrogels. J Biomater Sci Polym Ed 2009;20(12):1763-79

104. Ilagan BG, Amsden BG. Surface modifications of photocrosslinked biodegradable elastomers and their influence on smooth muscle cell adhesion and proliferation. Acta Biomater 2009;5(7):2429-40

105. Beamish JA, Fu AY, Choi AJ, Haq NA, Kottke-Marchant K, Marchant RE. The influence of RGD-bearing hydrogels on the re-expression of contractile vascular smooth muscle cell phenotype. Biomaterials 2009;30(25):4127-35

106. Beamish JA, Geyer LC, Haq-Siddiqi NA, Kottke-Marchant K, Marchant RE. The effects of heparin releasing hydrogels on vascular smooth muscle cell phenotype. Biomaterials 2009;30(31):6286-94

107. Oliviero O, Ventre M, Netti PA. Functional porous hydrogels to study angiogenesis under the effect of controlled release of vascular endothelial growth factor. Acta Biomater 2012;8(9):3294-301

108. Patel D, Vandromme S E, Reid ME, Taite LJ. Synergistic activity of αvβ3 integrins and the elastin binding protein enhance cell-matrix interactions on bioactive hydrogel surfaces. Biomacromolecules 2012;13(5):1420-8

109. Saik JE, Gould DJ, Keswani AH, Dickinson ME, West JL. Biomimetic hydrogels with immobilized ephrinA1 for therapeutic angiogenesis. Biomacromolecules 2011;12(7):2715-22

110. Tanahashi K, Mikos AG. Cell adhesion on poly(propylene fumarate-*co*-ethylene glycol):hydrogels. J Biomed Mater Res 2002;62(4):558-66

111. Tanahashi K, Jo S, Mikos AG. Synthesis and characterization of biodegradable cationic poly(propylene fumarate-*co*-ethylene glycol):copolymer hydrogels modified with

agmatine for enhanced cell adhesion. Biomacromolecules 2002;3(5):1030-7

112. Tanahashi K, Mikos AG. Protein adsorption and smooth muscle cell adhesion on biodegradable agmatine-modified poly(propylene fumarate-*co*-ethylene glycol):hydrogels. J Biomed Mater Res A 2003;67(2):448-57

113. Brown XQ, Bartolak-Suki E, Williams C, Walker ML, Weaver VM, Wong JY. Effect of substrate stiffness and PDGF on the behavior of vascular smooth muscle cells: implications for atherosclerosis. J Cell Physiol 2010;225(1):115-22

114. Zdrahala RJ, Zdrahala IJ. Biomedical applications of polyurethanes: a review of past promises present realities and a vibrant future. J Biomater Appl 1999;14(1):67-90

115. Park BJ, Seo HJ, Kim J, Kim HL, Kim JK, Choi JB, Han I, Hyun SO, Chung KH, Park JC. Cellular responses of vascular endothelial cells on surface modified polyurethane films grafted electrospun PLGA fiber with microwave-induced plasma at atmospheric pressure. Surf Coat Tech 2010;205 S222-6

116. Dubey G, Mequanint K. Conjugation of fibronectin onto three-dimensional porous scaffolds for vascular tissue engineering applications. Acta Biomater 2011;7(3):1114-25

117. Blit PH, Battiston KG, Yang M, Paul Santerre J, Woodhouse KA. Electrospun elastin-like polypeptide enriched polyurethanes and their interactions with vascular smooth muscle cells. Acta Biomater 2012;8(7):2493-503

118. Jiang X, Wang K, Ding M, Li J, Tan H, Wang Z, Fu Q. Quantitative grafting of peptide onto the nontoxic biodegradable waterborne polyurethanes to fabricate peptide modified scaffold for soft tissue engineering. J Mater Sci Mater Med 2011;22(4):819-27

119. Wang H, Feng Y, An B, Zhang W, Sun M, Fang Z, Yuan W, Khan M. Fabrication of PU/PEGMA crosslinked hybrid scaffolds by in situ UV photopolymerization favoring human endothelial cells growth for vascular tissue engineering. J Mater Sci Mater Med 2012;23(6):1499-510

120. Lin S, Sandig M, Mequanint K. Three-dimensional topography of synthetic scaffolds induces elastin synthesis by human coronary artery smooth muscle cells. Tissue Eng Part A 2011;17(11-12):1561-571

121. Sharifpoor S, Labow RS, Santerre JP. Synthesis and characterization of degradable polar hydrophobic ionic polyurethane scaffolds for vascular tissue engineering applications.

Biomacromolecules 2009;10(10):2729-39

122. Jiang X, Yu F, Wang Z, Li J, Tan H, Ding M, Fu Q. Fabrication and characterization of waterborne biodegradable polyurethanes 3-dimensional porous scaffolds for vascular tissue engineering. J Biomater Sci Polym Ed 2010;21(12):1637-52

Chapter II. Regulation of Smooth Muscle Cell Behavior on Biodegradable Network Substrates with Controllable Stiffness

Abstract

Substrates with controllable stiffness have emerged as important models in investigating cell-biomaterial interactions. Most substrates in the literature studies are hydrogels with a limited range of stiffness. Here, I developed a series of biodegradable photo-crosslinked PCLTA substrates with controllable stiffness by simultaneously varying the crosslinking density and crystallinity. I further evaluated the surface characteristics of these polymer substrates, including roughness, hydrophilicity, and capability of adsorbing proteins from cell culture media, and correlated these factors with regulation of primary rat SMC behavior. I found that stiffer substrates of semi-crystalline PCLTA networks induced stronger stress fibers, larger spread area, faster growth, higher motility, better conversion from the synthetic phenotype to the more functional contractile phenotype, and stronger focal adhesions of SMCs. Gene and protein expression was also performed to confirm that SMCs had higher expression levels of contractile gene markers and integrin subunits on the stiffer substrates of semi-crystalline PCLTA networks. As well as serving as model systems for regulating cell fate, these PCLTA networks with excellent tailorability of physicochemical properties have great potential for diverse tissue-engineering applications.

2.1 Introduction

Tissue engineering aims to develop substitutes for restoring normal functions of deficient organs and calls for cooperation of multi-disciplinary principles including materials science, engineering, medicine, and molecular cell biology. In tissue-engineered blood vessel research, it is crucial to develop suitable materials with desired properties for supplying a permissive environment for SMC functions. At the internal cellular level, genes must be activated in a correct order for expression of the proteins needed for cell proliferation, differentiation, and functional development. Meanwhile, extrinsic signals to cells from the surrounding extracellular matrix (ECM) are essential in guiding them through distinct development stages. External signals from the underlying biomaterial substrates are mainly chemical, topological, or mechanical [1]. Among these surface characteristics, substrate stiffness has been reported to create different magnitudes of static tension to cells, which can affect the growth, morphology, and functions of mechanosensitive cells [2,3], such as endothelial cells [4], fibroblasts [5], and SMCs [6-8]. Although many polymeric systems [9-13] have been employed to investigate the role of surface stiffness in regulating cell behaviors, they have limited elastic moduli (< 1 MPa) and thus it is still desirable to achieve model polymers with a wider range of mechanical properties without variance in surface chemistry and morphology.

Unlike weaker hydrogels, biodegradable hydrophobic polymer networks with controllable mechanical properties have been developed from multi-block copolymers of poly(propylene fumarate) (PPF) and poly(ε-caprolactone) (PCL) [14], PCL fumarate (PCLF) [15], PCL diacrylate (PCLDA), and their blends with PPF [16]. Distinct cell behaviors have been found in response to substrate stiffness, although other surface characteristics might also be involved [16-19]. In this study, I synthesized a series of photo-crosslinkable PCL triacrylates (PCLTAs) with six molecular weights from 2,000 to 20,000 g/mol (Fig. 2.1a) and crosslinked them into networks with high gel fractions and efficiently tunable mechanical properties through simultaneously controlling the crosslinking density and crystallinity. These PCLTAs can be molded into any desired shape and cured via UV initiation for diverse tissue engineering applications [20,21].

Cardiovascular disease is the number one killer in the U.S. [22]. Vascular tissue engineering

holds enormous potential by providing synthetic materials as vessel replacements. When SMCs are isolated and cultured out of a healthy body, they quickly revert from the contractile phenotype to the synthetic phenotype [23]. This transition is influenced in culture by ECM composition, soluble factors, and mechanical stress. Contractile SMCs in normal blood vessels are spindle-shaped with a prominent centrally located nucleus and proliferate at an extremely low rate but are suitable for contraction [23]. In contrast, SMCs with the synthetic phenotype do not have the contractile function and assume a morphology similar to fibroblasts, but they are more mobile and proliferative. It has been reported that the proliferation was faster, the projecting area was larger, and the focal adhesions (FAs) and stress fibers were more prominent for SMCs cultured on stiffer polymer substrates [6,24]. Here, I focus on the role of crystallite-strengthened substrate stiffness in influencing rat aortic SMC adhesion, spreading, migration, proliferation, and genetic and protein levels of the phenotypic marker expression using photo-crosslinked PCLTAs with a wide range of higher tensile moduli (*E*) from1.6 to 194 MPa, which demonstrated a non-monotonic dependence on the molecular weight of PCLTA.

2.2 Materials and Methods

2.2.1 Synthesis of PCLTAs and characterization

PCL triols were synthesized via the ring-opening polymerization of ε-caprolactone in the presence of initiator, trimethylolpropane (TMP), and catalyst, $Sn(Oct)_2$. To synthesize PCLTA, PCL triol, acryloyl chloride, and K_2CO_3 were measured at a molar ratio of 1:3:3. Acryloyl chloride dissolved in methylene chloride (1:10 v/v) was added dropwise into the slurry of PCL triol/K_2CO_3 in methylene chloride. After reaction at room temperature under nitrogen for 24 h, the mixture was filtered to remove the solids and then precipitated in diethyl ether. The molecular weights of PCL triols and PCLTAs were determined using Gel Permeation Chromatography (GPC; PL-GPC 20, Polymer Laboratories) at room temperature. Tetrahydrofuran (THF) was used as the eluent and standard monodisperse polystyrene samples (Polymer Laboratories) were used for calibration. Differential Scanning Calorimetric (DSC) measurements were performed by heating the polymer samples from room temperature to 100 ℃, cooling to −80 ℃ then heating from −80 to 100 ℃ at a rate of 10 ℃ min^{-1}.

2.2.2 Photo-crosslinking and characterization

Photo-initiator, phenyl bis(2,4,6-trimethyl benzoyl) phosphine oxide (BAPO, IRGACURE 819, Ciba Specialty Chemicals, Tarrytown, NY) was used in photo-crosslinking. Homogeneous PCLTA/BAPO/CH_2Cl_2 mixture was transferred into a Teflon mold composed of two glass plates and a Teflon spacer, and then placed under a high-intensity long-wave UV lamp (SB-100P, λ = 365 nm, Intensity: 4800 $\mu w/cm^2$) for 20 min. Crosslinked PCLTA sheets (10 × 0.5 mm, diameter × thickness) were soaked in acetone for two days to remove the residue of BAPO and the sol fraction, dried in vacuum, compressed between two glass plates to smoothen the semi-crystalline samples. Then the samples were sterilized in 70% alcohol solution and dried completely in vacuum. The gel fraction and swelling ratio of crosslinked PCLTA disks were determined in CH_2Cl_2 [11,17]. Linear viscoelastic properties of uncrosslinked and crosslinked PCLTAs were measured on a strain-controlled rheometer (RDS-2, Rheometric Scientific) at 37 and 60 ℃. The tensile properties of crosslinked PCLTAs (0.5 × 2.0 × 10 mm, thickness × width × length) were implemented using a dynamic mechanical analyzer (DMTA-5, Rheometric Scientific) at 37 ℃. Surface morphology of crosslinked PCLTA disks was characterized using a multimode atomic force microscopy (AFM) and the root-mean-square (rms) roughness was calculated from the height images. Water contact angles were determined at 37 ℃ using a Ramé-Hart NRC C. A. goniometer (Model 100-00-230, Mountain Lakes, NJ). Protein adsorption was determined using a micro-plate reader (SpectraMax Plus 384, Molecular Devices, Sunnyvale, CA) and MicroBCA protein assay kit (Pierce, Rockford, IL).

2.2.3 In vitro cell attachment and proliferation

Primary SMCs isolated from rat aorta were seeded onto crosslinked PCLTA disks (10 × 0.5 mm, diameter × thickness) at a density of 2 × 10^4 cells per cm^2 using TCPS as the positive control. SMC numbers at 4 h, days 1, 2, and 4 post-seeding were calculated based on the absorption values of MTS assay (CellTiter 96 Aqueous One Solution, Promega, Madison, WI) and a standard curve constructed using five known cell numbers of 5, 10, 15, 20, and 25 × 10^3 per well at 4 h post-seeding. The proliferation index (PI) of SMCs was calculated by dividing the cell number at day 4 by the initial number of attached cells at day 1. The growth rate and doubling time of SMCs were calculated using ln(PI)/3 and ln2/growth rate, respectively.

Attached SMCs on crosslinked PCLTA substrates were fixed in 4% paraformaldehyde (PFA) solution, permeabilised with 0.2% Triton X-100, and then stained using rhodamine-phalloidin for 1 h at 37 ℃ and DAPI at room temperature for photographing on an Axiovert 25 light microscope (Carl Zeiss, Germany). Using ImageJ software (National Institutes of Health, Bethesda, MD), cell area was determined and averaged on 20 non-overlapping cells at day 1.

2.2.4 Characterization of focal adhesions

SMCs cultured for 24 h were washed in PBS, fixed in 4% PFA solution, and permeabilised with 0.2% Triton X-100 for 5 min at room temperature. To reduce the background signal, samples were incubated in 1% BSA/PBS at 37 ℃ for 30 min then in monoclonal mouse antibody against vinculin (1:1000 in 1% BSA/PBS; Sigma) at room temperature for 1 h, and washed with PBS three times for 5 min each. Then the samples were cultured with goat anti-mouse IgG secondary antibody (1:200 in 1% BSA/PBS; Sigma) at room temperature for 1 h. Filaments of SMCs were stained using rhodamine-phalloidin for 1 h at 37 ℃ before photographing on a Leica DM6000B fluorescent confocal microscope. The area, density, and circularity of focal adhesions were determined and averaged on 20 non-overlapping cells using ImageJ.

2.2.5 Single cell motility and cell invasion migration assay

SMCs were incubated with fluorescent Calcein dye (Calcein AM, Invitrogen) at a concentration of 4 μM for 30 min and then transferred into transparent wells in a flow chamber at 37 ℃. Cell migration was monitored by tracking cells at the same location every 20 min using a camera and the velocity of cell migration was analyzed using ImageJ. The migration vector of the cell generated from two subsequent images was presented as a dot in an XY-diagram and characterized by its migration direction and distance. In cell monolayer migration study, cell seeding density on PCLTAs was adjusted by their attachment rates to ensure the same number of SMCs attached on each sample. A Teflon tip was placed gently onto the disk surface. After SMCs attached and proliferated for 24 h to form a monolayer, the Teflon tip was removed to allow cell migration into the blank area for one day before SMCs were fixed and stained with hematoxylin and eosin (Sigma-Aldrich, St. Louis, MO). For each image, the maximal migration distance was determined and averaged at five locations.

2.2.6 Gene expression analysis of phenotypic markers and integrins

Total RNA was isolated from SMCs cultured for 3 days using RNeasy Mini Kit (Qiagen, Valencia, CA) and then cDNA was obtained using DyNAmo cDNA synthesis kit (Thermo Scientific). Real-time PCR primers (Table 2.2) were designed using the Oligoperfect software (Invitrogen) and the reaction was conducted in 25 μL of a PCR mixture of cDNA samples and Power SYBR Green PCR Master Mix (Applied Biosystems, Carlsbad, CA). An appropriate amplification PCR protocol was set to 5 min at 95 °C followed by the same steps of 30 s at 95 °C, 30 s at 55 °C, and 30 s at 72 °C using the thermal cycler with fluorescence detection systems (PTC-200, MJ Research, Watham, MA). The expression of target genes was normalized to that of the house-keeping gene, glyceraldehyde 3-phosphate dehydrogenase (GAPDH). RT-PCR amplification was performed on a Peltier Thermo cycler (PTC-200, MJ Research) using specific RT-PCR primers (Table 2.3). The same thermal condition mentioned above was applied but the cycles for different genes varied according to their expression levels. Upon completion of the reaction, DNA products were electrophoresed in 1.5% agarose gel containing Gelgreen (Biotium, Hayward, CA) and visualized using an EpiChemi II darkroom imaging system (UVP, Upland, CA). For integrin expression, mRNA was isolated from SMCs cultured for 1 day and the real-time PCR procedure was similar to described above using integrin specific primers (Table 2.4).

Table 2.1 Molecular weight and thermal properties of uncrosslinked and crosslinked PCLTAs

Polymer	M_n (g mol^{-1})	M_w (g mol^{-1})	DPI	Thermal Properties		
				T_m (^oC)	ΔH_m (J/g)	χ_c (%)
PCLTA2k	2220	2990	1.3	21.3	21.2	15.7
PCLTA5k	5600	6520	1.2	27.2 38.1	61.6	45.6
PCLTA7k	6680	8490	1.3	34.8 43.4	66.2	49.0
PCLTA8k	8456	9983	1.2	45.2 49.5	65.0	48.1
PCLTA10k	9750	12310	1.3	45.1 50.9	66.8	49.5
PCLTA20k	20020	22670	1.1	52.4 54.6	65.4	48.4
Crosslinked PCLTA2k					0	0.0
Crosslinked PCLTA5k				13.8	3.3	2.4
Crosslinked PCLTA7k				22.9	24.6	18.3
Crosslinked PCLTA8k				40.08	39.0	28.9
Crosslinked PCLTA10k				44.7	44.5	32.9
Crosslinked PCLTA20k				50.4	56.7	42.0

Table 2.2 Primers for phenotypic makers in real-time PCR analysis

Gene	Primer sequence (5′ to 3′)	Length	% GC content	Tm (°C)	Product Size
NM-MHC	Forward GGATTGGCAGGTCTCTCTATCAG	23	52.2	64.6	220
	Reverse ATTGGGATCCTGGATATTGCT	21	42.9	58.7	
Calponin	Forward AGTCTACTCTCTTGGCTCTGGCC	23	56.52	57.3	122
	Reverse CCTGCCTTCTCTCAGCTTCTCAGG	24	58.33	58.5	
SM-M HC	Forward AAGCAGCTCAAGAGGCAG	18	55.6	59.9	178
	Reverse AAGGAACAAATGAAGCCTCGTT	22	40.9	58.9	
Transgelin (SM-22)	Forward GGCAGCTGAGGATTATGGAGTCACG	25	56.00	59.2	152
	Reverse TGGGATCTCCACGGTAGTGTCCA	23	56.52	58.6	
Smoothelin	Forward TCGGAGTGCTGGTGAATAC	19	52.6	60.2	197
	Reverse CCCTGTTTCTCTTCCTCTGG	20	55	62.4	
GAPDH	Forward TCTTCACCACCATGGAGAA	19	47.4	58	232
	Reverse ACTGTGGTCATGAGCCCTT	19	52.6	60.2	

Table 2.3 Reverse Transcription PCR primers for phenotypic markers

Gene	Primer sequence (5′ to 3′)	Length	% GC content	Tm (°C)	Product Size
NM-MHC	Forward GGATTGGCAGGTCTCTCTATCAG	23	52.2	64.6	220
	Reverse ATTGGGATCCTGGATATTGCT	21	42.9	58.7	
Calponin	Forward ACAAAAGGAAACAAAGTCAAT	21	28.6	52.8	375
	Reverse GGGCAGCCCATACACCGTCAT	21	61.9	66.5	
SM-M HC	Forward AAGCAGCTCAAGAGGCAG	18	55.6	59.9	178
	Reverse AAGGAACAAATGAAGCCTCGTT	22	40.9	58.9	
Transgelin (SM-22)	Forward TGTTCCAGACTGTTGACCTC	20	50	60.4	368
	Reverse GTGATACCTCAAAGCTGTCC	20	50	60.4	
smoothelin	Forward TCGGAGTGCTGGTGAATAC	19	52.6	60.2	197
	Reverse CCCTGTTTCTCTTCCTCTGG	20	55	62.4	
GAPDH	Forward TCTTCACCACCATGGAGAA	19	47.4	58	232
	Reverse ACTGTGGTCATGAGCCCTT	19	52.6	60.2	

Table 2.4 Real-time PCR primers for integrins

Integrin	Forward primer	Reverse primer
Integrin-av	5’-AAGACGCCCGAAAAGAATGAC-3’	5’-ATCCCGCTTGGTGATGAGAT-3’
Integrin-a1	5’-TCTGCCAAACTCAGTCCACGA-3’	5’-TGACGATCAGCAGGCTCTTTT-3’
Integrin-a5	5-’CCTTCCTTCATTGGCATGGA-3’	5-’TCTGCATCCTGTCAGCAATCC-3’
Integrin-b1	5’-AGAGTGCCGTGACAACTGTG-3’	5’-GAGCCCCAAAGCTACCCTAC-3’
Integrin-b2	5’-AGTCCCAGTGGAACAACGAC-3’	5’-AGCACTGGGGCTAGCTGTAA-3’
Integrin-b3	5’-GACCCGCTTCAATGACGAA-3’	5’-TCACAGACTGTAGCCTGCATGA-3’

2.2.6 Western blot

Total cellular proteins were obtained from SMCs cultured for 3 days on crosslinked PCLTA substrates. Briefly, proteins were extracted from the cell lysates in an ice-cold Radio-Immunoprecipitation Assay (RIPA) buffer that contained protease inhibitors. The same amount of protein for each sample was separated by sodium dodecyl sulfate polyacrylamide gel

electrophoresis (SDS-PAGE), and transferred to a polyvinylidene fluoride (PVDF) membrane (Immobilon-P, Millipore). Calponin and GAPDH protein were identified by using anti-calponin and anti-GAPDH primary antibodies (final concentration, 2 μg mL^{-1}; Santa Cruz) followed by a peroxidase-labeled anti-mouse secondary antibody (final concentration, 0.08 μg mL^{-1}). Specific protein bands were visualized using ECL-Plus (GE Healthcare, Piscataway, NJ) by exposure for 1 to 3 min with enhanced chemiluminescence.

2.3 Results and Discussion

2.3.1 Photo-crosslinked PCLTA with controllable stiffness

PCLTAs with number-average molecular weights (M_ns) of 2220, 5600, 6680, 8460, 9750, and 20020 g mol^{-1} were named as PCLTA2k, 5k, 7k, 8k, 10k, and 20k, respectively (Table 2.1). As illustrated in Fig. 2.1b, the stiffness of crosslinked PCLTA can be controlled efficiently through the molecular weight, which determines both the crosslinking density and crystallinity. In methylene chloride, crosslinked PCLTAs showed increasing swelling ratio from 2.2 ± 0.3 to 12.9 ± 0.3 when M_n increased from 2k to 20k. While in water or PBS, the original shape of all the six crosslinked PCLTAs remained, assuring their potential applications as polymer scaffolds in *in vivo* implantation. The gel fractions of all the samples were ~0.9 to ensure sample integrity with smooth surfaces after the sol fraction was removed through purification in acetone. As demonstrated in the DSC curves (Fig. 2.1c; Table 2.1), the six PCLTA samples were all semi-crystalline with T_m values of 33.7, 38.1, 43.4, 45.2, 50.9, and 52.4 ℃, respectively.

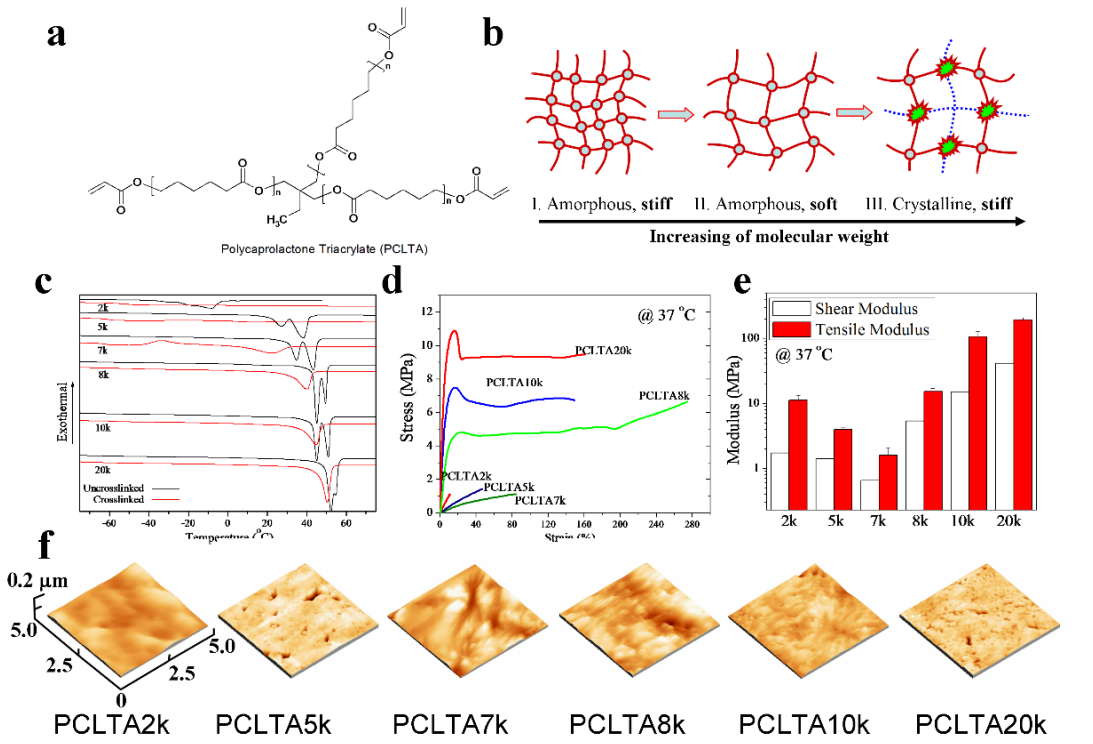

Figure 2.1 Photo-crosslinkable PCLTA with controllable thermal and mechanical properties. a, Chemical structure of PCLTA. b, Schematic change in crystallinity and stiffness of crosslinked PCLTA when the molecular weight increases. c, DSC curves of uncrosslinked and crosslinked PCLTAs. d, Tensile strain-stress curves of crosslinked PCLTAs at 37 ℃. e, The elastic moduli and shear moduli of the crosslinked PCLTAs at 37 ℃. f, AFM images of crosslinked PCLTAs in a scanning scope of 5 × 5 μm.

Because the crosslinks in PCL networks strongly restricted the crystallization of PCL segments[15], crosslinked PCLTAs had significantly suppressed crystallinity and T_m. PCLTA2k with the lowest crystallinity and T_m even became completely amorphous after crosslinking. Crosslinked PCLTA5k, 7k, 8k, 10k, and 20k showed decreased T_m values of 13.8, 22.9, 40.1, 44.7 and 50.4 °C (Fig. 2.1c; Table 2.1), indicating that the former two were amorphous while the latter three were still semi-crystalline at body temperature. The large, controllable differences in crystallinity and T_m in these polymer networks resulted in their distinct mechanical properties at 37 °C, as shown in the stress-strain curves in Fig. 2.1d. The three amorphous PCLTA networks that were not enhanced by the crystallites were weak and broke at a low stress and a low strain while the three semi-crystalline PCLTA networks were strong and

tough, showing yielding and necking phenomenon before they broke at a high stress and a high strain. The modulus for amorphous PCLTA networks was inversely proportional to the molecular weight M_c between two neighboring crosslinks. Given the same architecture for PCLTAs, M_c was proportional to M_n. Thus *E* decreased from 11.2 ± 2.2 to 4.0 ± 0.2 and 1.6 ± 0.5 MPa and the shear modulus (*G*) decreased from 1.72 to 1.42 and 0.65 MPa when the M_n of PCLTA increased from 2k to 5k and 7k, respectively (Fig. 2.1e). Similar to previous findings on crosslinked PCLF and PCLDA [16,17], crystallites formed a physical network to strengthen the chemical network in crosslinked PCLTA8k, 10k, and 20k. This effect was more prominent when the crystallinity was higher for a higher PCLTA molecular weight although the crosslinking density was lower (Fig. 2.1b). Among all the six samples, the most crystalline crosslinked PCLTA20k had the highest *E* and *G* values of 194 ± 16 and 41.1 MPa, respectively (Fig. 2.1e). For the three amorphous crosslinked PCLTAs, the strains at break increased from 7.5 ± 3.0% for crosslinked PCLTA 2k to 51.3 ± 4.5% for crosslinked PCLTA 7k and 97.4 ± 13.3% for crosslinked PCLTA 8k. In contrast, the values for semi-crystalline crosslinked PCLTAs were much higher and decreased from 275.7 ± 14.7% for crosslinked PCLTA 8k to 176.8 ± 55.0% for crosslinked PCLTA 10k and 169.7 ±103.2% for crosslinked PCLTA 20k.

Crosslinked PCLTA disks were compressed to achieve smooth surfaces before I characterized their surface morphology, hydrophilicity, and protein adsorption. AFM images in Fig. 2.1f showed no obvious differences in surface morphology and root-mean-square roughness (R_{rms}) was less than 10 nm for all these samples. The water contact angles on the three amorphous crosslinked PCLTAs were similar (~62.5 ± 1.0°) while they were higher on the three semi-crystalline crosslinked PCLTAs with values of 69.2 ± 1.5°, 77.7 ± 0.8°, and 77.8 ± 0.8° for 8k, 10k, and 20k, respectively. The result that a more crystalline polymer network had a higher hydrophobicity was in agreement with earlier reports on crosslinked PCLFs and PCLDAs with different crystallinities [17]. Compared with semi-crystalline crosslinked PCLTAs, less hydrophobic amorphous crosslinked PCLTAs adsorbed more serum proteins and fibronectin [25].

2.3.2 Regulation of SMC adhesion, spreading, and proliferation

Consistent with previous studies on different cell types [2,5,26-28], stiffer substrates of crosslinked PCLTAs better supported attachment of SMCs without showing cytotoxicity in the culture period. Stronger stress fibers and larger spread areas were observed for SMCs cultured on stiffer substrates of crosslinked PCLTAs for 8 and 24 h, as demonstrated in cell images (Fig. 2.2b). The dependence of the normalized number of attached SMCs at 4 h and the cell area at day 1 on the M_n of PCLTA followed the same trend as that in modulus, i.e., they decreased slightly on the amorphous substrates while increased significantly on the semi-crystalline ones when the M_n of PCLTA increased (Fig. 2.2c,d). The SMC numbers at days 1, 2, and 4 determined using the MTS assay (Fig. 2.2e) are consistent with the cell images by showing the same dependence on the substrate stiffness. The proliferation index (PI) of SMCs (Fig. 2.2f) increased from 2.4 ± 0.3 on the amorphous substrates to 2.7 ± 0.3 on the semi-crystalline ones while the corresponding doubling time decreased from 2.4 to 2.1 days.

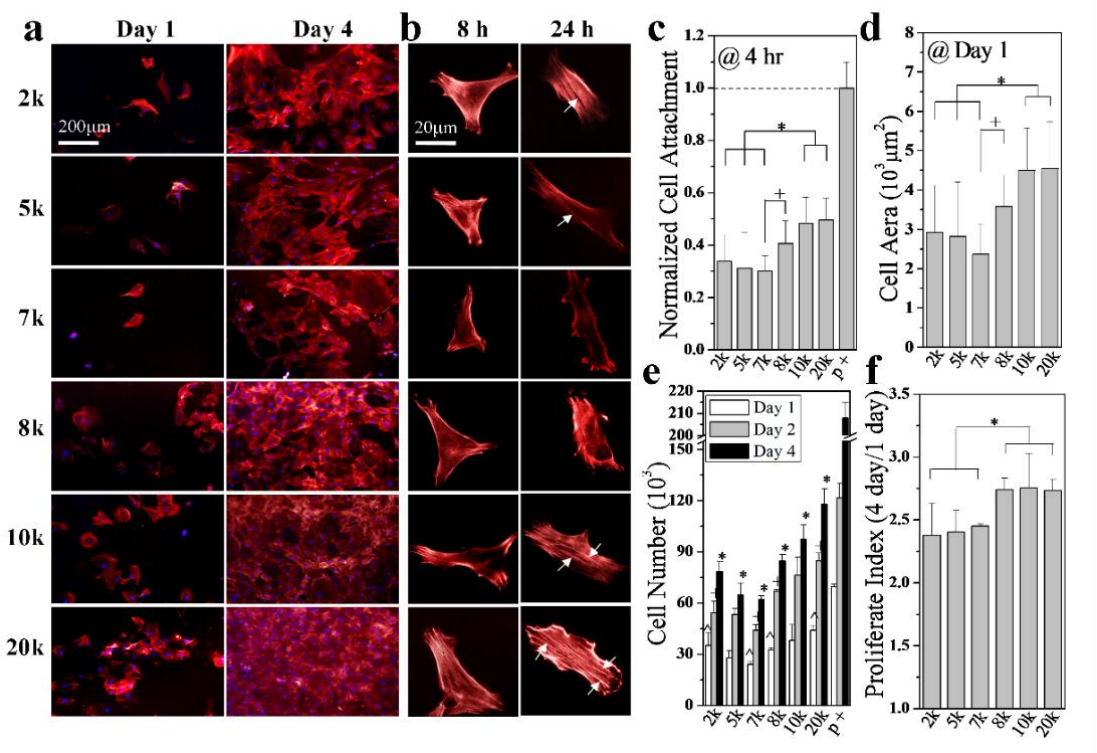

Figure 2.2 SMC behaviors on crosslinked PCLTAs. a, Fluorescent images of SMCs on crosslinked PCLTAs at days 1 and 4 post-seeding. Stained with rodamine-phalloidin (red) and DAPI (blue). b, Fluorescent images of SMCs to show filaments density and magnitude. The arrows point to the typical filaments in SMCs on stiff crosslinked PCLTAs. c, SMC had better attachment on stiffer substrates. d, SMC had significant larger projecting cell area ($p < 0.001$) on crosslinked PCLTA10k and 20k ($E > 100$ MPa) comparing to amorphous crosslinked PCLTA2k, 5k and 7k. For 7k and 8k, obvious difference also can be seen in cell area ($p < 0.01$). e, SMC number at days 1, 2, and 4 post-seeding using TCPS as positive control. The cell number pattern was quite consistent with the substrate stiffness trend. f, Proliferation Index of SMCs on crosslinked PCLTAs. +,^,* $p < 0.05$ between any two samples.

2.3.3 Distinct focal adhesion and integrin expression

Focal adhesions (FAs) are complicated, dynamic protein complexes consisting of >100 proteins through which the internal cytoskeleton of a cell connects to the ECM. FAs with functional diversity serve as the anchorage of a cell and signal carriers to report the ECM condition to cell nucleus and the feedback in turn affects the cell behavior. I characterized FAs of SMCs on three representative substrates of crosslinked PCLTA2k, 7k, and 20k at day 1 using confocal microscopy (Fig. 2.3a,b). The FA area on crosslinked PCLTA2k was larger than that on softer crosslinked PCLTA7k but lower than that on stiffer crosslinked PCLTA20k. The elongation of FAs, which is the inverse of circularity [6], was also significantly higher on crosslinked PCLTA20k compared with the softest crosslinked PCLTA7k. SMCs on crosslinked PCLTA20k also showed the highest FA number per cell, i.e., FA density, while those on crosslinked PCLTA7k showed the lowest. Because FAs are the direct contactors between ECM and cell body, they were the primary component in sensing ECM stiffness and transducing signals to cells through internal signal pathways.

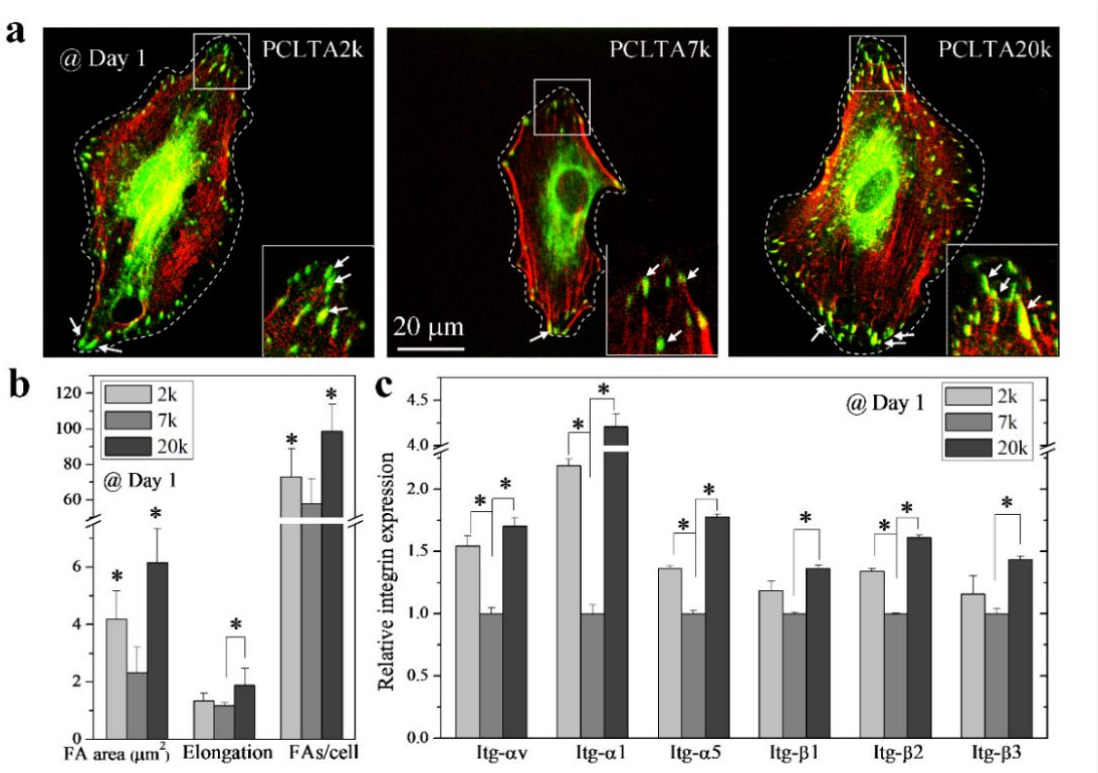

Figure 2.3 Focal adhesion characterization and integrin expression analysis. a, Confocal microscope images of SMC filaments and vinculin antibody stained focal adhesions. Comparing to soft crosslinked PCLTA7k, SMCs on stiffer crosslinked PCLTA20k have larger cell area, more focal adhesions per cell and larger average size for focal adhesions (the arrow points to the typical focal adhesions for SMC on each PCLTA). b, SMCs on crosslinked PCLTA20k have statistically higher value ($p < 0.01$) than crosslinked PCLTA7k in FA area, elongation and density. c, The relative expression of integrin α and β subunits using GAPDH as reference. There are significant higher expressions for the six α and β subunits in SMCs on stiffer crosslinked PCLTA20k than soft 7k ($p < 0.013$, 0.010, 0.017, 0.043, 0.020, and 0.040 for intergin α_v, α_1, α_5, β_1, β_2, and β_3, respectively). Differences also displayed between crosslinked PCLTA2k and 7k for α_v, α_1, α_5, and β_2 subunits ($p = 0.025$, 0.047, 0.002, and 0.041, respectively). * $p < 0.05$ between any two samples.

The interactions between FAs and ECM involve integrins, which are heterodimers of α and β subunits. Integrins cross through cell membrane and bind cytoskeleton with different ECM proteins such as talin, α-actinin, filamin and vinculin using their external end. This integrin-adapter protein-cytoskeleton complex is the basis of FA. I analyzed the integrin expression levels of SMCs on crosslinked PCLTAs at day 1 using real-time polymerase chain reaction (PCR) (Fig. 2.3c). Significantly higher expression ($p < 0.05$) levels of α_v, α_1, α_5, and β_2 subunits were found on crosslinked PCLTA2k and 20k relative to those on the softest crosslinked PCLTA7k. Higher expression ($p < 0.05$) levels of β_1 and β_3 subunits were observed on the stiffest crosslinked PCLTA20k compared to the softest crosslinked PCLTA7k by factors of 1.36 ± 0.03 and 1.43 ± 0.03, respectively. The combinations of these six integrin subunits, such as $\alpha_v\beta_3$, $\alpha_1\beta_1$, $\alpha_1\beta_3$, $\alpha_5\beta_1$, are of high importance in cell signaling, proliferation, spreading, and motility. The dependence of the integrin expression levels on the molecular weight of PCLTA was consistent with that of substrate stiffness, suggesting that integrins play an indispensable role in SMC mechanotransduction.

2.3.4 Promoted SMC migration on stiff PCLTA substrates

The mechanism for cell migration is closely related to the forces generated by FAs on the substrate [29]. For a steadily moving cell, the adhesion force is correlated to the cell-substrate viscous interaction, which is assumed to increase linearly with substrate rigidity [30]. In this study, single cell migration on six crosslinked PCLTAs showed a positive correlation between the speed of cell motility and the stiffness of the underlying substrate (Fig. 2.4a). The highest migration speed of 0.28 ± 0.11 μm min^{-1} was observed on the stiffest crosslinked PCLTA20k and the lowest speed of 0.17 ± 0.09 μm min^{-1} was on the softest crosslinked PCLTA7k (Fig. 2.4b). In agreement with the single cell motility, after scratch formation, the migration distance of SMC invasion (Fig. 2.4c,d) at day 1 reached the highest value of 267.4 ± 5.3 μm on crosslinked PCLTA20k. This value was more than two folds of the lowest value of 110.4 ± 8.2 μm on crosslinked PCLTA7k. The parabolic dependence of SMC migration on the PCLTA molecular weight suggested that SMC migration favored stiffer substrates in the studied stiffness range.

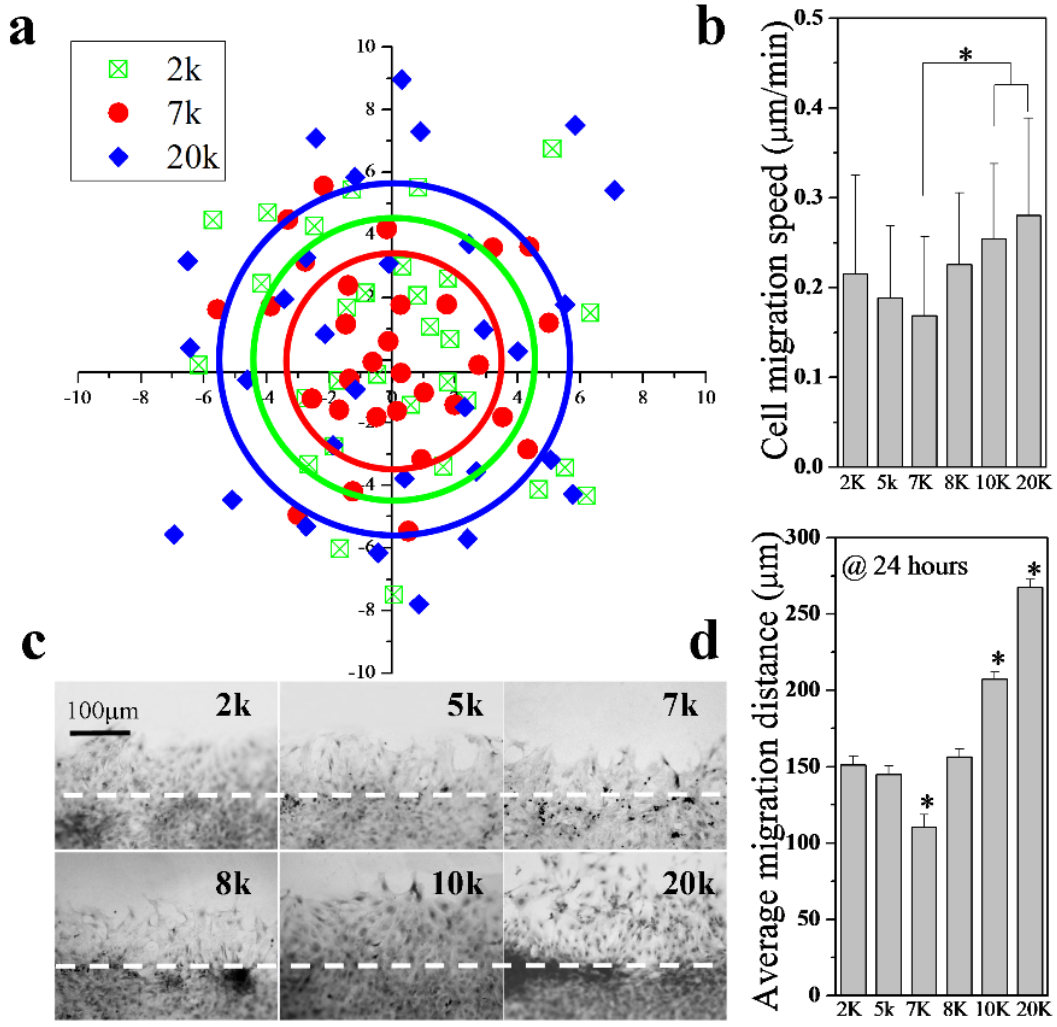

Figure 2.4 SMC migration on crosslinked PCLTAs. a, Single SMC motility pattern in an interval of 20 min. The migration vector, i.e., direction and length, of the cells was expressed as a dot in the XY-diagram. b, Cell migration speed obtained from (a) on crosslinked PCLTAs. Higher single cell motility ($p < 0.001$) speed is found on stiffer crosslinked PCLTA10k and 20k substrate ($E > 100$ MPa). c, Wound healing of SMC migration images at day 1 after scratch formation. d, Average migration distance measured from (c) on crosslinked PCLTAs. SMC layer invasion distances on crosslinked PCLTA7k were significant smaller than the other stiffer substrates ($p < 0.01$). SMCs on stiffest crosslinked PCLTA20k show the highest migration distance during the 1 day interval. * $p < 0.05$ between any two samples.

2.3.5 Controllable SMC conversion to functional contractile phenotype

I performed real-time PCR study on SMCs cultured on crosslinked PCLTA sheets for 3 days and analyzed the mRNA expression level of Non-muscle Myosin Heavy Chain (NM-MHC), a typical synthetic marker gene for SMCs. The expression level of NM-MHC was lower on stiffer substrates no matter in the amorphous or semi-crystalline groups (Fig. 2.5a,b), consistent with a previous study on phenotype modulation of SMCs on polyelectrolyte layers with different stiffnesses [31]. Contrary to the trend in the stiffness of crosslinked PCLTA when its M_n increased from 2k to 20k, the NM-MHC expression level first increased and then decreased. There was a larger portion of synthetic SMCs on the softer crosslinked PCLTAs compared with the stiffer ones, implying that conversion from the proliferative synthetic phenotype to the functional contractile phenotype was better supported by stiffer substrates. The expression level of NM-MHC on the semi-crystalline substrate was slightly higher than that on the amorphous one with a similar stiffness. This trend agreed with the SMC proliferation discussed above as fast growth of SMCs is related to elevated expression of the synthetic gene marker, which occurs during vascular development and involves a function of actin-myosin force generation [23].

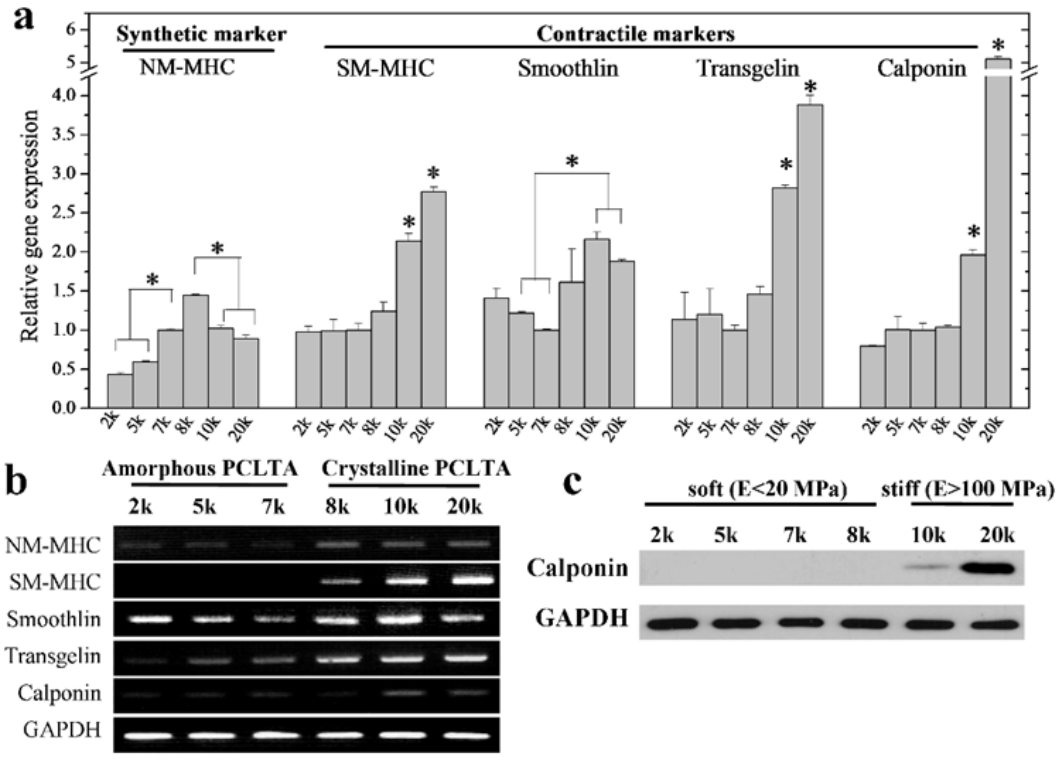

Figure 2.5 Gene and protein expression of SMCs on crosslinked PCLTAs. a, Real-time PCR gene expression of synthetic marker NM-MHC and contractile markers SM-MHC, smoothlin, trangelin and calponin using GAPDH as the reference and normalized to the expression in SMCs on crosslinked PCLTA7k, the softest substrates among all crosslinked PCLTAs. b, RT-PCR results also demonstrated significant higher contractile marker expression on stiff crystalline substrates. c, Western Blot showed there are much more calponin protein content in SMCs on stiffer crosslinked PCLTA 20k than 10k revealed by the band intensity. No obvious calponin protein content is for the soft PCLTAs (E < 20Mpa).* $p < 0.05$ between any two samples.

For four typical contractile gene markers, i.e., Smooth-muscle Myosin Heavy Chain (SM-MHC), smoothlin, transgelin, and calponin, their expression levels were substantially higher on semi-crystalline crosslinked PCLTA10k and 20k with E larger than 100 MPa, in contrast to the other four substrates with E lower than 20 MPa (Fig. 2.5a,b). To examine whether such upregulation of contractile gene expression was caused by the crystalline characteristics instead of solely surface stiffness, I compared the contractile marker expression of SMCs on semi-crystalline crosslinked PCLTA8k (E = 15.4 MPa) and amorphous crosslinked PCLTA2k (E =

11.2 MPa). Except in SM-MHC, no significant differences were found in the major markers on the different substrates with a similar stiffness. The expression levels of these four contractile markers were not significantly different among the substrates of crosslinked PCLTA2-8k with *E* in a narrow range of 1-20 MPa. When *E* increased to 106 MPa for crosslinked PCLTA10k, significantly higher ($p < 0.05$) expression levels were observed. The expression levels reached maxima for SM-MHC, transgelin, and calponin on crosslinked PCLTA20k (*E* = 194 MPa), which were 9.98, 2.20, and 2.77 times as much as those on the softest substrate of crosslinked PCLTA7k (*E* = 1.6 MPa). Consistent with real-time PCR analysis, reverse transcriptase-PCR (RT-PCR) results (Fig. 2.5b) further confirmed that larger contents of contractile markers, indicated by the higher band intensities, in SMCs cultured on the stiffer substrates of semi-crystalline crosslinked PCLTA10k and 20k. These results indicated that stiffer substrates could support a larger portion of functional contractile phenotype and conversion from the proliferative synthetic phenotype.

Smooth muscle basic calponin is a calcium-binding protein with a molecular weight of 32,000-36,000 g mol^{-1} to regulate the myosin ATPase activity in smooth muscle, also a signaling scaffold protein for ERK and PKC pathways [32]. In SMCs, calponin is also involved in force generation in the process of muscle fiber preparation and cell movement [33,34]. In this study, little calponin was detected in the SMCs cultured on the more compliant crosslinked PCLTAs (*E* < 20 MPa) but the expression level increased greatly when the substrates were crosslinked PCLTA10k and 20k. In the western blot result (Fig. 2.5c), calponin was not detected in SMCs on crosslinked PCLTA substrates with *E* < 20 MPa, although the exposure time was extended to 2 h. In contrast, there were obvious calponin contents in the cells on crosslinked PCLTA10k and 20k, and moreover, the band intensity was significantly higher on crosslinked PCLTA20k. The upregulated expression of contractile markers on the stiffer substrates at the both levels of mRNA and protein indicated that crystallite-strengthened polymer substrates could be more favorable for contractile phenotype and functions of SMCs.

2.3.6 Molecular mechanism model of stiffness on SMC behavior

I propose a molecular mechanism model (Fig. 2.6) for interpreting the observed better SMC adhesion, proliferation, migration and higher contractile marker expression on the stiffer substrates of semi-crystalline crosslinked PCLTAs. SMCs on stiffer substrates were reported to have higher focal adhesion kinase (FAK) phosphorylation, which further induces stronger stress fibers through the merlin and ezrin/radixin/moezin (MERM) family of cytoskeletal linkers [35,36]. Large amount and robust reorganization activity of F-actin facilitate formation of FAs and migration of SMCs. Increased assembly of F-actin stress fibers and FAs with increasing substrate stiffness found here could be correlated to complicated biological signal transductions [36]. The mechanical properties of ECM govern SMC migration speed mainly through regulating the activity of Ras homolog gene family, member A (RhoA) [8,37], which is a small GTPase protein known to regulate the signal transduction pathway linking membrane receptors to the assembly of FAs and actin stress fibers.

Cells interact with the substrate through FAs, where integrins cluster and bind to the matrix. SMCs could sense the substrate stiffness through the response to the integrin activity and density on the membrane [38]. Integrin activation and engagement enhanced by higher substrate stiffness are essential for the formation and stabilization of organized lipid membrane microdomains, which promote the efficiency of platelet-derived growth factor-β (PDGFR-β) signals [24]. PDGFR-β has links to cytoskeleton and FAs through the adapter Na^+/H^+ exchanger regulatory factor (NHERF), MERM, and FAK [36]. For SMCs attached to a soft substrate, there lacks sufficient force to generate high-level integrin activation and organize membrane domain lipid rafts, consequently PDGFR activation is weak. In contrast, PDGFR-β signaling is stronger on stiffer substrates as more activated PDGFRs and their downstream effectors are recruited to the membrane domain lipid rafts [24].

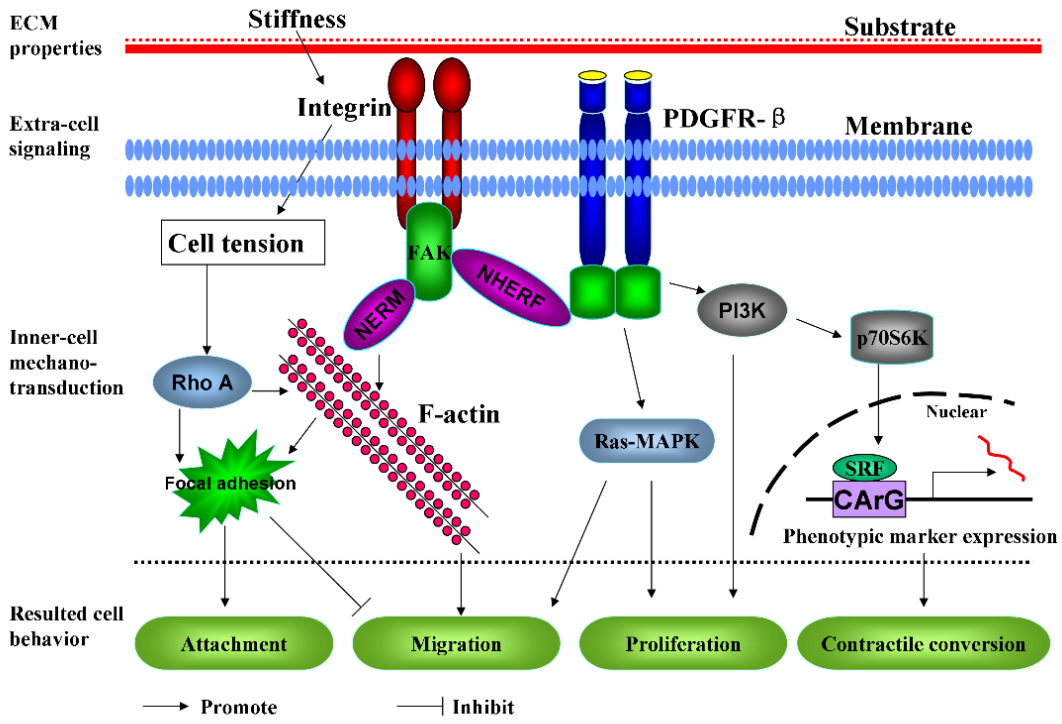

Figure 2.6 Proposed mechanisms model of mechanotransduction in SMCs. Cells cultured on rigid substrates presumably possess larger integrin activity, which promotes the formation of robust actin stress fibers and FAs via RhoA activity and MERM phosphorylation. High level integrin activity also leads to strong PDGFR-β activation and further triggers several signaling pathways like Ras-MAPK, PI3K and Akt, which are known to be involved in multiple cellular and developmental responses. PI3K pathway activation promotes actin reorganization, cell movements, cell growth, and inhibits cell apoptosis. Meanwhile, PDGFR-β activation can regulate the binding activity of SRF to CArG box via the PI3K/Akt/p70S6K pathway, therefore further modulate the transcriptional activation of the contractile marker proteins including SM-MHC, smoothlin, trangelin and calponin investigated in this study.

Activated PDGFR-β signaling triggers downstream signaling molecules such as G-protein Ras, GTPase Rho, Ras-mitogen-activated protein kinase (MAPK), and phosphatidylinositol 3-kinase (PI3K). These molecules are involved in multiple cellular and developmental responses [36]. MAPK signaling can activate gene transcription, leading to stimulation of cell growth, differentiation, and migration [39]. PI3K is a family of enzymes phosphorylating

phosphoinositides and the PI3K signaling pathway connects to enormous downstream effectors including serine/threonine kinases such as Akt/PKB [40,41], p70S6 kinase [42], and small GTPases of the Rho family [43]. Activation of the PI3K pathway by PDGFRs was reported to promote actin reorganization, direct cell movements, stimulate cell growth, and inhibit cell apoptosis [36]. PDGFR-β activation can also modulate the transcriptional activation of the contractile marker proteins via the PI3K/Akt/ p70S6 kinase (p70S6K) pathway [44], which has been found to promote both proliferation and, paradoxically, differentiation of SMCs [45,46]. Signaling transduction from PDGFR-β to p70S6K can enhance the binding ability of transcription factors especially serum response factor (SRF) to the CC[A/T]6GG (CArG) box, which is one of the DNA elements required for muscle-specific gene transcription and plays an indispensable role in the expression of almost all contractile gene markers of SMCs [47].

2.4 Conclusions

A series of biodegradable photo-crosslinked PCLTA substrates were developed with controllable stiffness achieved by simultaneously varying the crosslinking density and crystallinity. Surface characteristics of these polymer substrates were evaluated, including roughness, hydrophilicity, and capability of adsorbing proteins from cell culture media. Cell studies demonstrated stiffer semi-crystalline PCLTA networks induced stronger stress fibers, larger spread area, faster growth, higher motility, better conversion from the synthetic phenotype to the more functional contractile phenotype, and stronger focal adhesions of SMCs. Further gene and protein expression analysis showed higher expression levels of contractile gene markers and integrin subunits in SMCs on the stiffer substrates of semi-crystalline PCLTA networks. These biodegradable PCLTA networks with controllable stiffness can be used for diverse applications and regulation of different cell types, and various2D patterns and 3D structures can be readily fabricated using methods such as replica molding and stereolithography. The double bonds in PCLTA supply feasibility of being incorporated with other functional, bioactive components such as polyethylene glycol and poly(L-lysine) dangling chains to improve the biocompatibility.

References

1. Wong JY, Leach JB, Brown XQ. Balance of chemistry, topography, and mechanics at the cell-biomaterial interface: issues and challenges for assessing the role of substrate mechanics on cell response. Surf Sci 2004;570:119-33
2. Pelham RJ, Wang YL. Cell locomotion and focal adhesions are regulated by substrate flexibility. Pro Natl Acad Sci USA 1997;94:13661-5
3. Discher DE, Janmey P, Wang YL. Tissue cells feel and respond to the stiffness of their substrate. Science 2005;310:1139-43
4. Sieminski AL, Hebbel RP, Gooch KJ. The relative magnitudes of endothelial force generation and matrix stiffness modulate capillary morphogenesis *in vitro*. Exp Cell Res 2004;297:574-84
5. Yeung T, Georges PC, Janmey PA. Effects of substrate stiffness on cell morphology, cytoskeletal structure, and adhesion. Cell Motil Cytoskel 2005;60:24-34
6. Peyton SR, Raub CB, Keschrumrus VP , Putnam AJ. The use of poly(ethylene glycol) hydrogels to investigate the impact of ECM chemistry and mechanics on smooth muscle cells Biomaterials 2006;27:4881-93
7. Peyton SR, Kim PD, Ghajar CM, Seliktar D , Putnam AJ. The effects of matrix stiffness and RhoA on the phenotypic plasticity of smooth muscle cells in a 3-D biosynthetic hydrogel system. Biomaterials 2008;29:2597-607
8. Peyton S R, Putnam AJ. Extracellular matrix rigidity governs smooth muscle cell motility in a biphasic fashion. J Cell Physiol 2005;204:198-209
9. Brown XQ, Ookawa K, Wong JY. Evaluation of polydimethylsiloxane scaffolds with physiologically-relevant elastic moduli: interplay of substrate mechanics and surface chemistry effects on vascular smooth muscle cell response. Biomaterials 2005;26:3125-29
10. Teixeira AI, Ilkhanizadeh S, Wigenius JA, Duckworth JK, Inganäs O, Hermanson O. The promotion of neuronal maturation on soft substrates. Biomaterials 2009;30:4567-72
11. Wang S, Kempen DH, Simha NK, Lewis JL, Windebank AJ, Yaszemski MJ, Lu L. Photo-crosslinked hybrid polymer networks consisting of poly(propylene fumarate) and poly(caprolactone fumarate): controlled physical properties and regulated bone and nerve

cell responses. Biomacromolecules 2008;9:1229-41

12. Wang S, Kempen DHR, Yaszemski MJ , Lu L. The roles of matrix polymer crystallinity and hydroxyapatite nanoparticles in modulating material properties of photo-crosslinked composites and bone marrow stromal cell responses. Biomaterials 2009;30:3359-70
13. Nemir S, West FL. Synthetic materials in the study of cell response to substrate rigidity. Ann Biomed Eng 2010;38:2-20
14. Wang S, Lu L, Gruetzmacher JA, Currier BL, Yaszemski MJ. A biodegradable and cross-linkable multiblock copolymer consisting of poly(propylene fumarate) and poly(ε-caprolactone): synthesis, characterization, and physical prope rties. Macromolecules 2005;38:7358-70
15. Wang S, Yaszemski MJ, Gruetzmacher JA, Lu L. Photo-crosslinked poly(ε-caprolactone fumarate) networks: Roles of crystallinity and crosslinking density in determining mechanical properties. Polymer 2008;49:5692-9
16. Cai L, Wang S. Parabolic dependence of material properties and cell behavior on the composition of polymer networks via simultaneously controlling crosslinking density and crystallinity. Biomaterials 2010;31;7423-34
17. Cai L, Wang S. Poly (ε-caprolactone) acrylates synthesized using a facile method for fabricating networks to achieve controllable physicochemical properties and tunable cell responses. Polymer 2010;51:164-77
18. Cai L, Guinn AS, Wang S. Exposed hydroxyapatite particles on the surface of photo-crosslinked nanocomposites for promoting MC3T3 cell proliferation and differentiation. Acta Biomater 2011;7:2185-99
19. Wang K, Cai L, Hao F, Xu X, Cui M, Wang S. Distinct cell responses to substrates consisting of poly(ε-caprolactone) and poly(propylene fumarate) in the presence or absence of cross-links. Biomacromolecules 2010;11:2748-59
20. Wang K, Cai L, Zhang L, Dong J, Wang S. Biodegradable photo-crosslinked polymer substrates with concentric microgrooves for regulating MC3T3-E1 cell behavior. Adv Healthcare Mater 2012;1:292-301

21 Cai, L, Zhang, L, Dong, J , Wang, S Photocured biodegradable polymer substrates of varying stiffness and microgroove dimensions for promoting nerve cell guidance and differentiation

Langmuir 2012:28:12557-68

22. Roger VL, Go AS, Lloyd-Jones DM, Benjamin EJ, Berry JD, Borden WB, Bravata DM, Dai S, Ford ES, Fox CS, Fullerton HJ, Gillespie C, Hailpern SM, Heit JA, Howard VJ, Kissela BM, Kittner SJ, Lackland DT, Lichtman JH, Lisabeth LD, Makuc DM, Marcus GM, Marelli A, Matchar DB, Moy CS, Mozaffarian D, Mussolino ME, Nichol G, Paynter NP, Soliman EZ, Sorlie PD, Sotoodehnia N, Turan TN, Virani SS, Wong ND, Woo D, Turner MB; American Heart Association Statistics Committee and Stroke Statistics Subcommittee. Executive summary: heart disease and stroke statistics - 2012 update: a report from the american heart association. Circulation 2012;125:188-97
23. Beamish JA, He P, Kottke-Marchant K, Marchant RE. Molecular regulation of contractile smooth muscle cell phenotype: implication for vascular tissue engineering. Tissue Eng Part B 2010;16:467-91
24. Brown XQ, Bartolak-Suki E, Williams C, Walker ML, Weaver VM, Wong JY. Effect of substrate stiffness and PDGF on the behavior of vascular smooth muscle cells: implications for atherosclerosis. J Cell Physiol 2010;225:115-22
25. Wang S, Yaszemski MJ, Knight AM, Gruetzmacher JA, Windebank AJ, Lu L. Photo-crosslinked poly(ε-caprolactone fumarate) networks for guided peripheral nerve regeneration: material properties and preliminary biological evaluations. Acta Biomater 2009;5:1531-42
26. Schwartz U. Soft matters in cell adhesion: rigidity sensing on soft elastic substrates. Soft Matter ;2007;3:263-6
27. Choquet D, Felsenfeld DP, Sheetz MP. Extracellular matrix rigidity causes strengthening of integrin-cytoskeleton linkages. Cell 1997;88:39-48
28. Hadjipanayi E, Mudera V, Brown RA. Guiding cell migration in 3D: a collagen matrix with graded directional stiffness. Cell Motil Cytoskel 2009;66:121-128
29. Saez A, Buguin A , Ladoux B. Is the mechanical activity of epithelial cells controlled by deformations or forces? Biophys J 2005;89:L52-4
30. Dokukina IV, Gracheva ME. A model of fibroblast motility on substrates with different rigidities. Biophys J 2010;98:2794-03
31. Moussallem MD, Olenych SG, Scott SL, Keller III TCS, Schlenoff JB. Smooth muscle cell

phenotype modulation and contraction on native and cross-linked polyelectrolyte multilayers. Biomacromolecules 2009;10:3062-8

32. Leinweber B, Tang JX, Stafford WF, Chalovich JM. Calponin interaction with α-actinin-actin: evidence for a structural role for calponin. Biophys J 1999;77:3208-17

33. Shirinsky VP, Birukov KG, Hettasch JM, Sellers JR. Inhibition of the relative movement of actin and myosin by caldesmon and calponin. J Biol Chem 1992;267:15886-92

34. Haeberle JR. Calponin decreases the rate of cross-bridge cycling and increases maximum force production by smooth muscle myosin in an in vitro motility assay. J Biol Chem 1994;269:12424-31

35. Jin L, Hastings NE, Blackman BR, Somlyo AV. Mechanical properties of the extracellular matrix alter expression of smooth muscle protein LPP and its partner palladin; relationship to early atherosclerosis and vascular injury. Muscle Res Cell Motil 2009;30:41–55

36. Andrae J, Gallini R, Betsholtz C. Role of platelet-derived growth factors in physiology and medicine. Gene Dev 2008;22:1276-312

37. Peyton SR, Ghajar CM, Khatiwala CB, Putnam AJ. The emergence of ECM mechanics and cytoskeletal tension as important regulators of cell function. Cell Biochem Biophys 2007;47:300-20

38. Gerthoffer WT, Gunst SJ. Focal adhesion and small heat shock proteins in the regulation of actin remodeling and contractility in smooth muscle. J Appl Physiol 2001;91:963-72

39. Seger R, Krebs EG. The MAPK signaling cascade. FASEB J 1995;9:726-35

40. Burgering B , Coffer P. Protein kinase B (c-Akt) in phosphatidylinositol-3-OH kinase signal transduction. Nature 1995;76:599-602

41. Franke TF, Yang SI, Chan TO, Datta K, Kazlauskas A, Morrison DK, Kaplan DR, Tsichlis PN. The protein kinase encoded by the Akt proto-oncogene is a target of the PDGF-activated phosphatidylinositol 3-kinase. Cell 1995;81:727-736

42. Billington CK, Kong KC, Bhattacharyya R, Wedegaertner PB, Panettieri RA Jr, Chan TO, Penn RB. Cooperative regulation of p70S6 kinase by receptor tyrosine kinases and G protein-coupled receptors augments airway smooth muscle growth. Biochemistry 2005;44:14595-605

43. Ruse M, Knaus UG. New players in TLR-mediated innate immunity: PI3K and small Rho

GTPases. Immunol Res 2006;34:33-48

44. Chen CN, Li YS, Yeh YT, Lee PL, Usami S, Chien S, Chiu JJ. Synergistic roles of platelet-derived growth factor-BB and interleukin-1 in phenotypic modulation of human aortic smooth muscle cells. Proc Natl Acad Sci USA 2006;103:2665-2670

45. Liu ZP, Wang Z, Yanagisawa H, Olson EN. Phenotypic modulation of smooth muscle cells through interaction of Foxo4 and Myocardin. Dev Cell 2005;9:261-70

46. Duan C, Bauchat JR, Hsieh T. Phosphatidylinositol 3-kinase is required for insulin-like growth factor-I-induced vascular smooth muscle cell proliferation and migration. Circ Res 2000;86:15-23

47. Owens GK, Kumar MS, Wamhoff BR. Molecular regulation of vascular smooth muscle cell differentiation in development and disease. Physiol Rev 2004;84:767-801

Chapter III. Dynamic Substrates with Increasing Stiffness for Regulation of Smooth Muscle Cells

Abstract

Cardiovascular tissues bear constant blood shear and dynamic hardening under diseased conditions, which causes the tissue stiffness varies all the time. To mimic the dynamic changing environment in the vessel tissues and investigate the influence of dynamically changing substrate mechanical properties on the cell behaviors, I fabricated a model polymer network from poly(ε-caprolactone) triacrylate that can gradually stiffen in 24 h through impeded crystallization at body temperature (37 ℃). Rat primary SMCs were cultured on both static and dynamic substrates and distinct SMC attachment, proliferation and spreading were found. Quantification of contractile gene expression and protein content showed that the dynamic substrates could facilitate the contractile conversion process of SMCs. The analysis of focal adhesions and integrin expression indicated that the cellular abilities to sensing and adhering to the substrate surface were enhanced by the dynamic stiffening stimulation. These results extend the knowledge about SMC mechanosensing to dynamic substrates with increasing stiffness, and demonstrate a new method of regulating SMC adhesion, growth, and functional conversion on substrates.

3.1 Introduction

Substrate stiffness has been reported to initiate varied strength of static tension to cells, which can affect the attachment, growth, and morphology of mechanosensitive cells, for example, fibroblasts [1], endothelial cells [2], and SMCs [3-5]. In previous studies, SMCs were found to favor stiffer substrates by showing increased adhesion, spreading, and proliferation [6-10]. These findings suggest that SMC behavior could be affected by increasing the vessel stiffness resulted from the hardening of vascular tissue in disease development. However, most of the work was performed on static substrates with preset stiffness. In contrast, in real physiological conditions, SMCs are subjected to dynamic environment with changing mechanical stimulation from either blood shear or vascular hardening. Therefore, appropriate dynamic substrates with increasing stiffness are highly desired in cardiovascular tissue engineering studies.

There exist a limited number of dynamic substrates. Free DNA was crosslinked to be time-dependent stiffening hydrogels [11-13]. There are disadvantages of using this system such as slow reaction (1 day) [14,15], unfavorable negative charges from free DNA [15,16], long-term instability (>1 week), and potential dangerous mutations caused by DNA integration into cellular genomes [14,17]. In collagen-alginate composite hydrogels, the mechanical properties can be modified by introducing divalent cations but the external calcium ions may also alter cellular signaling [18]. UV-crosslinkable hyaluronic acid hydrogels modified with methacrylate groups were used as dynamic hydrogels [19-23]. The disadvantages are the requirements of addition of gelation reagent dithiothreitol (DTT), photoinitiator (Irgacure 2959) and exposure to UV light [20,21].

I have developed biodegradable and photo-crosslinkable poly(ε-caprolactone) triacrylates (PCLTAs) that can be photo-crosslinked into networks with high gel fractions and controllable thermal and mechanical properties [24,25]. Elastic modulus ranging from 1 to 200 MPa was achieved by modulating the crosslinking density and crystallinity through the nominal molecular weight (M_n) of the polymer [25]. When the molecular weight increases from 2000 to 20000 g/mol, the PCL network changes from an amorphous, compliant elastomer to a semi-crystalline, stiff material with a crystallinity of 42%. For the semi-crystalline PCLTA networks,

the melting temperature (T_m) of the substrate increased from 13.8 ℃ for M_n of 5000 g/mol to 50.4 ℃ for M_n of 20000 g/mol. Because of the constraints of the crosslinks, polymer crystallization in a network is suppressed and impeded, as demonstrated by reduced crystallinity and slower crystallization. By controlling the T_m of the PCLTA network to be slightly above 37 ℃, PCL segments in the network crystallized very slowly at 37 ℃ and the substrate stiffness increased gradually with the increase in crystallinity over a time period of 24 h, as schematically demonstrated in Fig. 3.1.

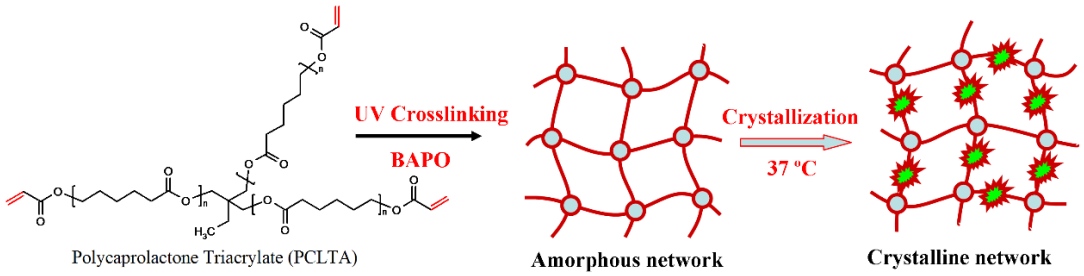

Figure 3.1 Scheme of PCLTA photocrosslinking and crystallization process at 37 ℃.

Based on this unique mechanism of impeded polymer crystallization in PCLTA networks, I explore to apply this spontaneously increasing substrate stiffness to regulate SMCs when they are seeded on the substrates and cell attachment occurs at the same time. To study the effect of the gradually increasing substrate stiffness on SMC adhesion, spreading, proliferation, and phenotypic conversion, I prepared a series of PCLTA networks, melted and crystallized at 37 ℃ for 0, 4, 8, or 24 h.

3.2 Materials and methods

3.2.1 Synthesis and photo-crosslinking PCLTA polymers

The PCLTA samples used in this study were synthesized in our lab using the method reported previously. The molecular weights of polymers were determined by using Gel Permeation Chromatography (GPC; PL-GPC 20, Polymer Laboratories, Inc.) with tetrahydrofuran (THF) as the solvent and monodisperse polystyrene samples (Polymer Laboratories) as the standard references. The PCLTA synthesized in this study had number-

average molecular weight of 7985 g/ mol, weight-average molecular weight of 9626 g/mol, and polymer molecular weight distribution of 1.206, as determined by GPC analysis. Thermal properties were determined by Differential Scanning Calorimetric (DSC) measurements, in which the samples were first heated from room temperature to 100 ℃, then cooled down to −80 ℃, followed by heated again to 100 ℃ at a rate of 10 ℃/min.

3.2.2 Photo-crosslinking and characterization

UV light generated from a high-intensity long-wave UV lamp (SB-100P, λ = 365 nm, Intensity: 4800 $\mu w/cm^2$) was used to facilitate photo-crosslinking of PCLTA. Phenyl bis(2,4,6-trimethyl benzoyl) phosphine oxide (BAPO, IRGACURE 819, Ciba Specialty Chemicals, Tarrytown, NY) was used as the photo-initiator. Homogeneous PCLTA/BAPO/CH_2Cl_2 mixture was transferred into a silicon mold consisting of two glass plates and a silicon spacer then placed under UV light for 20 min. In order to remove the residue of BAPO and sol fraction, the round crosslinked PCLTA disks (10 × 0.5 mm, diameter × thickness) were soaked in acetone for two days and washed with new acetone 3 times. Then the samples were dried in vacuum, compressed to remove the variance in surface roughness, sterilized in 70% alcohol solution, and dried completely in vacuum.

3.2.3 Crystallization process determination

Grazing incidence X-ray diffraction (GIXRD) was performed at an X-ray energy of 16.0 KeV using the beamline X6B of National Synchrotron Light Source in Brookhaven National Laboratory. Sample disks were placed on a thermal stage at 37 °C. The focused beam of 0.3 mm (vertical) × 0.3 mm (horizontal) was incident on the disks at an angle of 0.1 ° and the diffraction pattern was collected using a CCD detector (Princeton Instruments). Crystallinity was calculated from the area of crystalline peaks divided by the total area of crystalline peaks and amorphous halo. Crystallite size (τ) was calculated using the Scherrer equation $\tau = 0.89\lambda/\Delta\theta\cos 2\theta$ [26], where λ is the x-ray wavelength and $\Delta\theta$ is the line broadening at half the maximum intensity (FWHM) in radians.

3.2.4 Mechanical and rheological characterizations

The crystallization of PCLTA networks was monitored using elastic modulus (G′) a strain-controlled parallel-plate (8 mm) rheometer (RDS-2, Rheometric Scientific) at 37 ℃. The frequency was 1 Hz and the stress was 75 Pa in the measurements. The tensile properties of the crosslinked PCLTA specimens (0.5 × 2.0 × 10 mm, thickness × width × length) at a strain rate of 0.005/s were measured using a dynamic mechanical thermal analyzer (DMTA-5, Rheometric Scientific) at 37 ℃. The surface morphology of the crosslinked PCLTA disks was characterized using multimode atomic force microscopy (AFM) and the root mean square (RMS) roughness values were obtained from the height images. The hydrophilicity of the crosslinked PCLTA disks represented by the water contact angle was determined using a Ramé-Hart NRC C. A. goniometer (Model 100-00-230, Mountain Lakes, NJ) at 37 ℃. The amounts of serum proteins adsorbed on the disks from the culture media were determined on a micro-plate reader (SpectraMax Plus 384, Molecular Devices, Sunnyvale, CA) with assistance of a MicroBCA protein assay kit (Pierce, Rockford, IL), as described in our previous reports [27].

3.2.5 In vitro cell behaviors

Before cell studies, photo-crosslinked PCLTA disks were sterilized in 70% alcohol solution for 2 h and fully dried in vacuum. For cell attachment and proliferation, sterilized PCLTA disks were rinsed in PBS three times and seeded with SMCs at a density of ~15000 cells/cm^2 using TCPS as the positive control. UV absorbance at 496 nm was determined on the incubated MTS assay solution (CellTiter 96 Aqueous One Solution, Promega, Madison, WI) at 4 h, days 1, 2, and 4 post-seeding using the micro-plate reader described in Section 2.4. SMC numbers on these points were calculated using the standard curve constructed using known cell numbers. For observing the attached cells on the disks, SMCs were fixed in 4% paraformaldehyde (PFA) solution for 10 min and washed with PBS three times. Cell skeletons and nuclei were stained with rhodamine-phalloidin and 4',6-diamidino-2-phenylindole (DAPI), respectively. Cell images were taken using an Axiovert 25 light microscope (Carl Zeiss, Germany) and cell area was quantified from 20 non-overlapping cells in these images using ImageJ software.

3.2.6 Focal adhesion characterization

After 1 day culture on crosslinked PCLTA disks, SMCs were fixed with 4% PFA solution and cell membrane was permeabilised with 0.2% Triton X-100. Bovine Serum Albumin (BSA) in PBS (1%) was used to block SMCs at 37 ℃ for 1 h. The treated SMCs were incubated in monoclonal vinculin primary antibody (1:1000 in PBS; Sigma) for 1 h with gentle shaking at room temperature and washed three times by PBS to remove unconjugated antibodies. Then SMCs were further incubated in goat anti-mouse IgG secondary antibody (1:200 in PBS; Sigma) solution at 37 ℃ for 1 h. After vinculin staining, cells were further stained by rhodamine-phalloidin for 1 h at 37 ℃ for observing specific α-actins. Leica DM6000B confocal fluorescent microscope was used for photographing the stained cells. Quantification of focal adhesions (FAs) including the area of an FA and densities, i.e., the number of FAs per cell, was performed on 5 non-overlapping cells using ImageJ. The elongation of focal adhesion was calculated from the inverse of the circularity, a parameter defined by the equation of $4\pi \times \text{area/perimeter}^2$ to indicate how close an object is to a perfect circle [28].

3.2.7 Gene expression of contractile phenotypic markers and integrin subunits

Primers for gene expression using real-time polymerase chain reaction (PCR) were designed using Oligoperfect software, as listed in Table 3.1. After three days culture on the crosslinked PCLTA disks, SMCs were trypsinized and centrifuge collected at 1000 rpm for 2 min. The total RNA of SMCs was isolated using the RNeasy Mini Kit (Qiagen, Valencia, CA) and the total cDNA was obtained by reverse transcription using DyNAmo cDNA synthesis kit (Thermo Scientific) following the manufacturer's protocols. To make a comparable analysis, all the cDNAs were diluted to the same concentration of 1 ng/μL and the exact 5 μL of total cDNA were added as template to the real-time PCR reaction system. Power SYBR Green PCR Master Mix (Applied Biosystems, Warrington, UK) was used as PCR reaction solution and mixed with template cDNA to make a total 20 μL reaction volume. The PCR amplification process was conducted on a PTC-200 Peltier Thermal Cycler fluorescence detection system (MJ Research, Watham, MA). The reaction procedure was set as 5 min at 94 ℃ followed by cyclic steps of 94 ℃ for 30 s, 55 ℃ for 30 s, and 72 ℃ for 30 s. The relative gene expression levels were normalized to that of housekeeping gene glyceraldehyde-3-phosphate

dehydrogenase (GAPDH). Reverse transcription PCR (RT-PCR) amplification was performed on the Thermo cycler mentioned earlier using the same primers except Calponin and Transgelin listed in Table 3.2. The same thermal cycle steps were applied with varied cycle numbers for different genes according to their expression levels. After the reaction was completed, gene products were separated via electrophoresis in 1.0% agarose gels with Gelgreen (Biotium, Hayward, CA). An EpiChemi II darkroom imaging system (UVP, Upland, CA) was used for visualization of DNA bands. For expression of integrin subunits, mRNA was isolated from SMCs at day 1 post-seeding and the expression was analyzed by the same real-time PCR procedure described earlier for phenotypic gene markers, except using integrin specific primers listed in Table 3.3.

Table 3.1 Real-time PCR primers for phenotypic markers

Gene		Primer sequence (5′ to 3′)	Length (bp)	Product Size (bp)
NM-MHC	Forward	GGATTGGCAGGTCTCTCTATCAG	23	220
	Reverse	ATTGGGATCCTGGATATTGCT	21	
Calponin	Forward	AGTCTACTCTCTTGGCTCTGGCC	23	122
	Reverse	CCTGCCTTCTCTCAGCTTCTCAGG	24	
SM-M HC	Forward	AAGCAGCTCAAGAGGCAG	18	178
	Reverse	AAGGAACAAATGAAGCCTCGTT	22	
Transgelin	Forward	GGCAGCTGAGGATTATGGAGTCACG	25	152
(SM-22)	Reverse	TGGGATCTCCACGGTAGTGTCCA	23	
Smoothlin	Forward	TCGGAGTGCTGGTGAATAC	19	197
	Reverse	CCCTGTTTCTCTTCCTCTGG	20	
GAPDH	Forward	TCTTCACCACCATGGAGAA	19	232
	Reverse	ACTGTGGTCATGAGCCCTT	19	

Table 3.2 RT-PCR primers for phenotypic markers

Gene		Primer sequence (5′ to 3′)	Length (bp)	Product Size (bp)
Calponin	Forward	ACAAAAGGAAACAAAGTCAAT	21	375
	Reverse	GGGCAGCCCATACACCGTCAT	21	
Transgelin	Forward	TGTTCCAGACTGTTGACCTC	20	368
(SM-22)	Reverse	GTGATACCTCAAAGCTGTCC	20	

Table 3.3 Real-time PCR primers for integrin subunits

Gene	Forward primer	Reverse primer
Integrin-α_v	5'-AAGACGCCCGAAAAGAATGAC-3'	5'-ATCCCGCTTGGTGATGAGAT-3'
Integrin-α_1	5'-TCTGCCAAACTCAGTCCACGA-3'	5'-TGACGATCAGCAGGCTCTTTT-3'
Integrin-α_5	5'-CCTTCCTTCATTGGCATGGA-3'	5'-TCTGCATCCTGTCAGCAATCC-3'
Integrin-β_1	5'-AGAGTGCCGTGACAACTGTG-3'	5'-GAGCCCCAAAGCTACCCTAC-3'
Integrin-β_2	5'-AGTCCCAGTGGAACAACGAC-3'	5'-AGCACTGGGGCTAGCTGTAA-3'
Integrin-β_3	5'-GACCCGCTTCAATGACGAA-3'	5'-TCACAGACTGTAGCCTGCATGA-3'
GAPDH	5'-TCTTCACCACCATGGAGAA-3'	5'-ACTGTGGTCATGAGCCCTT-3'

3.2.8 Statistical analysis

All statistical calculations were performed using one way analysis of variance (ANOVA) followed by Tukey post-test if needed. Any two samples with a *p*-value lower than 0.05 were considered to be significantly different.

3.3 Results

3.3.1 Impeded crystallization in PCLTA networks

The gel fraction of crosslinked PCLTA was high as 0.92 ± 0.02 and the swelling ratio was 7.0 ± 0.01 in methyl chloride. As shown in the DSC curves in Fig. 3.2a, there existed one crystallization temperature (T_c) of 11.3 ℃ in the cooling curve and two melting peaks (T_m) of 42.0 and 49.8 ℃ in the heating curve for uncrosslinked PCLDA, whereas the crystallization peak shifted to a lower temperature at -1.05 ℃ and there was only one melting peak at 41.34 ℃ for the network. GIXRD patterns obtained at a penetration depth of 5 nm in Fig. 3.2b demonstrated that the crystallinity of crosslinked PCLTA increased progressively within a time scale of 30 h at 37 ℃.

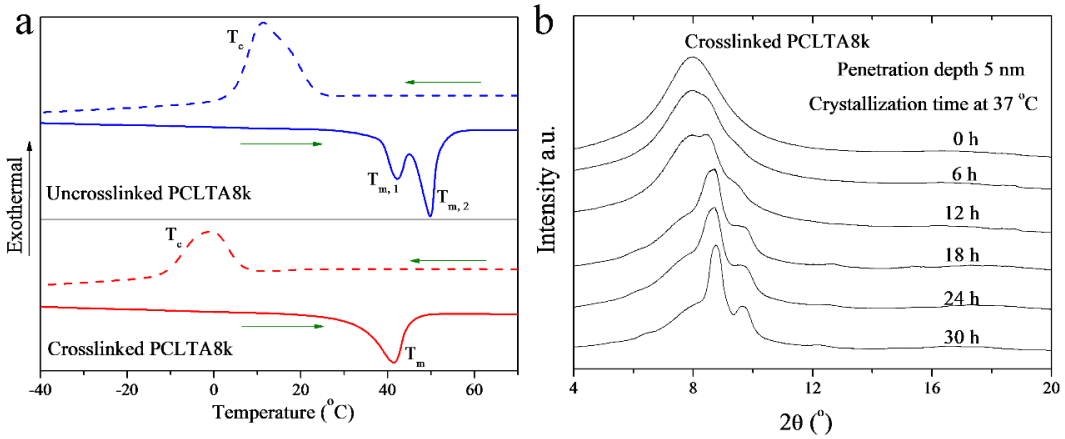

Figure 3.2 a). Thermal properties of uncrosslinked and crosslinked PCLTA. b). The chain segment crystallization processes in crosslinked PCLTA networks as monitored by the grazing incidence X-ray diffraction at the penetration depth of 5 nm and time scale of 30 h.

The crystallinities and crystallite sizes of crosslinked PCLTA at different penetration depths of 5 nm, 30 nm, and 15 mm were obtained from the GIXRD patterns, as shown in Fig. 3.3. Gradual increases in both crystallinity and crystallite size were found over a period of 30 h at 37 ℃. Both parameters increased with increasing the penetration depth, indicating that the bulk properties were distinct from the surface properties.

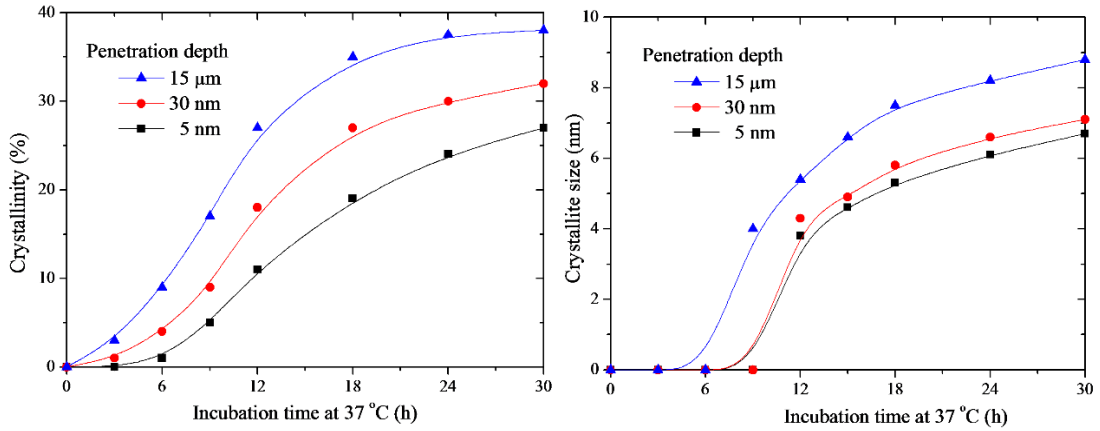

Figure 3.3 The a) crystallinities and b) crystallite sizes as tested by X-ray diffraction at varied penetration depths of 5 nm, 30 nm and 15 μm from the network surface at different incubation time.

3.3.2 Dynamic mechanical, rheological and surface properties

The shear modulus (G′) of crosslinked PCLTA increased gradually with time when it crystallized at 37 ℃ (Fig. 3.4a). The strain-stress curves in Fig. 3.4b from tensile tests at 37 ℃ also displayed the same trend. At time zero, crosslinked PCLTA was amorphous and elastomeric with low modulus and low stress/strain at break of 0.7 MPa/60%. Upon crystallization, the sample became stiffer with gradually increased modulus and stress/strain at break. When the sample crystallized for 24 h, it was a typical semi-crystalline polymer showing tough characteristics. After crystallization, the elastic region in the curves became much steeper and thus the tensile modulus calculated from the curves increased from 2.1 ± 0.9 for amorphous networks to 6.2 ±0.6, 9.9 ±0.7, and 15.1 ±0.6 MPa after crystallized at 37 ℃ for 4, 8, and 24 h, respectively. Meanwhile, the strain at break increased to 122%, 191%, and 226% and the stress at break increased to 2.9, 4.4, and 6.0 MPa, respectively.

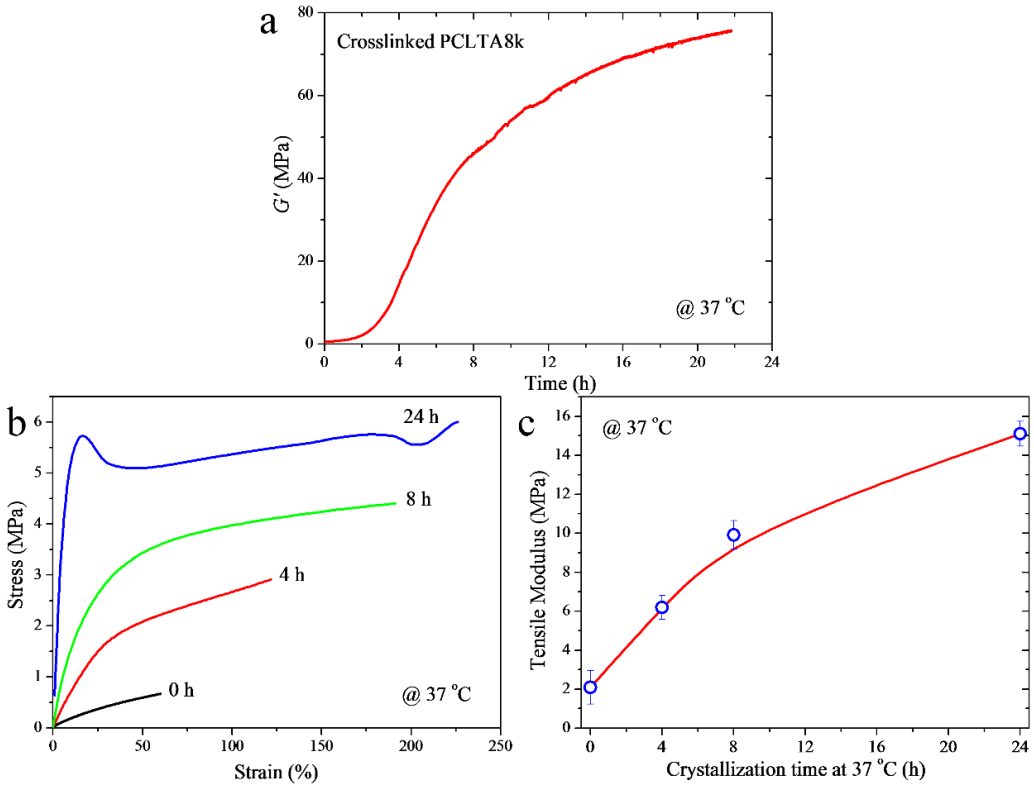

Figure 3.4 a). The elastic modulus (G′) of the PCLTA networks as monitored by rheometer with a constant temperature set at 37 ℃. b). The strain-stress curves for four melted amorphous PCLTA networks pretreated under 37 ℃ for 0, 4, 8 and 24 h, respectively. c). Tensile modulus of these networks at 37 ℃ as calculated from the strain-stress curves.

Crosslinked PCLTA disks were compressed to flatten the surfaces. AFM was used to characterize the surface morphology in crystallization. As shown the AFM images in Fig. 3.5, there were no obvious differences in surface morphology with a similar roughness of ~10 nm for crosslinked PCLTA disks crystallized for different time periods at 37 ℃. A slight increase was found in water contact angle on these disks when the crystallization time was prolonged, indicated by the values of 66.0 ± 1.6 °, 66.8 ± 1.9 °, 69.6 ± 2.3 ° and 69.8 ± 2.3 ° for 0, 4, 8 and 24 h, respectively. In contrast, the protein adsorption decreased slightly from 4.1 ± 0.2 to 3.7 ± 0.2 and 3.4 ± 0.2 μg/cm^2 for disks crystallized for 0 or 4 to 8 and 24 h, respectively.

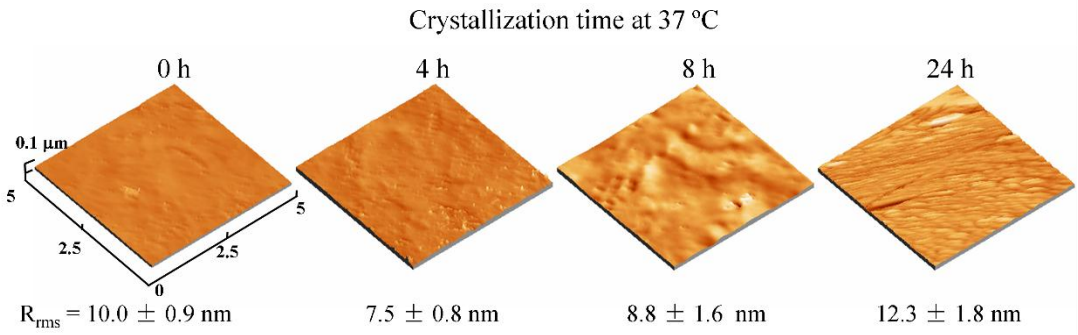

Figure 3.5 The surface features and roughness determined by AFM for four crosslinked PCLTA networks with pretreated time of 0, 4, 8 and 24 h, respectively.

3.3.3 SMC attachment, spreading, and proliferation on the substrates

At 4 h post-seeding, the highest cell attachment rate was found on the static substrate with the highest stiffness in the absence of dynamic stiffening stimulation. As shown in Fig. 3.6b, cells on the dynamic substrates, i.e., crosslinked PCLTA disks crystallized for 0 h, 4 h, and 8 h from their amorphous state, have smaller projected areas than on the stiffer static substrates at day 0.5 and day 1 post-seeding while the values were larger on the substrates crystallized for longer time.

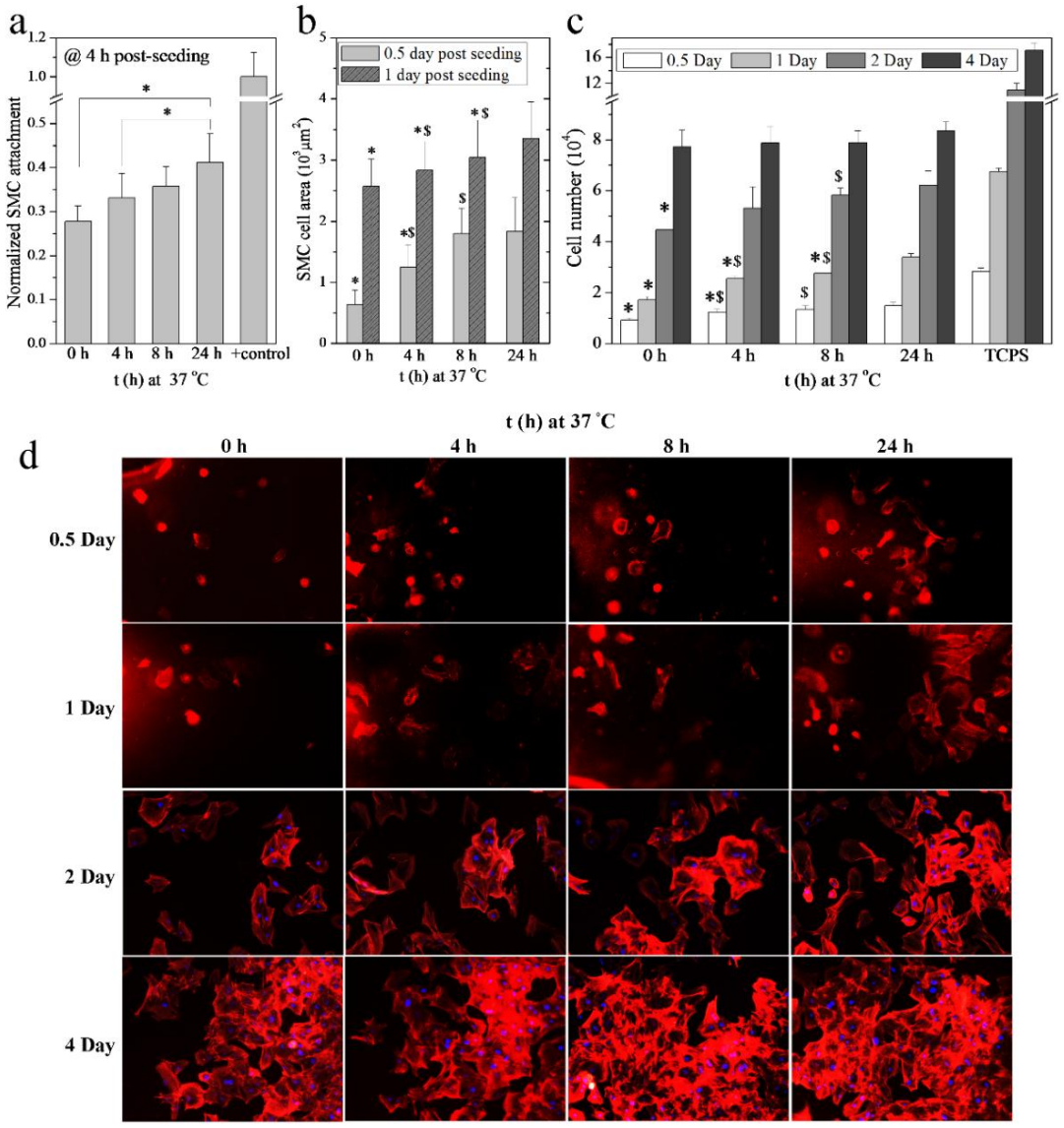

Figure 3.6 a). The SMC attachment rate on the dynamic and static networks at 4 h post-seeding, as normalized to that of TCPS positive control. b). The cell spread area calculated at 0.5 day (12 h) and 1 day post-seeding on these substrates. c). The cell numbers at 0.5, 1, 2 and 4 days post-seeding on the dynamic and static samples using TCPS as positive control. *: $p < 0.05$ to the 24 h static sample. $: $p < 0.05$ to the 0 h dynamic sample.

These differences may be attributed to the stiffness variance in these substrates. In the period of 24 h, dynamic substrates were more compliant than the static one because of their lower crystallinities, although they gradually stiffened with crystallization. In the stage of cell adhesion within a short period of 4 h, dynamic substrates were more compliant than the static

substrate, which enhanced SMC adhesion, as found in our previous study [25].

After crystallization for 24 h, the dynamic substrates reached the same stiffness as that for the static ones. Cells on the dynamic substrates experienced crystallization-induced stiffening stimulation while not on the static substrate. At 12 h and day 1, cell numbers on the dynamic substrates were still lower than that on the static substrate. Nevertheless, after two day culture, SMCs that experienced stiffening stimulation on the dynamic substrates had a higher growth rate than those on the static substrate. At day 2, the cell population on dynamic substrates made from crosslinked PCLTA that had crystallized for 4 and 8 h was similar to that on the static substrate. Cell images with filaments and nuclei stained further exhibited a similar trend in cell population (Fig. 3.6d).

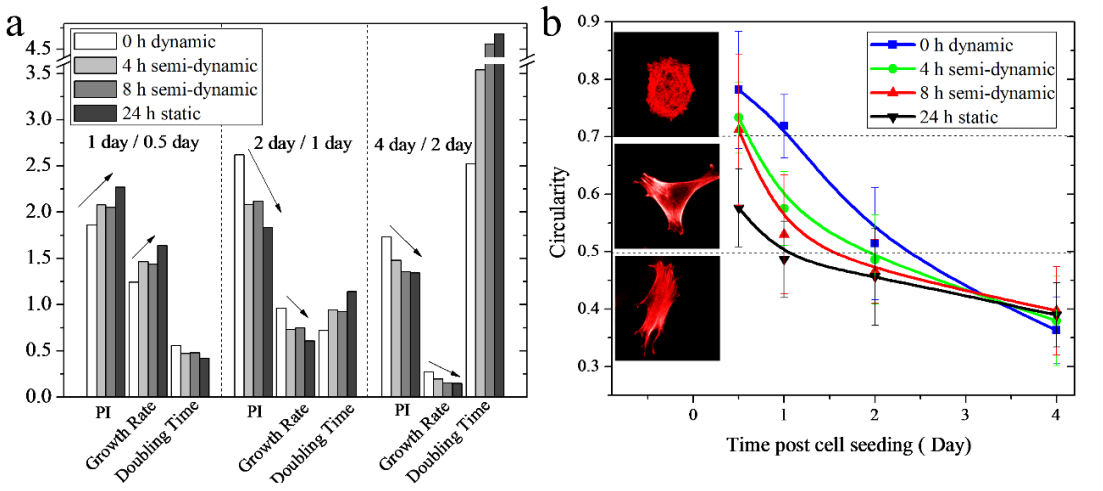

Figure 3.7 a). The separate proliferation index (PI), growth rate (fold per day) and doubling time (days) of the SMCs on the dynamic and static networks at different time period of 0.5 to 1 day, 1 day to 2 day, and 2 day to 4 day, respectively. b). Circularities of the cells on dynamic substrates were determined from cell images at varied post-seeding time points.

The proliferation index (PI) of SMCs was calculated by dividing the cell number by the initial number, as shown in Fig. 3.7a. From 12 h to 1 day, the PI value was lower for SMCs on the dynamic substrates compared with that on the static substrate. After 1 day, the PI was higher on the dynamic substrates instead, suggesting that stiffening mechanical stimulus could trigger stronger cellular activities in terms of growth and division. Cell growth rate was calculated by dividing the slope of ln(PI) by the time. The trend in cell growth rate was consistent with that

in the PI on these substrates (Fig. 3.7a). Cell doubling time, i.e., the time for cells to double their number decreased in the first day but increased later when the substrate varied from crosslinked PCLTA that crystallized for 0 to 4, 8, and 24 h. This trend reversion indicated that cells had faster division on the stiffer static substrates temporarily within 1 day whereas cells on the dynamic substrates receiving stiffening stimulation could gain a stronger ability in the long run. At day 4, cell numbers on the dynamic substrates were similar to that on the static substrate without distinguishable difference among the groups.

Besides cell area, the circularity calculated from the cell images quantifies cell roundness by equation 4π*area/perimeter^2. The circularity decreased when the substrates were crystallized from 0 to 4, 8, and 24 h. As displayed in Fig. 3.7, three SMC cellular morphologies of round, triangle and spindle shape were found at the circularity values of ≥ 0.7, ≥ 0.5 and ≤ 0.5, respectively. SMCs with the contractile phenotype spread well and exhibit the spindle shape (low circularities) while the synthetic phenotype divide frequently with a round shape (high circularities). From Fig. 3.7, in the period for substrate stiffening, i.e., within 1 day, SMCs on the dynamic substrates has higher circularity than that on the static substrate, showing that the higher stiffness of the static substrate resulted better cell adhesion relative to the softer dynamic substrates with stiffening stimulation. After 1 day, all the substrates crystallized fully and reached a similar stable stiffness and the S value of the cells that received dynamic mechanical stimulation decreased faster than that on the static substrate. At day 4, circularities on the dynamic substrates were even lower than that on the static substrate.

3.3.4 Focal adhesions and integrins of SMCs on the substrates

Focal adhesions are dynamic anchoring protein (e.g., paxillin, talin, and vinculin) complexes mostly located at the cell periphery to provide a structural connection between the internal cytoskeleton and the extracellular substrates [29]. Upon receiving mechanical stimulation, focal adhesions adjust their morphology and size to form various adhesion subtypes and simultaneously trigger signal transductions that relate to cell growth, spreading, and migration [30,31]. The focal adhesions in SMCs were stained green using immunofluorescent monoclonal vinculin primary antibody , as shown in the confocal images in Fig. 3.8a. Again, SMCs on the dynamic substrate spread less at day 1 relative to the static

substrate. However, the focal adhesions were denser in cells on the dynamic substrate than on the static one. In the protrusions, represented by the circled areas, cells on both dynamic and static substrates showed a high extent of vinculin proteins. Focal adhesions rarely developed in the cell body on the static substrate while cells on dynamic substrates demonstrated substantial focal adhesions similar to those in protrusions. Further quantification and statistical analysis in Fig. 3.8b-d indicated that the focal adhesions of the cells on dynamic substrates had significantly larger area, better elongation, and higher density.

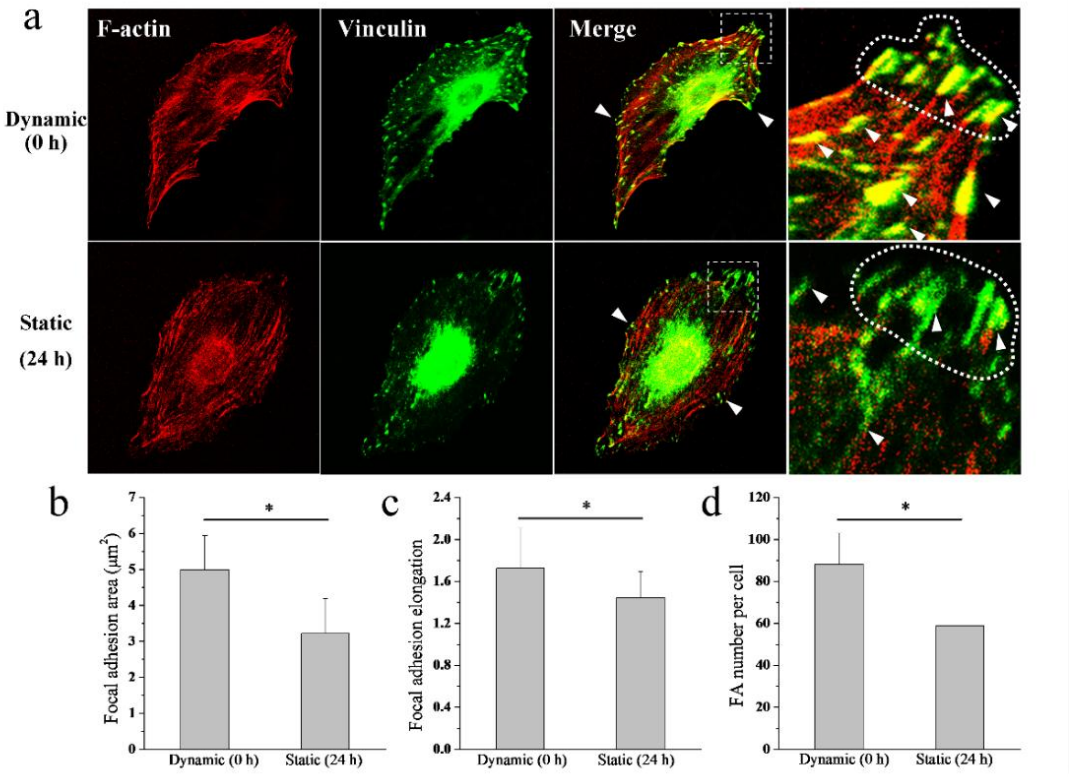

Figure 3.8 a). Immunostaining images of cytoskeleton actins (red) and focal adhesion vinculins (green). The arrows point to the typical focal adhesion sites and the dotted circles emphasize the protrusion in cell membrane. b-d). The focal adhesion area, elongation rate and density as calculated from the immunostaining images.

Integrins are heterodimers formed by two α and β subunits and different integrins bind to different extracellular matrix (ECM) proteins, though which cells sense the surface characteristics of the underlying substrates [32-36]. Integrin clusters activate the focal adhesion

kinase, induce the assembly of multicomponent signaling complexes, and trigger focal adhesion signal transduction, thus they play a critical role in cellular sensing process [29]. Consistent with the significant variance in focal adhesions, integrin α_1, α_v, α_5, β_1, β_2, and β_3 subunits were triggered to increase their expression levels by 1.2 to 2 folds in SMCs on dynamic substrates of crosslinked PCLTA that crystallized for 0 or 4 h from those on the static substrate, as shown in Fig. 3.9. The results on integrin expression indicated that the integrin subunits can be triggered by substrate stiffening stimulation and consequently determined focal adhesions and adhesion-mediated cell behavior.

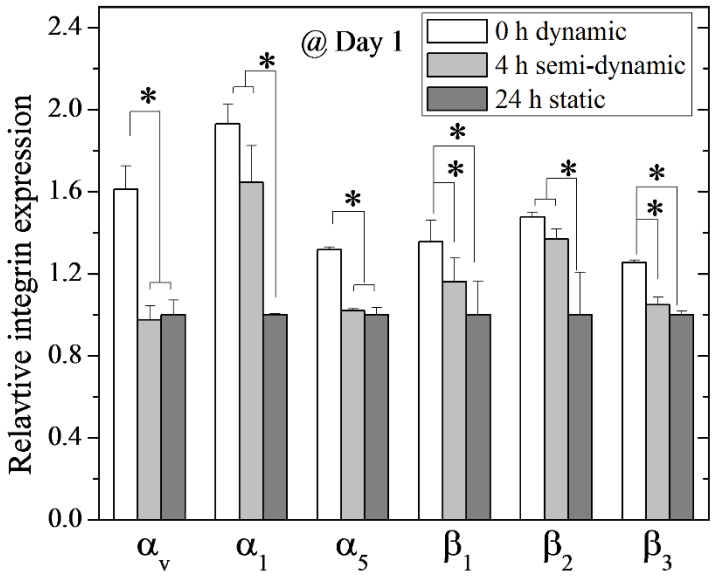

Figure 3.9 Gene expression of three integrin subunits α_v, α_1, α_5, β_1, β_2 and β_3, as normalized to that of the house keeping gene GAPDH.

3.3.5 Gene and protein expression

SMCs seeded onto scaffolds or substrates have the proliferative synthetic phenotype, which lacks functionality. After certain stage of growth and division, the synthetic phenotype convert to the contractile phenotype, which does not favor proliferation but mainly functionalized as extensible, elastic and contractible muscle unit [37-39]. Modulation of this phenotypic conversion is of critical importance for SMCs in blood vessel tissue engineering.

Smooth muscle myosin heavy chain (SM-MHC), smoothlin, transgelin and calponin are four representative gene markers for contractile SMCs [40,41]. As shown in Fig. 3.10a-e, real-

time PCR analysis on SMCs cultured for 1 day showed that the contractile markers have higher (approximately two folds) expression levels on the dynamic substrates of crosslinked PCLTA crystallized for 0 h than those of the static one. The gene expression levels of these contractile markers were higher for SMCs cultured for one more day and the values were again higher on the dynamic substrates than the static one. RT-PCR analysis in Fig. 3.10f also showed stronger band intensities for these markers on the dynamic substrates at both days 1 and 2, suggesting that dynamic mechanical stimulation facilitated SMC phenotypic conversion.

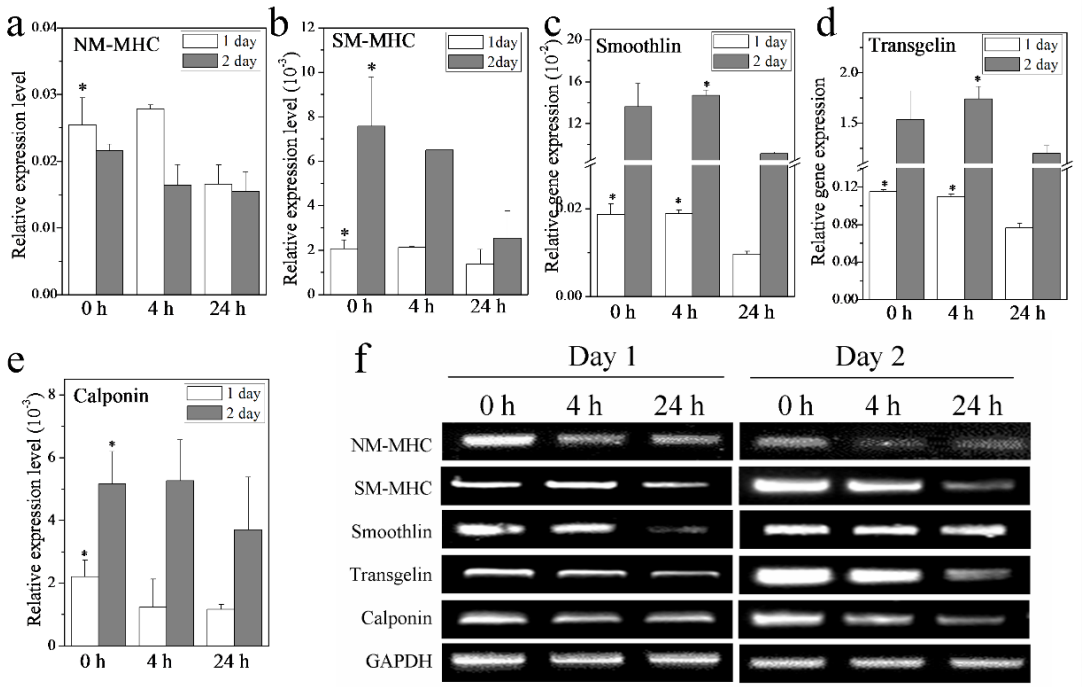

Figure 3.10 a-e). The real-time quantitative gene expressions of one synthetic phenotypic marker NM-MHC, and four contractile phenotypic markers SM-MHC, smoothlin, transgelin and calponin, as normalized to GAPDH. f). The RT-PCR band intensities of these makers.

To further substantiate the gene analysis, calponin protein expression was analyzed using immuostaining. As shown in Fig. 3.11, the nuclei and calponin in SMCs were stained blue and green, respectively. Consistent with cell proliferation discussed above, there were more cells on the static substrate. However, a larger portion of cells expressed calponin and protein expression in single cells was higher on dynamic substrates at both days 1 and 2, as indicated by stronger immunoflorescence intensity.

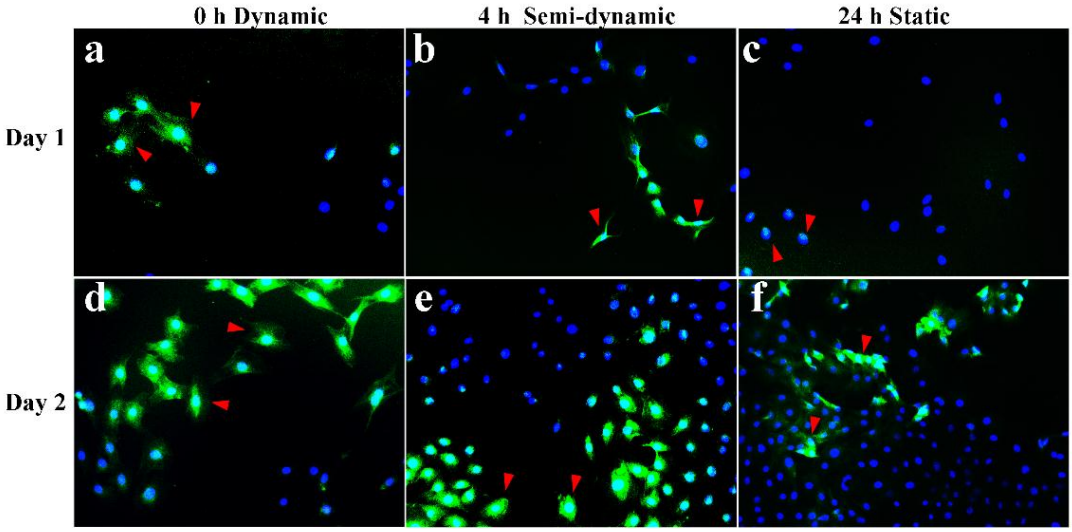

Figure 3.11 Expression of SMC contractile phenotypic marker proteins in SMCs on the dynamic, semi-dynamic and static networks examined at 1 day and 2 days post-seeding. Cells were subject to immunofluorescence staining with antibodies against calponin (green) and DAPI against nuclei (blue). Two red arrows were used to point out the calponin expressed cell examples in each image.

3.4 Discussion

Extensive studies have been performed using various cell types to reveal the instructive role of substrate stiffness in regulating cellular behaviors including adhesion, spreading, growth, differentiation, and gene/protein expression [28,42]. For example, in differentiation of multi-nucleated skeletal muscle myotubes, focal adhesion strength was enhanced monotonically by substrate stiffness from 1 kPa soft gel to stiff glass [43]. Vascular SMCs were also found to respond to substrate stiffness in their adhesion and proliferation processes [3-5,8]. Nevertheless, much of the evidence for these cellular responses to substrate stiffness was obtained from studies using static substrates with preset and invariant stiffness. In this study, our dynamic polymer substrates with gradually increasing stiffness provide an opportunity for investigating cell responses to dynamic mechanical stimulation. Using these unique dynamic substrates, I sought to mimic the hardening of cardiovascular tissue and investigated cellular responses under stiffening stimulation.

There exist several studies on cellular responses to substrates with gradually changing

mechanical properties. For example, in the in situ mechanosensing study of cells responding to external stimuli, myoblast cells exhibited pronounced stress fiber formation and flattening on dynamic pH-sensitive hydrogels made from an ABA triblock copolymer gelator when the hydrogel elasticity increased [44]. On DNA-crosslinked hydrogels with increasing stiffness to mimic the mechanical variations in the physiological conditions,, fibroblasts could adjust their cell projection area and polarity according to the magnitude and range of stiffness change [12]. In contrast, neuronal cells on hydrogels with gradually decreasing stiffness were found to have increased cellular population, focal adhesion kinase expression, and neurite outgrowth [17]. Human mesenchymal stem cells (hMSCs) were also found to adjust their live cellular functions including morphology, migration, integrin expression and differentiation on dynamic environment with real-time controlled mechanics [24].

In our previous studies using crosslinked PCLTA substrates with controllable *E* of 1-200 MPa, SMCs preferred stiffer ones by exhibiting larger and denser focal adhesions, larger spread area, stronger cytoskeleton actins, faster proliferation, and better expression of contractile phenotypic markers [25]. Based on the mechanism of crystallization-induced strengthening, I further investigated the effect of dynamic mechanical stimulation on SMC behaviors in this study. The initial stiffness of the substrates was critical for determining SMC adhesion and spreading, despite the stiffening, verifying the previous conclusion on the role of substrate stiffness. After the completion of crystallization in 1 day, both dynamic and static substrates reached similar stiffness and SMCs that experienced dynamic stiffening stimulation proliferated significantly faster, adjusted their cell shape faster, and converted to contractile phenotype better than those on the static substrate.

To understand why SMCs responded to the dynamic stimulation, I further revealed that the focal adhesions, which function as cell-biomaterial mechanosensors, were triggered to be larger, denser, and more elongated. Focal adhesions were a critical component in sensing substrate stiffness and transducing the corresponding intracellular signals for cell spreading and proliferation [45-47]. Focal adhesions in SMCs were found to be stronger and more elongated on stiffer substrates [4]. Here I found unique enhancement of focal adhesions in SMCs on substrates with lower initial stiffnesses but dynamic mechanical stimulation. This is the first time to report that SMC focal adhesions change in a dynamic environment, which is valuable

in understanding cellular mechanosensing in hardening tissues, e.g., blood vessels undergoing arteriosclerosis. Focal adhesions are two terminal molecules across cell membrane with the intracellular end linking to F-actin [43,48,49]. SMCs on more compliant static substrates had weaker F-actin [4,25]. In this study, the F-actin in SMCs on the dynamic substrates with low initial stiffness was not as weaker than that on the stiffer static substrate, suggesting that F-actin in cytoskeleton could be enhanced by the dynamic stiffening stimulation.

Integrins in cell membrane intermediate focal adhesions in sensing the mechanics of the underlying substrate [1]. Expression of integrin subunits in SMCs on the dynamic substrates was upregulated relative to that on the static substrate, showing that dynamic mechanical stimulation influences cell behavior through integrins. As proposed in a study using dynamic hydrogels, fibroblast cells probe the hydrogel stiffness by applying traction forces mainly through integrin linkage in focal adhesions [12]. When the external stiffness changes, cellular traction forces intensifies and feedback signals are transduced to cell body through integrin linkage and other biochemical pathways [12]. Upon receiving the environmental signals, cells respond by adjusting their spreading, proliferation and other related properties [12]. Our present results were consistent with the above literature discussion.

Enhanced focal adhesions and integrins further promoted cell proliferation and upreguated contractile gene expression. There may also exist other ECM sensing components in focal adhesions, e.g., paxillin and talin, or sensor proteins in cell membrane, e.g., additional integrin types involved in the environmental sensing and responsible intracellular biochemical activities. Further studies are under investigated for elucidating these concerns and achieving better understanding on cellular responses to dynamic mechanical stimulation. In addition, these model dynamic systems based on polymer crystallization can be extended to more novel one and modified to precisely tune their stiffness at time periods for other physiological processes and related cellular responses will also be conducted.

3.5 Conclusions

Dynamic mechanical stiffness stimulation plays an important role in influencing cell-biomaterial interactions. Photo-crosslinked PCLTA was employed as dynamic substrates as

impeded crystallization of PCL segments in the network resulted in a gradual increase in substrate stiffness. The advantage of using this unique polymer system is its free of external electrical, chemical, or photo stimulus, thus additional factors for influencing cellular behaviors could be excluded. SMCs receiving dynamic stiffening stimulation had stronger focal adhesions and higher expression of environmental sensing integrin subunits. SMC attachment, spreading, proliferation, and expression of contractile gene markers and calponin protein were all promoted upon receiving the dynamic mechanical stimulation. This study successfully outlines an approach to biomimic the mechanical variant environment for SMCs in the physiological conditions, and provides guidelines to regulate SMC behaviors through substrate stiffness, aiming for understanding related physiological processed in cardiovascular tissue engineering applications.

References

1. Yeung T, Georges PC, Janmey PA. Effects of substrate stiffness on cell morphology, cytoskeletal structure, and adhesion. Cell Motil Cytoskel 2005;60:24-34.
2. Sieminski AL, Hebbel RP, Gooch KJ. The relative magnitudes of endothelial force generation and matrix stiffness modulate capillary morphogenesis in vitro. Exp Cell Res 2004;297:574-584.
3. Peyton SR, Putnam AJ. Extracellular matrix rigidity governs smooth muscle cell motility in a biphasic fashion. J Cell Physiol 2005;204:198-209.
4. Peyton SR, Raub CB, Keschrumrus VP, Putnam AJ. The use of poly(ethylene glycol) hydrogels to investigate the impact of ECM chemistry and mechanics on smooth muscle cells. Biomaterials 2006;27:4881-4893.
5. Peyton SR, Kim PD, Ghajar CM, Seliktar D, Putnam AJ. The effects of matrix stiffness and RhoA on the phenotypic plasticity of smooth muscle cells in a 3-D biosynthetic hydrogel system. Biomaterials 2008;29:2597-2607.
6. Wong JY, Velasco A, Rajagopalan P, Pham Q. Directed movement of vascular smooth muscle cells on gradient-compliant hydrogels. Langmuir 2003;19:1908-1913.
7. Engler A, Bacakova L, Newman C, Hategan A, Griffin M, Discher D. Substrate compliance versus ligand density in cell on gel responses. Biophys J 2004;86:617-628.
8. Brown XQ, Ookawa K, Wong JY. Evaluation of polydimethylsiloxane scaffolds with physiologically-relevant elastic moduli: interplay of substrate mechanics and surface chemistry effects on vascular smooth muscle cell response. Biomaterials 2005;26:3125-3129.
9. McDaniel DP, Shaw GA, Elliott JT, Bhadriraju K, Meuse C, Chung KH, Plant AL. The stiffness of collagen fibrils influences vascular smooth muscle cell phenotype. Biophys J 2007;92:1759-1769.
10. Isenberg BC, DiMilla PA, Walker M, Kim S, Wong JY. Vascular smooth muscle cell durotaxis depends on substrate stiffness gradient strength. Biophys J 2009;97:1313-1322.
11. Yurke B, Turberfield AJ, Mills AP, Simmel FC, Neumann JL. A DNA-fuelled molecular machine made of DNA. Nature 2000;406:605-608.

12. Jiang FX, Yurke B, Schloss RS, Firestein BL, Langrana NA. The relationship between fibroblast growth and the dynamic stiffnesses of a DNA crosslinked hydrogel. Biomaterials 2010;31:1199-1212.
13. Previtera ML, Trout KL, Verma D, Chippada U, Schloss RS, Langrana NA. Fibroblast morphology on dynamic softening of hydrogels. Ann Biomed Eng 2012;40:1061-1072.
14. Lin DC, Yurke B, Langrana NA. Mechanical properties of a reversible, DNA-crosslinked polyacrylamide hydrogel. J Biomech Eng 2004;126:104-110.
15. Lin DC, Yurke B, Langrana NA. Inducing reversible stiffness changes in DNA-crosslinked gels. J Mater Res 2005;20:1456-1464.
16. Gawel K, Stokke BT. Logic swelling response of DNA-polymer hybrid hydrogel. Soft Matter 2011;7:4615-4618.
17. Jiang FX, Yurke B, Schloss RS, Firestein BL, Langrana NA. Effect of dynamic stiffness of the substrates on neurite outgrowth by using a DNA-crosslinked hydrogel. Tissue Eng Part A 2010;16(6):1873-1889.
18. Gillette BM, Jensen JA, Wang MX, Tchao J, Sia SK. Dynamic hydrogels: switching of 3D microenvironments using two-component naturally derived extracellular matrices. Adv Mater 2010;22:686-691.
19. Young JL, Engler AJ. Hydrogels with time-dependent material properties enhance cardiomyocyte differentiation in vitro. Biomaterials 2011;32:1002-1009.
20. Guvendiren M, Burdick JA. Stiffening hydrogels to probe short- and long-term cellular responses to dynamic mechanics. Nat Commun 2012;24(3):792.
21. Burdick JA, Prestwich GD. Hyaluronic acid hydrogels for biomedical applications. Adv Mater 2011;23:H41-H56.
22. Khetan S, Katz JS, Burdick JA. Sequential crosslinking to control cellular spreading in 3-dimensional hydrogels. Soft Matter 2009;5:1601-1606.
23. Kloxin AM, Kasko AM, Salinas CN, Anseth KS. Photodegradable hydrogels for dynamic tuning of physical and chemical properties. Science 2009;324:59-63.
24. Cai L, Wang S. Poly(ε-caprolactone) acrylates synthesized using a facile method for fabricating networks to achieve controllable physicochemical properties and tunable cell responses. Polymer 2010; 51: 164-177.

25. Liu X, Cai L, Hao F, Cui M, Wang S. Biodegradable elastomeric substrates with controllable stiffness for regulating smooth muscle cell behavior. 242nd ACS National Meeting, August 2011, Denver, Colorado. (PMSE Preprints, Am Chem Soc, Polymer Division 2011;105:124-6).

26. Murthy NS, Bednarczyk C, Minor H. Depth-profiles of structure in single- and multilayered commercial polymer films using grazing-incidence X-ray diffraction. Polymer 2000;41:277-284.

27. Cai L, Wang K, Wang S. Poly(ethylene glycol)-grafted poly(propylene fumarate) networks and parabolic dependence of MC3T3 cell behavior on the network composition. Biomaterials 2010;31:4457-4466.

28. Discher DE, Janmey P, Wang YL. Tissue cells feel and respond to the stiffness of their substrate. Science 2005;310(5751):1139-1143.

29. Burridge K, Chrzanowska-Wodnicka M. Focal adhesions, contractility, and signaling. Annu Rev Cell Dev Biol 1996;12:463-518.

30. Parsons JT, Horwitz AR, Schwartz MA. Cell adhesion: integrating cytoskeletal dynamics and cellular tension. Nat Rev Mol Cell Bio 2011;11:633-643.

31. Zamir E, Geiger B. Molecular complexity and dynamics of cell-matrix adhesions. J Cell Sci 2001;114:3583-90.

32. Ingber DE. Mechanosensation through integrins: cells act locally but think globally. Proc Natl Acad Sci 2003;100:1472-1474.

33. Wang HB, Dembo M, Hanks SK, Wang Y. Focal adhesion kinase is involved in mechanosensing during fibroblast migration. Proc Natl Acad Sci USA 2001;98:11295-11300.

34. Paszek MJ, Zahir N, Johnson KR, Lakins JN, Rozenberg GI, Gefen A, Reinhart-King CA, Margulies SS, Dembo M, Boettiger D, Hammer DA, Weaver VM. Tensional homeostasis and the malignant phenotype. Cancer Cell 2005;8:241-254.

35. Katsumi A, Orr AW, Tzima E, Schwartz MA. Integrins in mechanotransduction. J Biol Chem 2004;279:12001-12004.

36. Giancotti FG, Ruoslahti E. Integrin signaling. Science 1999;285:1028-1032.

37. Iyemere VP, Proudfoot D, Weissberg PL, et al. Vascular smooth muscle cell phenotypic

plasticity and the regulation of vascular calcification. J Intern Med 2006;260(3):192-210.

38. Rensen SSM, Doevendans PAFM, van Eys GJJM. Regulation and characteristics of vascular smooth muscle cell phenotypic diversity. Neth Heart J 2007;15(3):100-108.

39. Chan-Park MB, Shen JY, Cao Y, Xiong Y, Liu Y, Rayatpisheh S, Kang GC, Greisler HP. Biomimetic control of vascular smooth muscle cell morphology and phenotype for functional tissue-engineered small-diameter blood vessels. J Biomed Mater Res A 2009;88(4):1104-21.

40. Sobue K, Hayashi K, Nishida W. Expressional regulation of smooth muscle cell-specific genes in association with phenotypic modulation. Mol Cell Biochem 1999;190:105-118.

41. Wang C, Yin S, Cen L, Liu Q, Liu W, Cao Y, Cui L. Differentiation of adipose-derived stem cells into contractile smooth muscle cells induced by transforming growth factor-beta1 and bone morphogenetic protein-4. Tissue Eng Part A 2010;6(4):1201-1213.

42. Georges PC, Janmey PA. Cell type-specific response to growth on soft materials. J Appl Physiol 2005;98(4):1547-1553.

43. Engler AJ, Griffin MA, Sen S, Bonnemann CG, Sweeney HL, Discher DE. Myotubes differentiate optimally on substrates with tissue-like stiffness: Pathological implications for soft or stiff microenvironments. J Cell Biol 2004;66:877-887.

44. Yoshikawa HY et al. Quantitative evaluation of mechanosensing of cells on dynamically tunable hydrogels. J Am Chem Soc 2011;133(5):1367-1374.

45. Geiger B, Bershadsky A. Exploring the neighborhood: adhesioncoupled cell mechanosensors, Cell 2002;110:139-142.

46. Provenzano PP, Keely PJ. Mechanical signaling through the cytoskeleton regulates cell proliferation by coordinated focal adhesion and Rho GTPase signaling. J Cell Sci 2011; 124:1195-1205.

47. Wozniak MA, Modzelewska K, Kwong L, Keely PJ. Focal adhesion regulation of cell behavior. Biochim Biophys 2004;1692:103-119.

48. Hoffman BD, Grashoff C, Schwartz MA. Dynamic molecular processes mediate cellular mechanotransduction. Nature 2011;475:316-323.

49. Mitra SK, Hanson DA, Schlaepfer DD. Focal adhesion kinase: in command and control of cell motility. Nat Rev Mol Cell Bio 2005;6:56-68.

Chapter IV. Guidance of Smooth Muscle Cell Migration on Photo-Crosslinked Polymer Substrates with Stiffness Gradient

Abstract

I present the fabrication of a series of photo-crosslinked PCLTA substrates with defined gradients in stiffness and regulation of primary rat SMCs on them. The gradient strength was calculated to be 3.4, 13.4, 26.1 and 48.0 kPa/μm increasing along the direction from the soft end to the stiff end of the substrates. SMC migration was directed on the substrates from the soft end to the stiff end and faster cell migration emerged on the substrates with stronger gradient strengths.

4.1 Introduction

The *in vivo* environments for SMCs are complexes of biophysical and biochemical signals [1,2]. When vascular injury or tumor occurs, numerous signaling gradients created in the blood vessel walls (e.g., stiffness gradient) could influence SMC behaviors [3,4]. The mimic of SMC microenvironment thus is critical for better understanding of cell-materials interactions in cardiovascular tissue engineering [5-7]. In the past decades, many studies have reported that stiffness properties of extracellular microenvironment could influence SMC adhesion, growth, differentiation and migration [8-17].

Although there are extensive studies on how substrates stiffness affects cell behavior, fabrication of substrates with gradually changing stiffness and use of them to guide cell migration are still rather limited, especially for the stiffness higher than 1.0 MPa [18]. To explore, I fabricated a series of photo-crosslinked polymer substrates with stiffness gradient along the longitudinal direction [19-22]. Poly(ε-caprolactone) triacrylates (PCLTAs) developed in our research group can be photo-crosslinked into biodegradable polymer networks with high gel fractions and controllable thermal and mechanical properties (elastic modulus *E* in the range of 2-200 MPa) through varying the molecular weight of PCLTA [23,24]. The melting temperature (T_m) of semi-crystalline PCLTA network increased from 22.9 ℃ for the number-average molecular weight (M_n) of 7000 g/mol (PCLTA7k) to 50.4 ℃ for M_n of 20000 g/mol (PCLTA20k), and thus at 37 ℃ the former is an amorphous, compliant elastomer while the latter is a semi-crystalline, stiff polymer network with a substantial crystallinity of 42% [24].

Here I fabricated a series of photo-crosslinked PCLTA substrates with varied mechanical gradient strengths and evaluated primary rat vascular SMC migration on them. SMCs were able to detect and respond to the substrate stiffness, as indicated by the different spread areas along the continuously increasing stiffness in the gradient substrates. Moreover, SMC agglomerates were observed in the stiff regions of the substrate, whereas sparse cells were found in the soft regions. Further quantification of SMC motilities on these substrates demonstrated that a large fraction of the cells migrated distinctly toward the stiff region of the substrate, whereas cells on the uniform control substrates exhibited only random walks. All these findings suggest that cells could sense the mechanical differences of the underlying substrates and make

corresponding migration to the region with more favorable properties.

4.2 Materials and methods

4.2.1 PCLTA samples and other chemicals

Six PCLTAs with different number-average molecular weights (M_n) of 7050, 7790, 8570, 9230, 9760 and 19600 g mol^{-1} were synthesized in our research group as reported previously and were named as PCLTA7k, 8k, 8.6k, 9k, 10k, and 20k, respectively [23,24]. All other chemicals were purchased from Sigma-Aldrich (Milwaukee, WI) unless noted otherwise. Photo-initiator, phenyl bis(2,4,6-trimethyl benzoyl) phosphine oxide (BAPO, IRGACURE 819), was a gift from Ciba Specialty Chemicals (Tarrytown, NY).

4.2.2 Photo-crosslinking of PCLTA and mechanical characterization

Photo-crosslinking of PCLTA was facilitated under a high-intensity long-wave UV lamp (SB-100P, Spectroline) with a wavelength of 365 nm and intensity of 4800 $\mu w/cm^2$. PCLTA/BAPO/CH_2Cl_2 solution (100 g: 1 g: 50 ml) was transferred into a silicon mold consisting of two glass plates and a silicon spacer then placed under UV light for 20 min. Crosslinked PCLTA samples were soaked in acetone for two days and washed with new acetone 3 times to remove the residue of BAPO and sol fraction, followed by complete drying in vacuum. The tensile properties of three crosslinked PCLTA specimens (0.5 mm × 2.0 mm × 10 mm, thickness × width × length) were measured at 37 ℃ using a dynamic mechanical thermal analyzer (DMTA-5, Rheometric Scientific) at a strain rate of 0.005/s.

4.2.3 Fabrication and characterization of gradient substrates

As demonstrated in Fig. 4.1, PCLTA binary blends with compositional gradient were prepared by increasing the composition of the high-molecular-weight PCLTA, which was PCLTA8k, 8.6k, 10k, or 20k, in the low-molecular-weight PCLTA7k from one end to the other, prior to photo-crosslinking to cure the blends into substrates with stiffness gradients. A series of homogeneous PCLTA/BAPO/CH_2Cl_2 solutions was prepared with the composition of a higher-molecular-weight PCLTA in the blend with a lower-molecular-weight PCLTA ranging from 0 to 10, 20, 30, 40, 50, 60, 70, 80, 90, and 100%. These polymer solutions of varied

concentrations were transferred using micropipette at a fixed volume of 4 μl into a silicon mold (4 mm × 10 mm × 1 mm, width × length × thickness) between two glass plates. After a stable time of 10 second, another layer of different soft/stiff polymer composition was added. After all the polymer concentration layers were added, then the mold with polymers was kept stable for 5 minutes in order for the polymers to diffuse between boundaries. Then the silicon mold filled with polymer blends were placed under UV light and photo-crosslinked for 20 min. The tensile properties at varied gradient positions were tested at 37 ℃ using crosslinked PCLTA specimens (1.0 mm × 0.5 mm × 10 mm, thickness × width × length) at a strain rate of 0.005/s.

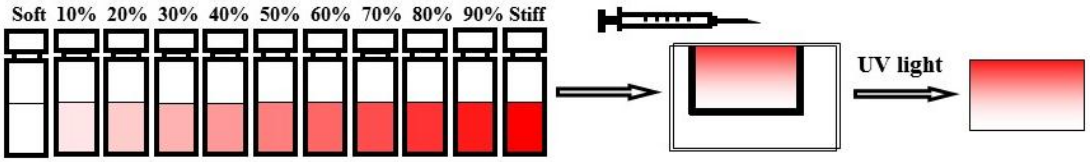

Figure 4.1 Fabrication of stiffness-gradient substrates by photo-crosslinking PCLTA binary homo-blends with compositional gradient along the longitudinal direction (darker color means stiffer region).

4.2.4 *In vitro* cell studies

Prior to cell studies, photo-crosslinked PCLTA disks were dried in vacuum, compressed between two glass plates to remove surface variance, sterilized in 70% alcohol solution, and dried completely in vacuum. Primary SMCs isolated from rat aorta were cultured in Dulbecco's modified eagle medium (DMEM) with 10% fetal bovine serum (FBS) in a 37 ℃ incubator with 5% CO_2 and 95% relative humidity prior to seeding. Sterilized photo-crosslinked PCLTA disks were seeded with SMCs at a density of ~15000 cells/cm^2 using TCPS as the positive control and empty wells without cells as the negative control. At days 1 post-seeding, SMCs were fixed with 4% paraformaldehyde (PFA) solution and then washed with PBS three times and permeabilised with 0.2% Triton X-100 at room temperature. Cytoplasm (F-actin) and cell nuclei were stained using rhodamine-phalloidin (RP, Cytoskeleton Inc) and 4',6-diamidino-2-phenylindole (DAPI, Sigma), respectively. Then the cells were photographed using an Eclipse Ti inverted microscope (Nikon, Japan). Cell density were calculated and averaged on 3 different

cell images. Cell area was quantified from 20 non-overlapping cells in these images using ImageJ software (National Institutes of Health, Bethesda, MD).

4.2.5 Analysis of cell motility

SMCs were incubated with fluorescent Calcein dye (Calcein AM, Invitrogen) at a concentration of 4 μM for 30 min to receive live staining and then transferred into transparent wells in a flow chamber at 37 ℃. Cell migration was monitored real-time by tracking the same cells every 10 min using an Axiovert 25 light microscope (Carl Zeiss, Germany). The direction of cell migration was analyzed from two subsequent images using ImageJ, according to a literature report [25,26]. To determine whether a 'live migration' existed or not on the gradient substrates in this study, I used real-time tracking method to record cell migration direction and migration path over a relatively long time period of 110 min. The migration path of a cell including both migration direction and displacement was generated from a series of continuous cell images and presented in an *XY*-diagram [19,27].

4.2.6 Statistical analysis

Statistical analysis was conducted using one-way analysis of variance (ANOVA). A *p*-value smaller than 0.05 indicated significant difference.

4.3 Results and Discussion

4.3.1 Photo-crosslinked PCLTA with controllable stiffness

Similar to previous findings on crosslinked PCLF and PCLDA [23,28-30], PCL crystallites formed a physical network to dramatically enhance the stiffness of the chemical network of PCLTA. As schematically demonstrated in Fig. 4.1, PCLTAs with different molecular weights had different crystallinities and different crosslinking densities after photo-crosslinking. When the PCLTA molecular weight was higher, the crystallinity was higher and thus the enhancing effect was more prominent although the crosslinking density was lower (Fig. 4.2b). Distinct mechanical properties were achieved by controlling both crystallinity and crosslinking density of the PCLTA networks simultaneously through the molecular weight, as shown in the stress-strain curves in Fig. 4.2b. Among all the six PCLTA samples, PCLTA7k with the smallest

molecular weight and the lowest crystallinity had the smallest *E* of 2.7 ± 1.0 MPa (Fig. 4.2c). With increasing the molecular weight of PCLTA, E increased to 19.9 ± 5.6, 34.4 ± 9.1, 56.8 ± 12.7, and 194.7 ± 13.4 MPa for PCLTA8k, 8.6k, 10k, and 20k, respectively.

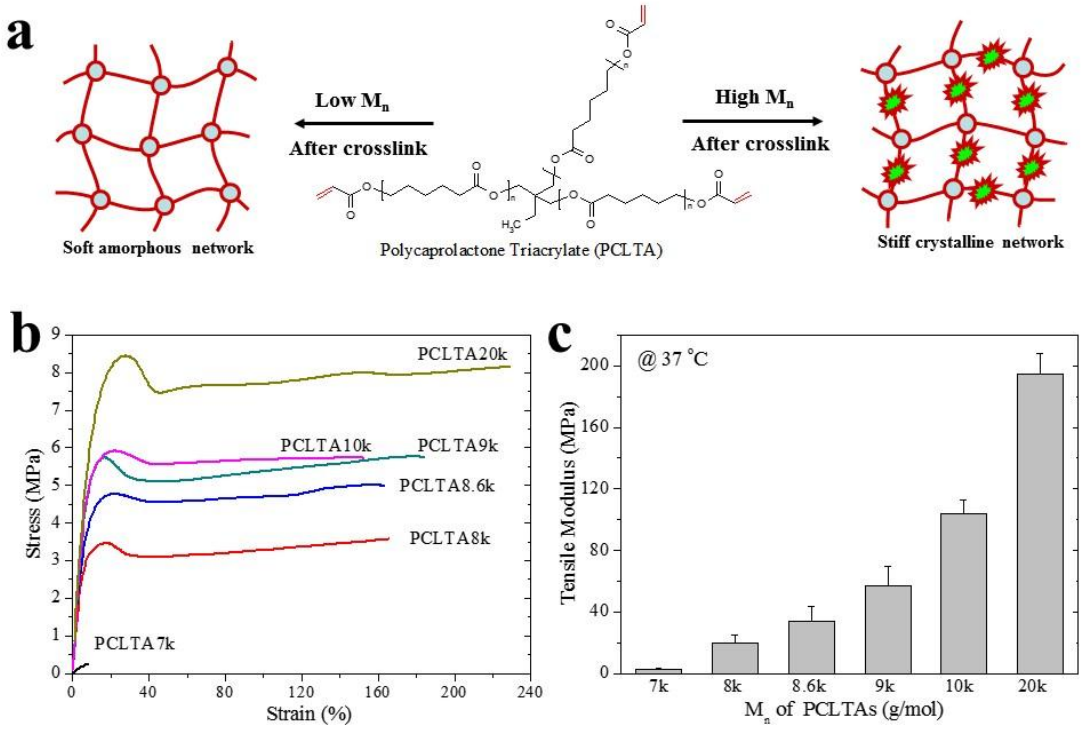

Figure 4.2 (a) Photo-crosslinking of PCLTA samples with different molecular weights from 7k to 20k g/mol, forming polymer networks with different crystallinties and mechanical properties. (b) Stress-strain curves of the PCLTA networks. (c) Tensile moduli of the PCLTA networks.

4.3.2 Gradient substrates of photo-crosslinked PCLTA

All the photo-crosslinked PCLTA substrates with stiffness gradients started from the soft end of crosslinked PCLTA7k to different stiff ends made from crosslinked PCLTA8k, 8.6k, 9k, 10k, and 20k. These gradient substrates also demonstrated gradients in transmission, i.e., gradual changes from the transparent, amorphous end to the opaque, crystalline ends, as can be seen from the optical images in Fig. 4.3a. The stiffness gradient strengths were calculated based on the differences in the *E* values on the two ends over a length of 4 mm to be 4.3, 7.9, 13.5, 25.4, and 48.0 kPa/μm when the stiff end was photo-crosslinked PCLTA8k, 8.6k, 9k, 10k, and

20k, respectively. Gradual increases in *E* along the soft end to the stiff end were demonstrated in Fig. 4.3b. It should be noted that the stiffness at the same position varied for different gradient substrates with different gradient strengths.

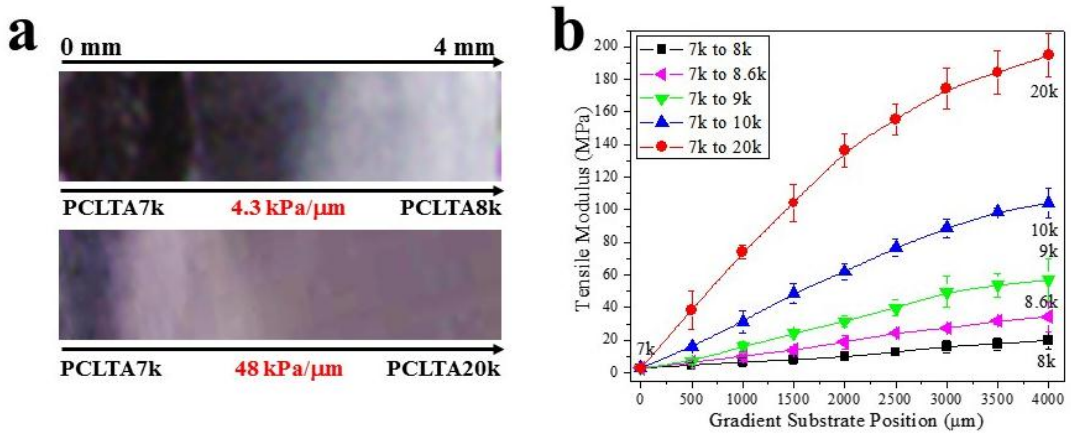

Figure 4.3 (a) Optical images of the gradient substrates from the transparent, amorphous soft end made from PCLTA7k network to the opaque, semi-crystalline stiff end made from PCLTA8k or PCLTA20k networks. (b) Tensile moduli of the samples at different positions along the longitudinal direction of the substrates.

4.3.3 SMC adhesion and proliferation on the gradient substrates

As demonstrated in the full-scale fluorescent images in Fig. 4.4, SMCs cultured for 1 day gathered on the stiff end with dense cell colonies while there was little cell attachment at the soft end. To observe the cell phenotype more clearly, enlarged cell images were taken in the four regions of 0-0.4 mm, 1.2-1.6 mm, 2.4-2.8 mm, and 3.6-4.0 mm starting from the soft end as zero along the longitudinal direction of the gradient substrates, as demonstrated in Fig. 4.5a. Again more SMCs were found to distribute on the stiffer regions on the gradient substrates. The cell densities (cell number per unit area) calculated from the cell images at day 1 in different regions of the gradient substrates are shown in Fig. 4.5b. The cell density increased continuously on all the five types of the gradient substrates when the studied area was shifted from left to right, i.e., from the region of 0-0.4 mm to 3.6-4.0 mm. Because these five substrates had different gradient strengths, the cell density in the same area was always higher when the gradient strength was higher. Cell spreading on the different areas of the gradient substrates at day 1, quantified as projected cell area in Fig. 4.5c, showed a trend similar in the cell density

as a larger cell area appeared on the area closer to the stiff end.

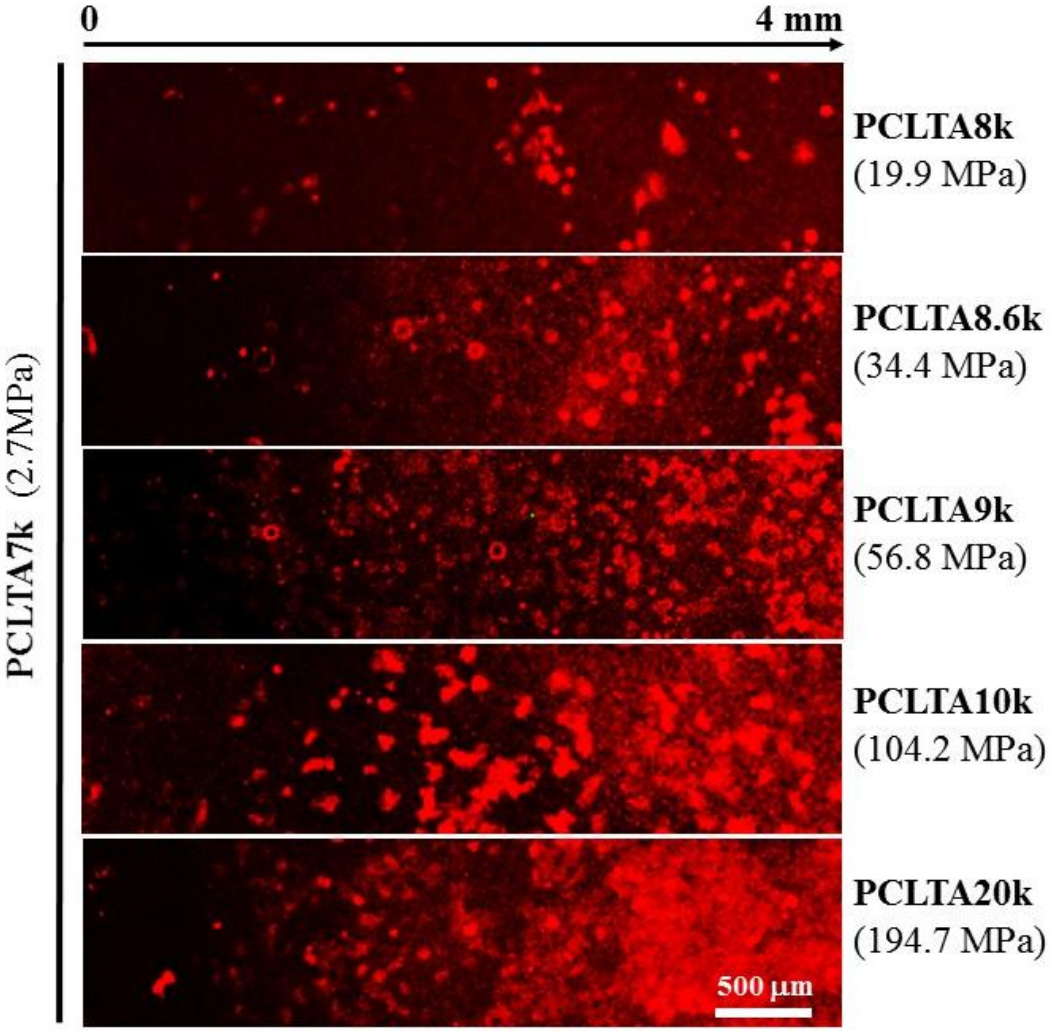

Figure 4.4 Full-scale fluorescent images of SMCs attached on the gradient substrates with different stiffness gradient strengths after 1 day culture.

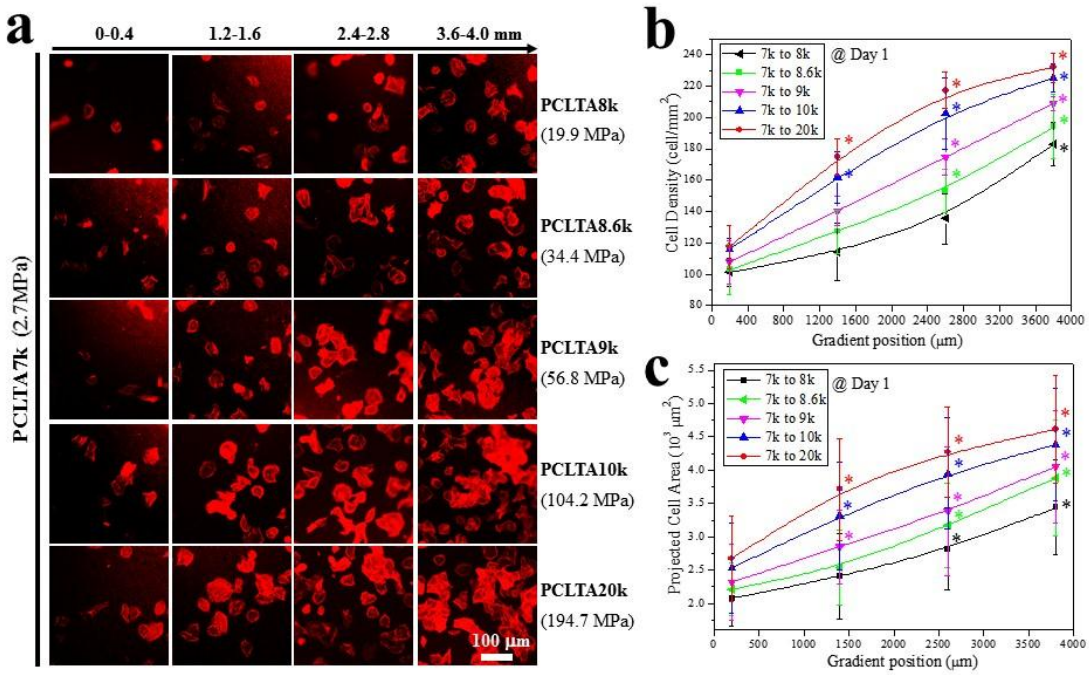

Figure 4.5 Fluorescent images (a), densities (b), and spread areas (c) of SMCs attached in four different regions (0-0.4 mm, 1.2-1.6 mm, 2.4-2.8 mm, and 3.6-4.0 mm) on the gradient substrates with different stiffness gradient strengths at day 1 post-seeding. *: $p < 0.05$ relative to cell numbers in other gel position on the same sample.

4.3.4 SMC migration on the gradient substrates

To monitor real-time SMC migration on these gradient substrates, live cells stained with fluorescent Calcein dye were photographed at the same location continuously with an interval time of 10 min. The migration of cells were marked with arrows to show the direction. As shown in Fig. 4.6a, almost all the cells migrated in the given time period of 10 min. The migration directions of multiple cells were complicated, especially for a large cell population. To address this issue, all the vectors were placed together into one *XY* diagram, as displayed in Fig. 4.6b. On the substrates with higher gradient strengths, there were more cells, as represented by denser vectors in the diagram. This trend was consistent with the cell adhesion discussed above [24]. Note that more vectors (> 70%) pointed to the stiff end of the gradient substrates than to the soft end, indicating that more cells migrated toward the stiff end. For comparison, SMC migration on homogenous substrate of photo-crosslinked PCLTA20k showed no preference in direction.

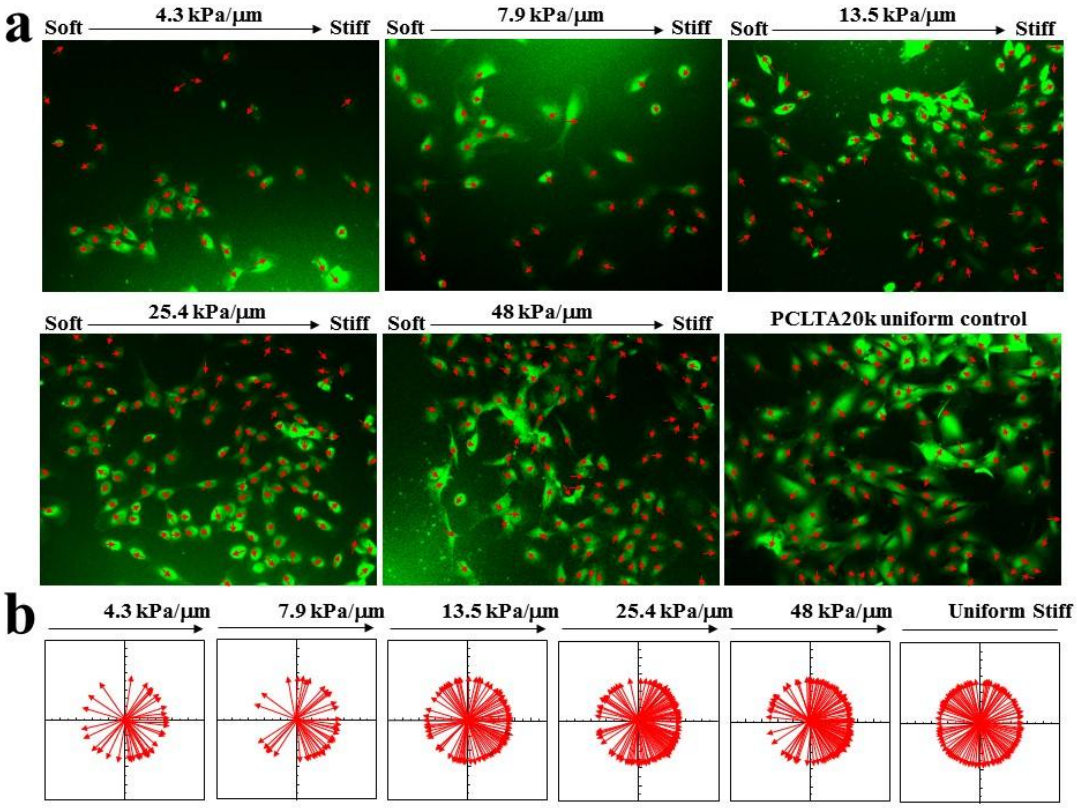

Figure 4.6 (a) Fluorescent images of live SMCs stained with Calcein dye migrating on the gradient substrates with different stiffness strengths and homogeneous crosslinked PCLTA20k substrate as the control. (b) SMC migration directions determined from two subsequent cell images.

To assess the generality of the finding in Fig. 4.6, I further examined the continuous migration paths of individual cells over a longer time period of 100 min in Fig. 4.7. Cell motility tended to follow principal stress orientation, as exemplified by the migration path toward the direction of increasing stiffness. As demonstrated in Fig. 4.7a-e, the direction of single cell migration was influenced by the gradient strength of the substrate. For the substrate with a low gradient strength of 4.3 kPa/μm, five cells migrated toward the stiff end with the longer migration distance whereas five cells migrated toward the soft end (Fig. 4.7a). For different stiffness gradient strengths, the profiles of cell migration varied dramatically. When the gradient strength was higher, more cells migrated toward the stiff end than to the soft end (Fig. 4.7b-e). For example, 7 cells migrated toward the stiff end whereas 3 migrated toward the soft end at the strongest gradient strength of 48 kPa/μm. On the control group of homogeneous

crosslinked PCLTA20k substrate, the cells did not show preference in their migration directions (Fig. 4.7f).

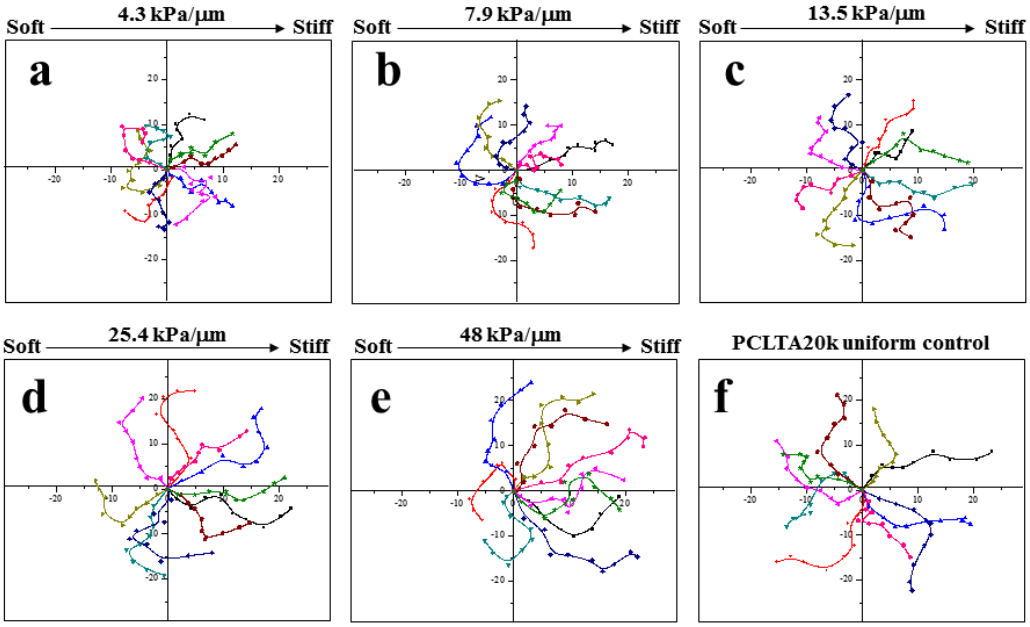

Figure 4.7 Two-dimensional paths of 10 individual SMCs on the gradient substrates with different stiffness gradient strengths from a-e) 4.3 to 48 kPa/μm and f) homogeneous photo-crosslinked PCLTA20k substrate as the control over 10*10 min. Cell paths were created by tracking cells every 10 min for ten continuous time points.

4.4 Discussion

The entire SMC population preferentially accumulated on the stiffer regions on the gradient substrates in this study, for all the groups with different absolute value of stiffness. SMCs could attach more and proliferate faster on the stiffer regions and they also have tendency to migrate to the stiffer regions, as our previous work demonstrated that SMCs could attach and proliferate better on stiffer substrates made from more crystalline PCLTA networks [24].

Similar migration trend to the stiff end after their attachment have been reported in several previous studies [27,31,32]. For example, bovine vascular SMCs on the gradient polyacrylamide substrates with a narrower range of lower Young's modulus of 2-12 kPa and a lower stiffness gradient strength of 0.001 kPa/ μm directly migrated from the soft region to

the stiff region and accumulated in the stiffer regions after 1 day culture [27]. In another study, bovine aortic vascular SMCs on the polyacrylamide gradient hydrogels withYoung's moduli of 1-80 kPa and stiffness gradient strengths of 0-0.04 kPa/μm also demonstrated a tendency to migrate toward the stiffer side of the substrates, which was terms as "*durataxis*" [31]. The morphology of the cells varied on different positions of the substrates with different moduli by showing increased spreading on stiffer gel positions [31]. The durotaxis quantified for a random walk was independent of the substrate modulus but increased with increasing the stiffness gradient strength [31]. Patterned silicone stiffness gradient substrates with a uniform soft PDMS membrane on the top were reported to modulate the motility of various cell types (NIH 3T3, hTERT fibroblasts, and C2C12 mouse myoblast cell line) and enable cellular patterning on the substrates through precise cell migration to the stiffer regions [32].

The mechanism for cell motility, however, is closely related to the internal forces generated by the focal adhesions (FAs) formed between cells and the substrate [33]. When cells proceed steady movement, the adhesion force is closely correlated to the cell-substrate viscous interactions, which are proposed to increase linearly with substrate stiffness [34]. Results in our study demonstrated that SMC migration occurred throughout the cell proliferation and was independent of local substrate stiffness, showing that cells favored to migrate towards the stiffer region regardless of which positions they attached and started. In contrast, the stiffness gradient strength of the gradient substrate was more critical and affected cell migration directly. This observation was consistent with the previous studies, despite much higher substrate stiffnesses and wider ranges of stiffness and gradient strengths here [27,31,32,35]. The correlation between the stiffness gradients in the substrates and SMC responses rendered in this study is helpful for fundamental understanding of cell-material interactions in stiffened vascular regions *in vivo* and the gradient substrates generated here can also serve as a platform for studying the effect of stiffness gradient strength on other cell types.

4.5 Conclusions

I developed a series of stiffness-gradient substrates along the longitudinal direction by photo-crosslinking PCLTA binary homo-blends made from two samples with different

molecular weights and crystallinities. These gradient substrates with the stiffness range of 2-200 MPa and gradient strengths of 4.3-48.0 kPa/μm were used to exam primary rat vascular SMC adhesion, spreading, and migration on them. The findings indicated that the stiffness gradient patterns of the underlying substrates were important for SMC adhesion, spreading, and accumulation. SMCs exhibited different spreading areas at different locations along the gradient on the substrates and they accumulated in the stiff regions of the substrates. Real-time observation of SMC motility showed that a large portion of cells migrated distinctly toward the stiff region of the substrate, especially when the gradient strength was higher.

References

1. Owens GK, Kumar MS, Wamhoff BR. Molecular regulation of vascular smooth muscle cell differentiation in development and disease. Physiol Rev 2004;84(3):767-801.
2. Gerthoffer WT. Mechanisms of vascular smooth muscle cell migration. Circ Res 200716;100(5):607-21.
3. Iadecola C. The pathobiology of vascular dementia. Neuron 2013;80(4):844-66.
4. Louis SF, Zahradka P. Vascular smooth muscle cell motility: From migration to invasion. Exp Clin Cardiol 2010;15(4):e75-85.
5. Khademhosseini A, Langer R, Borenstein J, Vacanti JP. Microscale technologies for tissue engineering and biology. Proc Natl Acad Sci USA 2006;103(8):2480-7.
6. Discher DE, Janmey P, Wang YL. Tissue cells feel and respond to the stiffness of their substrate. Science 2005;310:1139–43.
7. Engler AJ, Sen S, Sweeney HL, Discher DE. Matrix elasticity directs stem cell lineage specification. Cell 2006;126:677–89.
8. Wong JY, Leach JB, Brown XQ. Balance of chemistry, topography, and mechanics at the cell-biomaterial interface: issues and challenges for assessing the role of substrate mechanics on cell response. Surf Sci 2004;570:119-133.
9. Peyton SR, Putnam AJ. Extracellular matrix rigidity governs smooth muscle cell motility in a biphasic fashion. J. Cell Physiol 2005;204,198–209.
10. Peyton SR, Raub CB, Keschrumrus VP, Putnam AJ. The use of poly(ethylene glycol) hydrogels to investigate the impact of ECM chemistry and mechanics on smooth muscle cells. Biomaterials 2006;27:4881-4893.
11. Peyton SR, Kim PD, Ghajar CM, Seliktar D, Putnam A.J. The effects of matrix stiffness and RhoA on the phenotypic plasticity of smooth muscle cells in a 3-D biosynthetic hydrogel system. Biomaterials 2008;29:2597-2607.
12. Brown XQ, Ookawa K, Wong JY. Evaluation of polydimethylsiloxane scaffolds with physiologically-relevant elastic moduli: interplay of substrate mechanics and surface chemistry effects on vascular smooth muscle cell response. Biomaterials 2005;26:3125-3129.

13. Brown XQ, Bartolak-Suki E, Williams C, Walker ML, Weaver VM, Wong JY. Effect of substrate stiffness and PDGF on the behavior of vascular smooth muscle cells: implications for atherosclerosis. J Cell Physiol 2010;225(1):115-22.
14. Xu J, Chen C, Jiang X, Xu R, Tambe D, Zhang X, Liu L, Lan B, Cai K, Deng L. Effects of micropatterned curvature on the motility and mechanical properties of airway smooth muscle cells. Biochem Biophys Res Comm 2011;415(4):591-6.
15. McDaniel DP, Shaw GA, Elliott JT, Bhadriraju K, Meuse C, Chung KH, Plant AL. The stiffness of collagen fibrils influences vascular smooth muscle cell phenotype. Biophys J 2007;92(5):1759-69.
16. Smith BA, Tolloczko B, Martin JG, Grütter P. Probing the viscoelastic behavior of cultured airway smooth muscle cells with atomic force microscopy: stiffening induced by contractile agonist. Biophys J 2005;88(4):2994-3007.
17. Yim EK, Reano RM, Pang SW, Yee AF, Chen CS, Leong KW. Nanopattern-induced changes in morphology and motility of smooth muscle cells. Biomaterials 2005;26(26):5405-13.
18. Nemir S, West JL. Synthetic materials in the study of cell response to substrate rigidity. Ann Biomed Eng 2010;38(1):2-20.
19. Kloxin AM, Benton JA, Anseth KS. In situ elasticity modulation with dynamic substrates to direct cell phenotype. Biomaterials. 2010;31(1):1-8.
20. Wang S, Kempen DH, Simha NK, Lewis JL, Windebank AJ, Yaszemski MJ, Lu L. Photo-cross-linked hybrid polymer networks consisting of poly(propylene fumarate) and poly(caprolactone fumarate): controlled physical properties and regulated bone and nerve cell responses. Biomacromolecules 2008;9(4):1229-41.
21. Frey MT, Wang YL. A photo-modulatable material for probing cellular responses to substrate rigidity. Soft Matter 2009;5:1918-1924.
22. Vázquez CP, Boudou T, Dulong V, Nicolas C, Picart C, Glinel K. Variation of polyelectrolyte film stiffness by photo-cross-linking: a new way to control cell adhesion. Langmuir 2009;25(6):3556-63.
23. Cai L, Wang S. Poly(ε-caprolactone) acrylates synthesized using a facile method for fabricating networks to achieve controllable physicochemical properties and tunable cell

responses. Polymer 2010;51: 164-177.

24. Liu X, Cai L, Hao F, Cui M, Wang S. Biodegradable elastomeric substrates with controllable stiffness for regulating smooth muscle cell behavior. Polym Mater Sci Eng 2011;105:124-6.
25. Kaiser JP, Bruinink A. Investigating cell-material interactions by monitoring and analysing cell migration. J Mater Sci Mater Med 2004;15(4):429-35.
26. Tambe DT, Hardin CC, Angelini TE, Rajendran K, Park CY, Serra-Picamal X, Zhou EH, Zaman MH, Butler JP, Weitz DA, Fredberg JJ, Trepat X. Collective cell guidance by cooperative intercellular forces. Nat Mater. 2011;10(6):469-75.
27. Wong JY, Velasco A, Rajagopalan P, Pham Q. Directed movement of vascular smooth muscle cells on gradient compliant hydrogels. Langmuir 2003;19:1908–1913.
28. Wang S, Yaszemski MJ, Gruetzmacher JA, Lu L. Photo-crosslinked poly(ε-caprolactone fumarate) networks: Roles of crystallinity and crosslinking density in determining mechanical properties. Polymer 2008;49:5692-9
29. Wang S, Yaszemski MJ, Knight AM, Gruetzmacher JA, Windebank AJ, Lu L. Photo-crosslinked poly(ε-caprolactone fumarate) networks for guided peripheral nerve regeneration: Material properties and preliminary biological evaluations. Acta Biomaterialia 2009;5:1531-42
30. Cai L, Wang S. Parabolic dependence of material properties and cell behavior on the composition of polymer networks via simultaneously controlling crosslinking density and crystallinity. Biomaterials 2010;31(29):7423-34.
31. Isenberg BC, Dimilla PA, Walker M, Kim S, Wong JY. Vascular smooth muscle cell durotaxis depends on substrate stiffness gradient strength. Biophys J 2009;97(5):1313-22.
32. Cortese B, Gigli G, Riehle M. Mechanical gradient cues for guided cell motility and control of cell behavior on uniform substrates. Adv Funct Mater 2009;19:2961–2968.
33. Saez A, Buguin A, Ladoux B. Is the mechanical activity of epithelial cells controlled by deformations or forces? Biophys J 2005;89: L52-L54.
34. Dokukina IV, Gracheva ME. A model of fibroblast motility on substrates with different rigidities. Biophys J 2010;98:2794-2803.
35. Zaari N, Rajagopalan P, Kim SK, Engler AJ, Wong JY. Photopolymerization in microfluidic

gradient generators: microscale control of substrate compliance to manipulate cell response. Adv Mater 2004;16:2133-2137.

Chapter V. Photo-Cured Polymer Micro-Pillar Arrays to Control Smooth Muscle Cells

Abstract

Vascular SMCs are sensitive to the topographical features of the extracellular matrix (ECM) through the sensing molecules in cell membrane. The desirable landscape of ECM at the micron, submicron, or even nanometer scales attracts vascular cell adhesion to the surface, promotes cell proliferation and differentiation, and supports formation of functional blood vessels. Here I fabricated cylindrical pillars with three different heights of 3.4, 7.4, and 15.1 μm by photo-crosslinking PCLTA in silicon molds with predesigned micropatterns. Then I studied SMC adhesion, spreading, elongation, proliferation, and differentiation on these substrates with micro-pillar arrays. The micro-pillars were found to facilitate the cellular attachment and elongation whereas they inhibited cellular spreading and proliferation. Cell nuclei were smaller on the micro-pillar arrays than those on the flat substrates. Immuno-fluorescence imaging demonstrated that cellular filaments and punctate focal adhesions were intensely distributed around the micro-pillars. SMCs on the micro-pillar arrays had higher contractile marker expression levels, implying that the topography facilitated the phenotypic conversion from the proliferating synthetic one to the more functional contractile one.

5.1 Introduction

Cardiovascular diseases are No.1 killer in the U.S. [1]. Vascular tissue engineering is a promising solution for these diseases through developing synthetic vessel grafts. These materials should have biocompatibility, physical and chemical signal transferring abilities at the surfaces to contact biological components directly [2]. The physicochemical and geometrical properties of the substrate surface influence cellular behaviors through integrins, focal adhesions (FAs) and intracellular mechanotransduction pathways [3]. Geometric patterns at the micron and sub-micron scales of the underlying substrates and scaffolds affect the organization of cell adhesion molecular receptors and consequently cell morphology, migration, and differentiation [4-9].

Numerous novel biodegradable polymers have been developed as scaffold materials for promoting tissue formation in vascular tissue engineering [10-13]. Photo-crosslinkable poly(ε-caprolactone) triacrylates (PCLTAs) developed in our group are easy to synthesize, injectable, shapeable using stereolithography, and biodegradable through hydrolysis [14]. The mechanical properties and hydrophilicity of crosslinked PCLTA can be well modulated through controlling the crosslinking density and grafting with poly(ethylene glycol) (PEG) chains, respectively [14-16]. In our earlier study, crosslinked PCLTAs with varied crystallinities and stiffnesses were applied to regulate vascular SMC proliferation, migration, and differentiation [15]. As a widely used cell type in blood-vessel tissue engineering, SMCs are characteristic of phenotypic plasticity [17]. When there are sufficient nutrients and space in *in vivo* condition, SMCs adopt the proliferative synthetic phenotype [18]. When there is spatial limitation or nutrient shortage, the less-proliferative contractile phenotype dominates and it is essential for vascular formation and functioning. The growth and phenotypic conversion of SMCs is largely influenced by the mechanical, chemical and topographical properties of the underlying substrate [19].

In this study, I fabricated micro-pillar arrays with three pillar heights of 3.4, 7.4, and 15.1 μm by photo-crosslinking PCLTAs on different silicon molds. The morphology, hydrophilicity, and serum proteins adsorption abilities of these micro-pillar arrays and flat control samples were characterized. I further evaluated the attachment, spreading, proliferation, cytoplasm and

nuclei deformation, and phenotypic differentiation of SMCs on these substrates to achieve a better understanding of the roles of micro-pillar morphology in regulating SMC responses.

5.2 Materials and Methods

5.2.1 Polymer synthesis and fabrication of micro-pillar arrays

Ring-opening polymerization of ε-caprolactone into PCL triols was initiated by 1,1,1-tris(hydroxymethyl) propane (TMP) in the presence of $Sn(Oct)_2$ as the catalyst. Crosslinkable PCLTAs were further synthesized through acrylation of PCL triol in the presence of potassium carbonate (K_2CO_3) as the proton scavenger and purified according to our previous reports [14,15,20]. Phenyl bis(2,4,6-trimethyl benzoyl) phosphine oxide (BAPO, IRGACURE819, Ciba Specialty Chemicals, Tarrytown, NY) was used as the photo-initiator in crosslinking of PCLTAs. The solution of 1.5 g PCLTA in 500 μL CH_2Cl_2 was mixed with 75 μL of BAPO/CH_2Cl_2 (300 mg/1.5 mL) solution as the resin for crosslinking. As demonstrated in Fig. 5.1, the silicon molds with micro-pillar heights of 3.4, 7.4, and 15.1 μm were fabricated by using a standard micro-fabrication procedure including photo-lithography, physical vapor deposition, lift-off, and dry plasma etching processes [6]. Then the PCLTA/BAPO/CH_2Cl_2 mixture were poured onto the silicon molds and photo-crosslinked for 30 min under a UV lamp (SB-100P, Spectroline; wavelength = 365 nm, intensity = 4800 μw/cm^2), as described in our previous studies [14,15,20].

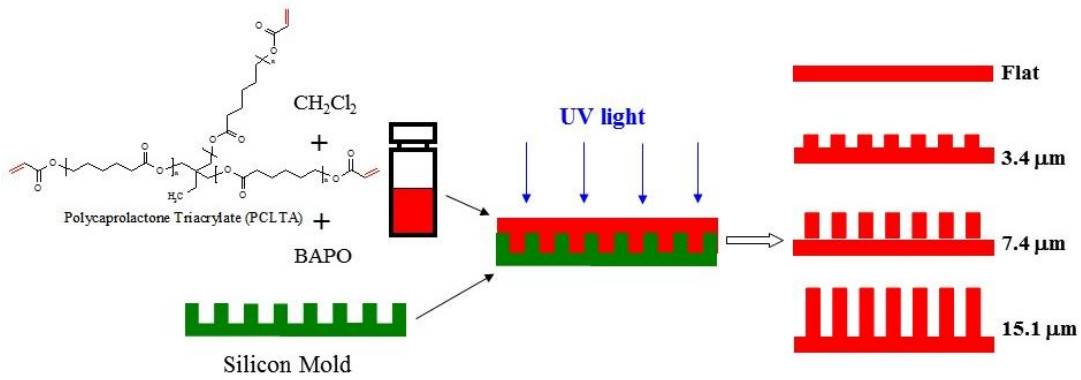

Figure 5.1 Fabrication of photo-crosslinked PCLTA substrates with micro-pillar arrays using silicon molds.

5.2.2 Characterization of polymer properties

Gel Permeation Chromatography (GPC; PL-GPC 20, Polymer Laboratories) was used to determine the molecular weights of PCLTAs with tetrahydrofuran (THF) as the eluent and standard monodisperse polystyrene samples (Polymer Laboratories) as the reference. Photo-crosslinked PCLTA micro-pillar arrays were soaked in an acetone/water (20:80) mixture for 2 days before complete drying in vacuum. The water contact angles on the substrates were determined using a Ramé-Hart NRC C.A. goniometer (Model 100-00-230, Mountain Lakes, NJ) at 37 ℃ and read and averaged over 4 droplets (20 μL for each) using ImageJ software (National Institutes of Health, Bethesda). To analyze serum protein adsorption on the surfaces, crosslinked PCLTA substrates were soaked in Dulbecco's modified eagle medium (DMEM) for 2 h. Then the substrates were washed with 1% sodium dodecyl sulfate (SDS) three times to collect the adsorbed proteins. The protein concentrations were detected on a micro-plate reader (SpectraMax Plus 384, Molecular Devices, Sunnyvale, CA) using MicroBCA protein assay kit (Pierce, Rockford, IL) [14]. The micro-pillar arrays on the substrates were characterized using scanning electron microscopy (SEM; S-3500, Hitachi Instruments, Tokyo, Japan) at a voltage of 2 kV. To obtain the edge view of the micro-pillar arrays, the substrates were frozen in liquid nitrogen for 10 min and then broken using a tweezer.

5.2.3 In vitro cell studies

Primary SMCs isolated from rat aorta were cultured in DMEM with 10% fetal bovine serum (FBS) on regular tissue culture flasks in a 5% CO_2 incubator with 95% relative humidity at 37 ℃ [21]. For the cell studies, crosslinked PCLTA substrates were cut into round disks (10 mm × 0.5 mm, diameter × thickness), sterilized in 70% alcohol solution and completely dried in vacuum. Prior to the cell studies, the substrates were attached onto the bottom of 48-well tissue culture polystyrene (TCPS) plates using autoclave-sterilized inert silicon-based grease (Dow Corning, Midland, MI). After SMCs were confluent on culture flasks, they were trypsinized, centrifuged, re-suspended in the culture media, and seeded onto the substrates at a density of 1.5×10^4 cells/cm^2. TCPS wells seeded cells at the same density in the absence of samples were used as the positive control whereas empty wells were the negative control. Then the substrates seeded with cells were incubated for 4 h and 1, 2, 4 days before the cell numbers

were determined using the MTS assay (CellTiter 96 Aqueous One Solution, Promega, Madison, WI) and the same micro-plate reader in Section 2.2 at 490 nm. For fluorescence imaging, cells on the substrates were washed twice with phosphate buffered saline (PBS) and then fixed in 4% paraformaldehyde (PFA) solution. Cellular membrane was permeabilised with 0.2% Triton X-100 for 10-20 min. To stain the filaments in cytoplasm, the fixed cells were incubated with rhodamine-phalloidin (RP) at 37 ℃ for 1 h. After that, cells were further incubated with 4',6-diamidino-2-phenylindole (DAPI) at room temperature for 10 min to stain cell nuclei. SMC images were visualized with an Axiovert 25 light microscope (Carl Zeiss, Germany). From these fluorescence cell images, cell area was determined using ImageJ and averaged over twenty single cells.

5.2.4 Characterization of focal adhesions

To characterize the focal adhesions, SMCs on the substrates were fixed and permeabilised at day 1 post-seeding, as described in Section 2.2. In order to block the unspecific antibody binding sites, cells were incubated in PBS with 1% Bovine Serum Albumin (BSA) at 37 ℃ for 1 h, as described in a previous report [22]. Then the cells were washed three times in PBS to remove BSA and incubated in monoclonal vinculin primary antibody (1:1000 in PBS; Sigma) at room temperature with gentle shaking for 2 h. After another three-time wash in PBS to remove unconjugated primary antibody, the cells were incubated in goat anti-mouse IgG secondary antibody (1:200 in PBS; Sigma) solution at room temperature for 1 h. For visualizing SMC F-actin, the cells were further stained using RP for an extra hour. The cells were then photographed on a Leica DM6000B confocal fluorescent microscope.

5.2.5 Gene expression of contractile phenotypic markers and integrins

For gene expression, SMCs were cultured on the substrates at the same density and proliferated at the same condition as described in Section 2.3. At day 1 post-seeding, the cells were trypsinized and centrifuged at 1000 rpm for 3 min. RNeasy Mini Kit (Qiagen, Valencia, CA) was used to extract the total RNA from these cells. DyNAmo cDNA synthesis kit (Thermo Scientific) was used to reverse transcript the unstable RNA into stable cDNA by following the manufacturer's instructions. The primers used in the real-time analysis process are listed as

follows: transgelin (SM-22): forward 5'-GGCAGCTGAGGATTATGGAGTCACG-3', reverse 5'-TGGGATCTCCACGGTAGTGTCCA-3'; smooth muscle myosin heavy chain (SM-MHC): forward 5'-AAGCAGCTCAAGAGGCAG-3', reverse 5'-AAGGAACAAATGAAGCCTCGTT-3'; calponin: forward 5'-AGTCTACTCTCTCTTGGCTCTGGCC-3', reverse 5'-CCTGCCTTCTCTCAGCTTCTCAGG-3'; smoothlin: forward 5'-TCGGAGTGCTGGTGAATAC-3', reverse 5'-CCCTGTTTCTCTTCCTCTGG-3'; and house-keeping gene glyceraldehyde-3-phosphate dehydrogenase (GAPDH): forward 5'-TCTTCACCACCATGGAGAA-3', reverse 5'-ACTGTGGTCATGAGCCCTT-3'. The real-time PCR reaction solution were prepared by mixing 2.5 μL of total cDNA at the same concentration of 5 ng/μL with power SYBR Green PCR Master Mix (Applied Biosystems, Warrington, UK) to make a total volume of 20 μL. A Peltier thermal cycler fluorescence detection system (MJ Research PTC-200 Thermo Cycler) was used for amplification and detecting process. The procedure for amplification was set as 5 min at 94 ℃ followed by cyclic steps of 30 s at 94 ℃, 30 s at 55 ℃, and 30 s at 72 ℃ for 30 times.

5.2.6 Calponin protein immunofluorescence staining

To substantiate the gene expression results, calponin, which is a typical SMC contractile marker, was stained for immunofluorescence imaging, as described in a previous study [23]. SMCs cultured for 4 days on the polymer substrates were fixed with 4% PFA and then stained using anti-rat calponin primary antibody produced in rabbit (sc-16604-R, Santa Cruz; 1:100 diluted in PBS) for 1 h at room temperature, followed by three-time wash with PBS. Fluorescein isothiocyanate (FITC) conjugated anti-rabbit secondary IgG antibody produced in goat (F0382; Sigma) was applied as the secondary antibody for visualization. Anti-calponin antibodies were localized in the solution of secondary antibody in PBS (1:80). The following steps were the same as described in Section 2.3, SMC nuclei were stained with DAPI for 10 min at room temperature and then imaged using an Axiovert 25 light microscope (Carl Zeiss, Germany). The protein expression levels of calponin in SMCs cultured on the polymer substrates were quantified by immunofluorescence intensity using ImageJ. The average intensity of SMCs on each sample was obtained by mean gray value 20 individual cells and then normalized to the

value on the flat PCLTA7k substrate.

5.2.7 Statistical analysis

All the statistical analysis was performed using one-way analysis of variance (ANOVA) in OriginLab software. A *p* value lower than 0.05 was considered as statistically different between two groups.

5.3 Results

5.3.1 Surface structure, hydrophilicity and protein adsorption

The surface patterns of the substrates with micro-pillar arrays were characterized using SEM, as demonstrated in Fig. 5.2. For all the three heights, the micro-pillar diameter and the inter-pillar distance were determined to be 3.7-3.8 and 2.0 μm, respectively (Fig. 5.2a-c). The tilted views of fractured substrates were also shown in Fig. 5.2d-f.

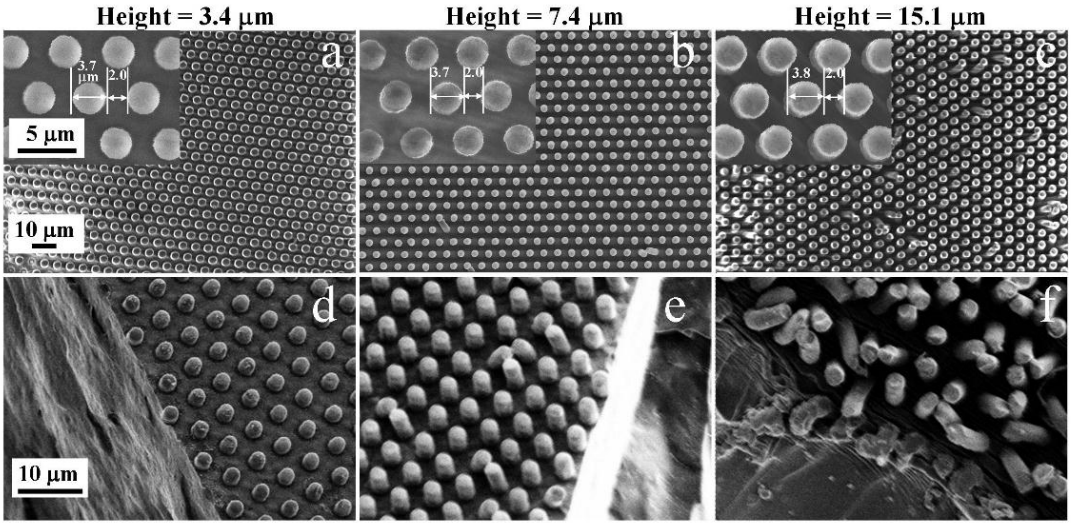

Figure 5.2 (a-c) Top-view and (d-f) edge-view SEM images of the crosslinked PCLTA substrates with micro-pillar arrays of different pillar heights of 3.4, 7.4, and 15.1 μm.

Substrate hydrophilicity was characterized using the water contact angles with the corresponding images of water droplets on different substrates shown in Fig. 5.3a and the water contact angles shown in Fig. 5.3b. The water contact angles on crystalline crosslinked PCLTA10k substrates were always higher than those on amorphous crosslinked PCLTA7k

substrates when the topography was the same. The water contact angles were higher when there were micro-pillar arrays on the substrates for both crosslinked PCLTA7k and PCLTA10k. For the same substrate material, increasing the pillar height could increase hydrophobicity, as indicated by higher water contact angles (Fig. 5.3b). These observations were consistent with several previous reports on the proportional relationship between micro-pillar height and surface hydrophobicity [24-26]. This phenomenon can be well explained by the Cassie and Baxter's model [27], with the essential equation listed in Eq. 1:

$$\cos\theta = f_{solid}\cos\theta_{s\text{-}l} + (1- f_{solid})\cos\theta_{a\text{-}l} \quad (1)$$

where θ is the overall contact angle presented on micro-pillar surfaces, $\theta_{s\text{-}l}$ is the solid-liquid contact angle on the material (crosslinked PCLTA) with a smooth surface, $\theta_{a\text{-}l}$ is the air-liquid contact angle. In a two-component system, f_{solid} is the fraction of the solid-liquid interface and $(1- f_{solid})$ is thus the air-liquid interface. At the condition when one component is air and the liquid used is pure water, $\theta_{a\text{-}l}$ is 180° with cos180 °= -1. Thus Eq. 1 is simplified to:

$$\cos\theta = f_{solid}\cos\theta_{s\text{-}l} - (1- f_{solid}) \quad (2)$$

With increasing the pillar height, the surface roughness increases and thus the fraction of the air-liquid interface is larger, as also explained previously [25,26,28]. The increased fraction of air-liquid interface results in a larger value of $(1- f_{solid})$ in the Eq. (2), rendering a higher water contact angle (θ) on the micro-pillar arrays with taller pillars.

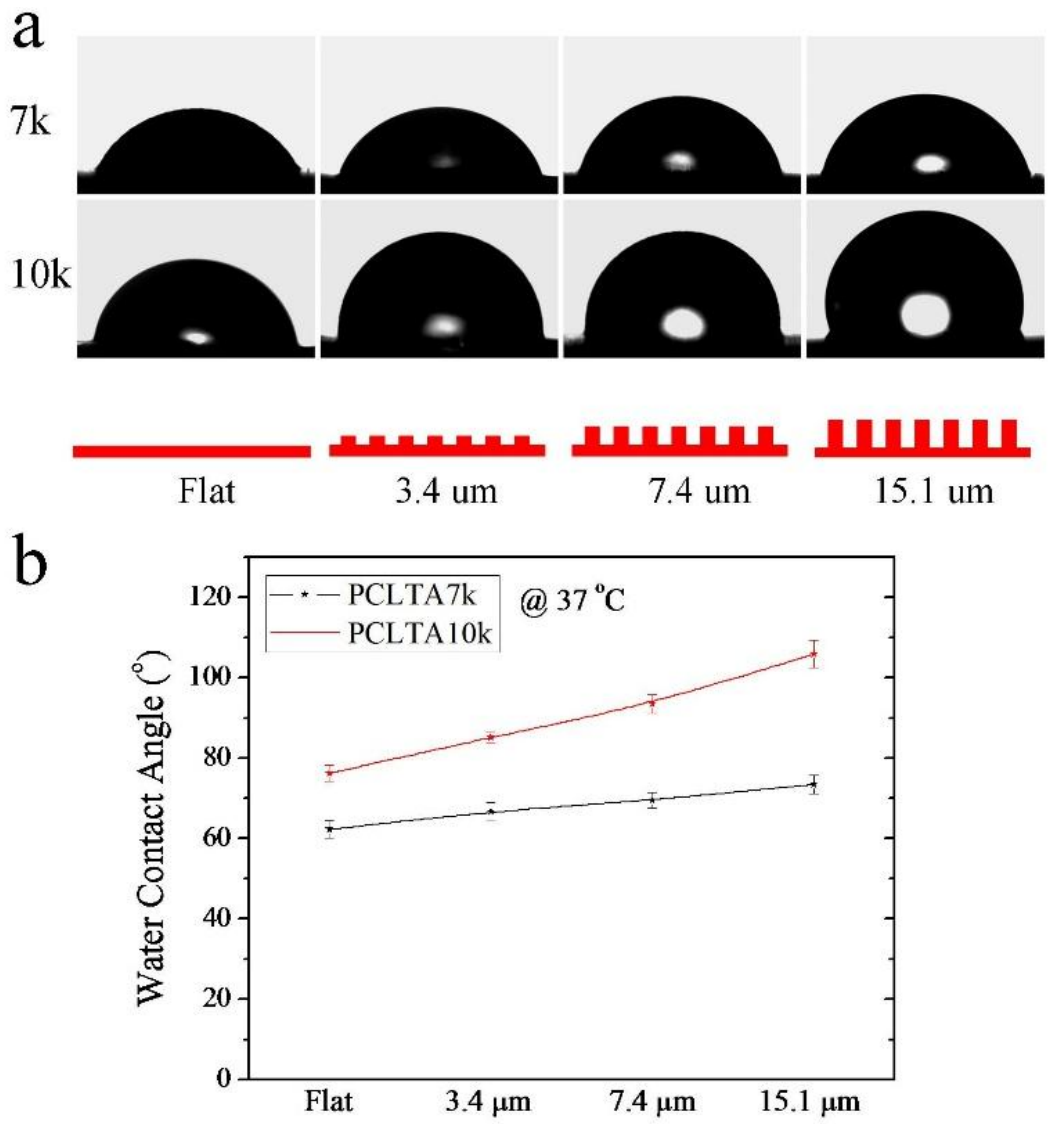

Figure 5.3 (a) Images of water droplets and (b) water contact angles on the crosslinked PCLTA7k and PCLTA10k substrates with flat surfaces or micro-pillar arrays at 37 °C.

The amounts of serum proteins adsorbed on the substrates are shown in Fig. 5.4. The values were higher on the substrates with micro-pillar arrays than that on the flat surfaces, especially when the micro-pillars were longer. When the topography was the same, substrates made from amorphous crosslinked PCLTA7k adsorbed more serum proteins than crosslinked PCLTA10k, in agreement with our previous studies [15].

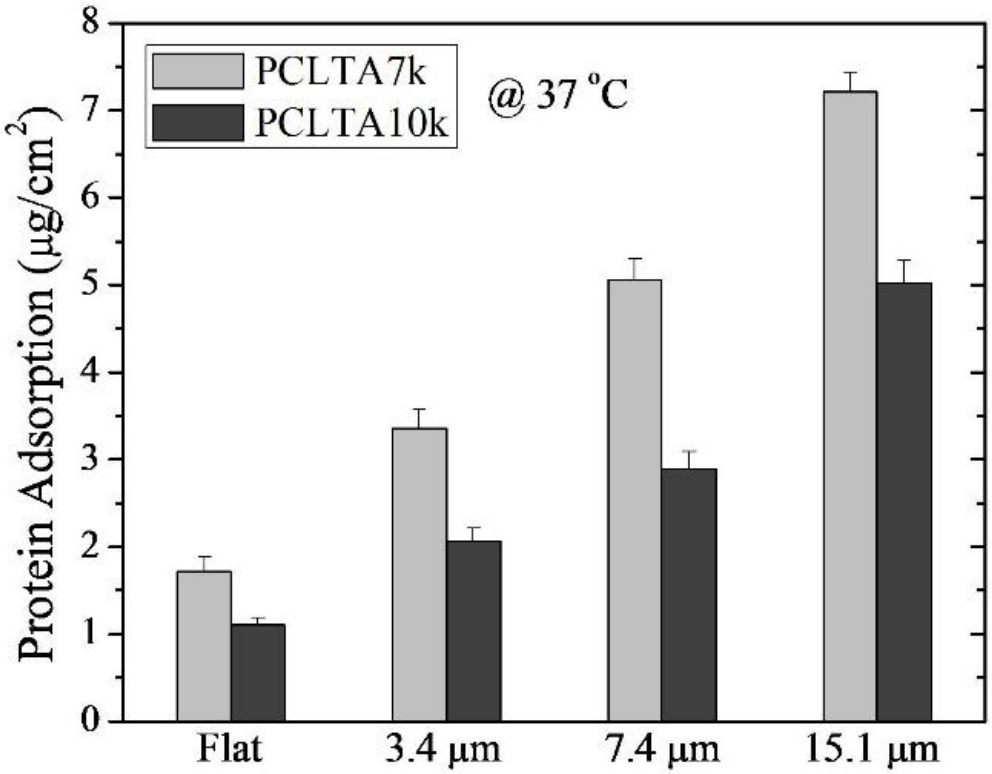

Figure 5.4 Adsorption of serum proteins from the culture media on the crosslinked PCLTA substrates with flat surfaces or micro-pillar arrays.

5.3.2 SMC behaviors on the micro-pillar substrates

At 4 h post-seeding, SMC attachment to the substrates normalized to the value on TCPS was determined, as shown in Fig. 5.5a. SMC attachment increased from 0.28 ± 0.02 on flat amorphous crosslinked PCLTA7k substrate to 0.42 ± 0.04, 0.48 ± 0.07, and 0.58 ± 0.05 for the substrates with 3.4, 7.4, and 15.1 μm micro-pillars, respectively. For crystalline crosslinked PCLTA10k, the value increased from 0.47 ± 0.03 to 0.62 ± 0.04, 0.74 ± 0.05, and 0.86 ± 0.07, respectively. In contrast to cell attachment, SMC spreading represented by the cell spread area in Fig. 5.5b was inhibited by the micro-pillars. This inhibition was more evident when the micro-pillars were longer for both crosslinked PCLTA7k and 10k, although the values were always higher on the later.

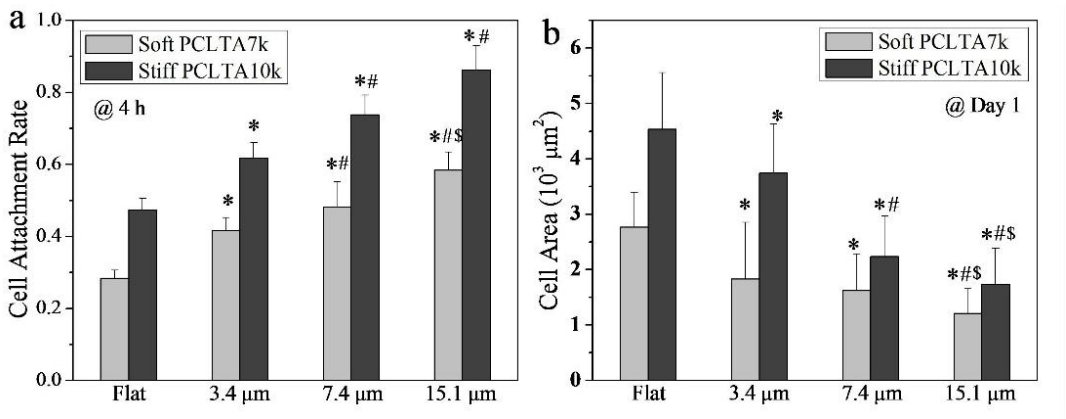

Figure 5.5 (a) SMC attachment rates on the crosslinked PCLTA substrates with flat surfaces and micro-pillar arrays relative to TCPS, the positive control. (b) SMC spread areas on the crosslinked PCLTA substrates with flat surfaces and micro-pillar arrays. *: $p < 0.05$ relative to the flat substrates; #: $p < 0.05$ relative to 3.4 μm micro-pillar substrates; $: $p < 0.05$ relative to 7.4 μm micro-pillar substrates.

To characterize the stretching effect of micro-pillar arrays on the cells, I calculated the circularity and major/minor axis ratio of SMCs on the substrates by using the equation of $4\pi \times \text{area/perimeter}^2$ and dividing the cell length by the width, respectively. For flat substrates, the major/minor axis ratio was 2.1 ± 0.8 and 2.4 ± 0.9 for crosslinked PCLTA7k and PCLTA10k, respectively. The major/minor axis ratio increased with increasing the pillar height (Fig. 5.6a). Unlike the major/minor axis ratio, the circularity of the SMCs decreased with increasing the micro-pillar height from the high values of 0.71 ± 0.12 and 0.66 ± 0.14 on flat substrates of crosslinked PCLTA7k and PCLTA10k, respectively (Fig. 5.6b). Both the major/minor axis ratio and circularity discussed above showed that SMCs were deformed by the underlying micro-pillar arrays, especially by the longer micro-pillars.

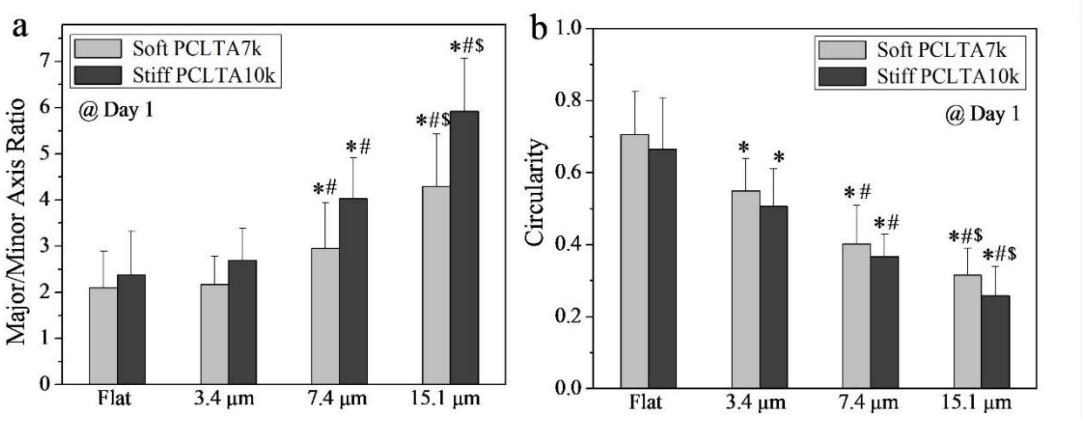

Figure 5.6 (a) Major/minor axis ratio and (b) circularity of the SMCs on the crosslinked PCLTA substrates with flat surfaces and micro-pillar arrays. *: $p < 0.05$ relative to the flat substrates; #: $p < 0.05$ relative to 3.4 μm micro-pillar substrates; $: $p < 0.05$ relative to 7.4 μm micro-pillar substrates.

Compared with the enhanced attachment by the micro-pillars, SMC proliferation however was inhibited. Although the cell numbers at day 1 on the micro-pillar arrays were higher than that on the flat substrates of crosslinked PCLTA7k (Fig. 5.7a), the proliferation index (PI) of SMCs calculated by dividing the cell number at day 1 by that at 4 h decreased (Fig. 5.7b). The SMC number on the flat substrate was similar to that on the micro-pillar arrays at day 2 and it became even higher at day 4 (Fig. 5.7a). The PI values based on the cell numbers at days 1, 2, and 4 were lower on micro-pillar arrays than on the flat substrates (Fig. 5.7b). SMC growth rate calculated by dividing ln(PI) by the time showed the same trend as the PI (Fig. 5.7b). The doubling time of the SMCs, i.e., the time needed for the cells to double their number, increased with increasing the micro-pillar length at all the time points (Fig. 5.7b). Cell images in Fig. 5.7c were consistent with the cell proliferation. On the flat substrate, cell number evidently increased from day 1 to day 4 but this trend was much weaker on the micro-pillar arrays.

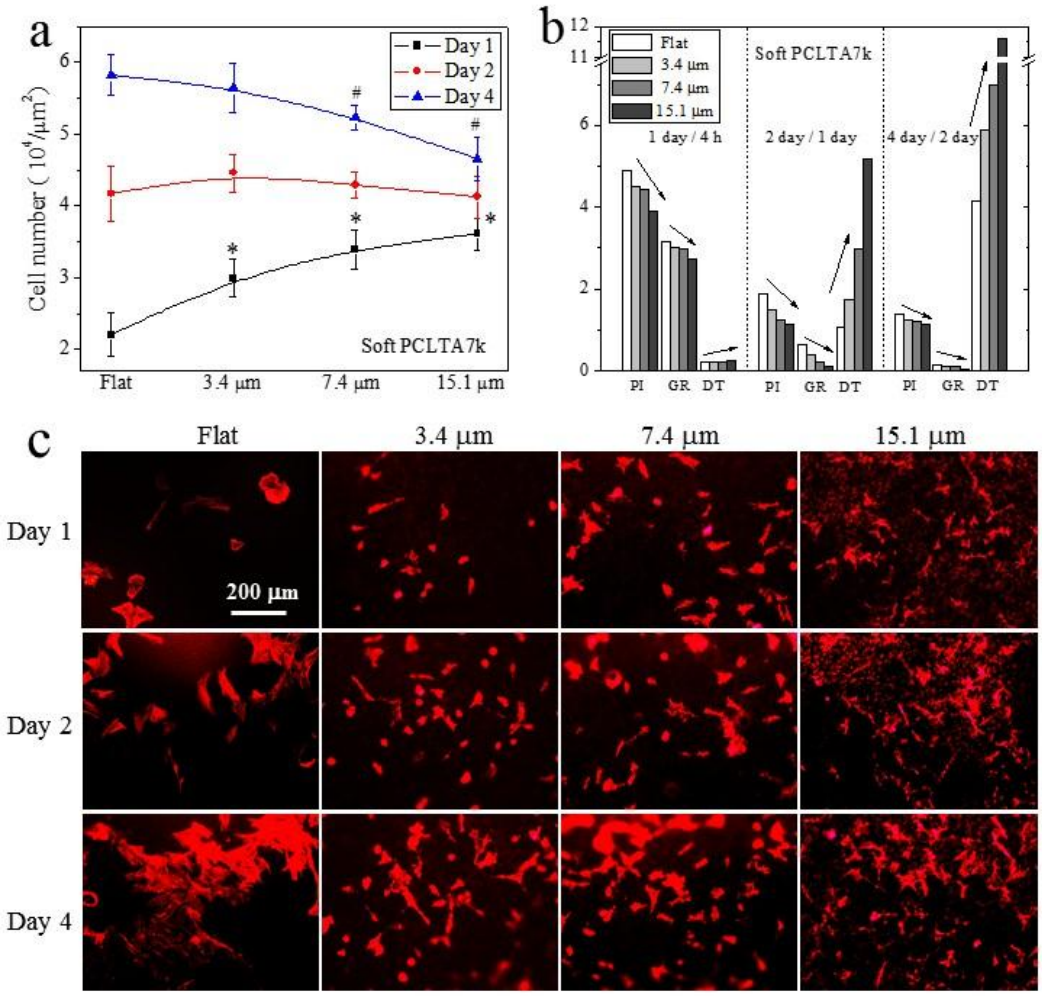

Figure 5.7 (a) SMC numbers at days 1, 2, and 4 post-seeding on the crosslinked PCLTA7k substrates with flat surfaces and micro-pillar arrays. (b) The proliferation index (PI), growth rate (GR) and doubling time (DT) of SMCs on these substrates. (c) Fluorescence images of SMCs on these substrates. *: $p < 0.05$ relative to the flat substrate (higher); #: $p < 0.05$ relative to the flat substrate (lower).

The SMCs on stiffer substrates of crosslinked PCLTA10k exhibited a similar proliferation ability, which was also inhibited by the micro-pillars in a stronger manner, as indicated by the lower PI, lower growth rate, and longer doubling time (Fig. 5.8a,b). The cell images in Fig. 5.8c were consistent with the data in Fig. 5.8a,b and also showed that the cells were highly stretched by the micro-pillar arrays while those on the flat substrate were well spread with a larger cell area.

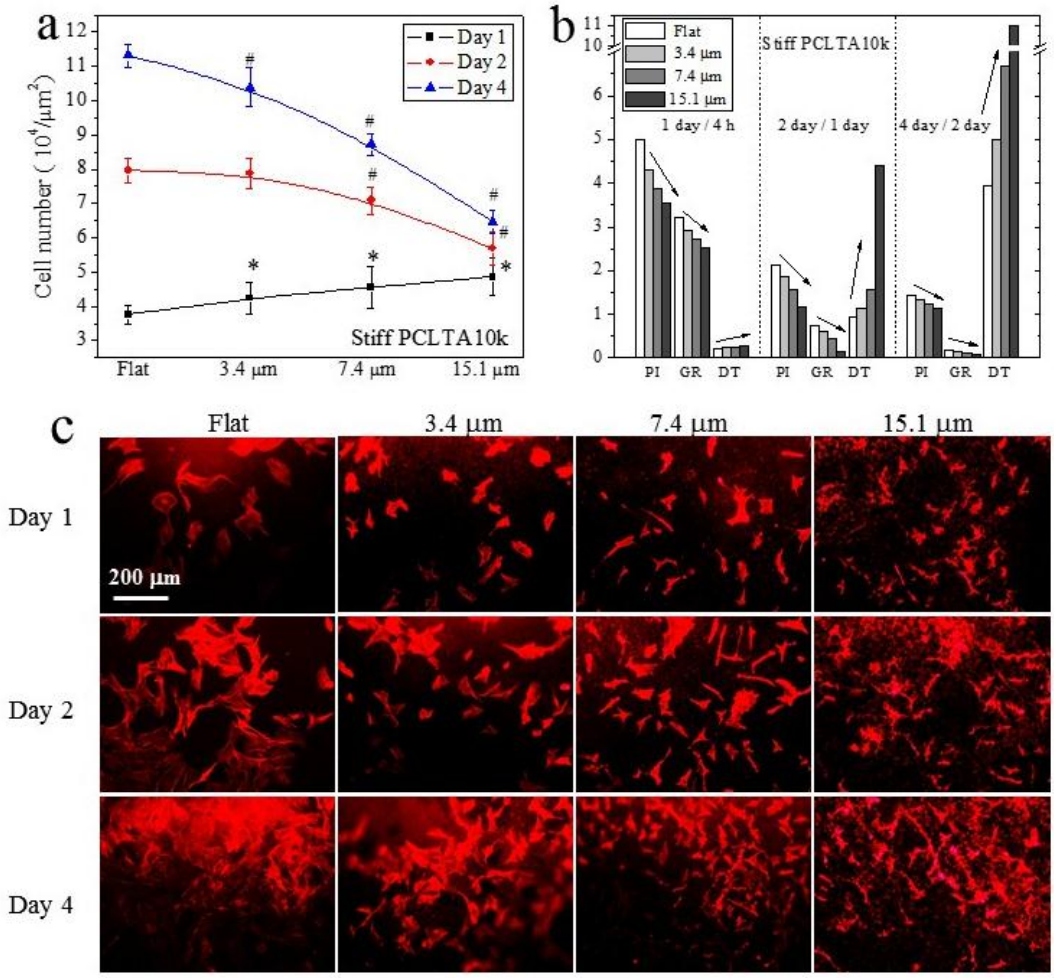

Figure 5.8 (a) SMC numbers at days 1, 2, and 4 post-seeding on the crosslinked PCLTA10k substrates with flat surfaces and micro-pillar arrays. (b) The proliferation index (PI), growth rate (GR) and doubling time (DT) of SMCs on these substrates. (c) Fluorescence images of SMCs on these substrates. *: $p < 0.05$ relative to the flat substrate (higher); #: $p < 0.05$ relative to the flat substrate (lower).

5.3.3 Cell and nuclei morphologies on the micro-pillar substrates

The SEM images of individual SMCs on the substrates in Fig. 5.9 were consistent with the fluorescence images discussed in Section 3.2. SMCs on flat crosslinked PCLTA7k were better spread than those on the micro-pillar arrays, especially when the micro-pillars were longer. Evidently the cells on flat stiffer crosslinked PCLTA10k were better spread than on flat crosslinked PCLTA7k. In contrast, SMCs were stretched and protruded their cytoplasm on the micro-pillar arrays as the inter-pillar gaps inhibited cell spreading and guided cytoplasm

extension and migration.

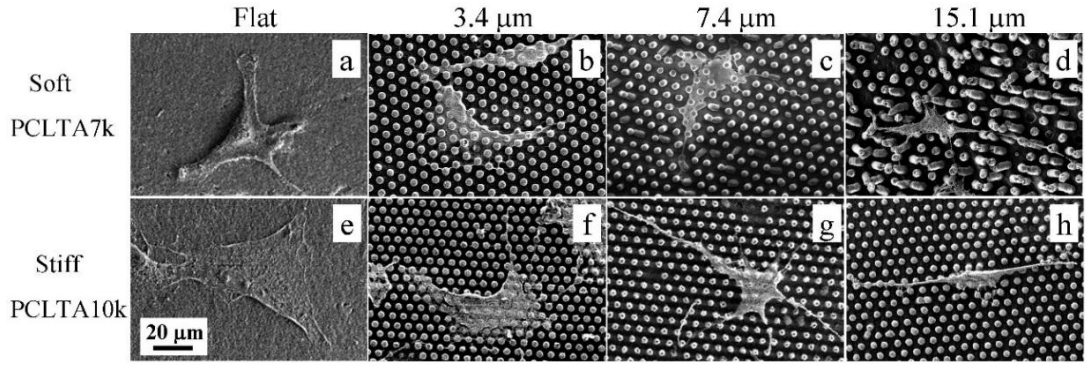

Figure 5.9 SEM images of SMCs on the (a-d) crosslinked PCLTA7k and (e-f) crosslinked PCLTA10k substrates with flat surfaces and micro-pillar arrays.

Filament development was visualized and quantified in RP-stained SMCs on the micro-pillar arrays in Fig. 5.10. SMCs on flat crosslinked PCLTA7k had regular distribution of filaments (Fig. 5.10a), as reported in our previous studies [Liu X 6 PCLTAs]. Meanwhile, the cells on the micro-pillar arrays showed bright dots around micro-pillars (Fig. 5.10b-d, green arrows) and dark dots on the micro-pillar points (Fig. 5.10b-d, white arrows). This phenomenon was more prominent for the cells on stiffer substrates of crosslinked PCLTA10k. For example, SMCs on crosslinked PCLTA10k 15.1-μm-high micro-pillar arrays were highly stretched with intensive bright fluorescence circles around the micro-pillars and weak dark fluorescence dots on the top of the pillars. This result indicated that cytoplasm was largely developed in the inter-pillar spaces with a small portion on the pillar top. To better illustrate the scenarios, schemes are shown in Fig. 5.10i-l. The cytoplasm of SMCs was uniformly supported by the flat substrate but it was mainly supported by the pillars and trapped in the inter-pillar spaces on the micro-pillar arrays. The situation was worse when the micro-pillars were longer because more cytoplasm was trapped between the pillars. The trapped cytoplasm resulted intensive bright fluorescence around the pillars.

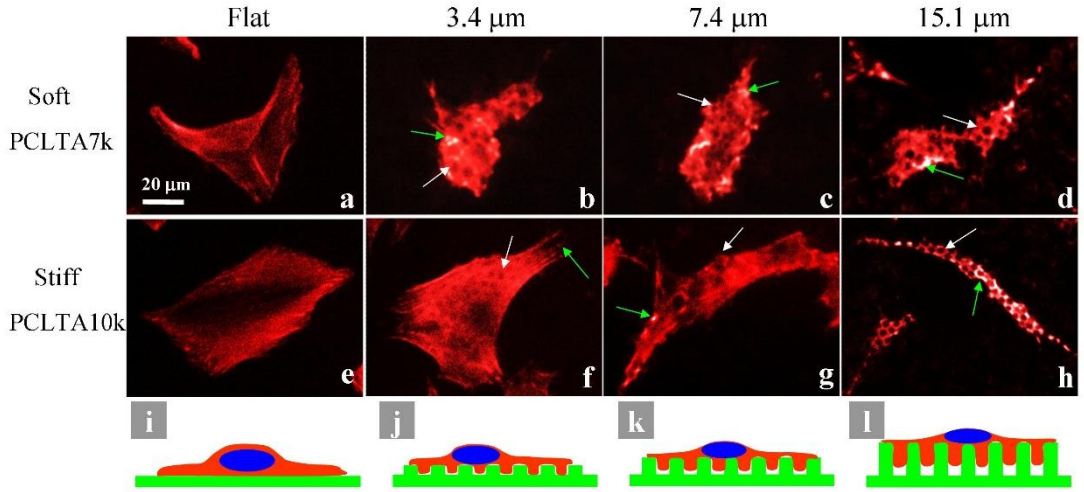

Figure 5.10 Fluorescence images of SMCs on the (a-d) crosslinked PCLTA7k and (e-f) crosslinked PCLTA10k with flat surfaces and micro-pillar arrays. The bottom schemes (i-l) demonstrate possible cell morphologies on the polymer substrates with flat surfaces or micro-pillar arrays of different pillar heights.

SMC nuclei at day 1 were also imaged and characterized on the substrates. As shown in Fig. 5.11a, cell nuclei on the flat substrates were round with a high fluorescence intensity. In contrast, cell nuclei on the micro-pillar substrates were smaller with weaker fluorescence and the nuclear size decreased with increasing the micro-pillar height (Fig. 5.11b). The circularities of cell nuclei, however, were similar among all the substrates except that the value on the 15.1-μm micro-pillar arrays was significantly lower, in both cases of crosslinked PCLTA7k and 10k (Fig. 5.11c).

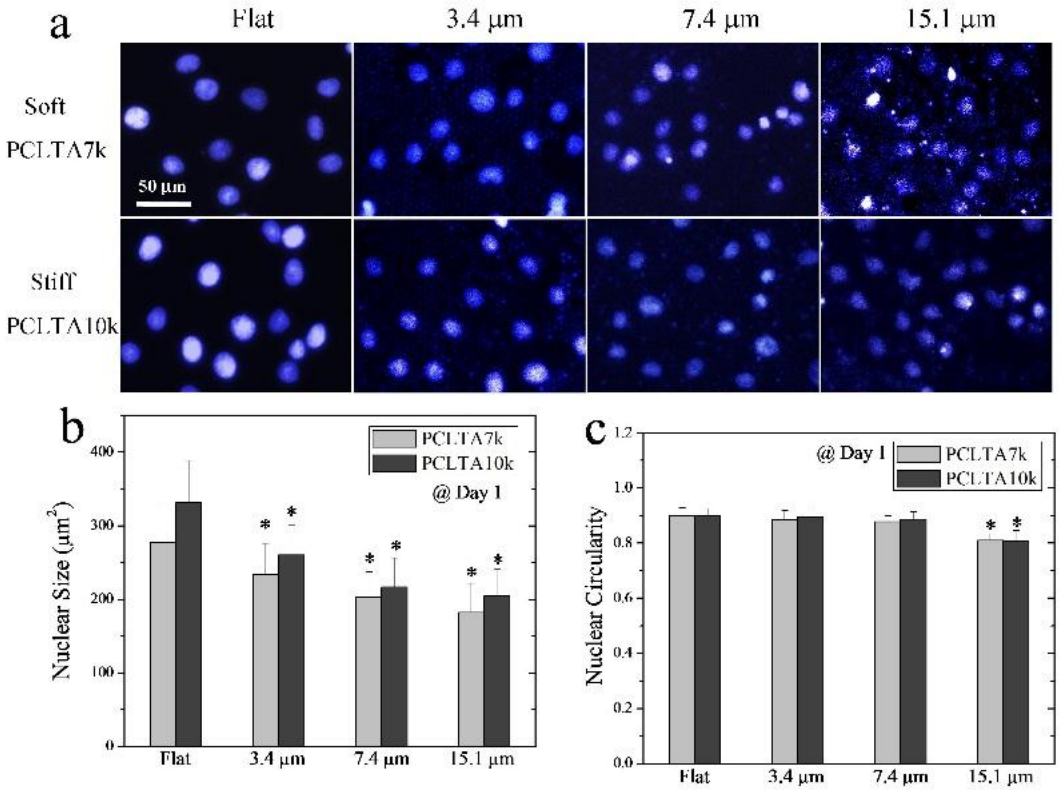

Figure 5.11 (a) Fluorescence images, (b) Size, and (c) circularity of SMC nuclei on the crosslinked PCLTA7k and PCLTA10k substrates with flat surfaces and micro-pillar arrays. *: $p < 0.05$ relative to flat substrates.

5.3.4 Focal adhesions in SMCs

Mammalian cells use focal adhesions, which are dynamic macromolecular assemblies composed of focal adhesion kinases, paxillins, vinculins and other adapter proteins, to help themselves adhere on the underlying substrate and sense the surrounding environment [29]. Strong focal adhesions normally develop on the cell periphery and have the abilities in responding to intracellular signals and adjusting their size and morphology correspondingly [30]. The changes in focal adhesions give further responsive signals to the intracellular signaling pathways, which ultimately influence cellular behavior vie mechanotransduction [31]. Here in this study, SMCs cultured on the flat substrate developed large, well-elongated focal adhesions, as shown in Fig. 5.12a. In contrast, SMCs cultured on the micro-pillar substrates were only able to develop weaker, irregular focal adhesions (Fig. 5.12b-d). The enlarged images showed clear focal adhesion dots on the flat substrate in Fig. 5.12e but weak dots on the micro-

pillar ones in Fig. 5.12f-h, which might be a reason for the slower proliferation on the micro-pillar substrates discussed in Section 3.2.

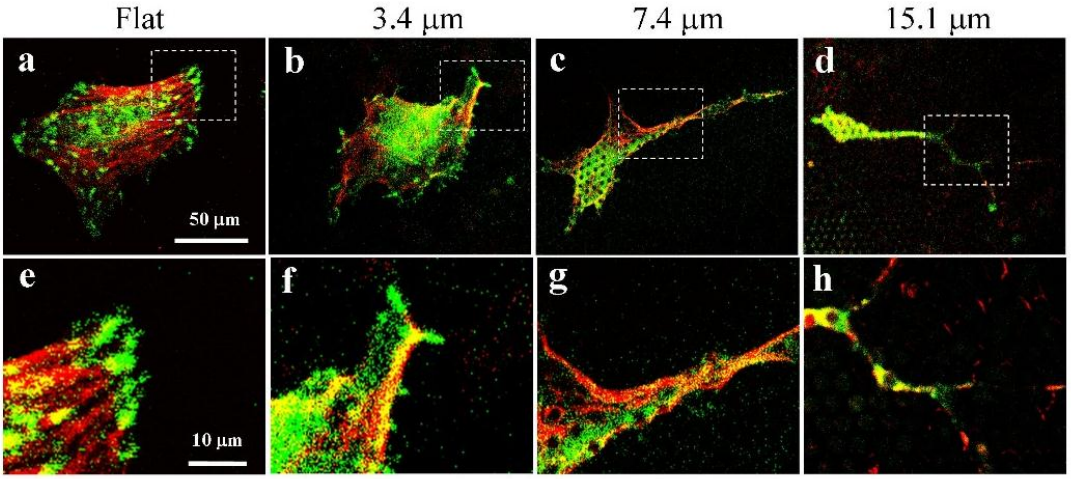

Figure 5.12 (a-d) Images of focal adhesions in SMCs on the crosslinked PCLTA10k substrates with flat surfaces and micro-pillar arrays, as visualized using vinclulin (green) and filaments (red). (e-f) Enlarged focal adhesion dots (green) in SMCs from the dotted rectangular areas in the corresponding images above them.

5.3.4 Phenotypic conversion abilities of SMCs

SMCs in proliferation have the ability in modulating their synthetic and contractile phenotypes by responding to changes in environmental conditions [32]. A commonly used method to define SMC phenotypes is characterization the levels of contractile phenotypic markers in the cells, which include α-smooth muscle actin (α-SMA), SM-MHC, smoothlin, SM22 and calponin [33]. These proteins are important in SMC contraction, either as structural components for contractile apparatus or as regulators in the contracting process. When one phenotype is converted to the other, SMCs express different levels of these phenotypic marker proteins. Therefore, the gene/protein expression levels of these markers in SMCs on different substrates can be used to determine their phenotypic conversion abilities.

The real-time PCR analysis of the expression of four typical contractile markers (SM-MHC, smoothlin, trangelin and calponin) using GAPDH as the reference is shown in Fig. 5.13. The expression levels of these four markers were all higher on 7.4 and 15.1 μm micro-pillar

substrates compared with those of the flat and 3.4 μm micro-pillar substrates (Fig. 5.13a-d), in both cases of crosslinked PCLTA7k and 10k, suggesting that micro-pillars could be used for phenotypic conversion. Together with the inhibited SMC proliferation in Section 3.2, these results suggested that long micro-pillars inhibited proliferative SMC spreading and proliferation, but facilitated their conversion into the functional contractile phenotype.

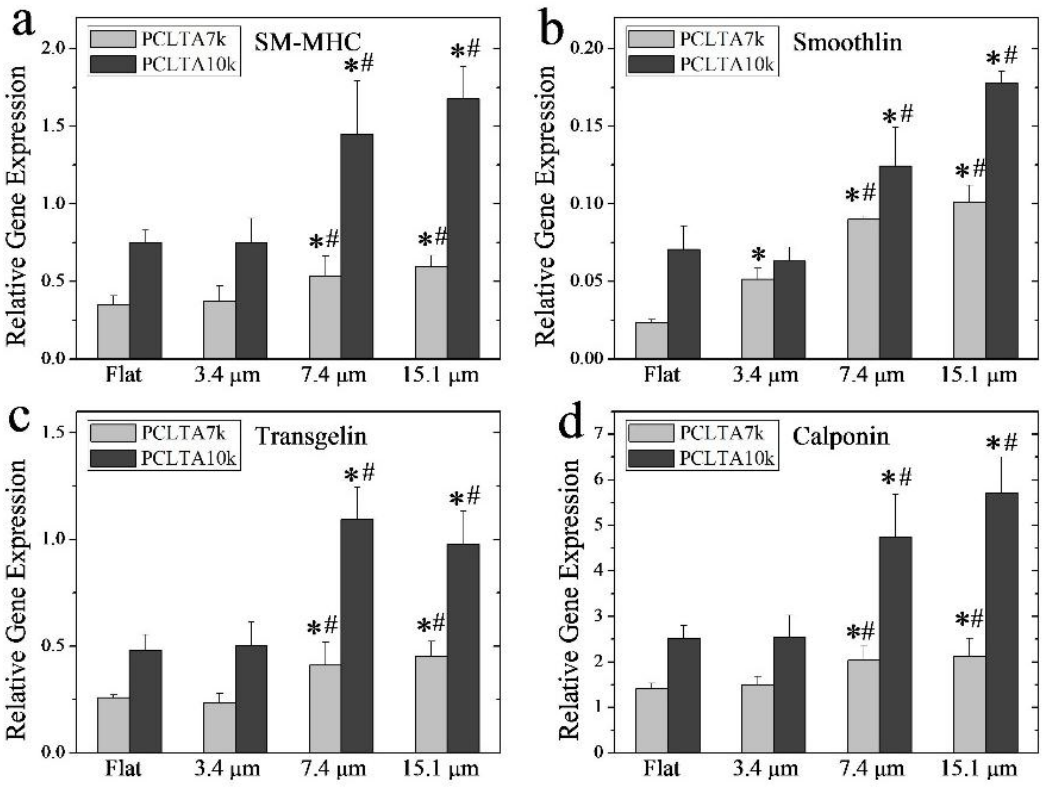

Figure 5.13 Relative gene expression levels of four contractile gene markers: (a) SM-MHC, (b) smoothlin, (c) transgelin, and (d) calponin using real-time PCR analysis. *: $p < 0.05$ relative to the flat substrates. #: $p < 0.05$ relative to 3.4 μm micro-pillar substrates.

The levels of calponin, an essential contractile phenotypic marker, in SMCs on the substrates were analyzed using fluorescence immunostaining. As shown in Fig. 5.14a,b, the calponin and cell nuclei in SMCs were visualized using green and blue fluorescence markers, respectively. The images showed consistent trends in SMC proliferation and spreading with those of Figs. 5.7c and 5.8c in Section 3.2, i.e., the cell numbers were lower and the cell spread areas were smaller on the micro-pillar substrates than on the flat substrates, for both crosslinked

PCLTA7k (Fig. 5.14a) and PCLTA10k (Fig. 5.14a). However, a larger fraction of SMCs showed contractile protein fluorescence on the micro-pillar substrates than on the flat substrates (Fig. 5.14c). In addition, the average immunofluorescence intensities were significantly stronger in SMCs cultured on the micro-pillar substrates with pillar heights of 7.4 and 15.1 μm than on the flat substrates (Fig. 5.14d). These results confirmed the conclusion from gene expression data in Fig. 5.13 that the micro-pillar substrates could support better conversion from the synthetic phenotype to the contractile one.

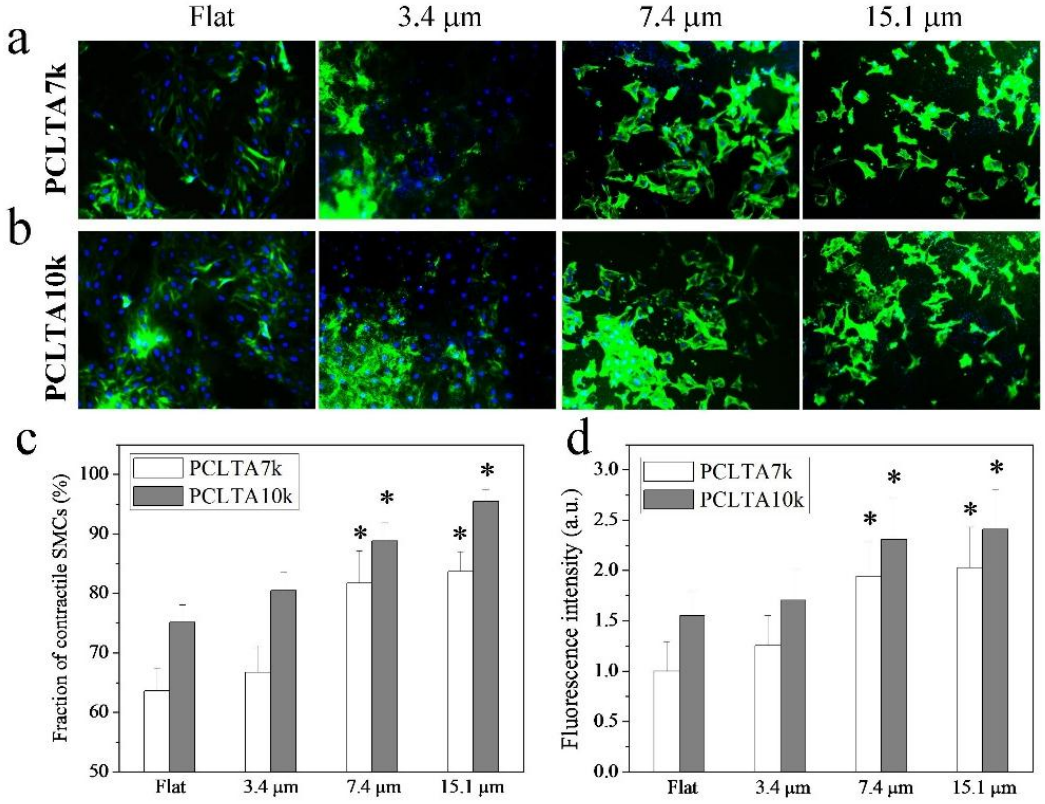

Figure 5.14 Immunostaining of contractile marker calponin protein (green) and nuclei (blue) in SMCs on the substrates of (a) crosslinked PCLTA7k and (b) crosslinked PCLTA10k with flat surfaces and micro-pillar arrays. (c) Percentage of contractile phenotypic SMCs at day 4 post-seeding determined from immunofluorescence images in (a) and (b). (d) Immunoflucorescence intensities of calponin protein stains in SMCs on the substrates, normalized by the value in SMCs on the flat substrate of cross-linked PCLTA7k. *: $p < 0.05$ relative to the flat substrates.

5.4 Discussion

As stated in an earlier report, micro-pillar arrays made from the same material but with different pillar lengths can be used to distinguish the role of substrate stiffness in regulating cell behavior from other material properties [34]. Initially I attempted to use the current micro-pillar arrays made from crosslinked PCLTA for the same purpose for SMCs. However, I found different results because of the larger inter-pillar space. The initial SMC attachment onto the micro-pillar substrates was significantly higher than that on a flat substrate, which can be interpreted as the micro-pillars could provide more contacting sites on the side walls [35]. Therefore, cells have better interactions with substrates and attach more strongly [36]. In contrast, SMC proliferation and spreading on the substrates with longer pillars were lower than those on the flat one. This phenomenon was also observed in previous studies [37-39]. Well spread cells on a large substrate area were reported to proliferate better than those poorly extended cells confined in a limited area and cell shape was tightly coupled to DNA synthesis and growth in cells [40], which was substantiated by further studies [41-44].

Cells grow and divide through regular cell-division cycle, including phases of G1, S, G2, and mitosis, which are influenced by types of factors, including cell adhesion, tension and shape changes [41,43]. Cell spreading was found to influence the cell-cycle as that 85% of the cells with a spread area larger than 300 μm^2 entered S-phase, whereas only 10% of those with an area smaller than 100 μm^2 did so in the same environment [45]. The above correlation between cell shape and cell cycle was also found in this study. SMCs cultured on the flat substrates were well spread and proliferated faster, whereas those on the substrates with long micro-pillars did not spread sufficiently. The nuclei of SMCs in this study were also deformed on the substrates with 15.1 μm pillars, in agreement with previous finding that microstructured surfaces cause severe deformation of cell nuclei [46,47]. The inhibited cell spreading could discourage the cells from entering the S-phase and decreased the proliferation rate of SMCs.

SMCs in this study exhibited different morphologies on the different substrates as that long micro-pillars (7.4 and 15.1 μm) guided SMCs to protrude in certain directions and aligned the cell body. In a previous study, SMCs also exhibited linear shapes by orienting along the lines on both poly(methyl methacrylate) (PMMA) and poly(dimethylsiloxane) (PDMS)

substrates with nanopatterned gratings (350 nm for linewidth, 700 nm for pitch, and 350 nm for depth) [48]. When the mico-pillars were shorter (3.4 μm), cell stretching and deformation were less significant and cell proliferation and spreading were better than those longer micro-pillars. Similar observation was reported on fibroblasts cultured on silicon substrates with pillars of 1, 5, and 10 μm high [39].

In addition, the distribution of filaments and focal adhesions in SMCs were influenced remarkably by the micro-pillar arrays as they were intensively anchored at the periphery of the pillar and the inter-pillar spaces, especially when the micro-pillars were longer. These observations were consistent with early studies on cell focal adhesions and mechanical behaviors on silicon elastomer substrates with deformable micro-pillars (1-2 μm, diameter; 1.6-6 μm, height) [49]. This phenomenon was called as topographical compensation because flat surfaces could not provide this effect in changing cell deformation and mechanical responses while micron-scale surface features can influence microfilaments, focal adhesions, and microtubules in cells [50-53]. A theoretical "*tensegrity*" model was proposed to summarize and explain mechanochemical transduction and morphogenetic regulation changes inside a cell when responding to external signals [54]. Cytoskeleton is dynamic and actin polymerization/depolymerization occurs all the time. External signals including environmental chemistry and structures are transduced to the focal adhesions and actin filaments in cells [55]. In this study, substrates with longer micro-pillars cause more severe topographical influences on the cells than the flat ones and thus the cell architecture on the micro-pillar arrays was rearranged to adapt the discontinuities.

The present study provides an insight into the understanding about the internal mechanisms in how topography can be used to regulate vascular cells, in particular, SMCs. It also serves in improving the strategies for designing and fabricating vascular grafts or scaffolds by using a convenient photo-crosslinkable and biodegradable polymer system with mechanical properties that can be modulated over a wide range of 1-200 MPa [15]. In future studies, the inter-pillar space can be reduced to ensure that SMCs are not trapped inside the spaces to experience the same topographical effect of the micro-pillar tops but different mechanical signals as different pillar heights result in different stiffness/compliance.

5.5 Conclusions

This study supplied a facial replica molding method to fabricate biodegradable photo-crosslinked PCLTA substrates with micro-pillar arrays and used them to regulate SMCs. The micro-pillar arrays significantly influenced surface hydrophilicity, protein adsorption, and SMCs on these substrates. The effects were highly related to the pillar height as the substrates with longer micro-pillars adsorbed more serum proteins and supported better SMC attachment than the others. However, the higher pillars inhibited both SMC spreading and proliferation, and deformed cell cytoplasm and nucleus more severely. Immunofluorescence and SEM images indicated that SMCs cultured on the high pillar arrays were positioned on the top of the pillars, aligned and stretched to a linear, narrow morphology. Focal adhesions in SMCs were formed around the periphery of the pillars where high tension exists. Gene and protein analysis of four phenotypic contractile markers, i.e., SM-MHC, smoothlin, transgelin, and calponin, showed that SMCs on the higher-pillar substrates converted more effectively into the functional contractile phenotype, in contrast with the cells undergoing fast growth on the flat and shorter-pillar ones.

References

1. Go AS, Mozaffarian D, Roger VL, Benjamin EJ, Berry JD, Borden WB, et al. American Heart Association Statistics Committee and Stroke Statistics Subcommittee. Heart disease and stroke statistics--2013 update: a report from the American Heart Association. Circulation 2013;127(1):e6-e245
2. Harbers GM, Grainger DW. Cell-material interactions: fundamental design issues for tissue engineering and clinical considerations. In: Guelcher SA, Hollinger JO, editors. Introduction to biomaterials. Boca Raton: CRC Press; 2005. p.15-45.
3. Ingber DE. Cellular mechanotransduction: putting all the pieces together again. FASEB J 2006;20:811-27.
4. Nikkhah M, Edalat F, Manoucheri S, Khademhosseini A. Engineering microscale topographies to control the cell-substrate interface. Biomaterials 2012;33(21):5230-46.
5. Cai L, Zhang L, Dong J, Wang S. Photocured biodegradable polymer substrates of varying stiffness and microgroove dimensions for promoting nerve cell guidance and differentiation. Langmuir 2012;28(34):12557-68.
6. Wang K, Cai L, Zhang L, Dong J, Wang S. Biodegradable photo-crosslinked polymer substrates with concentric microgrooves for regulating MC3T3-E1 cell behavior. Adv Healthcare Mater 2012;1(3):292-301.
7. Gittens RA, McLachlan T, Olivares-Navarrete R, Cai Y, Berner S, Tannenbaum R, et al. The effects of combined micron-/submicron-scale surface roughness and nanoscale features on cell proliferation and differentiation. Biomaterials 2011;32(13):3395-403.
8. Biela SA, Su Y, Spatz JP, Kemkemer R. Different sensitivity of human endothelial cells, smooth muscle cells and fibroblasts to topography in the nano-micro range. Acta Biomater 2009;5(7):2460-6.
9. Uttayarat P, Perets A, Li M, Pimton P, Stachelek SJ, Alferiev I, et al. Micropatterning of three-dimensional electrospun polyurethane vascular grafts. Acta Biomater 2010;6(11):4229-37.
10. Kim BS, Putnam AJ, Kulik TJ, Mooney DJ. Optimizing seeding and culture methods to engineer smooth muscle tissue on biodegradable polymer matrices. Biotechnol Bioeng

1998;57(1):46-54.

11. Timmer MD, Shin H, Horch RA, Ambrose CG, Mikos AG. In vitro cytotoxicity of injectable and biodegradable poly(propylene fumarate)-based networks: unreacted macromers, cross-linked networks, and degradation products. Biomacromolecules 2003;4:1026-33.
12. Hua J, Sun X, Ma H, Xie C, Chen YE, Ma PX. Porous nanofibrous PLLA scaffolds for vascular tissue engineering. Biomaterials 2010;31:7971-7.
13. Qu XH, Wu Q, Liang J, Zou B, Chen GQ. Effect of 3-hydroxyhexanoate content in poly(3-hydroxybutyrate-co-3-hydroxyhexanoate) on in vitro growth and differentiation of smooth muscle cells. Biomaterials 2006;27:2944-50.
14. Cai L, Wang S. Poly(ε-caprolactone) acrylates synthesized using a facile method for fabricating networks to achieve controllable physicochemical properties and tunable cell responses. Polymer 2010;51:164-77.
15. Liu X, Cai L, Hao F, Cui M, Wang S. Biodegradable elastomeric substrates with controllable stiffness for regulating smooth muscle cell behavior. Polym Mater Sci Eng 2011;105:124-6.
16. Liu X, Cai L, Wang S. Smooth muscle cell behavior on crosslinked poly(epsilon-caprolactone) triacrylate networks grafted with methoxy poly(ethylene glycol) monoacrylate of various composition and chain length. Abstracts of Papers of the American Chemical Society 2012;243.
17. Niklason LE, Gao J, Abbott WM, Hirschi K, Houser S, Marini R, et al. Functional arteries grown in vitro. Science 1999;284:489-93.
18. Owens GK. Regulation of differentiation of vascular smooth muscle cells. Physiol Rev 1995;75(3):487-517.
19. Wong JY, Leach JB, Brown XQ. Balance of chemistry, topography, and mechanics at the cell-biomaterial interface: issues and challenges for assessing the role of substrate mechanics on cell response. Surf Sci 2004;570:119-33.
20. Cai L, Wang K, Wang S. Poly(ethylene glycol)-grafted poly(propylene fumarate) networks and parabolic dependence of MC3T3 cell behavior on the network composition. Biomaterials 2010;31:4457-66.

21. Wang K, Cai L, Hao F, Xu X, Cui M, Wang S. Distinct cell responses to substrates consisting of poly(ε-caprolactone) and poly(propylene fumarate) in the presence or absence of cross-links. Biomacromolecules 2010;11:2748-59.
22. Peyton SR, Raub CB, Keschrumrus VP, Putnam AJ. The use of poly(ethylene glycol) hydrogels to investigate the impact of ECM chemistry and mechanics on smooth muscle cells. Biomaterials 2006;27:4881-93.
23. Wang C, Yin S, Cen L, Liu Q, Liu W, Cao Y, et al. Differentiation of adipose-derived stem cells into contractile smooth muscle cells induced by transforming growth factor-beta1 and bone morphogenetic protein-4. Tissue Eng Part A 2010;16(4):1201-13.
24. Shiu JY, Kuo CW, Chen PL, Mou CY. Fabrication of Tunable Superhydrophobic Surfaces by Nanosphere Lithography. Chem Mater 2004;16(4):561–564
25. Yeh YH, Cho KH, Chen LJ. Effect of softness of polydimethylsiloxane on the hydrophobicity of pillar-like patterned surfaces. Soft Matter 2012;8:1079-1086
26. Kiraly B, Yang S, Huang TJ. Multifunctional porous silicon nanopillar arrays: antireflection, superhydrophobicity, photoluminescence, and surface-enhanced Raman scattering. Nanotechnology 2013;24(24):245704.
27. Cassie ABD, Baxter S. Wettability of porous surfaces. Trans Faraday Soc 1944;40:546-551
28. Lai KY, Lin YR, Wang HP, He JH. Synthesis of anti-reflective and hydrophobic Si nanorod arrays by colloidal lithography and reactive ion etching. Cryst Eng Comm 2011;13:1014-1017
29. Geiger B, Spatz JP, Bershadsky AD. Environmental sensing through focal adhesions. Nat Rev Mol Cell Bio 2009;10:21-33.
30. Parsons JT, Horwitz AR, Schwartz MA. Cell adhesion: integrating cytoskeletal dynamics and cellular tension. Nat Rev Mol Cell Bio 2011;11:633-43.
31. Zamir E, Geiger B. Molecular complexity and dynamics of cell-matrix adhesions. J Cell Sci 2001;114:3583-90.
32. Owens GK, Kumar MS, Wamhoff BR. Molecular regulation of vascular smooth muscle cell differentiation in development and disease. Physiol Rev 2004;84:767-801.
33. Rensen SS, Doevendans PA, van Eys GJ. Regulation and characteristics of vascular smooth muscle cell phenotypic diversity. Neth Heart J 2007;15(3):100-8.

34. Fu J, Wang YK, Yang MT, Desai RA, Yu X, Liu Z, et al. Mechanical regulation of cell function with geometrically modulated elastomeric substrates. Nat Methods 2010;7(9):733-6.
35. Deutsch J, Motlagh D, Russell B, Desai TA. Fabrication of microtextured membranes for cardiac myocyte attachment and orientation. J Biomed Mater Res 2000;53(3):267-75.
36. Su WT, Liao YF, Lin CY, Li LT. Micropillar substrate influences the cellular attachment and laminin expression. J Biomed Mater Res A 2010;93(4):1463-9.
37. Wilkinson CDW, Curtis ASG, Crossan J. Nanofabrication in cellular engineering. J Vac Sci Technol B 1998;16:3132-3136.
38. Casey BG, Cumming DRS, Khandaker II, Curtis ASG, Wilkinson CDW. Nanoscale embossing of polymers using a thermoplastic die. Microelectron Eng 1999;46:125-128.
39. Su WT, Chu IM, Yang JY, Lin CD. The geometric pattern of a pillared substrate influences the cell-process distribution and shapes of fibroblasts. Micron 2006;37(8):699-706.
40. Folkman J, Moscona A. Role of cell shape in growth control. Nature 1978;273, 345-349.
41. Ingber DE, Prusty D, Sun Z, Betensky H, Wang N. Cell shape, cytoskeletal mechanics, and cell cycle control in angiogenesis. J Biomech 1995;28(12):1471-84.
42. Chen CS, Mrksich M, Huang S, Whitesides GM, Ingber DE. Micropatterned surfaces for control of cell shape, position, and function. Biotechnol Prog 1998;14(3):356-63.
43. Huang S, Ingber DE. The structural and mechanical complexity of cell-growth control. Nat Cell Biol 1999;1(5):E131-8.
44. Huang S, Ingber DE. Shape-dependent control of cell growth, differentiation, and apoptosis: switching between attractors in cell regulatory networks. Exp Cell Res 2000;261(1):91-103.
45. Meyers JR, Corwin JT. Shape change controls supporting cell proliferation in lesioned mammalian balance epithelium. J Neurosci 2007;27(16):4313-25.
46. Davidson PM, Öz çelik H, Hasirci V, Reiter G, Anselme K. Microstructured Surfaces Cause Severe but Non-Detrimental Deformation of the Cell Nucleus. Adv Mater 2009;21:3586–3590.
47. Pan Z, Yan C, Peng R, Zhao Y, He Y, Ding J. Control of cell nucleus shapes via micropillar patterns. Biomaterials 2012;33(6):1730-5.
48. Yim EKF, Reano RM, Pang SW, Yee AF, Chen CS, Leong KW. Nanopattern-induced

changes in morphology and motility of smooth muscle cells. Biomaterials 2005;26:5405-5413

49. Saez A, Buguin A, Silberzan P, Ladoux B Is the mechanical activity of epithelial cells controlled by deformations or forces? Biophys J 2005;89:L52-L54
50. Oakley C, Brunette DM. Topographic compensation: Guidance and directed locomotion of fibroblasts on grooved micromachined substrata in the absence of microtubules. Cell Motil Cytoskel 1995;31:45-58.
51. den Braber ET, de Ruijter JE, Smits HTJ, Ginsel LA, von Recum AF, Jansen JA. Quantitative analysis of cell proliferation and orientation on substrata with uniform parallel surface micro grooves. Biomaterials 1996;17:1093-1099.
52. Dalby MJ, Riehle MO, Sutherland DS, Agheli H, Curtis AS. Changes in fibroblast morphology in response to nano-columns produced by colloidal lithography. Biomaterials 2004;25(23):5415-22.
53. Ghibaudo M, Di Meglio JM, Hersen P, Ladoux B. Mechanics of cell spreading within 3D-micropatterned environments. Lab Chip 2011;11(5):805-12.
54. Ingber DE. Cellular tensegrity: defining new rules of biological design that govern the cytoskeleton. J Cell Sci 1993;104(3):613-27.
55. Banes AJ, Tsuzaki M, Yamamoto J, Fischer T, Brigman B, Brown T, et al. Mechanoreception at the cellular level: the detection, interpretation, and diversity of responses to mechanical signals. Biochem Cell Biol 1995;73(7-8):349-65.

Chapter VI. Photo-Crosslinked Polymer Nanowire Arrays for Regulating Smooth Muscle Cells

Abstract

Photo-crosslinked PCLTA nanowire arrays with diameters of 20, 100 and 200 nm were prepared using inorganic nanoporous aluminum oxide (AAO) templates. The lengths and morphologies of the nanowires can be controlled by adjusting the PCLTA solution concentration. The surface morphology, hydrophilicity and serum protein adsorption of crosslinked PCLTA nanowire arrays were characterized. I investigated SMC attachment, proliferation, spreading and differentiation as well as cellular sensing components as focal adhesions and integrins on these nanowire arrays. Nanowire arrays could adsorb more proteins and support SMC attachment, proliferation, spreading, and differentiation better than the smooth crosslinked PCLTA substrate, especially on nanowires with smaller diameters. Further analysis of cellular sensing components indicated that smaller nanowires triggered stronger focal adhesion dots and higher expression of integrins subunits.

6.1 Introduction

Cell morphology, cytoskeletal structure, and functionality are strongly influenced by the architectures of extracellular matrix (ECM) [1]. Cellular sensing of the structural cues in ECM or underlying substrates can be at the micron and nanometer levels [2]. Nanoscale topography of the substrates can be sensed by integrins and focal adhesions (FAs) on cell membrane and the signals are further passed onto cell nuleus through intracellular mechanotransduction pathways [3] and eventually induce corresponding alterations in cellular attachment, proliferation, and differentiation, as reported in many previous studies [4-8]. Therefore, substrates with architectures with different topographical features can serve as excellent platforms for studying cell-materials interactions.

Biomaterials with different nanostructures have been achieved by using a variety of methods [9,10]. Template-based approaches, including electro-chemical or electro-phoretic deposition, chemical conversion, and capillary force driven template filling, are effective in preparing arrays of nanorods, nanotubes and nanowires [11]. For polymers, direct template filling of a polymer melt or solution is the most straightforward method for preparing nanoscale arrays. Nanoporous aluminum oxide (AAO) membranes containing straight cylindrical nanopores with controllable, uniform sizes, have been used as templates to fabricate organic nanowires as they can be easily removed by exposure to sodium hydroxide or $CuCl_2$ solution [12-15]. When polymer melts or solutions were casted onto AAO membranes, they infiltrate into the nanopores via capillary action [16,17]. Using this method, the ultimate nanowire length can be modulated by the infiltration time, pore size, and melt/solution viscosity [18].

To regulate cellular behavior, substrates with well-controlled topographical features ranging from nanometer to micron scale have been fabricated to respond to micron-sized cells. In the nanometer range, strict requirements are needed for material properties to obtain and maintain stable desired patterns at such a tiny scale. Poly(dimethyl siloxane) (PDMS) is a widely used material for micro- and nano-fabrication; however, low elastic modulus PDMS (~2 MPa) is easy to deform or collapse and difficult to obtain high-aspect-ratio features below 100 nm [19,20]. Biodegradable poly(D,L-lactide) (PDLLA) was also used in fabrication of aligned nanorods with a diameter as small as 180 nm [21]. Poly(lactic acid)s (PLAs) are commonly

acknowledged as stiff materials for their high strength and tensile modulus (> 3 GPa); however, PLAs have deficits of easy brittleness for nanofabrication [22]. In nanoarray fabrication using poly(D,L-lactide-*co*-glycolide) (PLGA) and poly(ε-caprolactone) (PCL), PCL exhibited excellent outcomes by providing clear and stable morphological properties [23]. PCL nanowire patterns were also prepared for bone and neuron tissue-engineering applications [24,25]. In our research group, photo-crosslinkable and biodegradable PCL triacrylates (PCLTAs) have been prepared via condensation of acryloyl chloride and PCL diols with different molecular weights and can be molded into any desired shapes after photo-curing [26,27]. Through controlling the crosslinking density or grafting with hydrophilic chains, the mechanical properties and surface energy of photo-crosslinked PCLTA networks can also be well modulated [26-28]. These PCLTA networks with controllable elastic moduli of 1-200 MPa have been used to demonstrate the role of surface stiffness in regulating adhesion, spreading, proliferation, migration, and differentiation of vascular SMCs [27].

In the present study, I placed insights into the cell-matrix interactions by regulating 3D topographies of biodegradable PCLTA networks. All of these PCLTA networks have identical chemical compositions to minimize possible interference from the chemical properties of underlying substrates in regulation of cell behavior. AAO templates with different pore sizes were used to produce photo-crosslinked PCLTA nanowire arrays of wire diameters of 20, 100, and 200 nm. The topography, surface hydrophilicity, and protein adsorption abilities of these nanowire arrays were evaluated. SMC responses to these nanowire arrays were studied extensively, including adhesion, spreading, proliferation, morphologies of cytoplasm and nuclei, and phenotypic conversion.

6.2 Materials and Methods

6.2.1 Polymers and chemicals

The synthesis of PCLTA was reported by our research group previously [26,27,29]. The molecular weights of the synthesized PCLTAs (M_n = 9564 g mol^{-1}) were determined by Gel Permeation Chromatography (GPC; PL-GPC 20, Polymer Laboratories). Tetrahydrofuran (THF) was used as eluent and standard monodisperse polystyrene samples (Polymer

Laboratories) were used as the reference system. Three types of inorganic AAO templates (with varied pore diameters of 200, 100 and 20 nm were purchased from Anodisc, Whatman. All other chemicals used in this study were purchased from Sigma-Aldrich if not noted otherwise. The photo-initiator for polymer crosslinking, phenyl bis(2,4,6-trimethyl benzoyl) phosphine oxide (BAPO, IRGACURE819), was a gift from Ciba Specialty Chemicals (Tarrytown, NY).

6.2.2 Nanowire fabrication and characterization

Before photo-crosslinking, 1 g PCLTA was dissolved in 0.5 mL CH_2Cl_2. 300 mg BAPO was dissolved in 1.5 mL CH_2Cl_2. Prior to photo-crosslinking, 50 μL of BAPO/CH_2Cl_2 solution was added to the PCLTA/CH_2Cl_2 solution that contained 1 g of PCLTA. A layer (~100 μm) of PCLTA/BAPO/CH_2Cl_2 mixture was placed on glass slides (25.4 × 76.2 × 1.0 mm, width × length × thickness). The three types of inorganic AAO templates were placed onto the polymer layers. Then the templates with the polymers were placed under a UV lamp (SB-100P, Spectroline, wavelength = 365 nm, intensity = 4800 μw/cm^2) for 30 min to photo-crosslink, as described in our previous reports [26,27,29]. After photo-crosslinking, the templates together with the PCLTA films were immersed in 1 mol/L NaOH solution and stirred for 40 min to dissolve the AAO templates, as reported previously [30]. The as-obtained crosslinked PCLTA nanowire arrays were washed 10 times (30 min each) with distilled water. The nanowire arrays were further soaked in 1 L distilled water for 2 days to fully remove the residual NaOH, then dried in vacuum and stored in a desiccator prior to use. For simplicity, “crosslinked” is omitted in later discussion on “crosslinked PCLTA”.

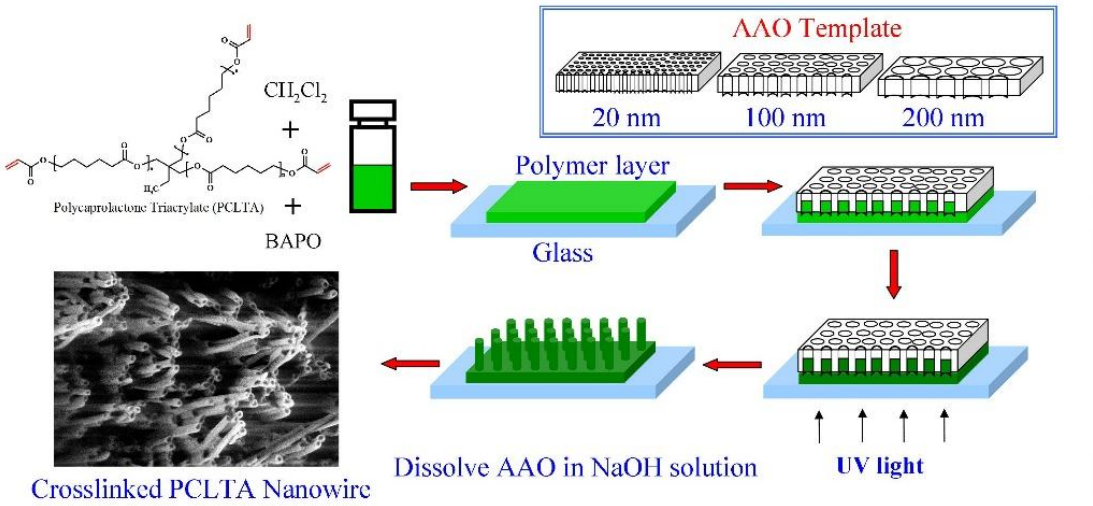

Figure 6.1 Scheme of the fabrication process of photo-crosslinked PCLTA nanowire arrays using Al_2O_3 templates.

6.2.3 Water contact angle and protein adsorption

These PCLTA nanowire arrays were characterized using scanning electron microscopy (SEM; S-3500, Hitachi Instruments, Tokyo, Japan) at a voltage of 2 kV. The water contact angles on the nanowire arrays were determined using a Ramé-Hart NRC C. A. goniometer (Model 100-00-230, Mountain Lakes, NJ) at 37 ℃. The contact angle values were calculated from the images of four water droplets (20 μl) using ImageJ software (National Institutes of Health, Bethesda). To determine the adsorption capabilities of serum proteins and fibronectin, PCLTA nanowire arrays were soaked in Dulbecco's modified eagle medium (DMEM) and fibronectin solution (40 μg/mL) for 2 h. Then the arrays were immersed in 1% sodium dodecyl sulfate (SDS) three times (1 h each time) with gentle shaking to collect the adsorbed proteins. The protein concentrations in the collected solutions were detected using a MicroBCA protein assay kit (Pierce, Rockford, IL) and the data were obtained by calibrating to the values of eight known concentrations on a micro-plate reader (SpectraMax Plus 384, Molecular Devices, Sunnyvale, CA) [26].

6.2.4 In vitro cell studies

Prior to cell studies, the nanowire arrays were sterilized in 70% alcohol solution and then completely dried in vacuum. To avoid swaying or even floating during the cell culture, these substrates were glued onto the bottom of 24-well tissue-culture polystyrene (TCPS) plates using autoclave-sterilized inert silicon-based grease (Dow Corning, Midland, MI) before cell seeding. Primary SMCs isolated from rat aorta were cultured in DMEM with 10% fetal bovine serum (FBS) in a 37 ℃ incubator with 5% CO_2 and 95% relative humidity prior to seeding [31]. When cells grew to approximately 70% confluency, they were seeded onto the nanowire arrays at a density of 1.5×10^4 cells per cm^2. TCPS wells seeded with cells at the same density but in absence of the arrays were used as positive controls and empty wells were negative controls in all the following process. After seeding, cells were cultured in the incubator. At 4 h and days 1, 2, and 4, cell numbers were accessed from the MTS assay solutions (CellTiter 96 Aqueous One Solution, Promega, Madison, WI) using the micro-plate reader mentioned in Section 2.3 at the wavelength of 490 nm, according to the manufacturer's instruction. For fluorescence visualization, SMCs cultured on the nanowire arrays were washed twice with phosphate buffered saline (PBS), fixed in 4% paraformaldehyde (PFA) solution, and permeabilised with 0.2% Triton X-100, followed by incubation with rhodamine-phalloidin (RP) for 1 h at 37 ℃ to stain cytoplasm and with 4',6-diamidino-2-phenylindole (DAPI) solution at room temperature for 10 min to stain cell nuclei. Then the cells were photographed using an Axiovert 25 light microscope (Carl Zeiss, Germany) and cell areas were calculated from the fluorescence images using ImageJ and averaged on 20 non-overlapping cells.

6.2.5 Characterization of focal adhesions

To characterize FAs, SMCs cultured for 1 day on the nanowire arrays were fixed and permeabilised, as described in Section 2.4. The cells were then incubated with 1% Bovine Serum Albumin (BSA) in PBS for 1 h at 37 ℃ to block unspecific antibody binding sites [32]. To remove BSA residue, cells were washed three times in PBS. Monoclonal vinculin primary antibody (1:1000 in PBS; Sigma) solution was then added and incubated with the cells for 2 h at room temperature, followed by three-time wash using PBS to remove unconjugated primary antibody. Goat anti-mouse IgG secondary antibody with green fluorescence (1:200 in PBS;

Sigma) solution was then applied to the cells at room temperature for 1 h. The cells were further stained using RP for 1 h to visualize F-actin with vinculin. Photographing was conducted using a Leica DM6000B confocal fluorescent microscope.

6.2.6 Gene expression of contractile phenotypic markers and integrins

To detect the expression levels of target gene markers in the cells, SMCs cultured for 4 days on the flat substrates and nanowire arrays were detached using trypsin-EDTA solution (Gibco) and collected using centrifuge at 1000 rpm for 3 min. Total RNAs were extracted from these cells using an RNeasy Mini Kit (Qiagen, Valencia, CA) according to the manufacturer's instruction. Stable cDNA was reverse-transcripted using a DyNAmo cDNA synthesis kit (Thermo Scientific) following the manufacturer's instruction. For real-time polymerase chain reaction (PCR) analysis, primers were designed using Oligoperfect software (Invitrogen) and their sequences are listed as follows. Calponin: forward 5'-AGTCTACTCTCTCTTGGCTCTGGCC-3', reverse 5'-CCTGCCTTCTCTCAGCTTCTCAGG-3'; smooth muscle myosin heavy chain (SM-MHC): forward 5'-AAGCAGCTCAAGAGGCAG-3', reverse 5'-AAGGAACAAATGAAGCCTCGTT-3'; smoothlin: forward 5'-TCGGAGTGCTGGTGAATAC-3', reverse 5'-CCCTGTTTCTCTTCCTCTGG-3'; and house-keeping gene glyceraldehyde-3-phosphate dehydrogenase (GAPDH): forward 5'-TCTTCACCACCATGGAGAA-3', reverse 5'-ACTGTGGTCATGAGCCCTT-3'; transgelin (SM-22): forward 5'-GGCAGCTGAGGATTATGGAGTCACG-3', reverse 5'-TGGGATCTCCACGGTAGTGTCCA-3'. A total reaction volume of 20 μL was prepared by mixing 2.5 μL of total cDNA at the same concentration of 5.0 ng/μL with power SYBR Green PCR Master Mix (Applied Biosystems, Warrington, UK). The amplification and detecting process in real-time PCR detection process were conducted on a Peltier Thermal Cycler fluorescence detection system (MJ Research PTC-200 Thermo Cycler). The running procedures for the amplification process were programmed as 94 ℃ for 5 min to denaturize DNA double strains, then 30 cyclic steps of 94 ℃ for 30 s, 55 ℃ for 30 s, and 72 ℃ for 30 s. The expression levels of the target gene markers were normalized by the value of GAPDH.

6.2.7 Statistical analysis

Statistical analysis was performed using the one-way analysis of variance (ANOVA) method contained in OriginLab software. Groups that have *p*-values lower than 0.05 were considered statistically different.

6.3 Results and Discussion

6.3.1 Surface structure, hydrophilicity and protein adsorption

The photo-crosslinked PCLTA nanowire arrays were observed using SEM (Fig. 6.1). As shown in Fig. 6.1a-c, different morphological patterns were created using AAO templates with varied pore sizes. From the edge-view SEM images of the nanowire arrays, the heights for the PCLTA nanowires with diameters of 200, 100 and 20 nm were determined to be 0.8, 1.0, and 0.7 μm, respectively. These results demonstrated that the AAO templates were effective in generating photo-crosslinked PCLTA nanowire arrays. When the AAO membranes were placed on the PCLTA solution layer, the solution penetrated into these membranes via the capillary effect [16,17]. The infiltration speed of polymer solution into the cylindrical nanopores was proportional to the pore diameter and surface tension (γ) but inversely propotional to solution viscosity (η) , as demonstrated in the equation $\frac{\mathrm{d}h}{\mathrm{d}t} = \frac{R\gamma\cos\theta}{4\eta h}$,

where h is the height or length of the polymer wires drawn into the AAO nanopores, t is penetration time, R is the hydraulic radius of nanopores (the ratio between the volume of the liquid in the capillary section and the area of the solid and liquid interface), and θ is the contact angle of liquid on the model wall [18,34]. Therefore, the length of the photo-crosslinked PCLTA nanowires could be well controlled through modulating the parameters in the equation.

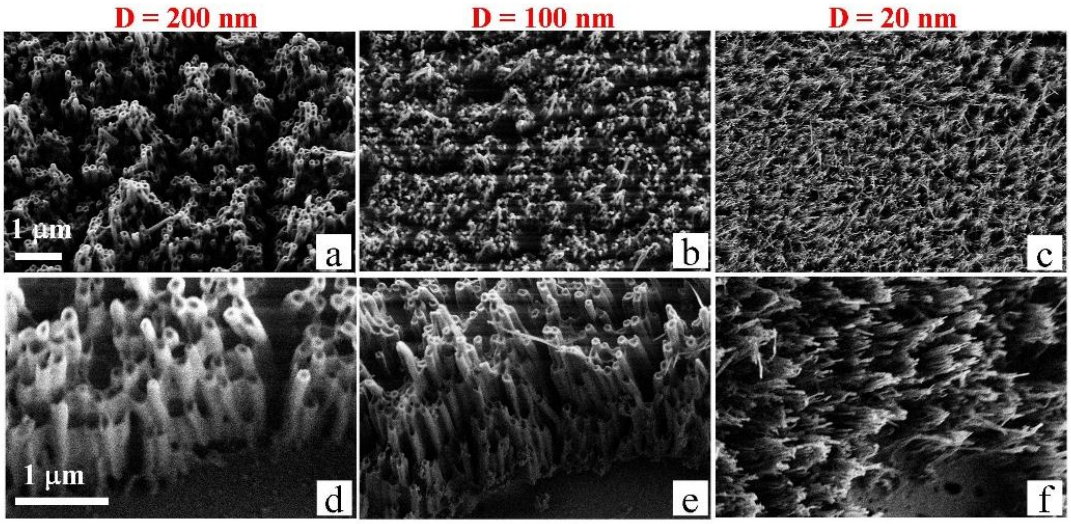

Figure 6.2 Top-view (a-c) and edge-view (d-f) SEM images of photo-crosslinked PCLTA nanowire arrays with three different wire diameters of 200, 100, and 20 nm.

Surface wettability is an important characfactor in developing biomaterials for tissue-engineering applications. Because the nanowire arrays were prepared by dissolving AAO templates in NaOH solution, flat substrates of photo-crosslinked PCLTA were treated in the same NaOH solution for comparison. The water contact angle on the flat substrate of photo-crosslinked PCLTA was higher than on the NaOH-treated counterpart, as indicated by the images of water droplets on these substrates in Fig. 6.3a. When there were nanowires on the surfaces, the water contact angles were higher than on the flat control (Fig. 6.3a). The smaller was the nanowire diameter, the larger the water contact angle, as displayed in the data in Fig. 6.3b.

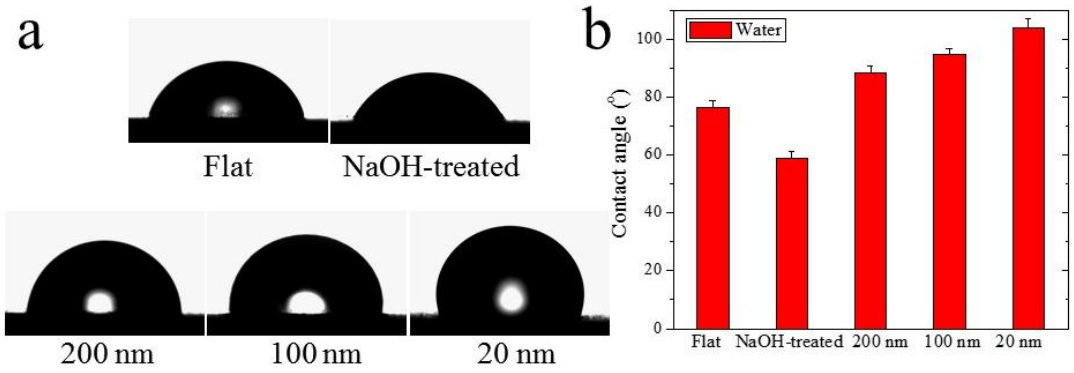

Figure 6.3 Water droplets (a) and water contact angles (b) on the original and NaOH-treated flat substrates and nanowire arrays of photo-crosslinked PCLTA at 37 °C.

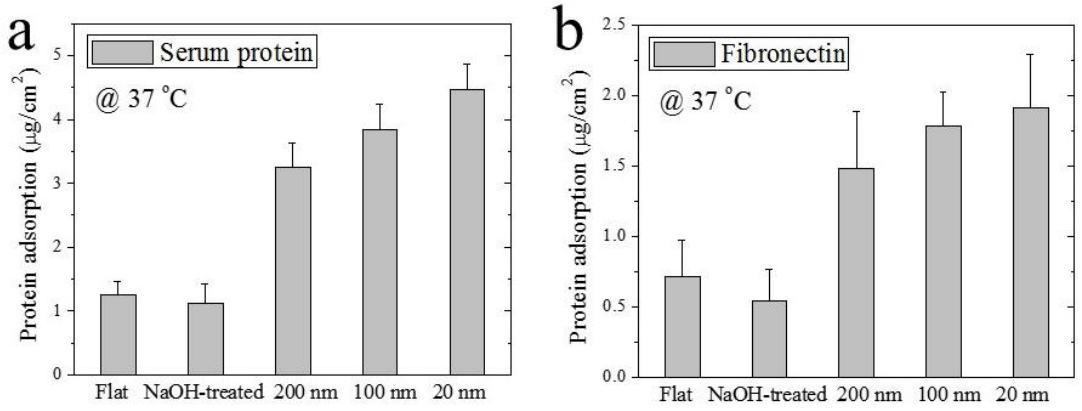

Figure 6.4 Adsorption of (a) serum proteins and (b) fibronectin on the original and NaOH-treated flat substrates and nanowire arrays of photo-crosslinked PCLTA.

For synthetic matrices without cell binding ligands on the surface, they need to adsorb external proteins to mediate cellular recognition and adhesion to the substrate surface [35]. Therefore, the protein absorption ability is important for evaluating biocompatibility and bioactivity of biomaterials. The amounts of serum proteins adsorbed on all the photo-crosslinked PCLTA substrates from cell culture media were determined, as shown in Fig. 6.4a. The amounts of adsorbed proteins on the nanowire arrays were apparently higher than those on the flat surfaces. In addition, protein adsorption was highly related to the nanowire size. When the nanowire diameter was smaller, a larger amount of proteins was adsorbed on the arrays with the same projected surface area. Fibronectin adsorption on these substrates were also evaluated

and demonstrated the same profile, as shown in Fig. 6.3b. The results here were consistent with a previous study, in which PCL nanowire arrays were found to adsorb more bovine serum albumin (BSA) and fibrinogen proteins compared with the flat surface samples [30].

6.3.2 SMC adhesion and proliferation on the nanowire arrays

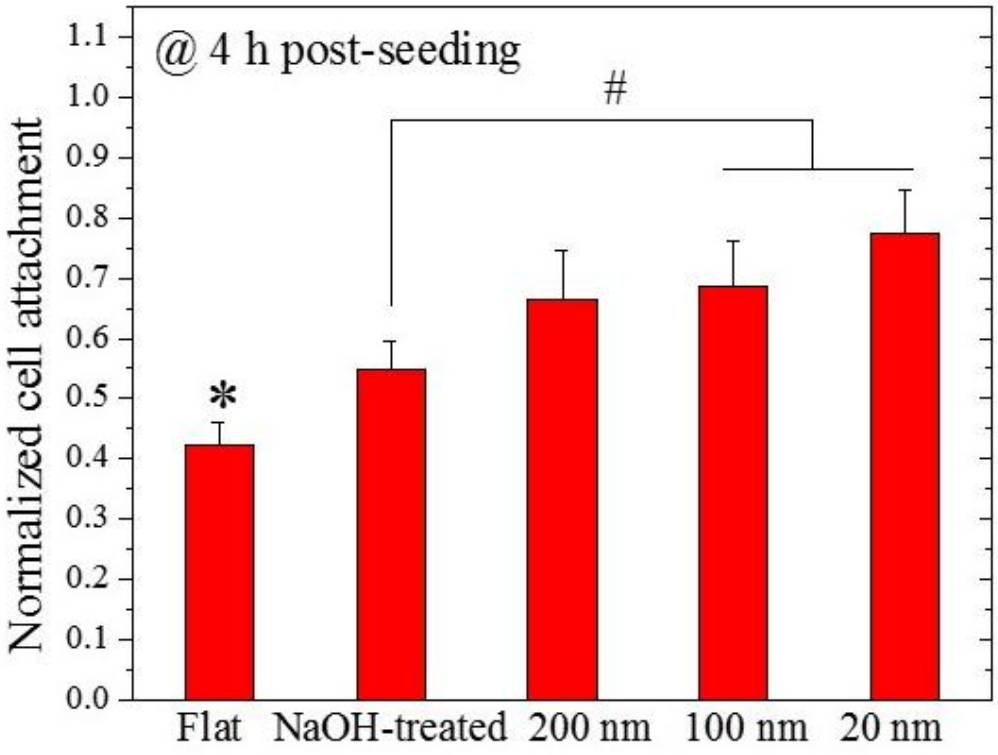

Figure 6.5 SMC attachment on the original and NaOH-treated flat substrates and nanowire arrays of photo-crosslinked PCLTA normalized to that on TCPS, the positive control. *: $p < 0.05$ relative to the others; #: $p < 0.05$.

SMC attachment to the photo-crosslinked PCLTA substrates with flat topography or nanowire arrays was evaluated at 4 h and normalized to that on TCPS. As shown in Fig. 6.5, the nanowire arrays had better SMC attachment than the flat substrates and the NaOH-treated surface was better than the original one. When the nanowire diameter was smaller, SMC attachment was higher. These results indicated that the nanowire structure provided a more preferable environment than the smooth surface for SMC attachment.

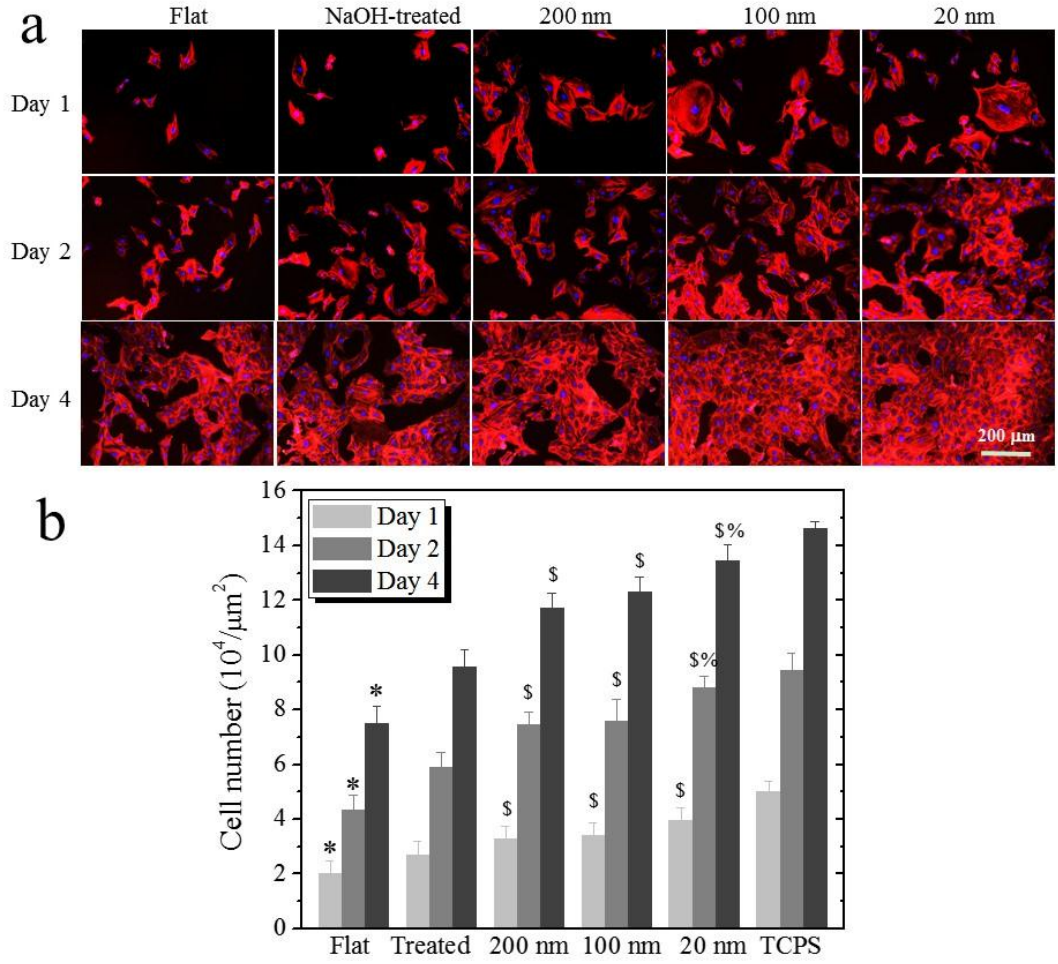

Figure 6.6 (a) Fluorescence images, (b) numbers and (c) PI and Growth Rate of SMCs on the original and NaOH-treated flat substrates and nanowire arrays of photo-crosslinked PCLTA at days 1, 2, and 4 post-seeding. *: $p < 0.05$ relative to the others; $: $p < 0.05$ relative to NaOH-treated flat substrates; %: $p < 0.05$ relative to 200 nm nanowire arrays.

SMC proliferation over 4 days in Fig. 6.6 showed the same trend as the attachment. The fluorescence images of SMCs on the substrates taken at days 1, 2, and 4 are demonstrated in Fig. 6.6a. Clear increases in SMC number occurred to all the substrates, while they were stronger on the nanowire arrays. The cell numbers on the NaOH-treated flat substrate and three nanowire arrays were significantly higher than that on the flat substrate while the cell numbers on the three nanowire arrays were higher than the NaOH-treated flat substrate. SMCs cultured on the nanowire arrays with the smallest diameter of 20 nm were significantly more than those on the nanowire arrays with the largest diameter of 200 nm. To quantify SMC proliferation, the proliferation index (PI) was obtained by dividing the cell number at day 2 by the number at 4

h. The PIs of SMCs on the original and NaOH-treated flat substrates of photo-crosslinked PCLTA were 8.67 and 9.14, respectively. It increased to 9.49, 9.36, and 9.64 on the nanowire arrays with diameters of 200, 100, and 20 nm, respectively.

6.3.3 Cell spreading and morphology of cytoplasm and cell nuclei

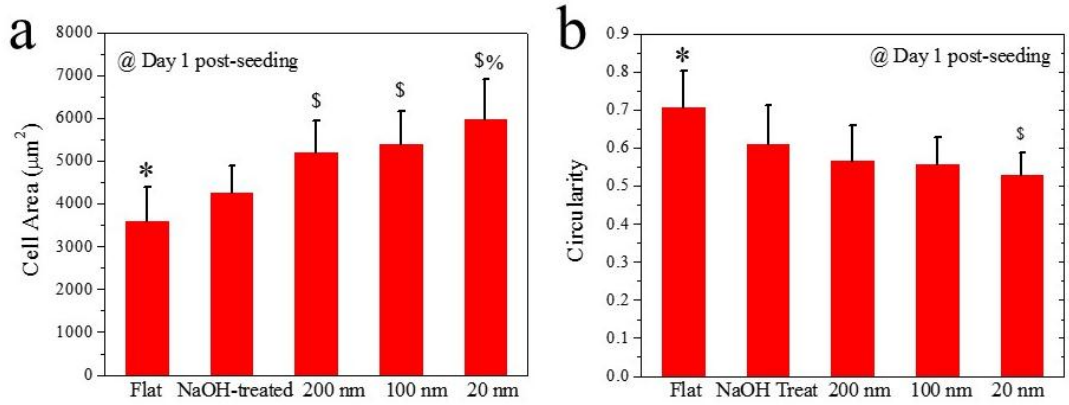

Figure 6.7 (a) SMC spread area and (b) circularity on the original and NaOH-treated flat substrates and nanowire arrays of photo-crosslinked PCLTA. *: $p < 0.05$ relative to the others; $: $p < 0.05$ relative to NaOH-treated flat substrate; %: $p < 0.05$ relative to 200 nm.

Cell spreading is closely related to cell division and proliferation on substrates [36,37]. As shown in Fig. 6.7a, cell area determined from the cell images at day 1 was the smallest on the original flat substrate of photo-crosslinked PCLTA and increased on the NaOH-treated flat substrate. Cell area was significantly higher on the nanowire arrays and the value increased with decreasing the wire diameter. As defined by the equation of $4\pi \times \text{area/perimeter}^2$, cell circularity, was quantified to indicate how close a cell was to being perfectly round with a measure of 1 for a perfect circle and the closer to 0 the less circular. As shown in Fig. 6.7b, cell circularity gradually decreased when the original flat substrate was changed to NaOH-treated one and nanowire arrays, especially when the nanowires were thinner, indicating that SMCs were stretched and deformed more strongly than those on the flat substrates.

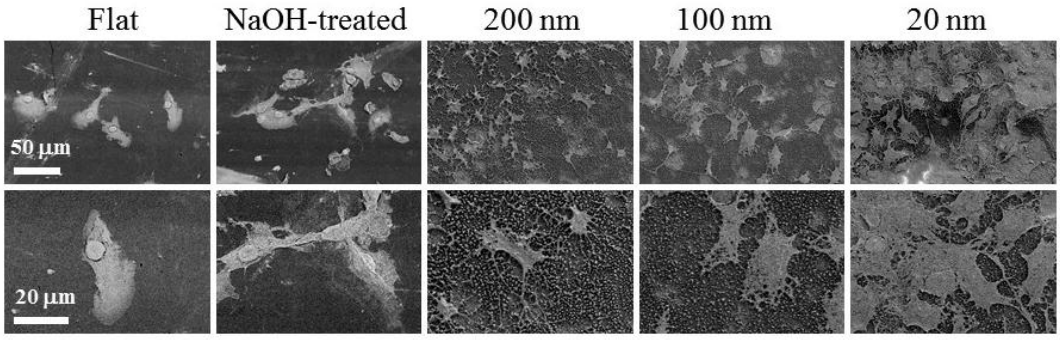

Figure 6.8 SEM images of SMCs on the original and NaOH-treated flat substrates and nanowire arrays of photo-crosslinked PCLTA.

To substantiate the conclusions from the cell images, I further conducted SEM imaging of dehydrated SMCs on the substrates and found that the SEM images in Fig. 6.8 were consistent with the fluorescence images in Fig. 6.6a. On the NaOH-treated substrate, SMCs spread better than on the original one. On the nanowire arrays, thinner nanowires could trigger better SMC adhesion and spreading as there were more nanowires in unit projected area. As demonstrated in Fig. 6.8, the best spreading and the largest cytoplasm appeared on the nanowire arrays with the smallest diameter of 20 nm.

I further characterized the nuclei of SMCs cultured for 1 day on these substrates. As shown in Fig. 6.9a, cell nuclei on the flat substrates were mainly round. Compared with those on the flat substrates, cell nuclei on the nanowire arrays were larger and brighter. Quantification of cell nuclei in Fig. 6.9b also indicated significantly larger nuclei on the NaOH-treated substrate and nanowire arrays than on the original flat substrate and the thinnest nanowires triggered largest nuclei. The average circularity of SMC nuclei was close to each other (~0.87) on the substrates except the 20 nm nanowire array, which showed a significantly lower value of 0.83.

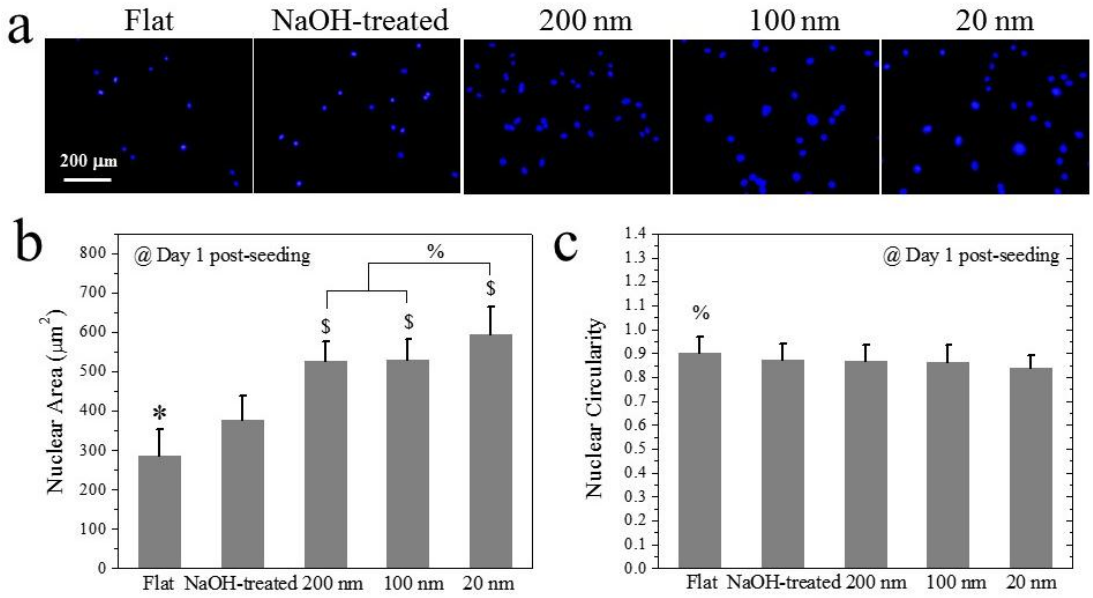

Figure 6.9 (a) Fluorescent images of SMC nuclei stained with DAPI on the original and NaOH-treated flat substrates and nanowire arrays of photo-crosslinked PCLTA at day 1 post-seeding. (b) Average area and (c) circularity of SMC nuclei on these substrates. *: $p < 0.05$ relative to the others; $: $p < 0.05$ relative to the NaOH-treated flat substrate; %: $p < 0.05$ relative to the 20 nm nanowire array.

6.3.4 Focal adhesions in SMCs

FAs in cells are macromolecular assemblies of multiple components including focal adhesion kinases, paxillins, and vinculins, and play key roles during the cellular adhesion and later proliferation process by holding cells on the underlying substrates and at the same time sensing the surrounding environments. [38]. Here in this study, SMCs developed evident FAs on all the substrates of photo-crosslinked PCLTA, as shown in Fig. 6.10a. In contrast with weak FAs on the flat substrates, the clear and punctate FA dots on the nanowire arrays were also more, showing stronger cell adhesion. Quantification of focal adhesions from the images in terms of FA average area, elongation (inverse of circularity), and densities (number per cell) confirmed that FAs on the NaOH-treated flat substrate were larger, more elongated, and denser than on the original one and those on the nanowire arrays were even better environments for FA development, especially when the nanofiber diamater was 20 nm, as shown in Fig. 6.10b-d.

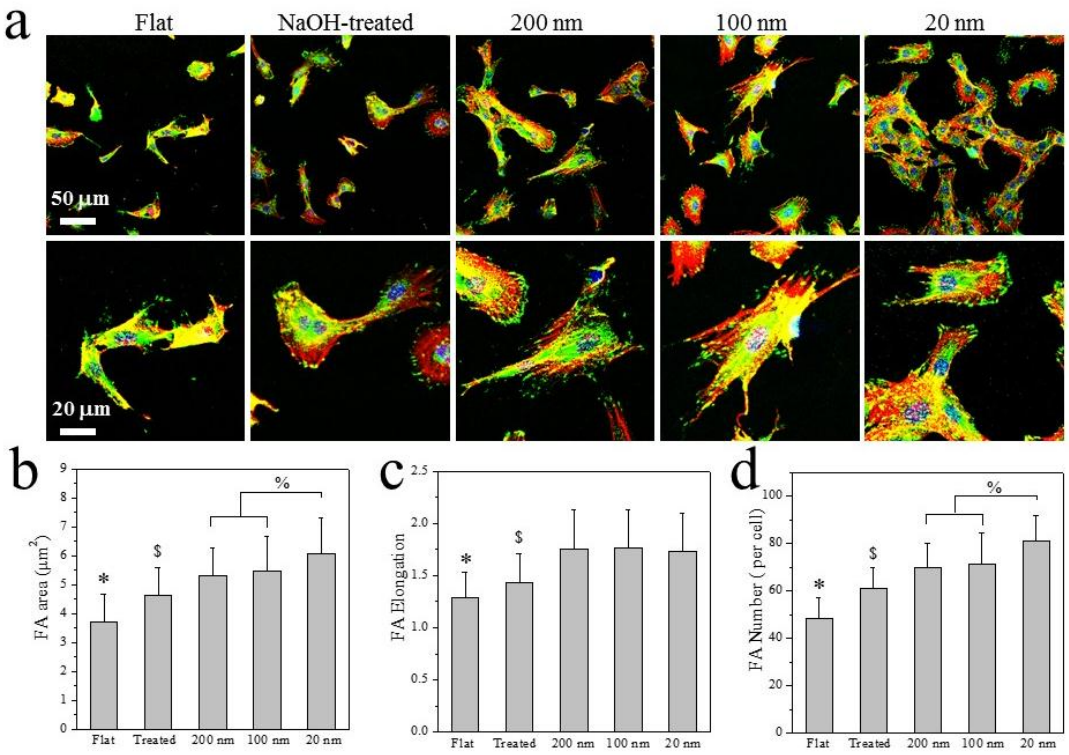

Figure 6.10 Characterizations of FAs in SMCs cultured for 1 day on the original and NaOH-treated flat substrates and nanowire arrays of photo-crosslinked PCLTA. (a) Immunofluorescence images of FAs in the cells with vinculin stained green, F-actin stained red, and nuclei stained blue. The images in the bottom row are enlarged ones of their corresponding images in the top row. Scale bars of 50 and 20 μm are applicable for the images in the top and bottom rows, respectively. Quantification of FAs in terms of (b) FA area (c) FA elongation, and (d) FA density from the images in (a). *: $p < 0.05$ relative to the others; $: $p < 0.05$ relative to the othersNaOH treated flat samples; %: $p < 0.05$ relative to the nanowire array with a diameter of 20 nm.

6.3.5 Gene expression

SMCs adopts two phenotypes: synthetic and contractile whose conversion can be modulated in the proliferation through responding to external mechanical, chemical, and topographical signals from ECM or the underlying substrate [39]. There are corresponding gene makers for these two phenotypes. For the contractile phenotype, gene markers that are most relevant to contractile SMC functions include α-smooth muscle actin, SM-MHC, smoothlin, transgelin, and calponin [40]. Thus evaluation the expression levels of contractile phenotypic

gene markers in SMCs is crucial to characterize their content of phenotype and functionality [40].

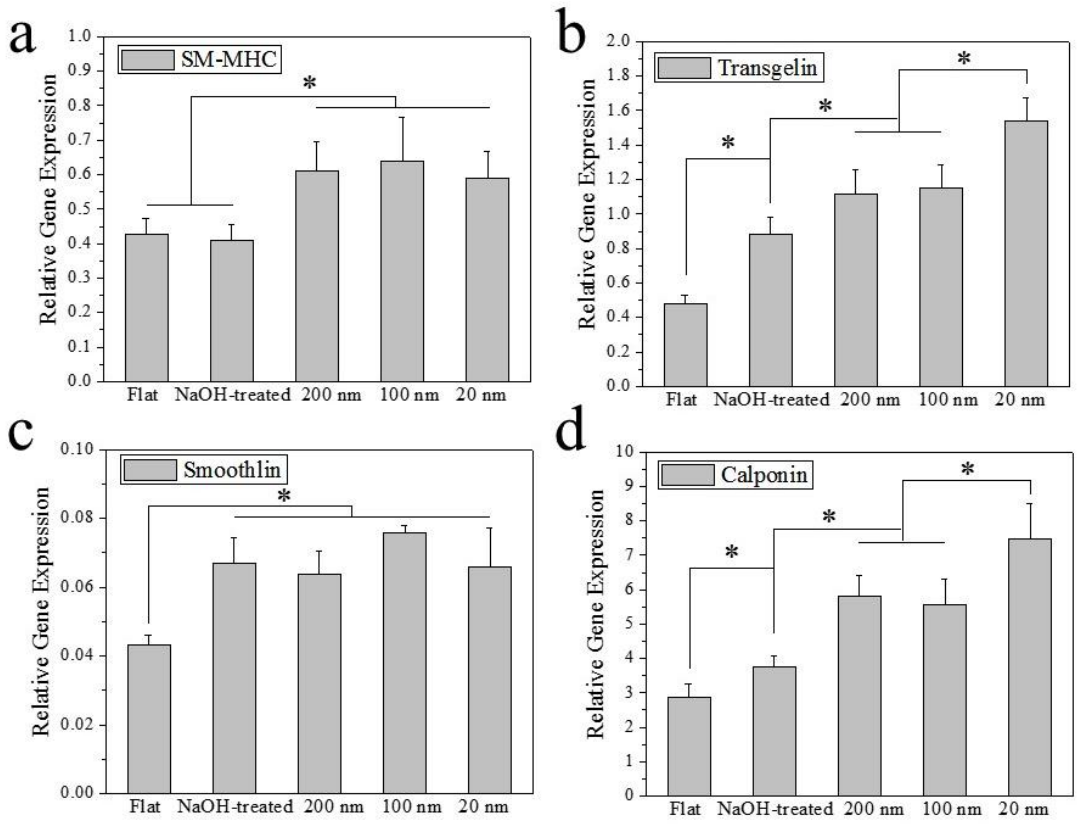

Figure 6.11 Expression levels for gene contractile markers of (a) SM-MHC, (b) transgelin, (c) smoothlin, and (d) calponin in SMCs cultured for 4 days on the original and NaOH-treated flat substrates and nanowire arrays of photo-crosslinked PCLTA, relative to that of GAPDH using real-time PCR. *: $p < 0.05$.

I performed real-time PCR analysis of four typical contractile markers of SM-MHC, smoothlin, transgelin and calponin to characterize their expression levels in SMCs cultured for 4 days on the substrates. The relative expression levels of these gene markers using GAPDH as the reference are shown in Fig. 6.11. All these four typical contractile markers had higher expression levels in SMCs on the nanowire arrays than on the flat substrates, except that smoothlin expression was similar on the NaOH-treated flat substrate, suggesting that nanowires could promote phenotypic conversion from the proliferative synthetic phenotype to the more functional contractile phenotype. For transgelin and calponin markers, their expression levels

were significantly higher when the nanowire diameter was the smallest (20 nm) than on the other substrates.

6.3.6 Integrin expression

Integrins are a category of heterodimers composed of two distinct chains named as α and β subunits [41]. Integrins normally form across the lipid bilayer membranes in active cells and function as linkage to various ECM proteins, thus playing critical roles in FA signal transduction [41].

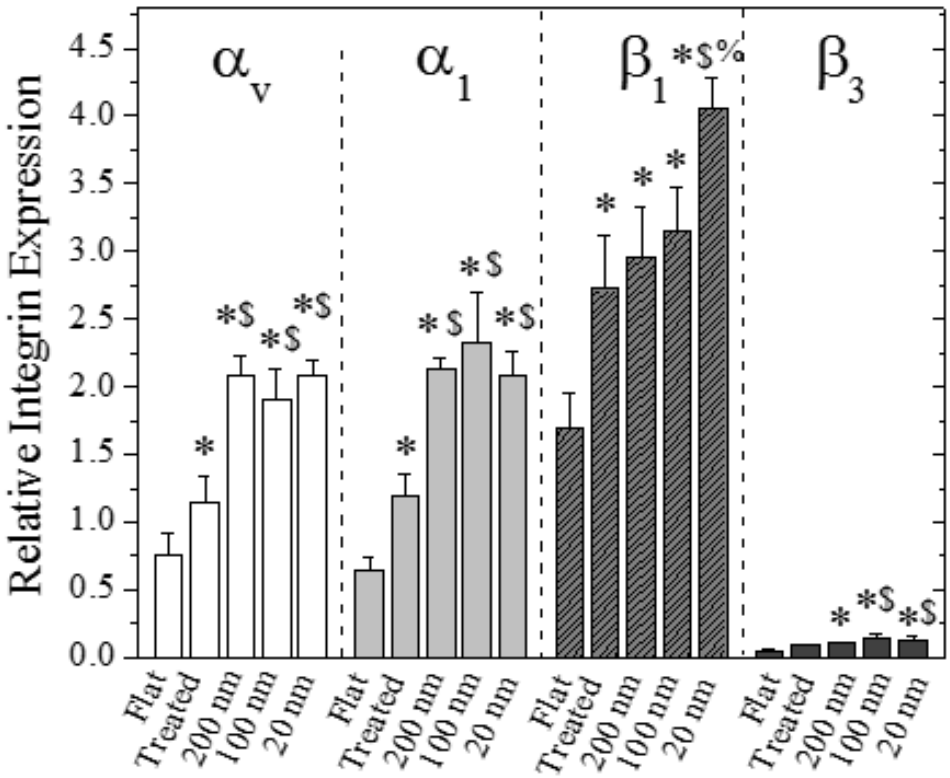

Figure 6.12 Relative expression levels of α_v, α_1, β_1, and β_3 integrin subunits normalized to that of GAPDH in SMCs cultured for 1 day on the original and NaOH-treated flat substrates and nanowire arrays of photo-crosslinked PCLTA. *: $p < 0.05$ relative to the original flat substrate; $: $p < 0.05$ relative to NaOH-treated flat substrate; %: $p < 0.05$ relative to the nanowire array with a diameter of 200 nm.

To understand better distinct FAs in SMCs when they were cultured on the different substrates, I further analyzed the expression level of four major integrin subunits (α_v, α_1, β_1, and β_3) in SMCs at day 1 using real-time PCR. I found that integrin expression in SMCs was greatly altered by the surface chemistry and topographical feature of the substrates. As shown in Fig. 6.12, the expression levels of the two α subunits were significantly higher on the nanowire arrays than on the original flat substrates and also higher on the NaOH-treated flat substrate than on the original flat one. Expression of the two β subunits could be further promoted by the smallest nanowire diameter of 20 nm. For β_1 subunit, its expression levels were significantly higher on the NaOH-treated flat substrate and the nanowire arrays than on the original flat one, and the expression level was the highest when the nanowire diameter was smallest (20 nm). For β_3 subunit, the expression levels on the nanowire arrays with diameters of 100 and 20 nm were significantly higher than on the flat substrates, whereas the value on the nanowire array with the diameter of 200 nm was only significantly higher than on the original flat substrate. Upregulated expression of these integrin subunits in SMCs on the nanowire arrays allowed them to form more and stronger integrin combinations such as $\alpha_v\beta_1$, $\alpha_1\beta_1$, $\alpha_v\beta_3$, and $\alpha_1\beta_3$, which play pivotal roles in signal transduction and modulating cellular behavior [42].

6.4 Discussion

Understating how ECM or underlying substrate properties influence cell survival, growth, and function is critical for biomaterial design and tissue-engineering applications [43-46]. Previous studies in our lab demonstrated the topographical features on extracellular substrates, e.g., microgrooves and honeycomb structures, could exert large influences on behaviors of bone cells and nerves cells [5,47-50]. For cardiovascular tissue engineering, morphological architectures of the underlying substrates provide necessary contact guidance for better vascular cell functions. Here in this study, the material was identical for all the nanowire arrays although it was indeed more hydrophilic than the original flat substrate after the NaOH treatment. The differences in surface hydrophilicity among the nanowire arrays and NaOH-treated flat substrate should be attributed to the effect of nanofibrous topography. The dominant factor in these nanowire arrays to affect SMC behavior was the topography and nanowire diameter.

Compared with the flat substrates, the nanowire arrays with the same projected area adsorbed three-fold higher amounts of serum proteins or fibronectin because of much higher surface areas, which could support cell adhesion to the substrate.

SMC behavior and function were greatly influenced by the presence of the nanowires. The initial attachment rates of SMCs were already higher and their spread areas were also larger on the nanowire arrays because of higher amounts of adsorbed protein and again the nanofibrous topography with a larger surface area, which were more evident when the nanowire diameter was smaller. It is known that well-spread cells could proliferate better than those poorly extended cells [36]. The underlying mechanism for this phenomenon was proposed as that cell shape was tightly coupled to nuclear acid synthesis and thus cell division for proliferation [36,37,51-53]. In the same external environment, cells with different spread areas were found to have remarkably different cell cycle progression [54]. Our present results also substantiated the above mechanism as better SMC spreading and faster proliferation appeared simultaneously on the nanowire arrays, in particular, when the nanowire diameter was smaller In addition, SMC nuclei were larger on the nanowire arrays than on the flat substrates as the result of better cell spreading and this nuclear expansion was similar to alignment of nuclei because deformation of cell nuclei is correlated with gene expression.

Adherent cells develop FAs with high alignment and strength to mechanically hold onto the underlying substrate so that other cell functions can proceed in a stable environment. On the other hand, FAs are also important ECM sensing components with the ability to adjust their size and morphology in responding to extracellular signals [55]. Signals that detected by FA complexes were further transduced to the intracellular signaling pathways, which ultimately altered cell behavior through multiple mechanotransduction pathways [56]. In this study, larger and more elongated FAs with denser distribution in SMCs were observed on the nanowire arrays, especially when the nanowire diameter was smaller. The correlation between FA profiles and cell spreading indicated that strong FAs appeared in the cells receiving intensified stretching tension. Several previous studies using topographical factors to regulate cell behavior also reported similar phenomenon that micron and submicron features can influence microfilaments, FA dots, and microtubules [57-59]. This unique effect was also called as topographical compensation because these surface architectures altered substrate properties and

then induced cell deformation [60].

Sensing of ECM through FAs was recognized to involve components including vinculin, talin, paxillin, focal adhesion kinase, and integrins [61]. For integrins, with variance in α and β subunits, they can form different types that are capable of binding to different ECM proteins. In SMCs, $\alpha_2\beta_1$ and $\alpha_5\beta_1$ generate important cellular receptors to help cells adhere to collagen and fibronectin in ECM while $\alpha_v\beta_5$ and $\alpha_v\beta_3$ are responsible for recognizing and helping cells link to vitronectin and osteopontin in ECM [62]. In this study, the two α and two β subunits analyzed are components for combinations of $\alpha_v\beta_3$, $\alpha_1\beta_1$, and $\alpha_1\beta_3$, which play critical roles in signal transduction in regulating cell adhesion, spreading, and proliferation [42]. The upregulated expression of these integrin subunits in SMCs on the nanowire arrays can be correlated with stronger FAs and better cell spreading, attachment, and proliferations.

6.5 Conclusions

Photo-crosslinked PCLTA nanowire arrays with three different nanowire diameters of 200, 100, and 20 nm were fabricated using nanoporous aluminum oxide templates, which was an efficient approach for preparing polymeric nanowire architectures for cardiovascular tissue-engineering applications. These nanowires increased the surface hydrophobicity of substrates and induced higher protein absorption capacity than both original and NaOH-treated flat substrates. Better SMC affinity, growth, spreading, and phenotypic conversion were observed on the nanowire arrays than on the flat substrates, especially when the nanowire diameter was the smallest, 20 nm. Stronger development of sensing components such as FAs and integrins emerged in SMCs with high cytoplasm tensions on the nanowire arrays.

References

1. Singhvi R, Stephanopoulos G, Wang DI. Effects of substratum morphology on cell physiology. Biotechnol Bioeng 1994;43(8):764-71.
2. Nikkhah M, Edalat F, Manoucheri S, Khademhosseini A. Engineering microscale topographies to control the cell-substrate interface. Biomaterials 2012;33(21):5230-46.
3. Ingber DE. Cellular mechanotransduction: putting all the pieces together again. FASEB J 2006;20:811-27.
4. Cai L, Zhang L, Dong J, Wang S. Photocured biodegradable polymer substrates of varying stiffness and microgroove dimensions for promoting nerve cell guidance and differentiation. Langmuir 2012;28(34):12557-68.
5. Wang K, Cai L, Zhang L, Dong J, Wang S. Biodegradable photo-crosslinked polymer substrates with concentric microgrooves for regulating MC3T3-E1 cell behavior. Adv Healthcare Mater 2012;1(3):292-301.
6. Gittens RA, McLachlan T, Olivares-Navarrete R, Cai Y, Berner S, Tannenbaum R, Schwartz Z, Sandhage KH, Boyan BD. The effects of combined micron-/submicron-scale surface roughness and nanoscale features on cell proliferation and differentiation. Biomaterials 2011;32(13):3395-403.
7. Biela SA, Su Y, Spatz JP, Kemkemer R. Different sensitivity of human endothelial cells, smooth muscle cells and fibroblasts to topography in the nano-micro range. Acta Biomater 2009;5(7):2460-6.
8. Uttayarat P, Perets A, Li M, Pimton P, Stachelek SJ, Alferiev I, Composto RJ, Levy RJ, Lelkes PI. Micropatterning of three-dimensional electrospun polyurethane vascular grafts. Acta Biomater 2010;6(11):4229-37.
9. Xia Y, Yang P, Sun Y, Wu Y, Mayers B, Gates B, Yin Y, Kim F, Yan H. One-dimensional nanostructures: synthesis, characterization, and applications. Adv Mater 2003;15: 353-389.
10. Burda C, Chen X, Narayanan R, El-Sayed MA. Chemistry and properties of nanocrystals of different shapes. Chem Rev 2005;105(4):1025-102.
11. Cao G, Liu D. Template-based synthesis of nanorod, nanowire, and nanotube arrays. Adv Colloid Interface Sci 2008;136(1-2):45-64.

12. Furneaux RC, Rigby WR, Davidson AP. The formation of controlled-porosity membranes from anodically oxidized aluminum. Nature 1989;337:147.
13. Duran H, Steinhart M, Butt HJ, Floudas G. From heterogeneous to homogeneous nucleation of isotactic poly(propylene) confined to nanoporous alumina. Nano Lett 2011;11(4):1671-5.
14. Lazzara TD, Kliesch TT, Janshoff A, Steinem C. Orthogonal functionalization of nanoporous substrates: control of 3D surface functionality. ACS Appl Mater Interfaces 2011;3(4):1068-76.
15. Haberkorn N, Weber SA, Berger R, Theato P. Template-based preparation of free-standing semiconducting polymeric nanorod arrays on conductive substrates. ACS Appl Mater Interfaces 2010;2(6):1573-80.
16. Chen JT, Chen D, Russell TP. Fabrication of hierarchical structures by wetting porous templates with polymer microspheres. Langmuir 2009;25(8):4331-5.
17. Zhang MF, Dobriyal P, Chen JT, Russell TP, Olmo J, Merry A. Wetting transition in cylindrical alumina nanopores with polymer melts. Nano Lett 2006; 6:1075-1079.
18. Kim E, Xia Y, Whitesides GM. Polymer microstructures formed by moulding in capillaries. Nature 1995;376: 581-584.
19. Zhang B, Xiao Y, Hsieh A, Thavandiran N, Radisic M. Micro- and nanotechnology in cardiovascular tissue engineering. Nanotechnology 2011;22(49):494003.
20. Kim P, Kim DH, Kim B, Choi SK, Lee SH, Khademhosseini A, Langer R, Suh KY. Fabrication of nanostructures of polyethylene glycol for applications to protein adsorption and cell adhesion. Nanotechnology 2005;16(10):2420-6.
21. Grimm S, Martin J, Rodriguez G, Fernandez-Gutierrez M, Mathwig K, Wehrspohn RB, Gosele U, San Roman J, Mijangos C, Steinhart M. Cellular interactions of biodegradable nanorod arrays prepared by nondestructive extraction from nanoporous alumina. J Mater Chem 2010;20: 3171-3177.
22. Jamshidian M, Tehrany EA, Imran M, Jacquot M, Desobry S. Poly-lactic acid: production, applications, nanocomposites, and release studies. Compr Rev Food Sci F 2010;9:552-571.
23. Tao SL, Desai TA. Aligned arrays of biodegradable poly(ε-caprolactone) nanowires and nanofibers by template synthesis. Nano Lett 2007;7(6):1463-8.

24. Porter JR, Henson A, Popat KC. Biodegradable poly(ε-caprolactone) nanowires for bone tissue engineering applications. Biomaterials 2009;30(5):780-8.
25. Bechara SL, Judson A, Popat KC. Template synthesized poly(ε-caprolactone) nanowire surfaces for neural tissue engineering. Biomaterials 2010;31(13):3492-501.
26. Cai L, Wang S. Poly(ε-caprolactone) acrylates synthesized using a facile method for fabricating networks to achieve controllable physicochemical properties and tunable cell responses. Polymer 2010;51:164-77.
27. Liu X, Cai L, Hao F, Cui M, Wang S. Biodegradable elastomeric substrates with controllable stiffness for regulating smooth muscle cell behavior. Abstracts of Papers of The American Chemical Society 2011;242: 260-PMSE.
28. Liu X, Cai L, Wang S. Smooth muscle cell behavior on crosslinked poly(ε-caprolactone) triacrylate networks grafted with methoxy poly(ethylene glycol) monoacrylate of various composition and chain length. Abstracts of Papers of The American Chemical Society 2012;243:458-POLY.
29. Cai L, Wang K, Wang S. Poly(ethylene glycol)-grafted poly(propylene fumarate) networks and parabolic dependence of MC3T3 cell behavior on the network composition. Biomaterials 2010;31:4457-66.
30. Du K, Gan Z. Cellular interactions on hierarchical poly(ε-caprolactone) nanowire micropatterns. ACS Appl Mater Interfaces 2012;4(9):4643-50.
31. Wang K, Cai L, Hao F, Xu X, Cui M, Wang S. Distinct cell responses to substrates consisting of poly(ε-caprolactone) and poly(propylene fumarate) in the presence or absence of cross-links. Biomacromolecules 2010;11:2748-59.
32. Peyton SR, Raub CB, Keschrumrus VP, Putnam AJ. The use of poly(ethylene glycol) hydrogels to investigate the impact of ECM chemistry and mechanics on smooth muscle cells. Biomaterials 2006;27:4881-93.
33. Wang C, Yin S, Cen L, Liu Q, Liu W, Cao Y, Cui L. Differentiation of adipose-derived stem cells into contractile smooth muscle cells induced by transforming growth factor-beta1 and bone morphogenetic protein-4. Tissue Eng Part A 2010;16(4):1201-13.
34. Kim E, Xia Y, Whitesides GM. Micromolding in capillaries: applications in materials science. J Am Chem Soc 1996;118 (24):5722-5731

35. Ayala R, Zhang C, Yang D, Hwang Y, Aung A, Shroff SS, Arce FT, Lal R, Arya G, Varghese S. Engineering the cell-material interface for controlling stem cell adhesion, migration, and differentiation. Biomaterials 2011;32(15):3700-11.
36. Folkman J, Moscona A. Role of cell shape in growth control. Nature 1978;273:345-349.
37. Huang S, Ingber DE. Shape-dependent control of cell growth, differentiation, and apoptosis: switching between attractors in cell regulatory networks. Exp Cell Res 2000;261(1):91-103.
38. Geiger B, Spatz JP, Bershadsky AD. Environmental sensing through focal adhesions. Nat Rev Mol Cell Bio 2009;10:21-33.
39. Owens GK, Kumar MS, Wamhoff BR. Molecular regulation of vascular smooth muscle cell differentiation in development and disease. Physiol Rev 2004;84:767-801.
40. Rensen SS, Doevendans PA, van Eys GJ. Regulation and characteristics of vascular smooth muscle cell phenotypic diversity. Neth Heart J 2007;15(3):100-8.
41. Giancotti FG, Ruoslahti E. Integrin signaling. Science 1999;285(5430):1028-32.
42. Hynes RO. Integrins: bidirectional, allosteric signaling machines. Cell 2002;110:673-87.
43. Matschegewski C, Staehlke S, Loeffler R, Lange R, Chai F, Kern DP, Beck U, Nebe BJ. Cell architecture-cell function dependencies on titanium arrays with regular geometry. Biomaterials 2010;31(22):5729-40.
44. Harbers GM, Grainger DW. Cell-material interactions: fundamental design issues for tissue engineering and clinical considerations. In: Guelcher SA, Hollinger JO, editors. Introduction to biomaterials. Boca Raton:CRC Press;2005. p. 15-45.
45. Wong JY, Leach JB, Brown XQ. Balance of chemistry, topography, and mechanics at the cell-biomaterial interface: issues and challenges for assessing the role of substrate mechanics on cell response. Surf Sci 2004;570:119-33.
46. Saltzman WM, Kyriakides TR. Cell interactions with polymers. In: Lanza R, Langer R, Vacanti J, editors. Principles of tissue engineering. 3rd ed. San Diego: Elsevier Academic Press; 2007. p. 279-96.
47. Cai L, Zhang L, Dong J, Wang S. Photocured biodegradable polymer substrates of varying stiffness and microgroove dimensions for promoting nerve cell guidance and differentiation. Langmuir 2012;28(34):12557-68.
48. Wu X, Wang S. Regulating MC3T3-E1 cells on deformable poly(ε-caprolactone)

honeycomb films prepared using a surfactant-free breath figure method in a water-miscible solvent. ACS Appl Mater Interfaces 2012;4(9):4966-75.

49. Wu X, Wang S. Biomimetic calcium carbonate concentric microgrooves with tunable widths for promoting MC3T3-E1 cell functions. Adv Healthc Mater 2013;2(2):326-33.
50. Wu X, Wang S. Integration of photo-crosslinking and breath figures to fabricate biodegradable polymer substrates with tunable pores that regulate cellular behavior. Polymer 2014;55(7):1756-62
51. Ingber DE, Prusty D, Sun Z, Betensky H, Wang N. Cell shape, cytoskeletal mechanics, and cell cycle control in angiogenesis. J Biomech 1995;28(12):1471-84.
52. Chen CS, Mrksich M, Huang S, Whitesides GM, Ingber DE. Micropatterned surfaces for control of cell shape, position, and function. Biotechnol Prog 1998;14(3):356-63.
53. Huang S, Ingber DE. The structural and mechanical complexity of cell-growth control. Nat Cell Biol 1999;1(5):E131-8.
54. Meyers JR, Corwin JT. Shape change controls supporting cell proliferation in lesioned mammalian balance epithelium. J Neurosci 2007;27(16):4313-25.
55. Parsons JT, Horwitz AR, Schwartz MA. Cell adhesion: integrating cytoskeletal dynamics and cellular tension. Nat Rev Mol Cell Bio 2011;11:633-43.
56. Zamir E, Geiger B. Molecular complexity and dynamics of cell-matrix adhesions. J Cell Sci 2001;114:3583-90.
57. den Braber ET, de Ruijter JE, Smits HTJ, Ginsel LA, von Recum AF, Jansen JA. Quantitative analysis of cell proliferation and orientation on substrata with uniform parallel surface micro grooves. Biomaterials 1996;17:1093-9.
58. Dalby MJ, Riehle MO, Sutherland DS, Agheli H, Curtis AS. Changes in fibroblast morphology in response to nano-columns produced by colloidal lithography. Biomaterials 2004;25(23):5415-22.
59. Ghibaudo M, Di Meglio JM, Hersen P, Ladoux B. Mechanics of cell spreading within 3D-micropatterned environments. Lab Chip 2011;11(5):805-12.
60. Oakley C, Brunette DM. Topographic compensation: Guidance and directed locomotion of fibroblasts on grooved micromachined substrata in the absence of microtubules. Cell Motil Cytoskel 1995;31:45-58.

61. Wozniak MA, Modzelewska K, Kwong L, Keely PJ. Focal adhesion regulation of cell behavior. Biochim Biophys Acta 2004;1692:103-19.
62. Srivatsa SS, Fitzpatrick LA, Tsao PW, Reilly TM, Holmes DR, Schwartz RS, Mousa SA. Selective αvβ3 integrin blockade potently limits neointimal hyperplasia and lumen stenosis following deep coronary arterial stent injury: evidence for the functional importance of integrin αvβ3 and osteopontin expression during neointima formation. Cardiovasc Res 1997;36:408-28.

Chapter VII. Controllable Crystallinity of Poly(L-lactide acid) Networks for Regulation of Smooth Muscle Cells

Abstract

Polymer crystallinity influences the morphological and mechanical properties, thus it is of interest to use it as a factor to regulate cell behavior in tissue engineering applications of semi-crystalline polymers. Here we report a series of novel photo-crosslinkable poly(L-lactic acid) triacrylates (PLLATAs) that were synthesized and photo-crosslinked under UV light into network substrates. With increasing the annealing time from 0 to 5, 7, 10, and 20 h at 70 ℃, both crystallinity and surface roughness increased for PLLATA networks without variance in chemical composition. Both water contact angle and the capability of adsorbing serum proteins from the culture media on the crystallized PLLATA networks were lower than on the amorphous one. Primary rat smooth muscle cells (SMCs) were found to respond to the substrate crystallinity by exhibiting reduced attachment, proliferation, and differentiation on the crystalline, rough surfaces of the PLLATA networks than on the amorphous, smooth one. Down-regulated integrin expression and weakened focal adhesions (FAs) in terms of size, elongation, and density in SMCs were also observed on the crystalline PLLATA networks. After removal of surface roughness through compression, SMCs exhibited little variance among compressed PLLATA networks regardless of the difference in bulk crystallinity.

7.1 Introduction

Cardiovascular diseases, for example, heart disease and stroke, are major causes of death in the U.S. [1]. Cardiovascular tissue engineering holds critical importance by providing vessel replacements or supportive tissue scaffolds made from natural or synthetic biomaterials. Widely studied cardiovascular tissue engineering polymers include polyethylene [2], poly(glycolic acid) (PGA) [3], poly(ethylene glycol) (PEG) [5,6], poly(ε-caprolactone) (PCL) [6-8], and poly(L-lactic acid) (PLLA) [9]. PLLA and its copolymers have favorable chemical properties such as biodegradability through hydrolysis, physical properties such as high stiffness, and good efficiency in supporting vascularization [10-12]. In 2000, PLLA-based stents were used in human coronary arteries without showing inflammatory reactions in 6 months [13]. Based on this finding, researchers conducted continuous clinical trials on PLLA-based stents, which paved the way to using PLLA for further vascular tissue engineering applications [14,15].

The processing methods for PLLA determine the properties of the final products and consequently influence cellular responses to them when used for tissue engineering applications such as implants. As a semi-crystalline polymer, PLLA undergoes crystallization in the bulk and its surface can be roughened by the spherulites formed in crystallization. PLLA has been studied in terms of crystallization-induced surface characteristics and their effects on cell behavior [16-18]. Because the glass transition temperature (T_g) for PLLA is higher than 37 ℃, amorphous PLLA substrates can be prepared by quenching the melt at a temperature well below its T_g. The crystallinity of PLLA can be tuned when it is crystallized isothermally at a crystallization temperature (T_c) between its T_g and melting temperature (T_m) [16]. Hepatocyte spheroid formation was faster on crystalline PLLA substrates while 3T3 fibroblasts proliferated better on amorphous PLLA ones [16]. A gradient of polymer crystallinity was also achieved on PLLA films by using different annealing temperatures (or T_c) from 45 to 100 ℃ and a gradient of root-mean-square surface roughness (R_{rms}) from 0.5 to 13 nm was formed on the substrate [17]. The proliferation rate of MC3T3-E1 cells was found to be monotonically dependent on R_{rms}: it was greater on the smooth area of the PLLA film than on the rough one [17]. Despite these results, the origin and mechanism of distinct cell responses to crystallization-induced surface characteristics compared with amorphous, smooth polymer substrates are still unclear

and these results for cell adhesion and proliferation are not always consistent, especially among different semi-crystalline polymers.

In this study, novel photo-crosslinkable PLLA triacrylates (PLLATAs) with different molecular weights (Table 7.1) were synthesized and photo-crosslinked under UV light to achieve network substrates. When the number-average molecular weight (M_n) of PLLATA was 28,010 g/mol, the crystallinity of the obtained PLLATA28k network was modulated by varying the annealing time at T_c of 70 ℃, which is slightly higher than its T_g. After being annealed for increased length of time from 0 to 5, 7, 10, and 20 h, PLLATA networks with the same chemical composition had increased crystallinity and surface roughness. Surface properties including hydrophilicity, surface energies, and protein adsorption were determined. Primary rat smooth muscle cells (SMCs) were cultured on these PLLATA networks and their attachment, proliferation, spreading, focal adhesions (FAs), expression of integrin subunits and phenotypic gene markers were evaluated.

Table 7.1 The synthesized PLLATA with varied molecular weights and thermal properties before and after photocrosslinking.

Polymer	M_n (g mol^{-1})	M_w (g mol^{-1})	DPI	T_m (℃)	ΔH_m (J/g)	χ_c (%)
PLLATA 9k	9,320	10,090	1.1	137.5	32.9	35.1
PLLATA 11k	11,360	12,420	1.1	142.1	46.5	49.7
PLLATA 13k	13,280	15,910	1.2	152.6	55.5	59.3
PLLATA 28k	28,010	34,640	1.2	163.7	57.0	60.9
PLLATA 55k	55,020	76,500	1.4	170.0	55.2	59.0
Crosslinked PLLATA 9k				-	-	-
Crosslinked PLLATA 11k				139.2	33.7	36.0
Crosslinked PLLATA 13k				149.1	37.0	39.6
Crosslinked PLLATA 28k				160.1	42.3	45.2
Crosslinked PLLATA 55k				168.8	41.1	43.9

7.2 Materials and methods

7.2.1 Synthesis and photo-crosslinking of PLLATA

PLLA triols were synthesized via the ring-opening polymerization of L-lactide initiated by 1,1,1-tris(hydroxymethyl) propane (TMP), in the presence of $Sn(Oct)_2$ as the catalyst (Figure

1). Five different molecular weights (see Table 7.1) were achieved by using different ratios of L-lactide and TMP. Then PLLA triol was reacted with acryloyl chloride (AC) at room temperature for 24 h under nitrogen protection in the presence of K_2CO_3 as the proton scavenger at a molar ratio of 1:3:3 (PLLA triol:AC:K_2CO_3) in methylene chloride with ratio of 50 ml per 10 g polymer to synthesize PLLATA. After the reaction, the mixture was centrifuged at 3000 rpm for 3 min to remove inorganic solids (KCl, $KHCO_3$, and unreacted K_2CO_3) followed by precipitation in diethyl ether and complete drying in vacuum. PLLATA networks were formed by photo-crosslinking PLLATAs in methylene chloride under a UV lamp (SB-100P, Spectroline; wavelength: 365 nm, Intensity: 4800 μw/cm^2) for 20 min. Phenyl bis(2,4,6-trimethyl benzoyl) phosphine oxide (BAPO, IRGACURE 819; Ciba Specialty Chemicals, Tarrytown, NY) was used as the photo-initiator with a ratio of 100 g : 50 ml : 1 g for PLLATA, CH_2Cl_2, and BAPO. The crystallinities of PLLATA28k networks were modulated by varying the annealing time from 0 to 5, 7, 10, or 20 h at 70 ℃.

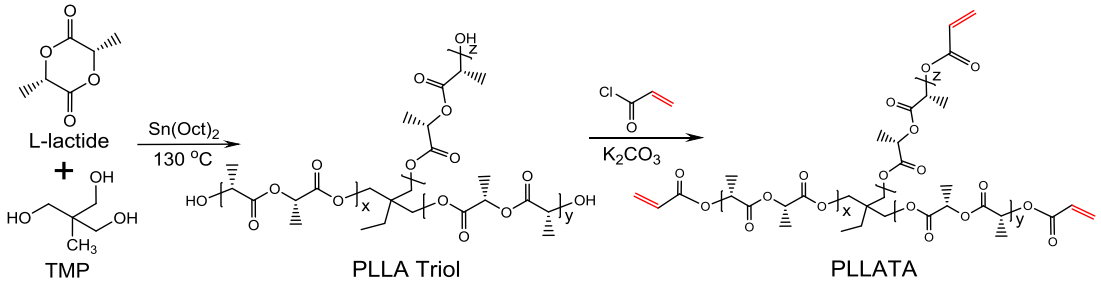

Figure 7.1 Synthesis of PLLA triol and PLLA triacrylate.

7.2.2 Characterization of polymer properties

The chemical structures of PLLATAs were analyzed by ^{1}H Nuclear Magnetic Resonance (NMR) on a Varian Mercury 300 spectrometer using $CDCl_3$ solutions containing tetramethylsilane (TMS). Their molecular weights were determined using Gel Permeation Chromatography (GPC) with tetrahydrofuran as the eluent and standard monodisperse polystyrene samples as the references. The swelling ratios and gel fractions of crosslinked PLLATA networks were obtained in CH_2Cl_2 according to the method reported previously by our research group [19]. Thermal properties were measured using Differential Scanning Calorimetry (DSC) by heating the samples to 200 ℃, then cooling to 0 ℃, and reheating to 200

℃ at a rate of 10 ℃/min. For crystallinity determinations in annealed crosslinked PLLATAs, the samples were heated from 0 to 200 ℃ at a rate of 10 ℃/min using the same DSC. Surface morphology of crosslinked PLLATA substrates was characterized using atomic force microscopy (AFM; Veeco Instruments, Santa Barbara, CA) and R_{rms} was calculated from a 10 μm × 10 μm area. Surface free energy was calculated from the water contact angle determined at 37 ℃ using a Ramé-Hart NRC C. A. goniometer (Model 100-00-230, Mountain Lakes, NJ) [19]. Total serum proteins adsorbed on the sample surface from the cell culture media were collected using a MicroBCA protein assay kit (Pierce, Rockford, IL) and detected using a micro-plate reader using the method reported previously by our research group [19].

7.2.3 In vitro cell behaviors

Crosslinked PLLATA thin films were prepared through spin-coating PLLATA/CH_2Cl_2 /BAPO solution (100 g : 50 ml : 1 g) using WS-400-6NPP Spin Coater (Laurell Technologies, North Wales, PA) on microscope slides (Fisher Scientifi c, Pittsburgh, PA) at 2000 rpm for 6 s. Then the samples were photo-crosslinking under UV light for 20 min immediately after spin-coating. Crosslinked PLLATA thin films were sterilized in 70% alcohol solution overnight and dried completely in vacuum prior to cell studies. Primary SMCs isolated from rat aorta were cultured using the method reported by our research group previously [20]. Sterile polymer films were seeded with SMCs at a density of 15000 cells/cm^2, with tissue-culture polystyrene (TCPS) as the positive control. Cell numbers at 4 h, days 1, 2, and 4 post-seeding were determined using the MTS method reported previously by our research group [21]. The cells attached on the polymer films were fixed with 4% paraformaldehyde (PFA) solution for 10 min, washed twice in phosphate buffered saline (PBS), and permeabilized in 0.2% Triton X-100 solution for 10 min, all at room temperature. Then their cytoplasm and cell nuclei were stained using rhodamine-phalloidin (RP) and 4',6-diamidino-2-phenylindole (DAPI), respectively, before photo-graphing using an Axiovert 25 light microscope (Carl Zeiss, Germany). From the fluorescence cell images, cell area was determined and averaged on 20 non-overlapping cells using ImageJ software (National Institutes of Health, Bethesda, MA).

7.2.4 Characterization of FAs in SMCs on crosslinked PLLATA

SMCs cultured for 1 day on the PLLATA films were fixed and permeabilized, as described in Section 2.3, before they were incubated with 1% Bovine Serum Albumin (BSA) in PBS for 1 h at 37 ℃ to block unspecific binding cites. Monoclonal vinculin primary antibody (1:1000 in PBS; Sigma) was then used to target FA vinculin by incubating the cells at room temperature with gentle shaking for 1 h. After that, unconjugated primary antibody was washed away using PBS three times, followed by further incubation with goat anti-mouse IgG secondary antibody (1:200 in PBS; Sigma) solution in dark at room temperature for 2 h. After vinculin staining, SMC specific filaments were also stained using RP for 1 h at 37 ℃. The cells were observed using a Leica DM6000B confocal fluorescent microscope. Quantification of FAs such as FA area, FA density (number of FAs per cell), and FA elongation defined as the inverse of circularity, i.e., perimeter^2/(4π × area), were performed and averaged on five non-overlapping cells using ImageJ according to a previous report [4].

7.2.5 Gene expression analysis of contractile phenotypic markers and integrins

Polymerase Chain Reaction (PCR) was used to quantify the expression levels of contractile phenotypic markers, smooth muscle myosin heavy chain (SM-MHC), calponin, and transgelin in SMCs cultured for 4 days on these polymer substrates. Total RNA was isolated using the RNeasy Mini Kit (Qiagen, Valencia, CA) following the manufacturer's instruction. cDNA was obtained by reverse transcription using DyNAmo cDNA synthesis kit (Thermo Scientific, Waltham, MA). The primers for different gene markers were designed using Oligoperfect software, as listed in Table 7.2. For each PCR well, 2.5 μL of total cDNA with the same concentration (1 ng/μL) was added as the template to make a mixture with Power SYBR Green PCR Master Mix (Applied Biosystems, Warrington, UK) for a total 20 μL reaction system. For each sample, this step was done in triplicates. The amplification and detection process was performed on a Peltier Thermal Cycler fluorescence detection system (MJ Research PTC-200). The software procedure were set as 94 ℃ for 5 min followed by the cyclic steps of 94 ℃ for 30 s, 55 ℃ for 30 s, and 72 ℃ for 1 min. The expression levels of target gene markers were normalized to that of the housekeeping gene, glyceraldehyde-3-phosphate dehydrogenase (GAPDH).

Table 7.2 Primers for different gene markers used in the real-time PCR analysis.

Gene markers	Forward primer	Reverse primer
Calponin	5'-AGTCTACTCTCTCTTGGCTCTGGCC-3'	5'-CCTGCCTTCTCTCAGCTTCTCAGG-3'
SM-MHC	5'-AAGCAGCTCAAGAGGCAG-3'	5'-AAGGAACAAATGAA GCCTCGTT-3'
Transgelin	5'-GGCAGCTGAGGATTATGGAGTCACG-3'	5'-TGGGATCTCCACGGTAGTGTCCA-3';
Integrin-α_v	5'-AAGACGCCCGAAAAGAATGAC-3'	5'-ATCCCGCTTGGTGATGAGAT-3'
Integrin-α_1	5'-TCTGCCAAACTCAGTCCACGA-3'	5'-TGACGATCAGCAGGCTCTTTT-3'
Integrin-α_5	5'-CCTTCCTTCATTGGCATGGA-3'	5'-TCTGCATCCTGTCAGCAATCC-3'
Integrin-β_1	5'-AGAGTGCCGTGACAACTGTG-3'	5'-GAGCCCCAAAGCTACCCTAC-3'
Integrin-β_3	5'-GACCCGCTTCAATGACGAA-3'	5'-TCACAGACTGTAGCCTGCATGA-3'
GAPDH	5'-TCTTCACCACCATGGAGAA-3'	5'-ACTGTGGTCATGAGCCCTT-3'

7.2.6 Statistical analysis

All statistical computations were performed by one-way analysis of variance (ANOVA) in Origin8 software and followed by Tukey post-test if necessary. The values were considered significantly different if the *p*-value calculated between them was lower than 0.05.

7.3 Results

7.3.1 Structure characterization and photocrosslinking

The chemical structures of PLLATAs were determined using ^{1}H NMR spectra, as displayed in Fig. 7.2.All the chemical shifts in the ^{1}H NMR spectra could be well assigned to corresponding protons, as marked in the polymer structures. As demonstrated in Fig. 7.2a, PLLA triols showed no vinyl groups in (-CH=CH-) in the chemical shift at 5.7-6.5 ppm. However, after acrylation, PLLATA showed an apparent chemical shift at 5.7-6.5 ppm, indicating successful addition of vinyl groups in the ends. PLLATA samples with M_ns of 9320, 11360, 13280, 28010, and 55020 g/mol were named as PLLATA9k, 11k, 13k, 28k, and 55k, respectively. After photo-crosslinking, all the PLLATA networks had high gel fractions of ~90%, as shown in Fig. 7.3a. Meanwhile, the swelling ratio of PLLATA network in methylene chloride increased evidently with increasing the molecular weight of PLLATA (Fig. 7.3b).

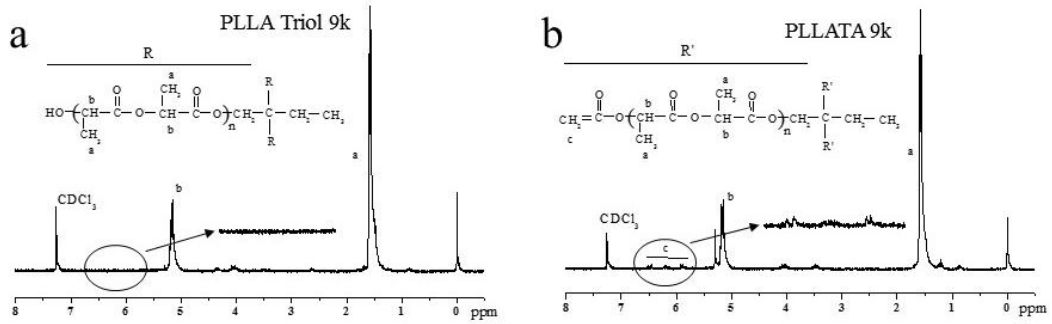

Figure 7.2 ^{1}H NMR spectra of (a) PLLA triol and (b) PLLATA. Solvent: $CDCl_3$.

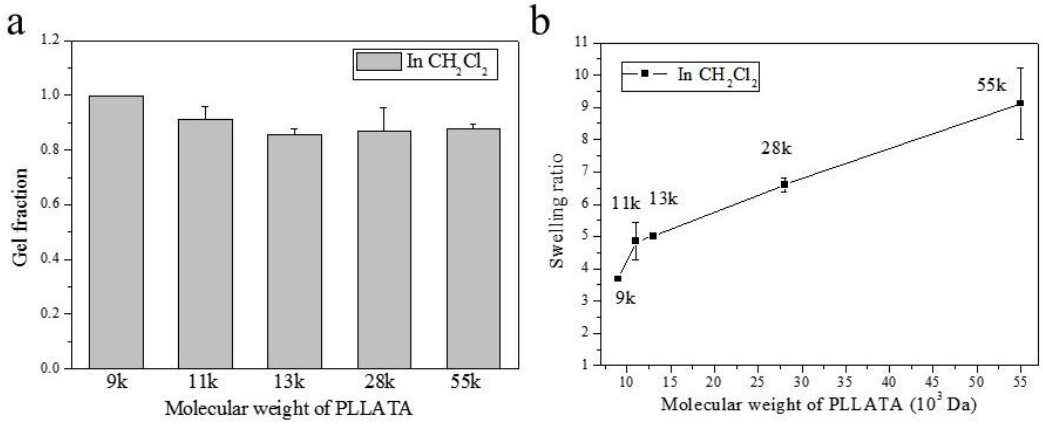

Figure 7.3 (a) Swelling ratios and (b) gel fractions of photo-crosslinked networks of PLLATAs with different molecular weights from 9320 to 55020 g/mol.

7.3.2 Thermal properties, surface hydrophilicities and protein adsorption

Figure 4 shows the DSC curves of PLLATAs before and after crosslinking obtained in the heating run from 0 to 200 ℃. Their thermal properties including T_m, heat of fusion (ΔH_m), and degree of crystallinity (χ_c) obtained from these DSC curves are listed in Table 7.1. T_m was the highest peak temperature in all the exothermal peaks. Crystallinity (χ_c) was estimated using the equation of $\chi_c = [\Delta H_m/\phi_{PLA}\Delta H_0] \times 100\%$, where ΔH_0 was the heat of fusion for fully crystalline PLLA with a value of 93.6 J/g [22] and ϕ_{PLLA} was the PLLA fraction in PLLATA, which was approximately 100%. These five PLLATAs with different molecular weights were all semi-crystalline with different values in T_m and crystallinity. T_m increased gradually from 137.5 to 142.1, 152.6, 163.7, and 170.0 ℃ when the molecular weight increased from 9k to 11k, 13k, 28k, and 55k, respectively. After crosslinking, both T_m and crystallinity decreased significantly

because the crystallization process of PLLA chain segments was strongly prohibited by the crosslinks [23]. As demonstrated in Fig. 7.4, crosslinked PLLATA9k became fully amorphous. Meanwhile, crosslinked PLLATA11k, 13k, 28k, and 55k were still semi-crystalline and had reduced T_m values of 139.2, 149.1, 160.1, and 168.8 ℃, respectively.

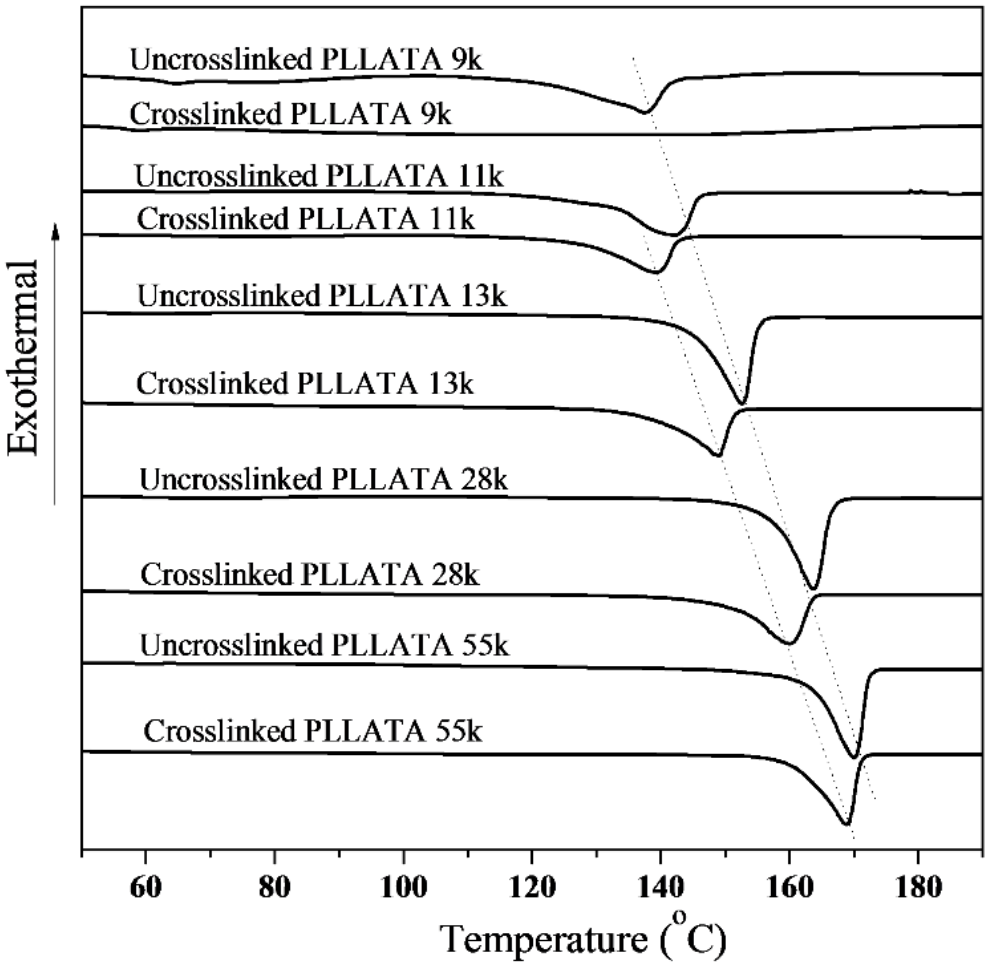

Figure 7.4 DSC curves of the PLLATAs with different molecular weights before and after photo-crosslinking.

7.3.3 Crystallinity differences achieved by varying crystallization time

Photo-crosslinked PLLATA28k networks were melted at 200 ℃ then annealed at 70 ℃ for 0, 5, 7, 10, and 20 h to achieve samples with different crystallinities. As shown in the DSC curves in Fig. 7.5a, the crystallization peak gradually diminished with increasing the annealing time. The calculated χ_c increased from 3.5% to 18.7%, 29.0%, 41.3%, 49.0%, and 49.3% when the annealing time increased from 0 to 5, 7, 10, 20, and 40 h, respectively.

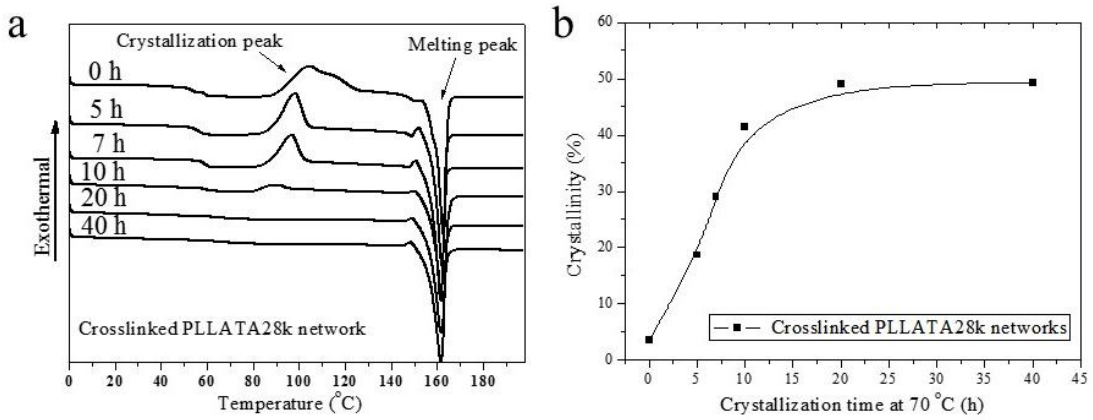

Figure 7.5 (a) DSC curves and (b) crystallinities of PLLATA28K networks annealed for different time at 70 °C.

The surface of amorphous PLLATA was homogeneous with dominant amorphous regions. When it was annealed, crystals nucleated and grew larger. The crystalline microstructures of PLLATA spherulites resulted in surface roughness. As demonstrated in Fig. 7.6a, the surface of crosslinked PLLATA gradually became rougher when the annealing time was longer. R_{rms} increased from 20.8 ± 1.3 nm to 22.9 ± 3.9, 28.4 ± 2.8 and 48.1 ± 3.4 nm when the annealing time increased from 5 to 7, 10, and 20 h, respectively. In comparison, the samples after compression had lower R_{rms} values of 14.1 ± 1.1, 17.2 ± 0.9, 17.7 ± 0.7, and 15.8 ± 1.2 nm when the annealing time was 5, 7, 10, and 20 h (Fig. 7.6b), respectively. To determine whether cell culture media affected the surface structures of PLLATA networks, PLLATA network annealed at 70 ℃ for 20 h was placed in the culture medium used for SMCs here at 37 °C for 24 h. The sample had a similar R_{rms} value of 46.3 ± 2.8 nm, as displayed in Fig. 7.6c. Amorphous PLLATA network was the smoothest with the lowest R_{rms} of 3.1 ± 1.0 nm, as shown in Fig. 7.6d.

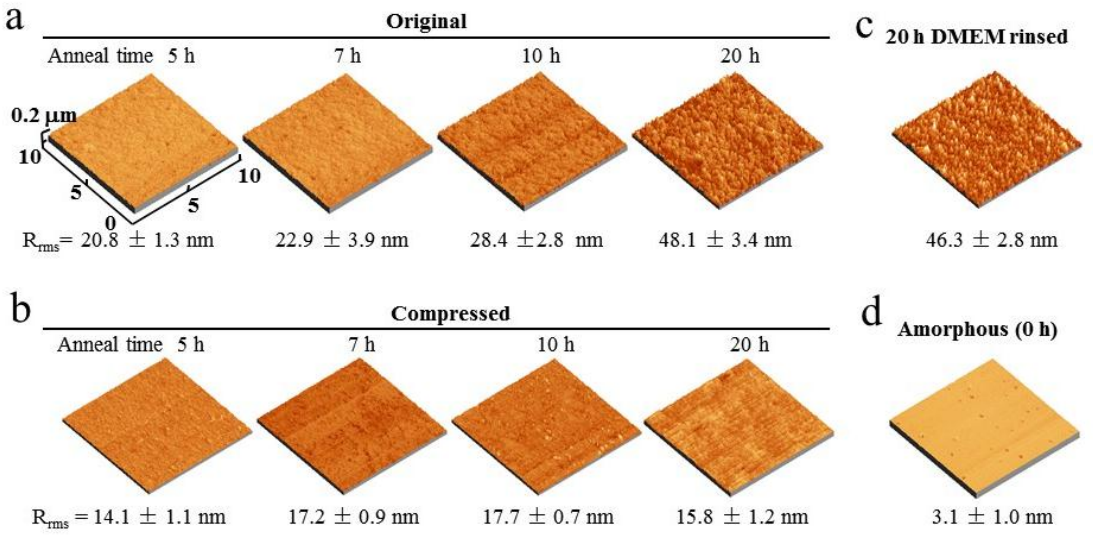

Figure 7.6 AFM images of (a) original and (b) compressed PLLATA network surfaces annealed for 0, 5, 7, 10, and 20 h at 70 ℃, (c) PLLATA network crystallized for 20 h and rinsed in DMEM for 1 day, and (d) amorphous PLLATA network (crystallized for 0 h).

Surface roughness can affect hydrophilicity [24]. As shown in Fig. 7.7a, a lower water contact angle was observed on the fully crystallized samples than the PLLATA networks annealed for shorter time periods. However, no obvious differences were observed in the water contact angle among all the smooth samples that were compressed. When methylene iodide was used to evaluate its interaction with the PLLATA networks, no significant differences were observed in the contact angles.

The total surface energy (γ) and the dispersive (γ^d) and polar (γ^p) components of the surface tension were calculated using the Owens-Wendt equation, as reported in literature [25-27]. As shown in Fig. 7.7b, the surface energy only increased slightly when the annealing time for crosslinked PLLATA increased because of the increase in χ_c. Meanwhile, the amount of serum proteins adsorbed on the PLLTA networks was significantly lower when the annealing time was 10 or 20 h than on those annealed for short time periods (Fig. 7.7c). The variance in serum protein adsorption was not seen for the compressed samples. The differences in surface energy and protein adsorption were attributed to the submicron surface morphologies in polymer crystallization, which also influenced SMC responses to these PLLATA networks.

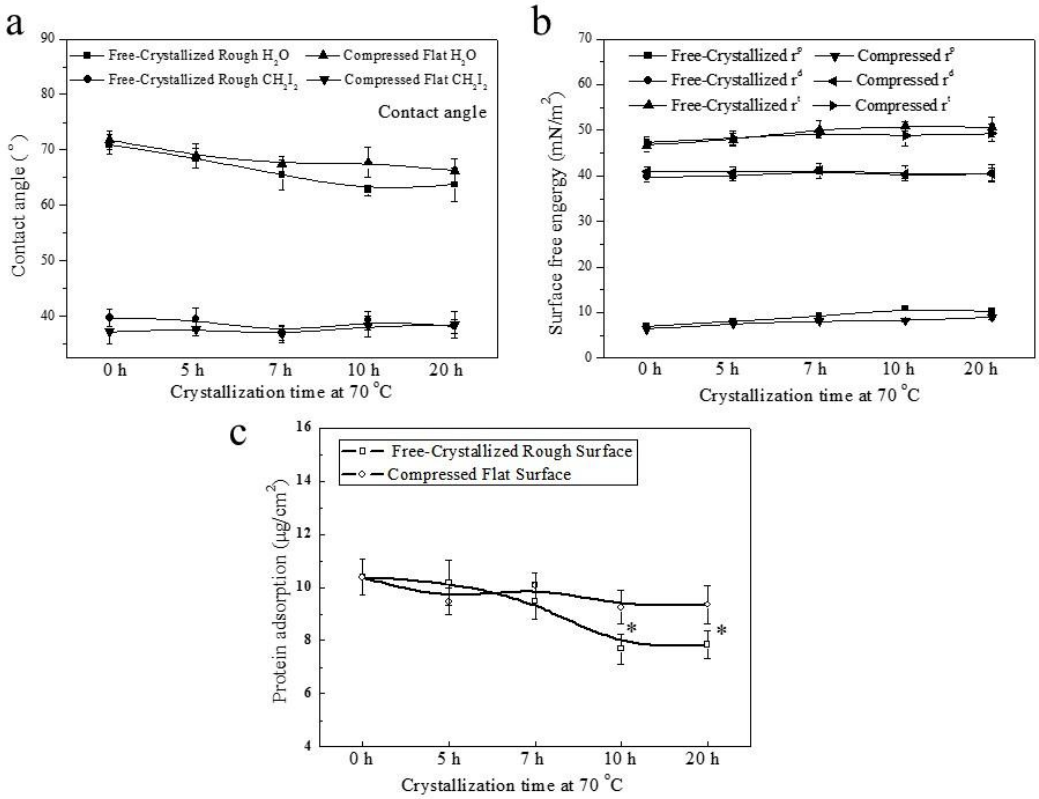

Figure 7.7 (a) Contact angles of water and CH_2I_2 on the original and compressed PLLATA networks annealed for different time periods. (b) Surface energies calculated from the contact angles on these PLLATA networks. (c) Protein adsorption on these PLLATA networks.

7.3.4 Cellular response to crystallinity differences

The SMC attachment rates determined at 4 h post-seeding on these crosslinked PLLATA films are shown in Fig. 7.8a. For the original films having surfaces from free crystallization without being compressed, SMC attachment decreased from 0.93 ± 0.05 on amorphous PLLATA network to 0.90 ± 0.02, 0.88 ± 0.02, 0.84 ± 0.03, and 0.73 ± 0.04 when the annealing time increased to 5, 7, 10, and 20 h, respectively. On the compressed substrates with similar R_{rms} values, little difference was seen in SMC attachment. To clarify whether the PLLATA surface structure diminished in the culture media, we also compared SMC attachment on the original and pre-wetted PLLATA network films. As shown in Fig. 7.8b, SMC attachment rates were similar on either original or pre-wetted substrates.

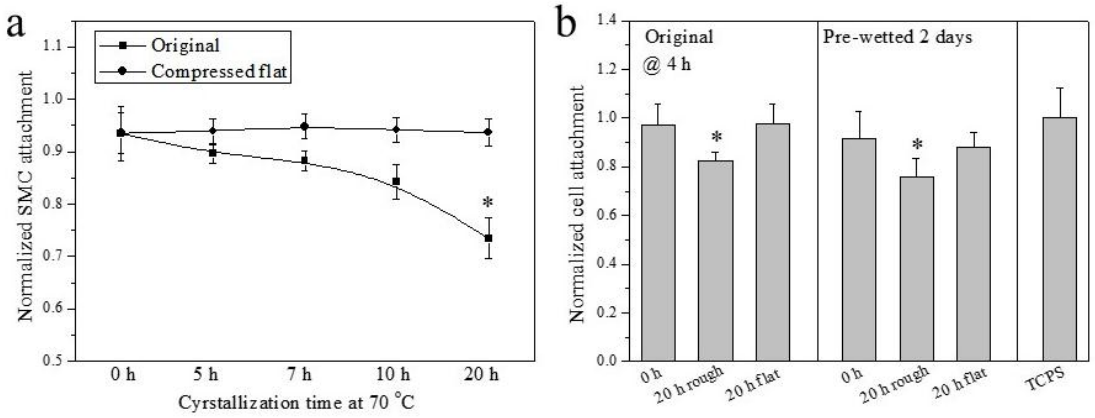

Figure 7.8 (a) SMC attachment rates on original and compressed PLLATA networks crystallized for different time, normalized by the positive control (TCPS) value at 4 h post-seeding. (b) SMC attachment rates on original PLLATA networks and the ones that were pre-wetted in cell culture media for two days, with TCPS as the positive control.

After adhesion onto a substrate, cells start to spread and cell spreading is important for subsequent events such as proliferation and migration [28]. SMC spread areas determined at day 1 on original and compressed PLLTA networks are shown in Fig. 7.9. For the original PLLATA network films, SMC spreading was altered dramatically by the textured surfaces formed in crystallization. When the annealing time was 7 h or longer, significant lower cell spread areas of ~3460, ~3040, and ~2870 μm^2 were found than the amorphous group and the samples annealed for a shorter period (Fig. 7.9a). In contrast, little variance was found for SMC spreading on the compressed substrates of PLLATA networks, indicated by similar cell spread areas of ~4000 μm^2 (Fig. 7.9b).

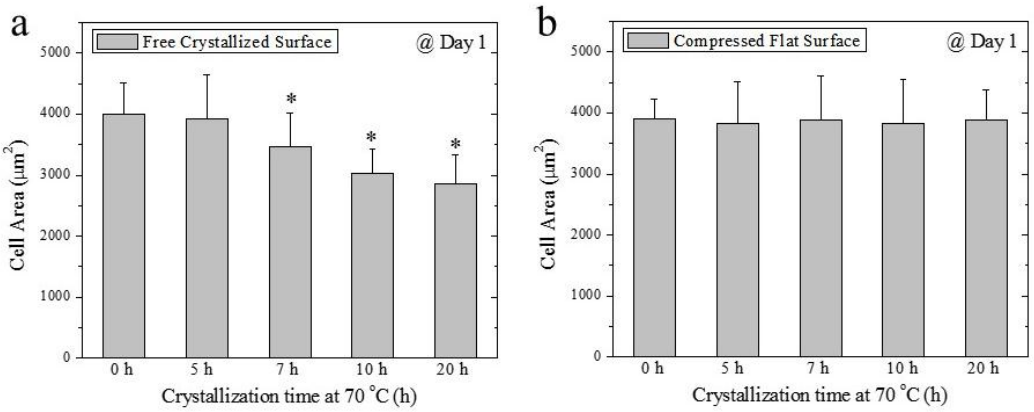

Figure 7.9 SMC spread area at day 1 post-seeding on (a) original and (b) compressed PLLATA networks crystallized for different time.

In agreement with cell attachment, SMC proliferation over 4 days on the PLLATA networks decreased substantially when the annealing time was 10 or 20 h (Fig. 7.10a). Again, the numbers of SMCs on the compressed films were all similar, regardless of the annealing time and culture time. The fluorescence cell images at days 1, 2, and 4 in Fig. 7.10b were consistent with the data of cell densities in Fig. 7.10a. When the PLLTA network films were not compressed, the highest cell density and the fast cell proliferation appeared on the amorphous one whereas cell proliferation was inhibited on the crystallized ones, especially when the annealing time was longer. On the other hand, the compressed films with similar R_{rms} values showed similar SMC densities and proliferation rates (Fig. 7.9b).

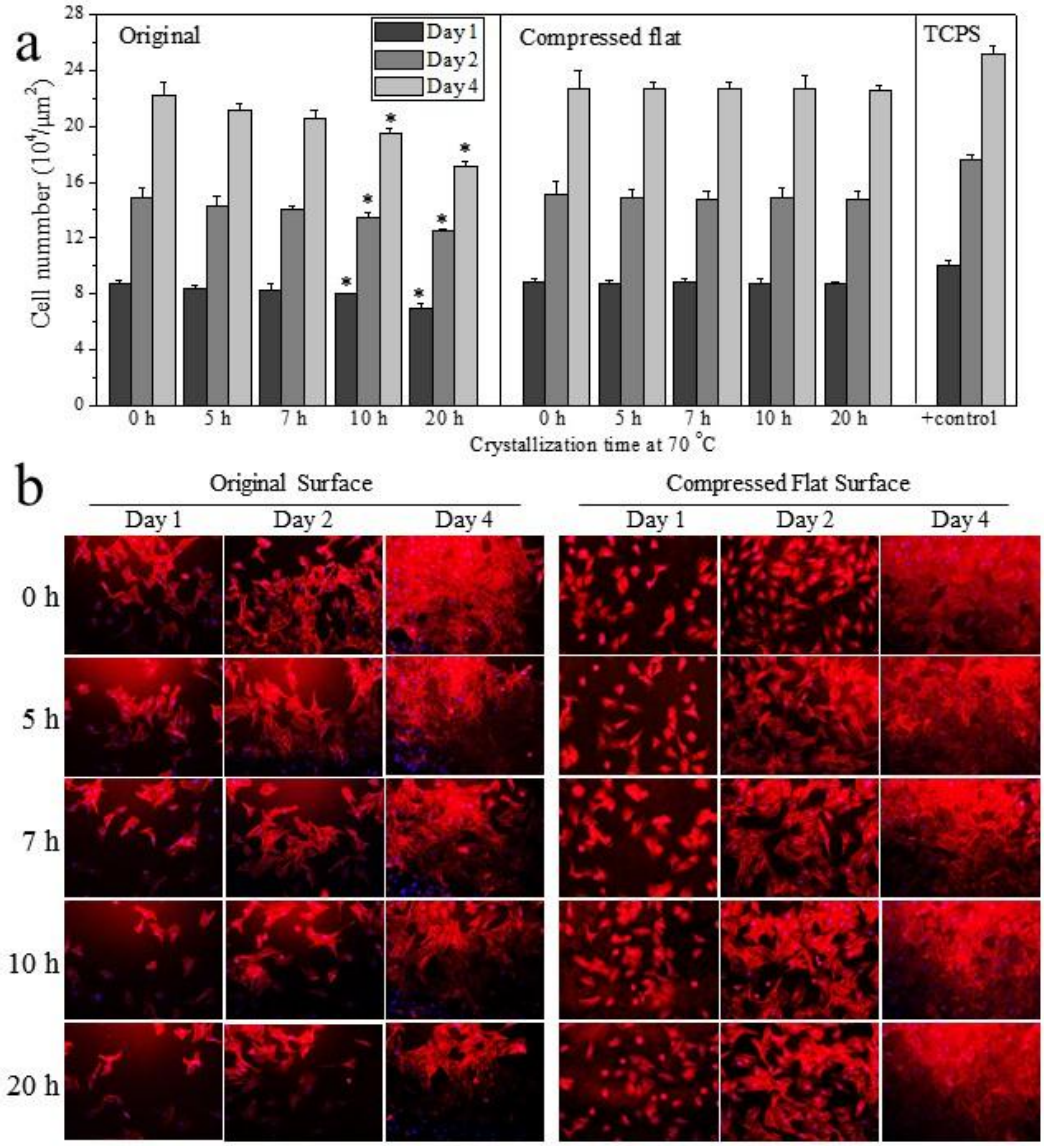

Figure 7.10 (a) SMC numbers and (b) fluorescence images of SMCs stained with RP and DAPI on original and compressed PLLATA networks crystallized for different time periods of 0, 5, 7, 10, and 20 h at days 1, 2, and 4 post-seeding, with TCPS as the positive control. *: $p < 0.05$ relative to amorphous PLLATA network (crystallized for 0 h).

7.3.5 FAs in SMCs on the substrates

FAs are a series of dynamic anchoring protein complexes composed of multiple components including paxillin, talin, and vinculin [29]. FAs are mostly located at the cell periphery to functionalize as structural connectors between internal cytoskeleton and extracellular matrix (ECM) [29]. FAs are able to respond to external mechanical signals and adjust their own properties and simultaneously trigger mechanotransductions for further

regulation of cell growth, spreading, and differentiation [30,31]. As demonstrated in Fig. 7.11a, FAs in SMCs on both original and compressed PLLATA network films were labeled as green dots, which were similar in their intensities. The cells on the original PLLATA network film annealed for 20 h exhibited weaker fluorescence intensities, suggesting that FA development was inhibited. As shown in Fig. 7.11b-d, FA area, elongation, and density quantified from the images in Fig. 7.11a were consistent in the trend.

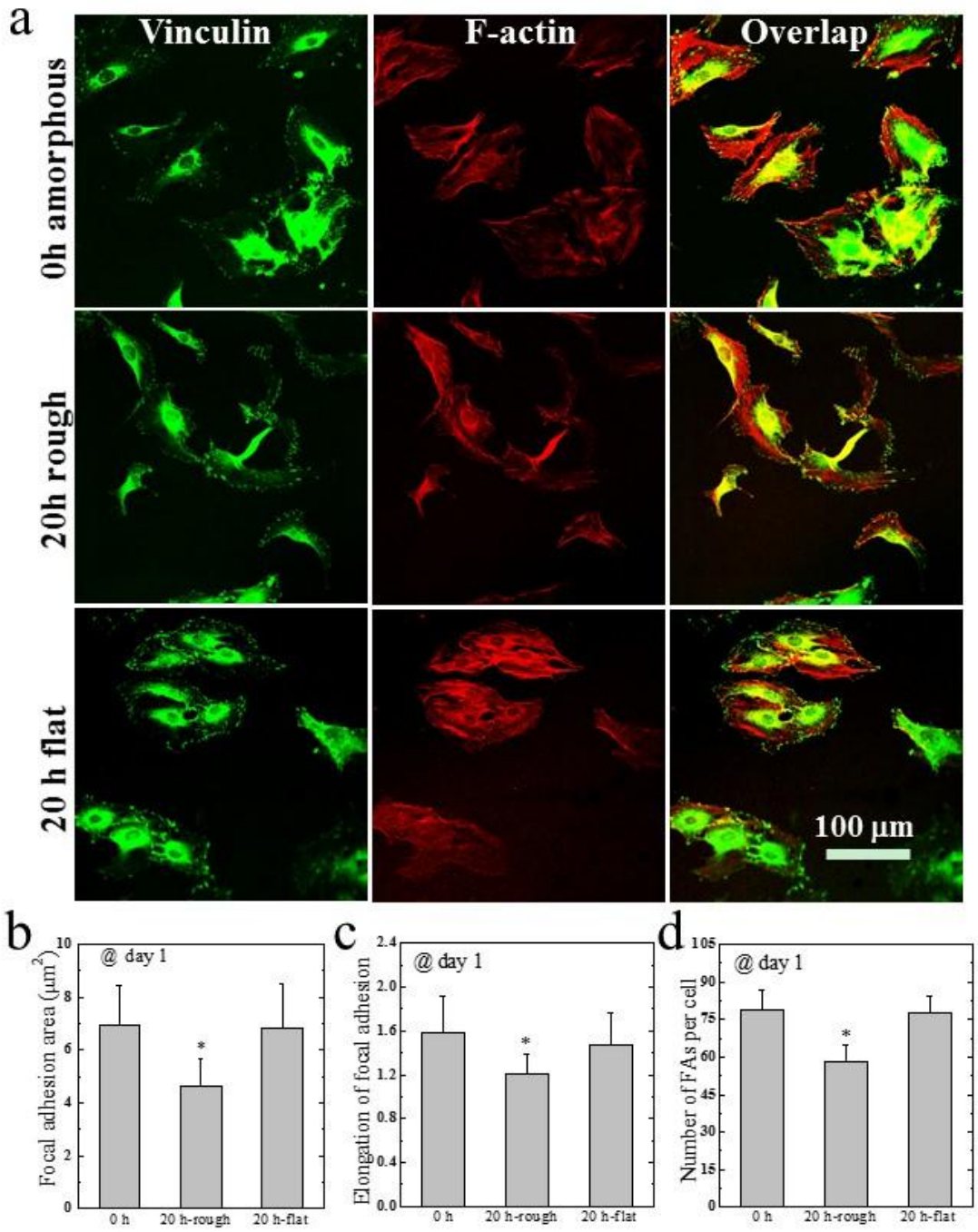

Figure 7.11 (a) Immunofluorescence images of FA vinculin (green) and cytoskeleton actin (red) in SMCs cultured on the original and compressed PLLATA networks crystallized for 0 and 20 h at day 1 post-seeding. (b) Area, (c) elongation, and (d) density of FAs in the fluorescence images in (a). *: $p < 0.05$ relative to all the other groups.

7.3.6 Gene expressions of phenotypic markers and integrin expression

After seeding, SMCs first adopt the proliferative synthetic phenotype that favors growth but lacks contractile functionality. When SMCs reach confluency, they tend to convert from the synthetic phenotype into the contractile phenotype, which develop functionality as elastic muscle units [32-34]. Regulation of this *phenotypic conversion* process is of critical importance for SMCs in cardiovascular tissue engineering. Here we chose three typical contractile gene markers, calponin, and transgelin, to evaluate phyenotypic conversion in SMCs [35,36]. As shown in Fig. 7.12a-c, all the three contractile gene markers had lower expression levels in SMCs on the original PLLATA network films. Meanwhile, the expression levels were similar on the amorphous and compressed films with R_{rms} values below 20 nm. The above gene expression results suggested that the surface pattern and roughness formed in crystallization resulted in different phenotypic conversion in SMCs.

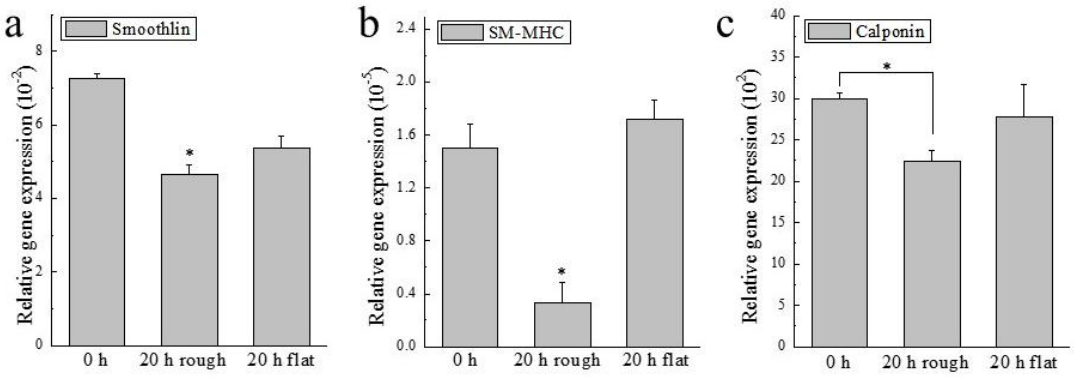

Figure 7.12 Gene expression levels of three contractile phenotypic markers, (a) smoothlin, (b) SM-MHC, and (c) calponin, in SMCs cultured for 4 days on the PLLATA substrates, as normalized to that of GAPDH, determined using real-time PCR. *: $p < 0.05$ relative to the other groups.

Integrins in cell membrane are a category of heterodimers consisted of a α subunit and a β subunit. Different integrins could bind to different ECM proteins and thus play a critical role in cell sensing [37-41]. Upon receiving stimulation from the external environment, integrin clusters are able to medicate intracellular signal transduction, e.g., activating FA kinase and

triggering FA signal transduction [29]. In this study the expression levels of integrin subunits were consistent with the characterizations of FAs. As demonstrated in Fig. 7.13a,b, the expression levels of two α integrin subunits (α_3 and α_5) and two β subunits (β_2 and β_3) were lower in the SMCs cultured on original PLLATA network films annealed for 20 h, compared with the amorphous one and the compressed one. These results indicated that the integrin subunits were also influenced by the surface roughness and thus different integrin expression further determined the differences in adhesion-mediated cellular behaviors.

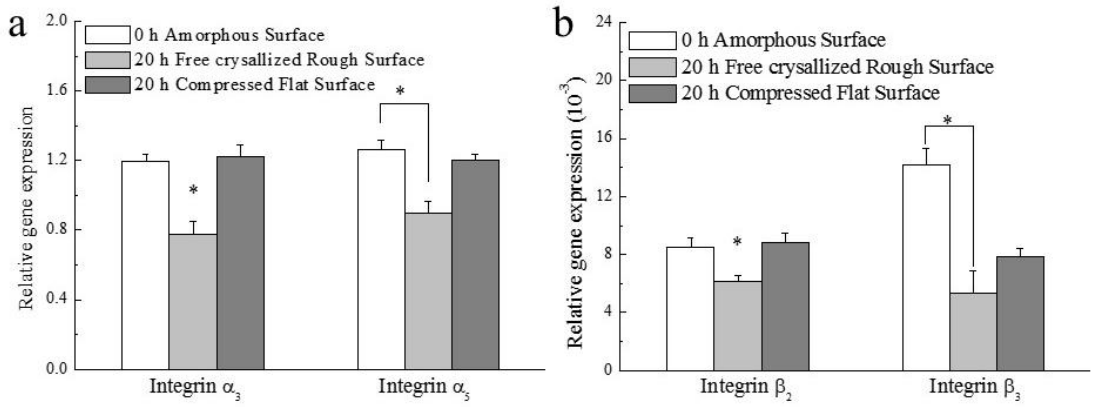

Figure 7.13 Expression levels of (a) two alpha integrin subunits α_3, α_5 and (b) two beta subunits β_2 and β_3, as normalized by that of GAPDH, determined using real-time PCR. *: $p < 0.05$ relative to the other groups.

7.4 Discussion

Cells can sense the structural components at the nanometer scale in the blood vessel wall [42,43]. There have been many reports on how the nano-scale features in the ECM influence vascular cell behaviors, including those of SMCs [42,43]. Decreased cell adhesion and proliferation and altered orientation were reported on crystalline PLLA substrates with rough surfaces, in comparison with on amorphous, smooth PLLA substrates [16,18]. Here we prepared photo-crosslinked PLLATA networks and achieved surface variance by controlling the anneal time and crystallinity. Different SMC adhesion, spreading, proliferation, and phenotypic conversion were observed on the PLLA network films with different crystallinities and roughnesses, whereas the chemical composition was identical. The differences in SMC

behaviors were associated with the different rough surfaces formed in crystallization.

Both enhancing and inhibiting effects of polymer roughness on cell functions have been reported [16,17,42-45]. For example, human umbilical vein endothelial cell adhesion and growth were better on polyurethane-PEG surfaces with higher nano-scale surface roughness [44]. In another study, bladder SMC adhesion was enhanced on poly(lactic-co-glycolic acid) (PLGA) and poly(ether urethane) (PU) film surfaces with higher roughnesses [42,43]. In clear contrast, lower cell adhesion and proliferation were found when surface roughness was higher on PLLA-related polymers, for example, the growth rate of 3T3 fibroblasts was lower on crystalline PLLA substrates than on the amorphous counterparts [16]. Pre-osteoblastic MC3T3-E1 cell proliferation on the smooth PLLA films was found to be significantly higher than that on the rough ones and such variation was a monotonic function of roughness [17]. Meanwhile, human vascular endothelial cell function was found to be improved on smooth solvent-cast PLLA films than electrospun ones with rough surfaces [45].

The distinct cell responses to smooth and rough surfaces may be attributed to several reasons. Surface energy is believed to be one important factor in affecting cell behaviors [46-50]. In the present study, no obvious differences in total surface energy were detected on PLLATA networks, implying that surface energy might not be a major reason for the differences in cellular responses. When a biomaterial surface contacts cell culture medium *in vitro* or blood *in vivo*, it adsorbs proteins onto the surfaces immediately before attracting cells to attach [51-54]. The adsorbed protein layer helps the recognition and adhesion of surrounding cells onto the biomaterial surface [55]. Thus the ability of a material surface to adsorb serum proteins from the cell culture media is also critical in affecting cell adhesion and other behaviors [56-59]. As discussed in Section 3.3, a decrease in protein adsorption was found on the PLLATA films annealed for a longer period. Therefore, the difference in the ability of adsorbing serum proteins, which was resulted from the different surface roughnesses and patterns in crystallization, might account for the distinct cell-material interactions.

Responding to the proteins adsorbed on the surfaces, cells express a family of receptors named integrins for the recognition and binding to a specific category of proteins, followed by formation of FAs, subcellular microstructures that connect the cells and the substrate surface [60-63]. FAs are further associated with intracellular cytoskeletons, thus the information in FA

activities can be transduced to cell nuclei for controlling cell proliferation, spreading, differentiation, and gene/protein expression [64,65]. In this study, upregulated integrin expression was found on amorphous, smooth PLLATA network films compared with the crystalline, rough ones. Characterizations of FAs again demonstrated a larger average size, better elongation, and a higher density on the amorphous, smooth films. Taken together, the enhanced protein adsorption, integrin expression, and FAs on smooth PLLATA network films implied a straightforward signal transduction route for regulating cellular behaviors. The extracellular recognition signals from these sensing components are thus believed to account for the distinct SMC responses to the surface topography developed in crystallization.

7.5 Conclusions

Novel photo-crosslinkable PLLATAs with different molecular weights from 9k to 55k were synthesized and photo-crosslinked under UV light to achieve network substrates. The PLLATA28k networks annealed at 70 ℃ for varied time periods of 0, 5, 7, 10, and 20 h had the same chemical composition but increased crystallinity and surface roughness. Primary rat SMCs responded to the substrate crystallinity by exhibiting reduced SMC attachment, proliferation, and differentiation on the crystalline PLLATA networks compared with the amorphous ones. FA size, elongation, and density, and integrin expression in SMCs were also weakened on the crystalline PLLATA networks with rough surfaces compared with the amorphous smooth ones. After removal of the difference in surface roughness through compression during crystallization, SMC adhesion, proliferation, and differentiation on the PLLA network films varied little regardless of the different bulk crystallinities. Surface hydrophilicity and free energy were similar among all the PLLA network films while the ability to adsorb serum proteins was lower on the PLLATA network films with higher crystallinity and surface roughness.

References

1. Go AS, Mozaffarian D, Roger VL, Benjamin EJ, Berry JD, Borden WB, et al.; on behalf of the American Heart Association Statistics Committee and Stroke Statistics Subcommittee. Heart disease and stroke statistics-2013 update: a report from the American Heart Association. Circulation 2013; 127:e6-e245
2. Venkatraman S, Boey F, Lao LL. Implanted cardiovascular polymers: natural, synthetic and bio-inspired. Prog Polym Sci 2008;33:853-74.
3. Gui L, Zhao L, Spencer RW, Burghouwt A, Taylor MS, Shalaby SW, et al. Development of novel biodegradable polymer scaffolds for vascular tissue engineering. Tissue Eng Part A 2011;17(9-10):1191-200.
4. Peyton SR, Raub CB, Keschrumrus VP, Putnam AJ. The use of poly(ethylene glycol) hydrogels to investigate the impact of ECM chemistry and mechanics on smooth muscle cells. Biomaterials 2006;27(28):4881-93.
5. Peyton SR, Kalcioglu ZI, Cohen JC, Runkle AP, Van Vliet KJ, Lauffenburger DA, et al. Marrow-derived stem cell motility in 3D synthetic scaffold is governed by geometry along with adhesivity and stiffness. Biotechnol Bioeng 2011;108(5):1181-93.
6. Bramfeldt H, Vermette P. Enhanced smooth muscle cell adhesion and proliferation on protein-modified polycaprolactone-based copolymers. J Biomed Mater Res A 2009;88(2):520-30.
7. Fu W, Liu Z, Feng B, Hu R, He X, Wang H, Yin M, Huang H, Zhang H, Wang W. Electrospun gelatin/PCL and collagen/PLCL scaffolds for vascular tissue engineering. Int J Nanomedicine 2014;9:2335-44.
8. Lee CH, Lim YC, Farson DF, Powell HM, Lannutti JJ. Vascular wall engineering via femtosecond laser ablation: scaffolds with self-containing smooth muscle cell populations. Ann Biomed Eng 2011;39(12):3031-41.
9. Hu J, Sun X, Ma H, Xie C, Chen YE, Ma PX. Porous nanofibrous PLLA scaffolds for vascular tissue engineering. Biomaterials 2010;31(31):7971-7.
10. Song W, Veiga DD, Custódio CA, Mano JF. Bioinspired degradable substrates with extreme wettability properties. Adv. Mater. 2009;21: 1830-1834.

11. Melchels FP, Feijen J, Grijpma DW. A poly(D,L-lactide) resin for the preparation of tissue engineering scaffolds by stereolithography. Biomaterials 2009;30(23-24):3801-9.
12. Hegen A, Blois A, Tiron CE, Hellesøy M, Micklem DR, Nör JE, et al. Efficient in vivo vascularization of tissue-engineering scaffolds. J Tissue Eng Regen Med 2011;5(4):e52-62.
13. Tamai H, Igaki K,Kyo E,KosugaK,KawashimaA,Matsui S, et al. Initial and 6-month results of biodegradable poly-L-lactic acid coronary stents in humans. Circulation;102:399–404.
14. Waksman R. Update on bioabsorbable stents: frombench to clinical. J Interv Cardiol 2006;19:414–21.
15. Isotalo T, Talja M, Valimaa T, Tormala P, Tammela TLJ. A bioabsorbable self-expandable self-reinforced poly l-lactic acid urethral stent for recurrent urethral strictures: long term results. J Endourol 2002;16:759–62.
16. Park A, Cima LG. In vitro cell response to differences in poly-L-lactide crystallinity. J Biomed Mater Res 1996;31(1):117-30.
17. Washburn NR, Yamada KM, Simon CG Jr, Kennedy SB, Amis EJ. High-throughput investigation of osteoblast response to polymer crystallinity: influence of nanometer-scale roughness on proliferation. Biomaterials 2004;25(7-8):1215-24.
18. Costa ME, Escobar IJL, Muñoz CI, Gómez RJL, Monleón PM, Salmerón SM. Effect of poly(L-lactide) surface topography on the morphology of in vitro cultured human articular chondrocytes. J Mater Sci Mater Med 2007;18(8):1627-32.
19. Cai L, Wang S. Poly(ε-caprolactone) acrylates synthesized using a facile method for fabricating networks to achieve controllable physicochemical properties and tunable cell responses. Polymer 2010;51:164-77.
20. Wang K, Cai L, Hao F, Xu XM, Cui MZ, Wang SF. Distinct Cell Responses to Substrates Consisting of Poly(epsilon-caprolactone) and Poly(propylene fumarate) in the Presence or Absence of Cross-Links. Biomacromolecules. 2010;11:2748-59.
21. Cai L, Wang SF. Parabolic dependence of material properties and cell behavior on the composition of polymer networks via simultaneously controlling crosslinking density and crystallinity. Biomaterials. 2010;31:7423-34.
22. Celli A, Scandola M. Thermal properties and physical ageing of poly (L-lactic acid). Polymer 1992; 33(13):2699-2703

23. Mandelkern L. Crystallization of polymers. 2nd ed., vol. 1. New York: McGraw-Hill; 2001 [chapter 7].
24. Lim JY, Hansen JC, Siedlecki CA, Hengstebeck RW, Cheng J, Winograd N, et al. Osteoblast adhesion on poly(L-lactic acid)/polystyrene demixed thin film blends: effect of nanotopography, surface chemistry, and wettability. Biomacromolecules2005;6:3319–3327.
25. Ajami-Henriquez D, Rodr ́guez M, Sabino M, Castillo RV, Müller AJ, Boschetti-de-Fierro A, et al. Evaluation of cell affinity on poly(L-lactide) and poly(ε-caprolactone) blends and on PLLA-b-PCL diblock copolymer surfaces. J Biomed Mater Res A 2008;87(2):405-417.
26. Sharma PK, Hanumantha Rao K. Analysis of different approaches for evaluation of surface energy of microbial cells by contact angle goniometry. Adv Colloid Interface Sci 2002;98:341–463.
27. Van Oss CJ, Good RJ, Chaudhury MK. Additive and nonadditive surface tension components and the interpretation of contact angles. Langmuir 1988;4(4):884–891.
28. Saltzman WM, Kyriakides TR. Cell interactions with polymers. In: Lanza R, Langer R, Vacanti J, editors. Principles of tissue engineering. 3rd ed. San Diego: Elsevier Academic Press; 2007. p. 279-296.
29. Burridge K, Chrzanowska-Wodnicka M. Focal adhesions, contractility, and signaling. Annu Rev Cell Dev Biol 1996;12:463-518.
30. Parsons JT, Horwitz AR, Schwartz MA. Cell adhesion: integrating cytoskeletal dynamics and cellular tension. Nat Rev Mol Cell Bio 2011;11:633-643.
31. Zamir E, Geiger B. Molecular complexity and dynamics of cell-matrix adhesions. J Cell Sci 2001;114:3583-90.
32. Iyemere VP, Proudfoot D, Weissberg PL, Shanahan CM. Vascular smooth muscle cell phenotypic plasticity and the regulation of vascular calcification. J Intern Med 2006;260(3):192-210.
33. Rensen SSM, Doevendans PAFM, van Eys GJJM. Regulation and characteristics of vascular smooth muscle cell phenotypic diversity. Neth Heart J 2007;15(3):100-108.

34. Chan-Park MB, Shen JY, Cao Y, Xiong Y, Liu Y, Rayatpisheh S, et al. Biomimetic control of vascular smooth muscle cell morphology and phenotype for functional tissue-engineered small-diameter blood vessels. J Biomed Mater Res A 2009;88(4):1104-21.
35. Sobue K, Hayashi K, Nishida W. Expressional regulation of smooth muscle cell-specific genes in association with phenotypic modulation. Mol Cell Biochem 1999;190:105-118.
36. Wang C, Yin S, Cen L, Liu Q, Liu W, Cao Y, et al. Differentiation of adipose-derived stem cells into contractile smooth muscle cells induced by transforming growth factor-beta1 and bone morphogenetic protein-4. Tissue Eng Part A 2010;6(4):1201-1213.
37. Ingber DE. Mechanosensation through integrins: cells act locally but think globally. Proc Natl Acad Sci USA 2003;100:1472-1474.
38. Wang HB, Dembo M, Hanks SK, Wang Y. Focal adhesion kinase is involved in mechanosensing during fibroblast migration. Proc Natl Acad Sci USA 2001;98:11295-11300.
39. Paszek MJ, Zahir N, Johnson KR, Lakins JN, Rozenberg GI, Gefen A, et al. Tensional homeostasis and the malignant phenotype. Cancer Cell 2005;8:241-254.
40. Katsumi A, Orr AW, Tzima E, Schwartz MA. Integrins in mechanotransduction. J Biol Chem 2004;279:12001-12004.
41. Giancotti FG, Ruoslahti E. Integrin signaling. Science 1999;285:1028-1032.
42. Thapa A, Miller DC, Webster TJ, Haberstroh KM. Nanostructured polymers enhance bladder smooth muscle cell function. Biomaterials 2003;17:2915-2926.
43. Thapa A, Webster TJ, Haberstroh KM. Polymers with nano-dimensional surface features enhance bladder smooth muscle cell adhesion. J Biomed Mater Res A 2003;67(4):1374-1383.
44. Chung TW, Liu DZ, Wang SY, Wang SS. Enhancement of the growth of human endothelial cells by surface roughness at nanometer scale. Biomaterials 2003;24:4655-4661.
45. Xu C, Yang F, Wang S, Ramakrishna S. In vitro study of human vascular endothelial cell function on materials with various surface roughness. J Biomed Mater Res A 2004;71(1):154-161.

46. Ruardy TG, Moorlag HE, Schakenraad JM, van Der Mei HC, Busscher HJ. Growth of fibroblasts and endothelial cells on wettability gradient surfaces. J Colloid Interf Sci;188:209-217.
47. Lee JH, Lee SJ, Khang G, Lee HB. The effect of fluid shear stress on endothelial cell adhesiveness to polymer surfaces with wettability gradient. J Colloid Interface Sci 2000;230:84-90.
48. Redey SA, Razzouk S, Rey C, Bernache-Assollant D, Leroy G, Nardin M, et al. Osteoclast adhesion and activity on synthetic hydroxyapatite, carbonated hydroxyapatite and natural calcium carbonate: relationship to surface energies. J Biomed Mater Res 1999;45:140-7.
49. Hallab NJ, Bundy KJ, O'connor K, Moses RL, Jacobs JJ. Evaluation of metallic and polymeric biomaterial surface energy and surface roughness characteristics for directed cell adhesion. Tissue Eng 2001;7:55-71.
50. Lee SJ, Khang G, Lee YM, Lee HB. The effect of surface wettability on induction and growth of neurites from the PC-12 cell on a polymer surface. J Colloid Interface Sci 2003;259:228-35.
51. Li S, Yang D, Tu H, Deng H, Du D, Zhang A. Protein adsorption and cell adhesion controlled by the surface chemistry of binary perfluoroalkyl/oligo(ethylene glycol) self-assembled monolayers. J Colloid Interface Sci 2013;402:284-90.
52. Kim DJ, Lee JM, Park JG, Chung BG. A self-assembled monolayer-based micropatterned array for controlling cell adhesion and protein adsorption. Biotechnol Bioeng 2011;108(5):1194-202.
53. Chen H, Song W, Zhou F, Wu Z, Huang H, Zhang J, et al. The effect of surface microtopography of poly(dimethylsiloxane) on protein adsorption, platelet and cell adhesion. Colloids Surf B Biointerfaces 2009;71(2):275-81.
54. Anselme K, Davidson P, Popa AM, Giazzon M, Liley M, Ploux L. The interaction of cells and bacteria with surfaces structured at the nanometre scale. Acta Biomater 2010;6(10):3824-46.
55. Nikolovski J, Mooney DJ. Smooth muscle cell adhesion to tissue engineering scaffolds. Biomaterials 2000;21:2025-2032.

56. Misra RD, Nune C, Pesacreta TC, Somani MC, Karjalainen LP. Interplay between grain structure and protein adsorption on functional response of osteoblasts: ultrafine-grained versus coarse-grained substrates. J Biomed Mater Res A 2013;101(1):1-12.
57. Allen LT, Tosetto M, Miller IS, O'Connor DP, Penney SC, Lynch I, et al. Surface-induced changes in protein adsorption and implications for cellular phenotypic responses to surface interaction. Biomaterials 2006;27(16):3096-108.
58. Lord MS, Cousins BG, Doherty PJ, Whitelock JM, Simmons A, Williams RL, et al. The effect of silica nanoparticulate coatings on serum protein adsorption and cellular response. Biomaterials 2006;27(28):4856-62.
59. Leibner ES, Barnthip N, Chen W, Baumrucker CR, Badding JV, Pishko M, et al. Superhydrophobic effect on the adsorption of human serum albumin. Acta Biomater 2009;5(5):1389-98.
60. Barczyk M, Carracedo S, Gullberg D. Integrins. Cell Tissue Res 2010;339(1):269-80.
61. Bacakova L, Filova E, Parizek M, Ruml T, Svorcik V. Modulation of cell adhesion, proliferation and differentiation on materials designed for body implants. Biotechnol Adv 2011;29(6):739-67.
62. Moser M, Legate KR, Zent R, Fässler R. The tail of integrins, talin, and kindlins. Science. 2009;324(5929):895-9.
63. Caswell PT, Vadrevu S, Norman JC. Integrins: masters and slaves of endocytic transport. Nat Rev Mol Cell Biol 2009;10(12):843-53.
64. Geiger B, Spatz JP, Bershadsky AD. Environmental sensing through focal adhesions. Nat Rev Mol Cell Biol 2009;10(1):21-33.
65. Parsons JT, Horwitz AR, Schwartz MA. Cell adhesion: integrating cytoskeletal dynamics and cellular tension. Nat Rev Mol Cell Biol 2010;11(9):633-43.

Chapter VIII. Tuning Smooth Muscle Cell Behavior on Poly(Ethylene Glycol)-Grafted Poly(ε-Caprolactone) Networks

Abstract

PCLTA is a promising photo-crosslinkable polymeric biomaterial as crosslinked PCLTA has excellent biocompatibility, biodegradability and readily controlled physical properties. However, the high hydrophobicity of semi-crystalline crosslinked PCLTA may limit its tissue engineering applications. Here I report that the hydrophobic nature of crosslinked PCLTA can be greatly relieved when PCLTA was photo-crosslinked with hydrophilic methoxy poly(ethylene glycol) monoacrylate (mPEGA). To further clarify the role of mPEGA in modification of crosslinked PCLTA, I utilized a series of photo-crosslinked mPEGA/PCLTA samples with various ϕ_m of 0-50% and different mPEGA number-average molecular weights of 350, 2000, and 10000 g/mol. Material properties including surface hydrophilicity, friction coefficient, roughness, thermal and mechanical properties were characterized. Crosslinked mPEGA/PCLTA samples with modified surface physicochemical characteristics were used to modulate primary rat SMC attachment, spreading, proliferation, and gene/protein expression. With increasing ϕ_m, SMC attachment on PCLTA networks grafted with short chains of mPEGA350 or mPEGA2000 showed a non-monotonic trend with a maximum at ϕ_m of 5% or 2%, respectively. When ϕ_m was higher, SMC attachment and proliferation decreased sharply. For the longest chain mPEGA10000 used in this study, SMC attachment decreased monotonically with ϕ_m to zero at ϕ_m of 7%. Sparsely tethered short PEG chains were found to significantly enhance SMC attachment, proliferation, and gene/protein expression by reducing the substrate hydrophobicity, while densely tethered short PEG chains or long PEG chains diminished SMC attachment and proliferation because of their strong repulsion to proteins and cells.

8.1 Introduction

Cardiovascular disease is the number one killer in the U.S. and vascular tissue engineering holds enormous potential by fabricating synthetic materials into vessel replacements [1]. Understanding cell-biomaterial interactions is critical in tissue engineering because biomaterial surface interacts with the biological environment directly [2]. The surface physicochemical properties and geometrical features of the underlying biomaterial substrates affect cells through integrins, focal adhesions (FAs), and various pathways [3]. In the past decades, novel degradable polymeric biomaterials have been developed to achieve desirable physical properties, biocompatibility, and degradability [4-8]. To ensure successful implantation, it is important to understand how candidate biomaterials can be used to tune cell behavior and tissue growth [2,9].

Among these candidates, photo-crosslinkable polymers are injectable and can be manufactured into biomimetic structures using stereolithography [10-18]. Photo-crosslinkable, biodegradable poly(ε-caprolactone) triacrylates (PCLTAs) synthesized in our group were fabricated into substrates and scaffolds with well-controlled mechanical properties by simultaneously regulating the crosslinking density and network crystallinity through the molecular weight of PCLTA [13,18]. When crosslinked PCLTA is semi-crystalline, its hydrophobicity may limit the potential tissue engineering applications. Thus it is desirable to modify PCLTA networks with hydrophilic polymer chains, for example, polyethylene glycol (PEG). PEG has been well applied in improving surface hydrophilicity/wettability, reducing protein adsorption and platelet adhesion, and inhibiting immunogenic activities, which are crucial for the blood compatibility of a material [19-25]. PEG can be copolymerized, blended, grafted, or covalently linked to surfaces mediated by proteins and other functional groups [26-29]. For example, incorporation of peptide-PEG segment into polyurethaneureas significantly enhances the adhesion, spreading, and migration of endothelial cells on the substrates but prohibits platelet adhesion [30]. For PCL, *in vitro* hemocompatibility experiments indicated chitosan-g-PCL-*b*-PEG/heparin-modified PCL resisted platelet adhesion effectively and showed good potential for use in vascular tissue engineering [31].

SMC is a cell type that is extensively used for blood-vessel engineering with a specific feature of phenotypic plasticity [32]. When SMCs are removed from a healthy body or encounter a large space for growth, they convert from the functional contractile phenotype to the proliferative synthetic one and start fast growth and division [33]. When SMCs are confluent, they revert into the contractile phenotype for vascular formation or other functional development. Both processes are essential in vascular engineering and the transition between the two phenotypes is affected by soluble factors in the culture medium, mechanical properties of the substrates, and characteristics of extracellular matrix (ECM) [33,34].

In this study, I photo-crosslinked PCLTA with three different methoxy PEG acrylates (mPEGAs) that were prepared from mPEG precursors with number-average molecular weights of 350, 2000 and 10000 g/mol with the compositions of mPEGA (ϕ_m) of 0-50%. After I characterized the mechanical, thermal, and surface properties of photo-crosslinked PCLTA/mPEGAs, including tensile modulus, melting temperature (T_m), crystallinity (χ_c), surface friction coefficient, water contact angle, and protein adsorption, I used these photo-crosslinked mPEGA/PCLTAs with well-controlled surface characteristics to modulate SMC adhesion, integrin expression, proliferation, and gene expression of contractile phenotypic markers. The goal of this study was to evaluate the potential of these photo-crosslinked polymers as cardiovascular tissue engineering materials and achieving a better understanding about regulating SMCs using polymer substrates.

8.2 Materials and methods

8.2.1 Polymer synthesis and photo-crosslinking

PCL triol precursor (Fig. 8.1) was synthesized via the ring-opening polymerization of ε-caprolactone, initiated by 1,1,1-tris(hydroxymethyl) propane (TMP) in the presence of $Sn(Oct)_2$ as the catalyst. PCLTA and mPEGA were synthesized through acrylation of PCL triol and methoxy PEG (mPEG; Sigma) in the presence of K_2CO_3, as reported by us [13,18,35]. Three mPEGAs, i.e., mPEGA350, mPEGA2000 and mPEGA10000, were named after the nominal molecular weights of their mPEG precursors. mPEGA/PCLTA blends with ϕ_m of 0, 2, 5, 7, 10, 20, 30, and 50% were dissolved in CH_2Cl_2 and fully mixed. Phenyl bis(2,4,6-trimethyl benzoyl)

phosphine oxide (BAPO, IRGACURE819, Ciba Specialty Chemicals, Tarrytown, NY) was used as the photo-initiator. Before crosslinking, 75 μL of BAPO/CH_2Cl_2 (300 mg/1.5 mL) was mixed with the solution of 1.5 g mPEGA/PCLTA in 500 μL CH_2Cl_2. Homogenous mPEGA/PCLTA blends were crosslinked in a mold, which was composed of two glass plates with a silicon spacer, under UV light (SB-100P, Spectroline, wavelength = 365 nm, intensity = 4800 μw/cm^2) for 20 min, as described previously [35].

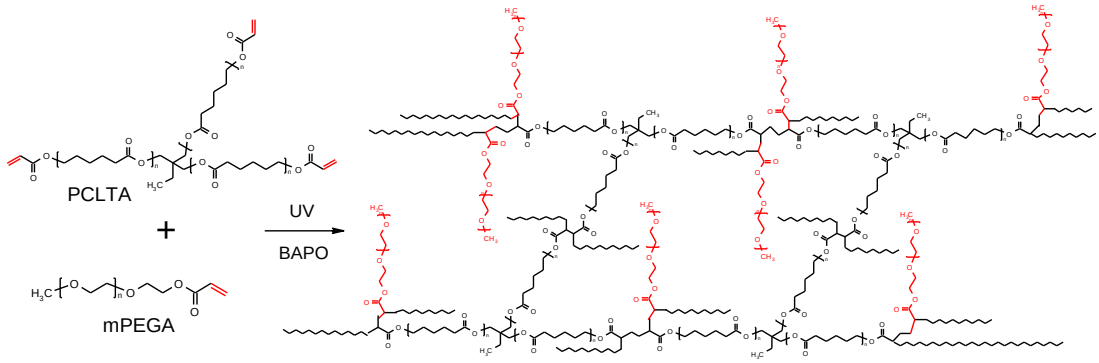

Figure 8.1 Photo-crosslinking of PCLTA and mPEGA.

8.2.2 Characterization of polymer properties

Determined using Gel Permeation Chromatography (GPC; PL-GPC 20, Polymer Laboratories) with tetrahydrofuran as the eluent and standard monodisperse polystyrene samples (Polymer Laboratories) as references, the PCLTA, mPEGA350, mPEGA2000 and mPEGA10000 used here had number-average molecular weights of 11350, 320, 2950 and 13390 g/mol, respectively. Crosslinked mPEGA/PCLTA disks (10 mm × 0.5 mm, diameter × thickness) were soaked in acetone for 2 days to remove the sol fraction and unreacted BAPO, followed by complete drying in vacuum. Then the dried polymer disks were compressed at 60 ℃ and recrystallized at 37 ℃ between two glass plates to flatten their surfaces. The swelling ratio and gel fraction of crosslinked mPEGA/PCLTA were obtained in CH_2Cl_2 using the method reported by our research group previously [12,33]. The surface morphology of the polymer disks was characterized using atomic force microscopy (AFM) and surface roughness was computed. Frictional forces between a stainless steel plate and hydrated polymer disks were determined using the rheological method reported previously [35]. The water contact angles on the polymer disks were determined at 37 ℃ using a Ramé-Hart NRC C. A. goniometer (Model

100-00-230, Mountain Lakes, NJ). Serum proteins from cell culture media adsorbed on the polymer disks were collected using MicroBCA protein assay kit (Pierce, Rockford, IL) and detected on a microplate reader [35]. Thermal properties of the polymer samples were characterized using Differential Scanning Calorimetric (DSC) measurements, in which the samples were first heated to 100 ℃, then cooled to -80 ℃, and reheated to 80 ℃ at a rate of 10 ℃/min. Tensile strain-stress curves of the polymer samples (0.5 × 2.0 × 10 mm, thickness × width × length) were obtained using a dynamic mechanical analyzer (DMTA-5, Rheometric Scientific) at a strain rate of 0.01/s at 37 ℃. Rheological properties of the polymer samples at both 37 and 60 ℃ were determined on a strain-controlled parallel-plate (diameter = 8 mm, gap = ~1 mm) rheometer (RDS-2, Rheometric Scientific) in the frequency range of 0.1-100 rad/s.

8.2.3 In vitro cell studies

Crosslinked mPEGA/PCLTA disks were sterilized in 70% alcohol solution and completely dried in vacuum prior to cell studies. Primary SMCs isolated from rat aorta were used to evaluate the cellular behaviors on these polymer disks. Cells were cultured with Dulbecco's modified eagle medium (DMEM) with 10% fetal bovine serum (FBS) on regular tissue culture flasks in the 37 ℃ incubator prior to seeding [16]. Sterilized polymer disks were rinsed in PBS and seeded with SMCs at a density of ~20000 cells/cm^2. Tissue culture polystyrene (TCPS) was used as the positive control. SMC number was calculated at 4 h, days 1, 2, and 4 post-seeding. Attached cells on the polymer disks were washed twice in PBS and fixed in 4% paraformaldehyde (PFA) solution with cell membrane permeabilised for 10 min using 0.2% Triton X-100. Then the cells were incubated with rhodamine-phalloidin (RP) for 1 h at 37 ℃ and 4',6-diamidino-2-phenylindole (DAPI) for 5 min at room temperature to stain cytoplasm and nuclei, respectively. Then fluorescent cell images were obtained on an Axiovert 25 light microscope (Carl Zeiss, Germany). From these images, cell area was determined using ImageJ software (National Institutes of Health, Bethesda) and averaged on 20 non-overlapping cells.

8.2.4 Characterization of focal adhesions

As described in Section 2.3, SMCs cultured on the polymer disks for 1 day were fixed and permeabilised. Then the cells were blocked with 1% Bovine Serum Albumin (BSA) in PBS at 37 ℃ for 1 h, followed by incubation in monoclonal vinculin primary antibody (1:1000 in PBS; Sigma) for 1 h with gentle shaking at room temperature. Then the cells were washed three times with PBS to remove unconjugated primary antibody, followed by incubation in goat anti-mouse IgG secondary antibody (1:200 in PBS; Sigma) solution for 1 h at room temperature. To examine SMC specific filaments, the cells were further stained using RP at 37 ℃ for 1 h after vinculin staining and photographed on a Leica DM6000B confocal fluorescent microscope. FA area and perimeter were measured using ImageJ and averaged on 20 individual FAs from 5 representative cells. FA elongation was calculated using the inverse of the circularity, which was defined by the equation of $4\pi \times \text{area}/\text{perimeter}^2$ [36]. FA density, i.e., the number of FAs per cell, was also obtained using ImageJ on 5 non-overlapping cells.

8.2.5 Gene expression of contractile phenotypic markers and integrins

For gene expression of phenotypic markers, primers listed below were designed using Oligoperfect software. Calponin: Forward 5'-AGTCTACTCTCTCTTGGCTCTGGCC-3', Reverse 5'-CCTGCCTTCTCTCAGCTTCTCAGG-3'; smooth muscle myosin heavy chain (SM-MHC): Forward 5'-AAGCAGCTCAAGAGGCAG-3', Reverse 5'-AAGGAACAAATGAAGCCTCGTT-3'; Transgelin (SM-22): Forward 5'-GGCAGCTGAGGATTATGGAGTCACG-3', Reverse 5'-TGGGATCTCCACGGTAGTGTCCA-3'; and house-keeping gene glyceraldehyde-3-phosphate dehydrogenase (GAPDH): Forward 5'-TCTTCACCACCATGGAGAA-3', Reverse 5'-ACTGTGGTCATGAGCCCTT-3'. Total RNA was isolated using the RNeasy Mini Kit (Qiagen, Valencia, CA) from SMCs that were cultured for 2 days and the total cDNA was reverse transcripted using the DyNAmo cDNA synthesis kit (Thermo Scientific) according to the manufacturer's instructions. For each sample, 2.5 μL of the total cDNA at the same concentration of 5 ng/μL was added as the template to prepare the mixture with Power SYBR Green Polymerase Chain Reaction (PCR) Master Mix (Applied Biosystems, Warrington, UK) for a total 20 μL reaction system. Real-time PCR amplification was conducted on a Peltier

Thermal Cycler fluorescence detection system (MJ Research PTC-200 Thermo Cycler) with a procedure set as 5 min at 94 ℃ followed by the cyclic steps of 30 s at 94 ℃, 30 s at 55 ℃, and 30 s at 72 ℃. The expression levels of contractile phenotypic markers were normalized to that of GAPDH. For integrin expression analysis, the designed primers are listed below. Integrin-α_v: Forward 5'-AAGACGCCCGAAAAGAATGAC-3', Reverse 5'-ATCCCGCTTGGTGATGAGAT-3'; Integrin-α_1: Forward 5'-TCTGCCAAACTCAGTCCACGA-3', Reverse 5'-TGACGATCAGCAGGCTCTTTT-3'; Integrin-α_5: Forward 5'-CCTTCCTTCATTGGCATGGA-3', Reverse 5'-TCTGCATCCTGTCAGCAATCC-3'; Integrin-β_1: Forward 5'-AGAGTGCCGTGACAACTGTG-3', Reverse 5'-GAGCCCCAAAGCTACCCTAC-3'; and Integrin-β_3: Forward 5'-GACCCGCTTCAATGACGAA-3', Reverse 5'-TCACAGACTGTAGCCTGCATGA-3'. The GAPDH primers in integrin expression were the same as those used in the expression of phenotypic markers. Total RNA was isolated from SMCs cultured for one day and integrin expression was analyzed using the same real-time PCR procedure as in phenotypic marker expression.

8.2.6 Calponin protein immunofluorescence staining

To further substantiate the gene results, immunofluorescence was performed on 4% PFA-fixed cells using anti-rat calponin primary antibody produced in rabbit (sc-16604-R; Santa Cruz). The reaction with primary antibody (1:100 diluted in PBS) was kept at room temperature for 60 min before cells were washed with PBS three times. Fluorescein isothiocyanate (FITC) conjugated anti-rabbit secondary IgG antibody produced in goat (F0382; Sigma) was used to detect the localization of anti-calponin antibodies with a dilution of 1:80 in PBS. Cell nuclei were stained with DAPI before photographing on the Axiovert 25 light microscope.

8.2.7 Statistical analysis

Statistical analysis was performed using one-way analysis of variance (ANOVA) followed by Tukey post-test. Any two samples with a *p*-value lower than 0.05 were considered to have a significant difference.

8.3 Results

8.3.1 Structural characterization

The gel fractions of all the polymer networks were larger than 90%, similar to that for crosslinked PCLTA, suggesting that mPEGAs were efficiently incorporated into the networks (Table 8.1). The swelling ratio of crosslinked mPEGA/PCLTA in CH_2Cl_2 increased with increasing ϕ_m or the molecular weight of mPEGA (Fig. 8.2a). The value of ~8.4 for crosslinked PCLTA increased to 9.3, 9.7, and 9.1 when 50% mPEGA350, 20% mPEGA2000, and 7% mPEGA10000 were tethered in the networks. No swelling was seen for all the disks in PBS, different from hydrogels made from polymers containing PEG blocks in the backbone [4].

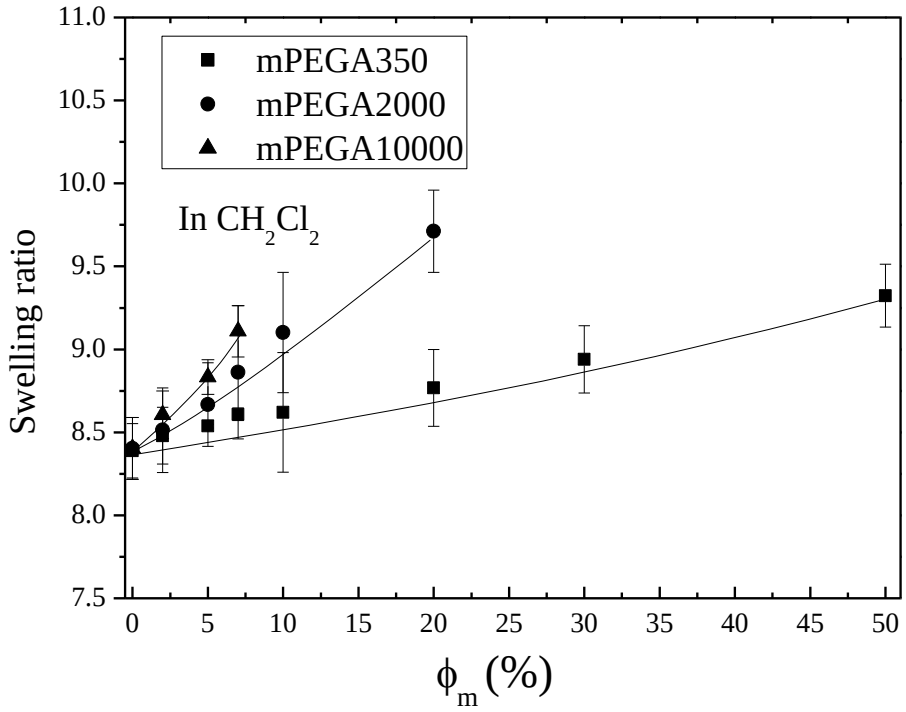

Figure 8.2 Swelling ratio of PCLTA and mPEGA/PCLTA networks in CH_2Cl_2.

Table 8.1 Thermal, mechanical, and surface roughness of PCLTA and mPEGA/PCLTA networks.

	ϕ_m	Φ_m	C	Gel Fraction (%)	T_m	ΔH_m	χ_c	E (MPa)	R_{rms} (nm)
Crosslinked PCLTA	0%	0	0	93.9 ±4.8	41.7	45.7	33.8	107 ±4	8.9 ±0.5
mPEGA350/PCLTA	2%	0.40	0.04	93.6 ±0.2	40.9	44.5	32.9	102 ±5	8.9 ±0.9
	5%	0.63	0.09	91.7 ±0.4	41.8	45.9	34.0	99 ±4	8.7 ±0.7
	7%	0.71	0.12	91.5 ±1.4	40.5	43.5	32.2	84 ±5	8.3 ±1.1
	10%	0.78	0.17	93.3 ±1.6	40.6	43.1	31.9	70 ±2	9.1 ±0.6
	20%	0.89	0.32	92.1 ±0.7	39.2	34.1	25.3	50 ±6	9.4 ±0.4
	30%	0.93	0.45	93.2 ±1.3	36.9	28.5	21.1	41 ±9	8.7 ±1.1
	50%	0.97	0.65	92.5 ±0.5	35.0	20.8	15.4	19 ±5	9.1 ±0.7
mPEGA2000/PCLTA	2%	0.90	0.09	95.1 ±5.0	41.0	45.6	33.8	88 ±7	8.4 ±1.0
	5%	0.77	0.20	94.0 ±2.6	40.6	45.1	33.4	66 ±8	9.1 ±0.6
	7%	0.70	0.26	93.9 ±2.9	40.0	42.2	31.2	52 ±6	8.9 ±0.6
	10%	0.61	0.35	91.9 ±4.3	39.0	32.1	23.8	40 ±8	9.0 ±0.8
	20%	0.41	0.54	95.9 ±4.3	37.2	26.3	19.5	24 ±4	8.7 ±0.6
mPEGA10000/PCLTA	2%	0.02	0.11	98.1 ±0.3	39.7	44.0	32.6	71 ±5	9.2 ±1.0
	5%	0.06	0.24	92.1 ±7.8	39.6	42.9	31.8	51 ±3	8.6 ±1.2
	7%	0.08	0.31	90.7 ±2.3	39.5	40.2	29.8	36 ±2	9.1 ±0.8

The chemical structures of mPEGAs and mPEGA/PCLTA networks were confirmed using the FTIR spectra in Fig. 8.3. The absorption bands at 2900, 1740, and 1635 cm^{-1} were ascribed to the C-H bond, ester carbonyl (C=O) group, and vinyl (-C=C-) groups, respectively [10,16]. For crosslinked PCLTA, the carbonyl (C=O) peak was obvious while the vinyl (-C=C-) group did not appear, suggesting that the double bonds were consumed in photo-crosslinking. mPEGA had apparent C=O and -C=C-, and C-O absorption bands at ~1100 cm^{-1}. With increasing the molecular weight of mPEGA, the C=O and -C=C- bands significantly weakened for mPEGA2000 because the density of the acrylate end groups was lower for a longer chain. For mPEGA10000, the -C=C- and C=O bands were indiscernible. After mPEGA was crosslinked with PCLTA, the absorption peaks for crosslinked PCLTA were dominant and the absorption peak at 1635 cm^{-1} no longer existed, indicating that they were fully consumed to ensure that mPEGA chains were well grafted into the network. This result was consistent with our previous study on grafting mPEGA into PPF networks [35].

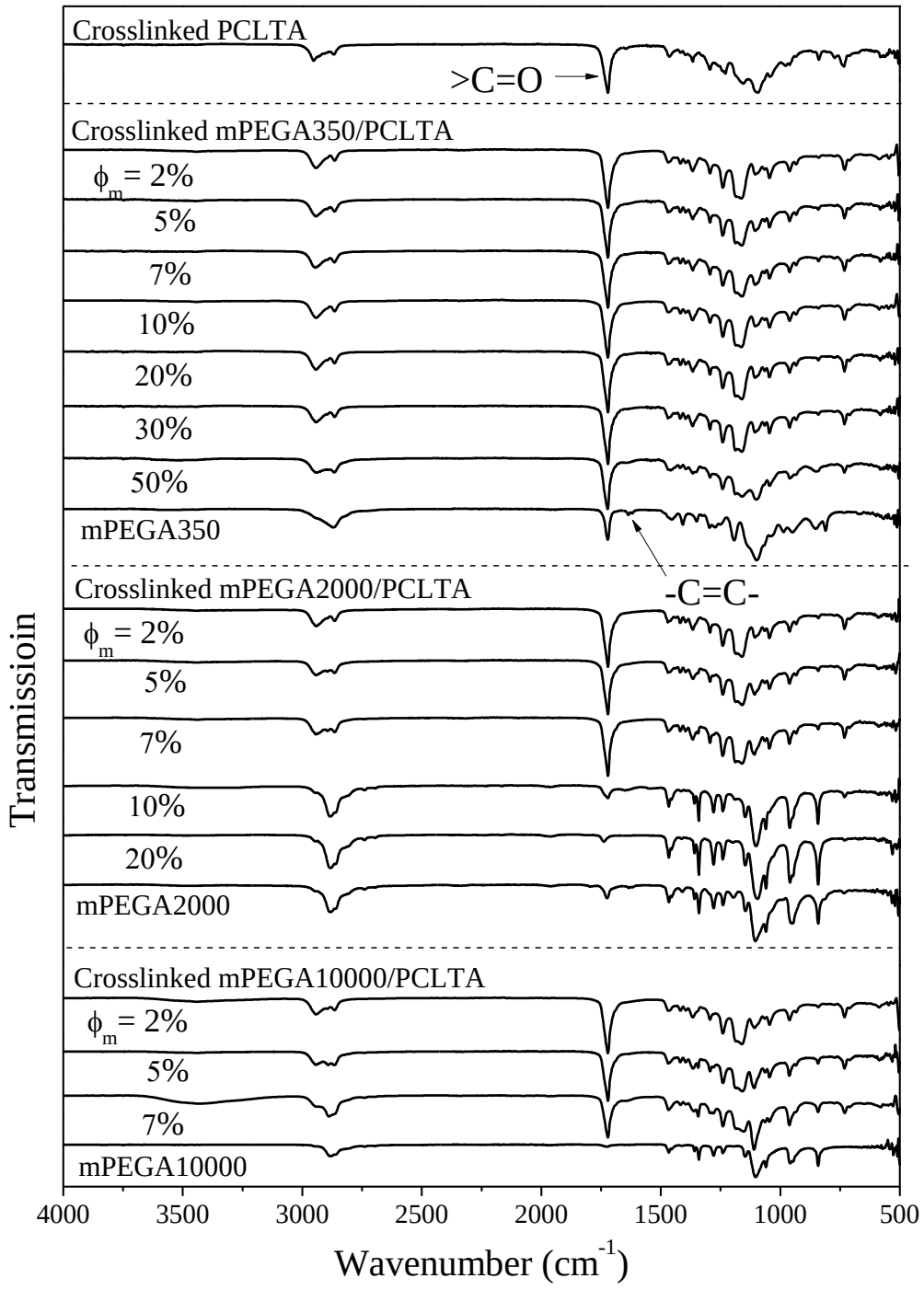

Figure 8.3 FTIR spectra of mPEGAs and networks of PCLTA and mPEGA/PCLTA.

8.3.2 Surface properties

AFM images of the surfaces of all these compressed crosslinked mPEGA/PCLTA disks are shown in Fig. 8.4a and the root-mean-square roughness (R_{rms}) values calculated from the images were less than 10 nm for all these compressed mPEGA/PCLTA networks (Table 8.1) without obvious differences in surface morphology among these samples. Therefore, the role of surface roughness in influencing SMC behavior was negligible in the discussion on cell-biomaterial interactions.

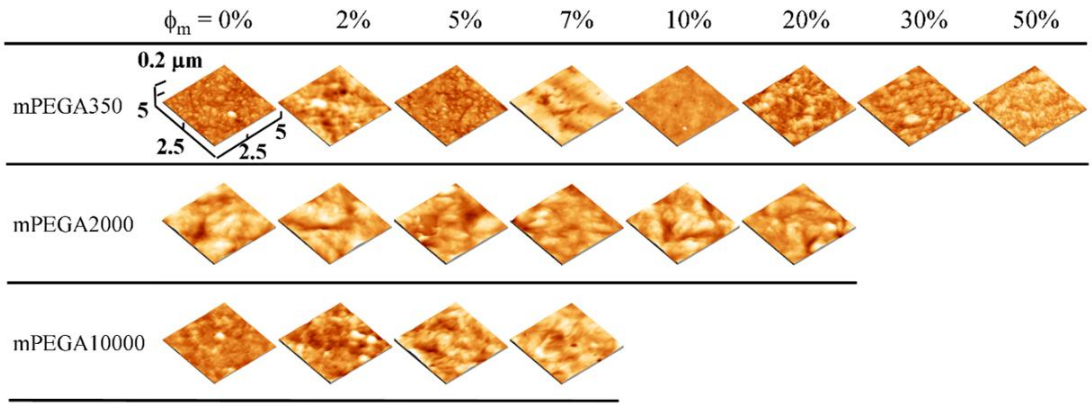

Figure 8.4 AFM images of mPEGA/PCLTA networks.

The tethered PEG chains in the networks formed coils to cover part of the exposed surface and the coverage was highly determined by ϕ_m and PEG chain length [35,37]. An approximate estimation of the coverage ratio of PEG chains in the networks was conducted to achieve a better understanding about the surface chemistry. The mean-square radii of gyration R_g^2 for both mPEGA and PCLTA chains were calculated using eq. 1. Based on the Kuhn length b of 0.7 nm for both PEG and PCL [35,38,39] and the number of repeating units N in the polymer chain, R_g^2 values were calculated to be 15.2, 0.9, 12.7, and 78.0 nm^2 for PCLTA, mPEGA350, mPEGA2000 and mPEGA10000, respectively. The molar compositions of mPEGA (Φ_m) in the mPEGA/PCLTA networks were converted from ϕ_m. The approximate coverage (C) of mPEGA chains on the network surface was calculated using eq. 2. Both Φ_m and C are listed in Table 8.1. At the same composition, a shorter mPEGA resulted in a lower C. For example, at ϕ_m of 2%, C increased from 0.04 for mPEGA350 to 0.09 and 0.11 for mPEGA2000 and mPEGA10000, respectively. When ϕ_m was 7%, the longer chain mPEGA10000 had a higher C value of 0.31 while mPEGA350 and mPEGA2000 had C values of 0.12 and 0.26, respectively. These

calculated R_g^2 and C values indicated that longer mPEGA chains formed larger coils and covered a larger portion of the polymer surface area.

$$R_g^{\ 2} = \frac{r_0^{\ 2}}{6} = \frac{(N^{3/5}b)^2}{6} \tag{1}$$

$$C = \frac{R^2_{g,m} \cdot \Phi_m}{R^2_{g,m} \cdot \Phi_m + R^2_{g,PCLTA} \cdot (1-\Phi_m)} \tag{2}$$

The hydrophilicity of PCLTA networks was greatly improved by tethering PEG chains, as indicated by a sharp decrease in the water contact angle from 79 ± 2 °on crosslinked PCLTA to 39 ± 4 °, 5 ± 2 °, and 14 ± 2 ° on PCLTA/mPEGA networks with 50% mPEGA350, 20% mPEGA2000, and 7% mPEGA10000, respectively (Fig. 8.5a). The improved hydrophilicity, which was more prominent at higher ϕ_m, indicated that hydrophilic PEG chains indeed appeared on the network surfaces efficiently. At the same ϕ_m, the surface grafted with longer PEG chains was more hydrophilic. For example, at ϕ_m of 7%, the water contact angles were 65 ± 2 °, 21 ± 3 °, and 14 ± 2 °for the networks grafted with mPEGA350, mPEGA2000, and mPEGA10000, respectively. Meanwhile, the ability of adsorbing serum proteins from the culture media decreased continuously with increasing ϕ_m for all three series of PCLTA/mPEGA networks because of the repulsive effect of grafted PEG chains, especially for the longer ones [37].

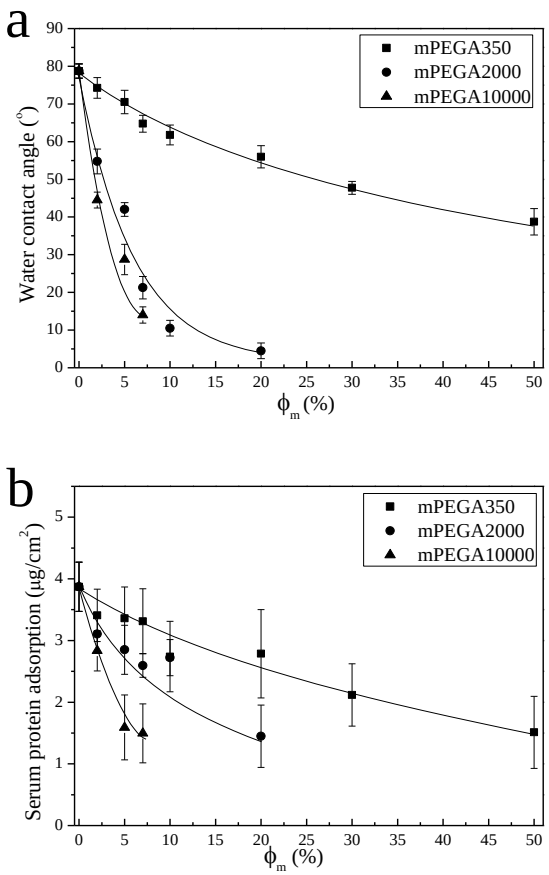

Figure 8.5 Surface wettability and protein adsorption capability. (a) Water contact angle. (b) Total serum protein adsorption from cell culture medium.

Surface lubrication to reduce friction can minimize inflammation and toxicity from wear debris, facilitate easy insertion and removal of biomedical devices, and improve the machinability of the materials [28]. Grafting PEG chains to surfaces is a widely used method to create low-friction surfaces [28,40,41]. For crosslinked mPEGA/PCLTA disks, a linear relationship between the frictional force F and the normal force W is shown in Fig. 8.6a based on Amonton's law $F = \mu W$ [40,41]. The frictional coefficient μ was obtained from the slope of the fitted line [35]. As shown in Fig. 8.6b, μ was 0.82 ± 0.02 for crosslinked PCLTA and it decreased continuously after PEG was tethered into the networks. The μ values for 50% mPEGA350, 20% mPEGA2000 and 7% mPEGA10000 were 0.18 ± 0.01, 0.12 ± 0.01 and 0.22 ± 0.03, respectively. The reduced friction coefficients confirmed that PEG chains appeared on the network surface, similar to the finding in PPF/mPEGA networks reported previously by our research group [35]. Moreover, the ability of longer tethered PEG chains in reducing friction

was higher, as demonstrated in Fig. 8.6b. At the same ϕ_m of 5%, the μ values were 0.54 ± 0.04, 0.34 ± 0.03, and 0.31 ± 0.02 for networks grafted with mPEGA350, mPEGA2000, and mPEGA10000, respectively.

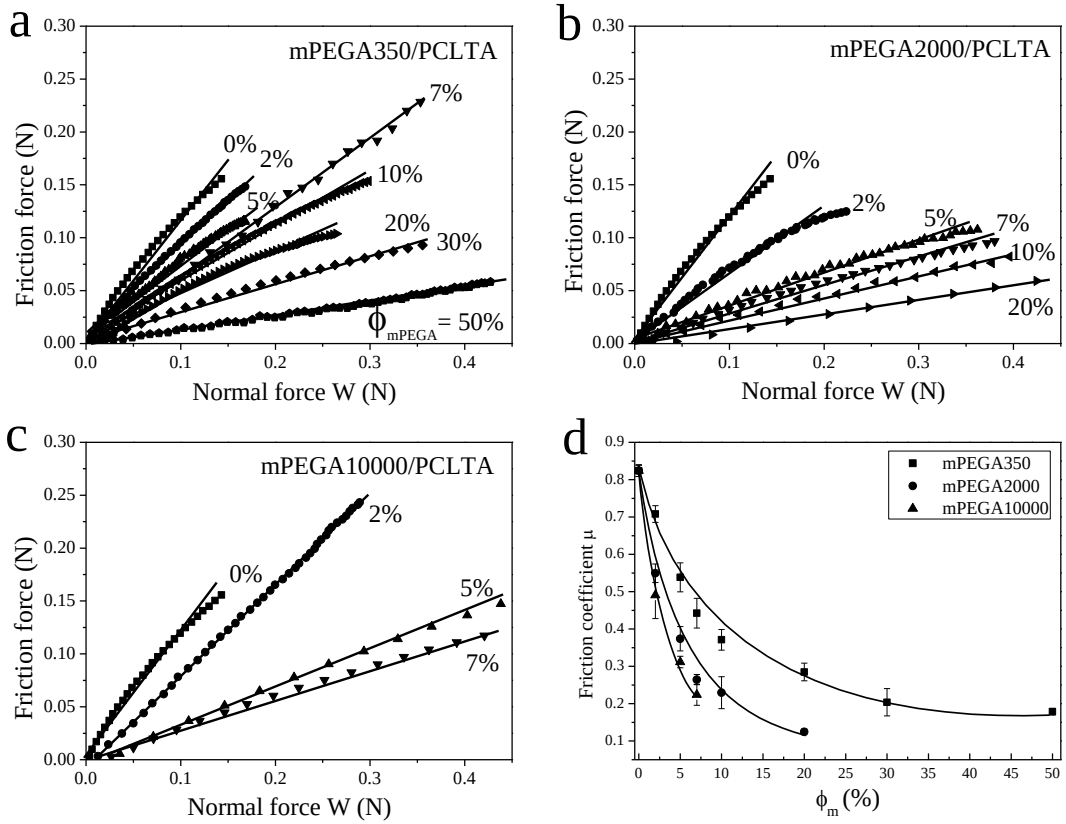

Figure 8.6 Surface lubrication characterization. (a) Normal force and Friction force curves between a stainless steel plate and disk of mPEGA/PCLTA networks. (b) Frictional coefficient calculated from the slope of these curves.

8.3.3 Thermal, mechanical, and rheological properties

DSC curves in Fig. 8.7 were used to characterize the thermal properties of mPEGA/PCLTA networks. T_m, heat of fusion (ΔH_m), and χ_c obtained from the DSC curves are listed in Table 8.1. With increasing ϕ_m, a small decrease in T_m was seen because that the tethered mPEGA chains in the networks interrupted the crystallization process of PCL segments. For the networks with ϕ_m lower than 10%, the decrease in T_m was almost negligible. When ϕ_m was greater than 10%, the T_m of the network decreased to 39.2, 36.9, and 35.0 ℃ for 20%, 30%, 50% mPEGA350, and to 37.2 ℃ for 20% mPEGA2000, respectively.

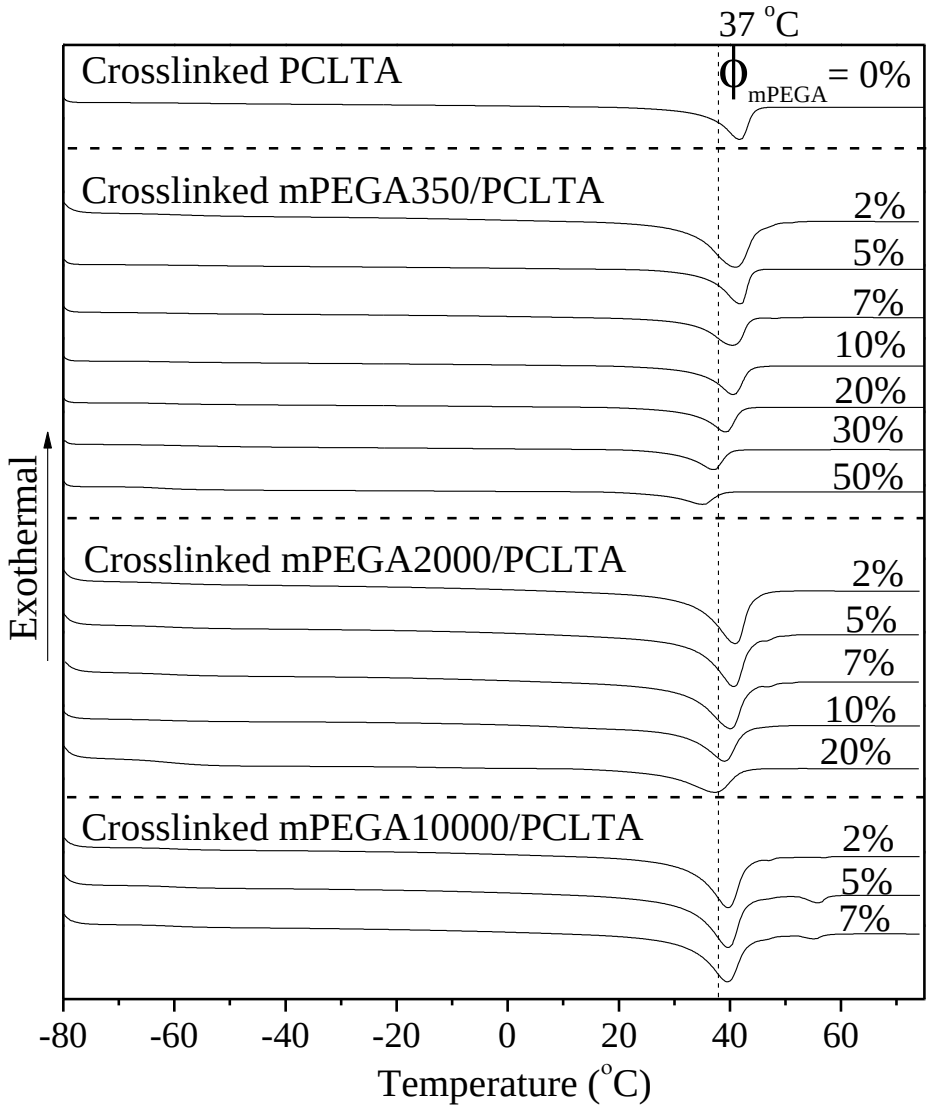

Figure 8.7 DSC curves of the samples.

Representative stress-strain curves of mPEGA/PCLTA networks obtained at 37 ℃ are shown in Fig. 8.8a-c. The networks gradually became weaker at higher ϕ_m and the strain at break (ε_b) generally increased with increasing ϕ_m, indicating that mPEGA/PCLTA networks were more elastomeric than stiffer and stronger crosslinked PCLTA. Tensile moduli (*E*) calculated from the curves decreased significantly with increasing ϕ_m in the networks (Fig. 8.8d). The reason was that mPEGA with only one acrylate group lowered both crystallinity and crosslinking density. At the same ϕ_m, longer PEG chains reduced the tensile modulus of the PCLTA network more, as also observed in mPEGA/PPF networks [35]. The rheological properties of PCLTA/mPEGA networks at both 37 and 60 ℃ are demonstrated in Figs. 9a-f. The storage modulus (*G'*) decreased continuously with increasing ϕ_m at 37 ℃, indicating that

both crystallinity and crosslinking density were reduced after incorporation with mPEGA (Fig. 8.9a-c). At 60 ℃, mPEGA/PCLTA networks were amorphous. In this scenario, *G′* was only determined by the crosslinking density and decreased by increasing ϕ_m (Fig. 8.9d-f). At the same ϕ_m, *G′* decreased gradually when mPEGA was shorter because its number of double bonds was more to be graft points to cause imperfect networks.

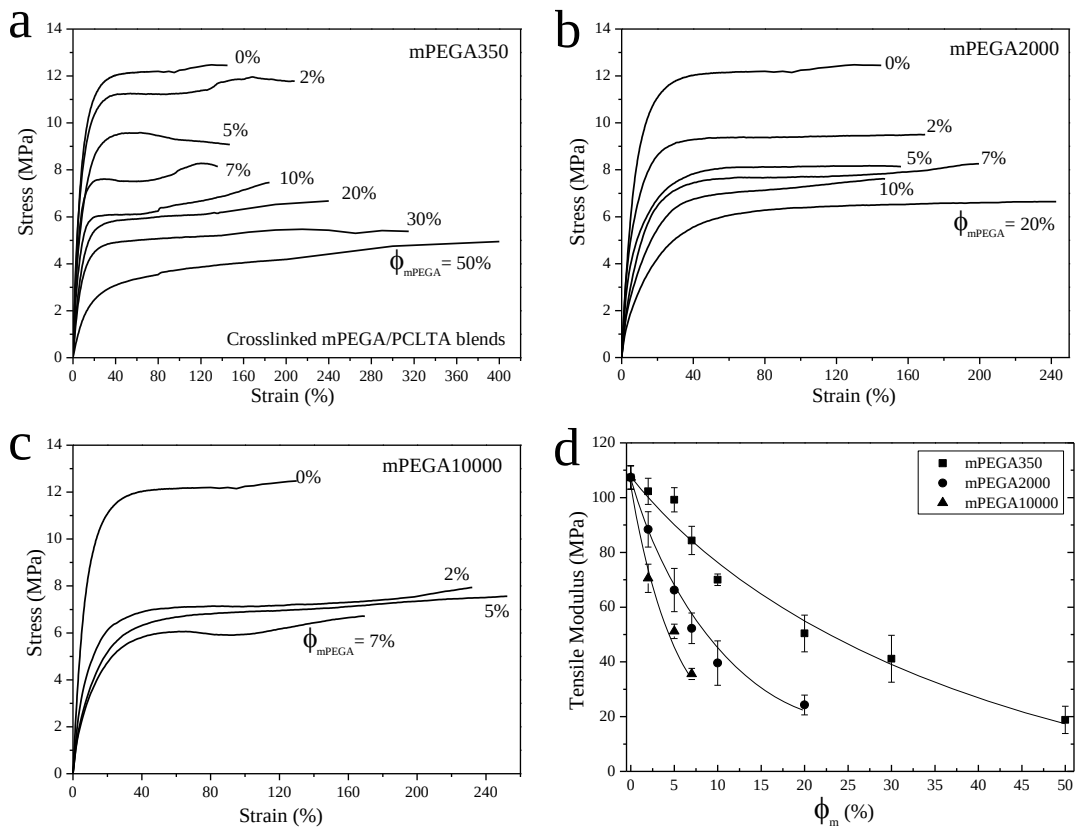

Figure 8.8 Strain-stress curves for crosslinked (a) mPEGA350/PCLTA, (b) mPEGA2000/PCLTA and (c) mPEGA10000/PCLTA networks at 37 ℃. (d) Tensile moduli.

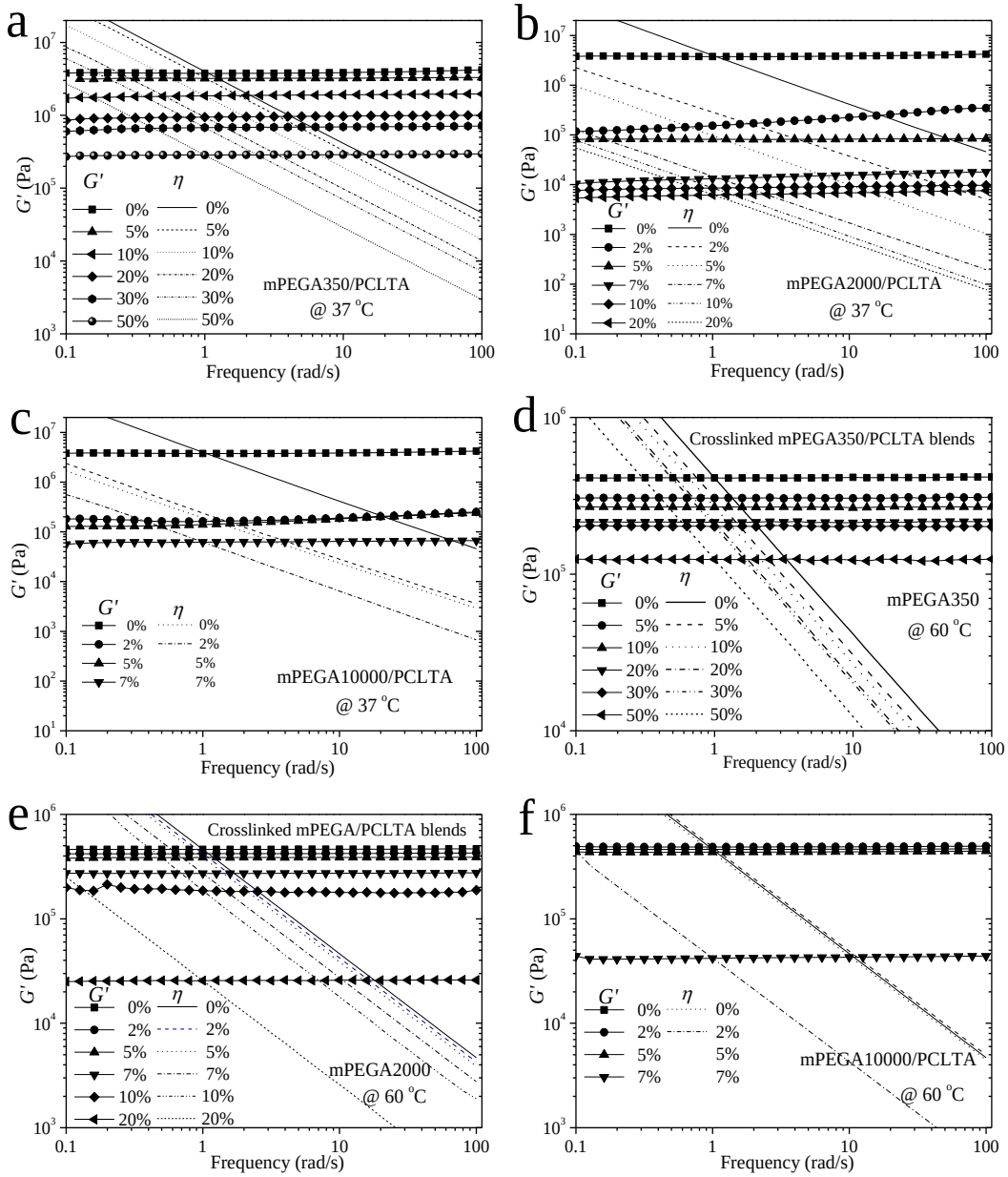

Figure 8.9 G' and η vs. frequency of the crosslinked mPEGA/PCLTA networks measured at (a-c) 37 ℃ and (d-f) 60 ℃.

8.3.4 SMC behavior on the polymer disks

SMC attachment on the polymer disks at 4 h post-seeding normalized by the positive control value is shown in Fig. 8.10a. For the networks grafted with mPEGA350 and mPEGA2000, SMC attachment showed a non-monotonic trend with increasing ϕ_m. For crosslinked mPEGA350/PCLTA, SMC attachment increased 0.48 ± 0.07 to 0.55 ± 0.05 and 0.60 ± 0.02 when ϕ_m increased from 0% to 2% and 5%, respectively. Beyond 5%, SMC attachment decreased sharply to almost zero at ϕ_m of 50%. Crosslinked mPEGA2000/PCLTA had a similar

trend with a lower ϕ_m of 2% to show the maximal attachment and also a lower ϕ_m of 20% to show almost zero attachment because of the stronger repellent effect of the densely grafted PEG chains on the network surface. For crosslinked mPEGA10000/PCLTA, SMC attachment was reduced dramatically and monotonically in a narrow composition range of 2-7%. The effect of the length of tethered PEG chains on SMC attachment was evident and can be exemplified using ϕ_m of 5%, at which the value decreased from 0.60 ± 0.02 for mPEGA350 to 0.45 ± 0.04 and 0.11 ± 0.05 for mPEGA2000 and mPEGA10000, respectively.

Cell spreading is critical for cell migration and proliferation [42]. It can be quantified using cell area after 1 day culture. As demonstrated in Fig. 8.10b, cell area followed the same trend as in cell attachment in terms of dependence on both ϕ_m and the length of tethered PEG chains. These data indicated that a small fraction of tethered PEG short chains lowered the surface hydrophobicity of crosslinked PCLTA and SMC attachment was therefore improved. In contrast, mPEGA10000 with a longer length dramatically decreased the water contact angle to values lower than $50°$ and generated a strong repulsion to protein adsorption and SMC attachment even at ϕ_m of 2%. When ϕ_m was 5%, mPEGA2000 also showed repulsion to SMCs, as their attachment and spread area were reduced to 0.45 ± 0.04 and 4100 ± 570 μm^2, respectively. At this ϕ_m, mPEGA10000 resulted in even lower SMC attachment of 0.11 ± 0.05 and spread area of 1870 ± 460 μm^2 while mPEGA350 resulted in higher values of 0.60 ± 0.02 and 4960 ± 840 μm^2. mPEGA350 did not show cell adhesion inhibition effect until when ϕ_m was 7%, at which SMC attachment and spread area were reduced to 0.48 ± 0.05 and 4190 ± 730 μm^2, respectively. In contrast, SMC adhesion was fully prohibited on the substrates grafted with 7% mPEGA10000. As found in attachment, SMC proliferation over 4 days on the networks of mPEGA350/PCLTA and mPEGA2000/PCLTA also demonstrated non-monotonic dependence on ϕ_m by showing a peak at ϕ_m of 5% and 2% before sharp decrease to almost zero at ϕ_m of 50% and 20%, respectively. SMC proliferation on mPEGA10000/PCLTA networks was reduced substantially and continuously as expected.

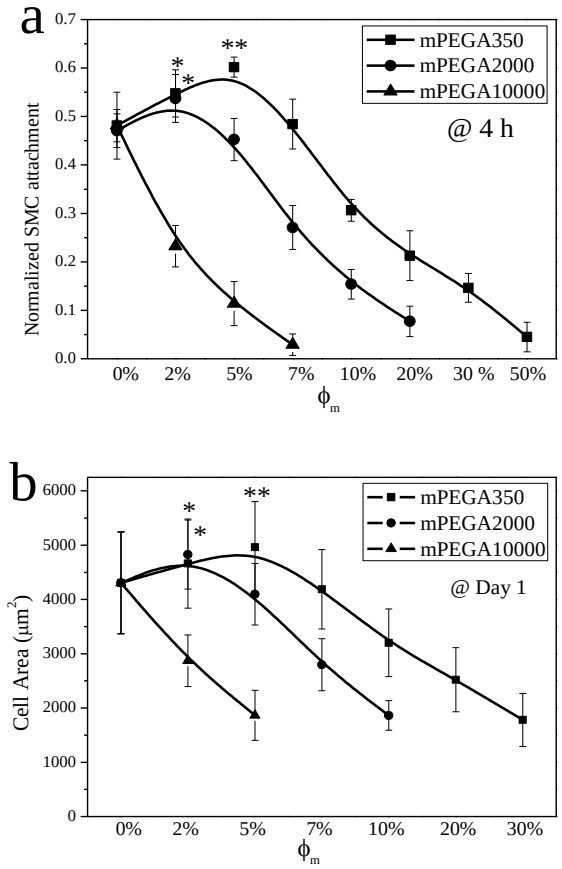

Figure 8.10 SMC attachment and spread area. (a) SMC attachment at 4 h post-seeding on crosslinked mPEGA/PCLTA networks. (b) SMC area after 1 day culture on these networks. **: significant difference ($p < 0.05$) between mPEGA350/PCLTA ($\phi_m = 5\%$) and PCLTA ($\phi_m = 0\%$). *: significant difference ($p < 0.05$) between mPEGA2000/PCLTA ($\phi_m = 2\%$) and PCLTA ($\phi_m = 0\%$).

The images of SMCs stained with both RP and DAPI at different time points are demonstrated in Fig. 8.11b and the cell numbers were consistent with those in Fig. 8.11a. The best spread-out cell phenotype and the fastest cell proliferation were found on crosslinked PCLTA/mPEGA350 with ϕ_m of 5% and crosslinked PCLTA/mPEGA2000 with ϕ_m of 2%. On the networks tethered with either short PEG chains at high ϕ_m or long PEG chains at any ϕ_m, SMCs were small and round in morphology and slow in proliferation. SMCs cultured on crosslinked PCLTA/mPEGA10000 for several days still showed a sparsely distributed pattern because of the strong repulsive effect of the tethered PEG chains [19,23,24,26,28].

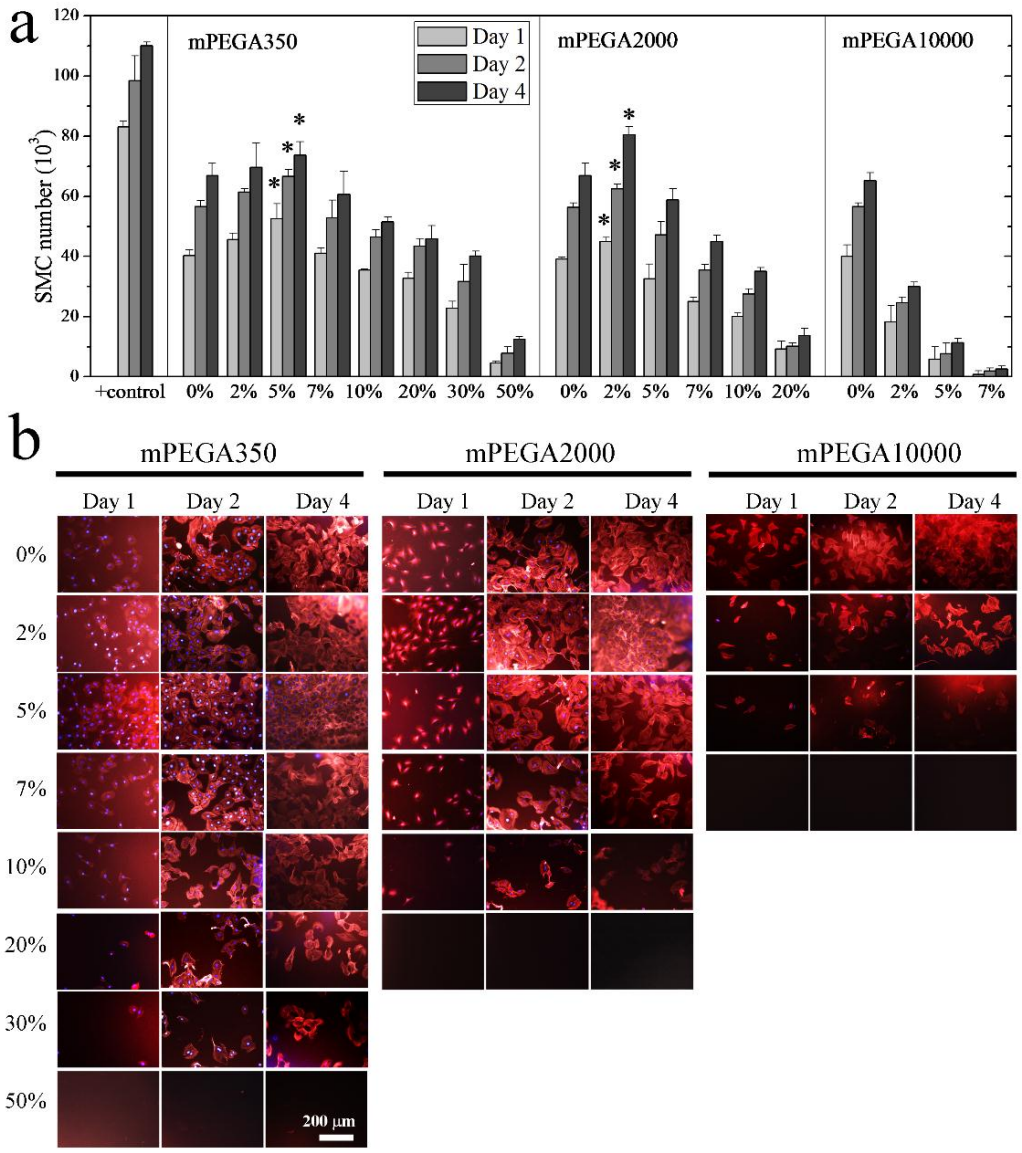

Figure 8.11 SMC proliferation and images. (a) SMC number at days 1, 2, and 4 post-seeding using TCPS as positive control. (b) Cells on these networks stained by RP and DAPI at days 1, 2, and 4 post-seeding. *: significant higher ($p < 0.05$) than corresponding value on crosslinked PCLTA ($\phi_m = 0\%$) network.

SMCs are not terminally differentiated and have the potential to modulate their phenotype as the response to changes in environmental conditions including substrate stiffness, growth factors, surface proteins, and ECM chemical properties [43]. Based on that fact that SMC attachment and proliferation were improved on PCLTA networks tethered with a small portion of short PEG chains, I further analyzed the expression levels of representative contractile

markers on these substrates using real-time PCR. Among the contractile markers analyzed in this study, smoothlin, calponin, and SM-MHC showed significant differences in SMCs cultured on PCLTA/mPEGA350 networks with three representative ϕ_m of 0%, 5%, and 10%. After normalization to the value on crosslinked PCLTA, the expression level of smoothlin was significantly higher ($p < 0.05$) at ϕ_m of 5% compared with the value at ϕ_m of 10% (Fig. 8.12a). The expression levels of calponin and SM-MHC at ϕ_m of 5% were significantly higher than the values at the other two ϕ_m (Fig. 8.12b-c).

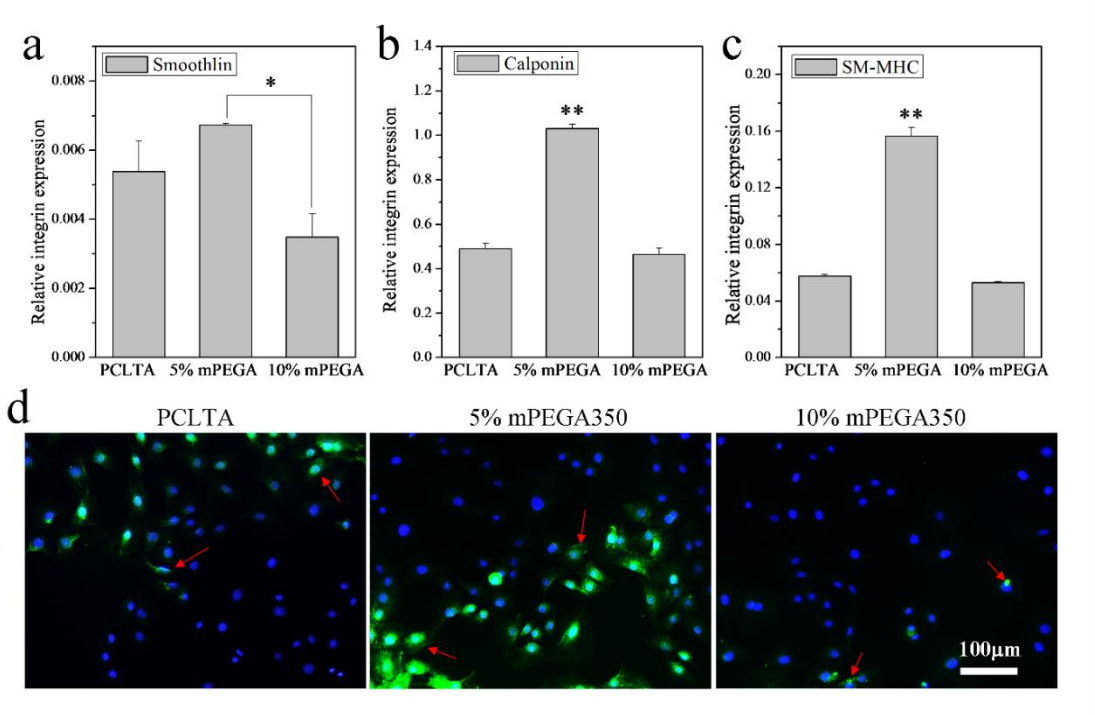

Figure 8.12 Normalized relative expression level of contractile marker (a) smoothlin, (b) calponin and (c) SM-MHC in SMCs on mPEGA350/PCLTA networks with different ϕ_m at day 2 post-seeding. (d) The immunofluorescence staining of a contractile marker protein, calponin, in SMCs on mPEGA350/PCLTA networks with different ϕ_m at day 2 post-seeding. *: $p < 0.05$; **: $p < 0.05$ relative to the other samples.

The content of calponin, a critical contractile phenotypic marker, was analyzed using fluorescence immunostaining. As shown in Fig. 8.12d, the nuclei and calponin in SMCs were stained blue and green, respectively. Consistent with SMC proliferation discussed in Section 3.4, more cells appeared on the network grafted with 5% mPEGA compared with crosslinked

PCLTA and 10% mPEGA. As indicated by stronger immunofluorescence intensity, a larger fraction of SMCs expressing calponin and more calponin in each cell were found on the network grafted with 5% mPEGA. The result that SMCs on PCLTA/mPEGA350 networks with ϕ_m of 5% had upregulated expression of contractile markers indicated that modification of PCLTA networks with a small fraction of short PEG chains better supported phenotypic conversion from synthetic to contractile SMCs as well as SMC attachment and proliferation.

8.3.5 Focal adhesions of SMCs

FAs are dynamic anchoring protein complexes that connect the internal cell cytoskeleton to the ECM [44]. Elongated FAs are mostly located at the cell periphery and contain a set of different proteins, in particular, paxillin and vinculin [44]. FAs can respond to different intracellular tensions and adjust their elongation and size to form super-mature adhesion subtypes [45]. Changes in formation of adhesion complexes give responsive signals to the pathways of intracellular signaling and cytoskeletal transduction, and ultimately affect cellular behaviors [46].

Stronger, denser, and larger FAs were observed in SMCs cultured on PCLTA/mPEGA (ϕ_m = 5%) networks for 1 day compared with ϕ_m of 0 and 10%, shown as bright green punctate spots in Fig. 8.13a. Quantification of FAs is shown in Fig. 8.13b-d. At ϕ_m of 10%, the FAs in SMCs were the smallest and their density was also the lowest. In Fig. 8.13c, elongation of FAs quantified using the inverse of FA circularity was significantly higher at ϕ_m of 5% than that at 10%. The FA density, defined as the number of FAs per cell, was significantly higher at ϕ_m of 5% than the values at ϕ_m of 0 and 10% (Fig. 8.13d). All these significant differences in the characteristics of FAs in SMCs on substrates with different PEG grafting densities confirmed that FAs can sense the substrate properties and adjust themselves accordingly. PCLTA networks grafted with short chain mPEGA350 at ϕ_m of 5% could trigger stronger FAs and facilitate SMCs to attach onto the substrate surface than ϕ_m of 0 or 10%.

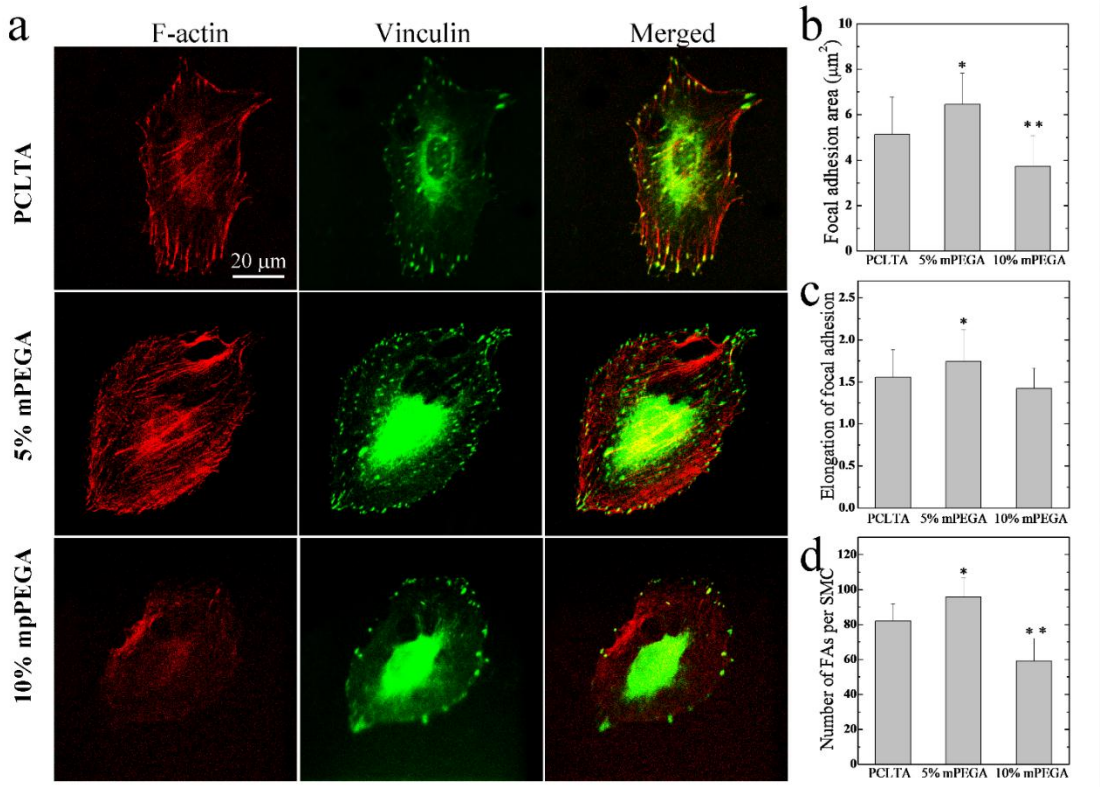

Figure 8.13 Characterizations of focal adhesions. (a) Confocal microscope images of SMC filaments and focal adhesions stained using RP and vinculin antibodies at day 1 post-seeding. (b) Focal adhesion area, (c) elongation in SMCs, and (d) density on crosslinked mPEGA350/PCLTA substrates. *: $p < 0.05$ relative to the other samples; **: $p < 0.05$ relative to crosslinked PCLTA.

8.3.6 Integrin expression

The sensing process of FAs in cells to the ECM was recognized to involve different subunits in FA complexes. More than 20 functional sub-components have been identified in FA complexes, including vinculin, talin, paxillin, focal adhesion kinase (FAK), and integrins [47]. Integrins are a series of heterodimers formed by two distinct chains named as α and β subunits [48]. Integrins located across the cell membrane can link to different ECM proteins with the external end and to intracellular molecules via adapter proteins, thus they play critical roles in signal transduction in FAs [48]. Various combinations of integrin subunits are capable of binding to different proteins, for example, $\alpha_2\beta_1$ and $\alpha_5\beta_1$ are important cellular receptors for SMC adhesion to collagen and fibronectin while $\alpha_v\beta_5$ and $\alpha_v\beta_3$ are for vitronectin and

osteopontin [49].

To understand why distinct FAs appeared in SMCs cultured on the networks grafted with different ϕ_m, I further analyzed expression levels of several major integrin subunits in SMCs at day 1 using real-time PCR. Three α subunits (α_v, α_1, and α_5) and two β subunits (β_1 and β_3) all had significantly different expression levels ($p < 0.05$) on the three selected PCLTA/mPEGA350 networks with ϕ_m of 0, 5, and 10% (Fig. 8.14). For integrin subunits α_v, α_5, and β_3, their expression levels were significantly higher ($p < 0.03$) when ϕ_m was 5% than those on crosslinked PCLTA. For integrin subunits α_1 and β_1, there were no significant differences between crosslinked PCLTA and the network with ϕ_m of 5%. In contrast, the expression levels of α_1 and β_1 were significantly lower at ϕ_m of 10% compared with those at ϕ_m of 5%. Upregulated expression of these integrin subunits in SMCs on PCLTA/mPEGA350 networks with ϕ_m of 5% was well correlated with the results on FAs, cell spreading, attachment, and proliferation as these integrin subunits are capable of forming different integrin combinations such as $\alpha_v\beta_3$, $\alpha_1\beta_3$, $\alpha_1\beta_1$, $\alpha_5\beta_1$, which play critical roles in signal transduction regulating cellular adhesion, spreading, and proliferation [50].

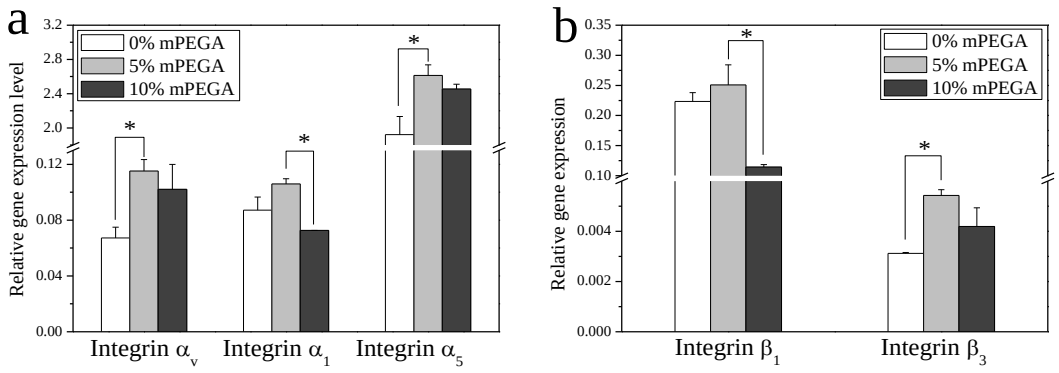

Figure 8.14 The integrin alpha subunit (a) and beta subunit (b) gene expression level in SMCs on PCLTA networks with 0, 5, and 10% of mPEGA350 at day 1 post-seeding. The expression was normalized to the house keeping gene GAPDH. *: $p < 0.05$.

8.4 Discussion

In order to improve surface hydrophilicity, hydrophobic polymer substrates are often modified by grafting PEG chains on the surface through a variety of methods [51,52]. For example, PEG chains were immobilized on the surface through atmospheric pressure glow discharge treatment to improve biocompatibility of hydrophobic intraocular lens and repellency of the attachment, spreading and growth of platelets, macrophages and lens epithelial cells was observed on the PEG-modified lens [51]. In another study, anti-fouling and blood compatibility were highly improved by esterifying PEG chains on the surface of poly(acrylonitrile-*co*-maleic acid) membranes [52]. The effectiveness of surface modification was influenced by the PEG chain length and the best performance was achieved when the molecular weight of PEG was 400 g mol^{-1} [52]. Unlike the above surface grafting methods, the PCLTA networks grafted with PEG chains in this study were homogeneous not only on the surface but also in the bulk, even after degradation. In addition, the density of grafted PEG chains can be readily controlled by adjusting the mPEGA/PCLTA blend composition and consequently their surface and bulk material properties were all tuned in a monotonic manner. Tethered PEG chains in the networks reduced the crosslinking density and inhibited the crystallization process of PCL segments. Therefore, with the increase of ϕ_m, evidently decreased T_m, χ_c, and tensile modulus were found. In our previous reports, crosslinked PCL acrylate substrates with lower χ_c and stiffness are believed to less support pre-osteoblastic MC3T3-E1 cell and SMC adhesion and proliferation [13,18]. The surface morphology of the underlying substrate can also influence cell responses; however, this effect was ruled out because all the samples were compressed to achieve a similar surface roughness. After more PEG chains were grafted into the networks, the original hydrophobic surface became more hydrophilic continuously. When the water contact angle was ~50 °, surface energy and hydrophilicity were reported to be the most appropriate for cell attachment and proliferation [34,42].

The protein adsorption ability of a polymer surface is often related to its hydrophilicity [2]. Neither too hydrophilic nor too hydrophobic surfaces favor cells attachment because of low protein or non-adhesive protein adsorption [2]. In molecular models in Fig. 8.15, the PEG layer grafted on a polymer substrate provides an interfacial barrier to prevent the serum proteins from

reacting with the substrate [53,54]. Proteins approach to the substrate surface by diffusion and this step is influenced by the hydrophobic interaction free energies, van der Waals attraction, and steric repulsion between the surface and proteins [53,54]. Closer approaching of proteins to the surface compresses the PEG grafted chains and induces a steric repulsion effect while the van der Waals component with the substrate weakens with increasing the grafting density and the PEG chain length [53-55]. These models can well explain that serum protein adsorption by the networks studied here was not significantly changed when a small amount of short PEG chains was grafted onto the network but it was reduced significantly when the PEG grafted chains were more or longer.

The effect of PEG grafted chain density on SMC behavior was well demonstrated by a non-monotonic trend of SMC adhesion and proliferation, gene expression of integrin subunits and contractile phenotypic markers on mPEGA350/PCLTA networks. Hydrophobic surfaces can adsorb non-adhesive proteins and denature adhesive proteins [2]. Sparsely grafted short PEG chains on the surface could relieve the hydrophobic property to a favorable extent and thus increase the wettability and adsorption of adhesive proteins, which consequently facilitated SMCs to attach and proliferate better (Fig. 8.15a). However, the hydrophilicity and antifouling ability increased with increasing the density of PEG grafted chains [56]. The gathering of crowded PEG chains on the surface repel serum proteins and cells [23,24,57]. The repulsion originates from the steric stabilization force and chain mobility effect of the grafted PEG chains [58]. Proteins, blood components, or cells have to be in contact with the foreign surface longer than certain time to reach stable adhesion while rapid movements of the densely hydrated chains on the substrate prevent the stagnation on the surface, shorten the contact time, and then inhibit adhesion [58].

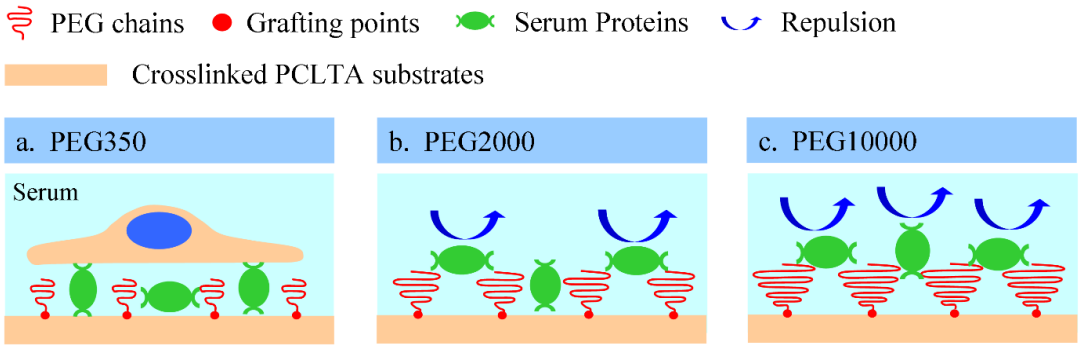

Figure 8.15 Scheme of grafted PEG chain coils on the surface of crosslinked PCLTA networks. Three different lengths PEG chains of (a) PEG350, (b) PEG2000 and (c) PEG 10000 form varied chain coverage on the surface, hence differed protein repelling effects resulted by covering PEG chains motilities.

As discussed in Results, longer PEG chains formed larger coils to cover a larger fraction of the surface at the same ϕ_m (Fig. 8.15b-c). Thus the critical ϕ_m for mPEGA10000 to exhibit strong repulsion was much lower than that for mPEGA350. Cell attachment, spreading and proliferation increased for the networks grafted with mPEGA350 and mPEGA2000 when ϕ_m was sufficient low. The same surface coverage of 0.09 was achieved when 5% mPEGA350 or 2% mPEGA2000 was grafted into the PCLTA network. mPEGA10000 had stronger ability in reducing surface hydrophobicity, larger volume restriction, and higher chain mobility (Fig. 8.15c). To reach the same surface coverage of 0.09, ϕ_m for mPEGA10000 should be only 1.4%, lower than the lowest value of 2% tested in this study. Therefore, mPEGA10000 prohibited SMC attachment and proliferation even throughout the composition range, in agreement with previous reports on stronger protein repellence and cell adhesion elimination for longer PEG graft chains [37,59]. This protein/cell repellency from the tethered PEG chains in polymer networks was also reported by us to be effective for MC3T3-E1 cells and nerve cells [35,60]. The effective repellency of proteins and cells together with reduced surface friction at high ϕ_m while promoted cell behavior and improved surface wettability at low ϕ_m suggest the high potential of crosslinked mPEGA/PCLTA used as candidate materials in fabricating biomedical devices. Based on the current findings on tuning surface properties and cell behavior, I will further investigate better design and modification strategies for biomaterials and scaffolds for cardiovascular tissue engineering applications.

8.5 Conclusions

A series of photo-crosslinked mPEGA/PCLTA networks with various ϕ_m and three mPEGA molecular weights was developed to modulate bulk and surface properties and then to regulate SMC behavior. The PEG chains grafted on the surface of crosslinked PCLTA networks significantly reduced surface hydrophobicity, frictional coefficient, and serum protein adsorption. Longer PEG chains had a more prominent effect in modifying these surface properties. Unlike the continuous change in surface properties, rat primary SMC adhesion and proliferation exhibited non-monotonic dependence on ϕ_m and maximized at ~5% for the networks grafted with mPEGA350 and ~2% for those with mPEGA2000. The expression levels of three contractile gene markers for SMCs cultured on crosslinked mPEGA350/PCLTA substrates also demonstrated a similar trend by having maxima at ϕ_m of 5%. For mPEGA10000 with the longest chain length, a sharp, monotonic decrease was found in both SMC attachment and proliferation. This study clearly demonstrated that grafting a small fraction of short PEG chains to PCLTA networks promoted the behaviors of SMCs cultured on them by reducing surface hydrophobicity. In contrast, a high fraction or long PEG tethered chains could significantly prohibit SMC adhesion and proliferation via strong repulsion to cells and cell-adhesive proteins.

References

1. Go AS, Mozaffarian D, Roger VL, Benjamin EJ, Berry JD, Borden WB, et al. American Heart Association Statistics Committee and Stroke Statistics Subcommittee. Heart disease and stroke statistics--2013 update: a report from the American Heart Association. Circulation 2013;127(1):e6-e245
2. Harbers GM, Grainger DW. Cell-material interactions: fundamental design issues for tissue engineering and clinical considerations. In: Guelcher SA, Hollinger JO, editors. Introduction to biomaterials. Boca Raton: CRC Press;2005. p.15-45.
3. Ingber DE. Cellular mechanotransduction: putting all the pieces together again. FASEB J 2006;20:811-27.
4. Kim BS, Putnam AJ, Kulik TJ, Mooney DJ. Optimizing seeding and culture methods to engineer smooth muscle tissue on biodegradable polymer matrices. Biotechnol Bioeng 1998;57(1):46-54.
5. Timmer MD, Shin H, Horch RA, Ambrose CG, Mikos AG. In vitro cytotoxicity of injectable and biodegradable poly(propylene fumarate)-based networks: unreacted macromers, cross-linked networks, and degradation products. Biomacromolecules 2003;4:1026-33.
6. Suggs LJ, West JL, Mikos AG. Platelet adhesion on a bioresorbable poly(propylene fumarate-co-ethylene glycol) copolymer. Biomaterials 1999;20:683-90.
7. Hua J, Sun X, Ma H, Xie C, Chen YE, Ma PX. Porous nanofibrous PLLA scaffolds for vascular tissue engineering. Biomaterials 2010;31:7971-7.
8. Qu XH, Wu Q, Liang J, Zou B, Chen GQ. Effect of 3-hydroxyhexanoate content in poly(3-hydroxybutyrate-co-3-hydroxyhexanoate) on in vitro growth and differentiation of smooth muscle cells. Biomaterials 2006;27:2944-50.
9. Chan-Park MB, Shen JY, Cao Y, Xiong Y, Liu Y, Rayatpisheh S, Kang GC, Greisler HP. Biomimetic control of vascular smooth muscle cell morphology and phenotype for functional tissue-engineered small-diameter blood vessels. J Biomed Mater Res A 2009;88(4):1104-21.
10. Wang S, Kempen DH, Simha NK, Lewis JL, Windebank AJ, Yaszemski MJ, et al. Photo-crosslinked hybrid polymer networks consisting of poly(propylene fumarate) and

poly(caprolactone fumarate): controlled physical properties and regulated bone and nerve cell responses. Biomacromolecules 2008;9:1229-41.

11. Wang S, Kempen DH, Yaszemski MJ, Lu L. The roles of matrix polymer crystallinity and hydroxyapatite nanoparticles in modulating material properties of photo-crosslinked composites and bone marrow stromal cell responses. Biomaterials 2009;30:3359-70.
12. Wang S, Yaszemski MJ, Gruetzmacher JA, Lu L. Photo-crosslinked poly(ε-caprolactone fumarate) networks: Roles of crystallinity and crosslinking density in determining mechanical properties. Polymer 2008;49:5692-99.
13. Cai L, Wang S. Poly(ε-caprolactone) acrylates synthesized using a facile method for fabricating networks to achieve controllable physicochemical properties and tunable cell responses. Polymer 2010;51:164-77.
14. Cai L, Wang S. Parabolic dependence of material properties and cell behavior on the composition of polymer networks via simultaneously controlling crosslinking density and crystallinity. Biomaterials 2010;31:7423-34.
15. Cai L, Guinn AS, Wang S. Exposed hydroxyapatite particles on the surface of photo-crosslinked nanocomposites for promoting MC3T3 cell proliferation and differentiation. Acta Biomater 2011;7(5):2185-99.
16. Wang S, Lu L, Gruetzmacher JA, Currier BL, Yaszemski MJ. A biodegradable and cross-linkable multiblock copolymer consisting of poly(propylene fumarate) and poly(ε-caprolactone): synthesis, characterization, and physical properties. Macromolecules 2005;38:7358-70.
17. Wang K, Cai L, Hao F, Xu X, Cui M, Wang S. Distinct cell responses to substrates consisting of poly(ε-caprolactone) and poly(propylene fumarate) in the presence or absence of cross-links. Biomacromolecules 2010;11:2748-59.
18. Liu X, Cai L, Hao F, Cui M, Wang S. Biodegradable elastomeric substrates with controllable stiffness for regulating smooth muscle cell behavior. Polym Mater Sci Eng 2011;105:124-6.
19. Lee JH, Lee HB, Andrade JD. Blood compatibility of polyethylene oxide surfaces. Prog Polym Sci 1995;20:1043-79.
20. Sefton MV, Gemmell CH. Nonthrombogenic treatments and strategies. In: Ratner BD,

Hoffman AS, Schoen FJ, Lemons JE, editors. Biomaterials science. 2nd ed. Amsterdam: Elsevier Academic Press; 2002. p. 456-60.

21. Chaikof EL, Merrill EW, Callow AD, Connolly RJ, Verdon SL, Ramberg K. PEO enhancement of platelet deposition, fibrinogen deposition, and complement C3 activation. J Biomed Mater Res 1992;26:1163-8.

22. Nagaoka S, Mori Y, Takiuchi H, Tanzawa H, Nishiumi S. Interaction between blood components and hydrogels with poly(oxyethylene) chains. In: Shalaby SW, Hoffman AS, Ratner BD, Horbett TA, editors. "Polymers as biomaterials". New York: Plenum Press; 1984. p. 361-74.

23. Mougin K, Lawrence MB, Fernandez EJ, Hillier AC. Construction of cell-resistant surfaces by immobilization of poly(ethylene glycol) on gold. Langmuir 2004;20:4302-5.

24. Blümmel J, Perschmann N, Aydin D, Drinjakovic J, Surrey T, Lopez-Garcia M, Kessler H, Spatz JP. Protein repellent properties of covalently attached PEG coatings on nanostructured SiO_2-based interfaces. Biomaterials 2007;28:4739-47.

25. Kingshott P, Griesser HJ. Surfaces that resist bioadhesion. Curr Opin Solid State Mater Sci 1999;4:403-12.

26. Elbert DL, Hubbell JA. Surface treatment of polymers for biocompatibility. Annu Rev Mater Sci 1996;26:365-94.

27. Desai NP, Hubbell JA. Solution technique to incorporate polyethylene oxide and other water-soluble polymers into surfaces of polymeric biomaterials. Biomaterials 1991;12:144-53.

28. Chawla K, Lee S, Lee BP, Dalsin JL, Messersmith PB, Spencer ND. A novel low-friction surface for biomedical applications: modification of poly(dimethylsiloxane) (PDMS) with polyethylene glycol(PEG)-DOPA-lysine. J Biomed Mater Res A 2009;90(3):742-9.

29. Wattendorf U, Merkle HP. PEGylation as a tool for the biomedical engineering of surface modified microparticles. J Pharm Sci 2008;97(11):4655-69.

30. Jun HW, West JL. Modification of polyurethaneurea with PEG and YIGSR peptide to enhance endothelialization without platelet adhesion. J Biomed Mater Res Part B: Appl Biomater 2005;72B:131-9.

31. Liu L, Guo S, Chang J, Ning C, Dong C, Yan D. Surface modification of polycaprolactone

membrane via layer-by-layer deposition for promoting blood compatibility. J Biomed Mater Res Part B: Appl Biomater 2008;87B:244-50.

32. Niklason LE, Gao J, Abbott WM, Hirschi K, Houser S, Marini R, et al. Functional arteries grown in vitro. Science 1999;284:489-93.
33. Owens GK. Regulation of differentiation of vascular smooth muscle cells. Physiol Rev 1995;75(3):487-517.
34. Wong JY, Leach JB, Brown XQ. Balance of chemistry, topography, and mechanics at the cell-biomaterial interface: issues and challenges for assessing the role of substrate mechanics on cell response. Surf Sci 2004;570:119-33.
35. Cai L, Wang K, Wang S. Poly(ethylene glycol)-grafted poly(propylene fumarate) networks and parabolic dependence of MC3T3 cell behavior on the network composition. Biomaterials 2010;31:4457-66.
36. Peyton SR, Raub CB, Keschrumrus VP, Putnam AJ. The use of poly(ethylene glycol) hydrogels to investigate the impact of ECM chemistry and mechanics on smooth muscle cells. Biomaterials 2006;27:4881-93.
37. Kingshott P, Thissen H, Griesser HJ. Effects of cloud-point grafting, chain length, and density of PEG layers on competitive adsorption of ocular proteins. Biomaterials 2002;23:2043-56.
38. Schultz KM; Baldwin AD; Kiick KL; Furst EM. Gelation of covalently cross-linked PEG-heparin hydrogels. Macromolecules 2009;42:5310-16.
39. Herrera D, Zamora J, Bello A, Grimau M, Laredo E, Muller AJ, Lodge TP. Miscibility and crystallization in polycarbonate/poly(ε-caprolactone) blends: Application of the self-concentration model. Macromolecules 2005;38:5109-17.
40. Gong JP, Kagata G, Osada Y. Friction of gels. 4. Friction on charged gels. J Phys Chem B 1999:103(29):6007-14.
41. Gong JP, Osada Y. Surface friction of polymer gels. Prog Polym Sci 2002;27:3-38.
42. Saltzman WM, Kyriakides TR. Cell interactions with polymers. In: Lanza R, Langer R, Vacanti J, editors. Principles of tissue engineering. 3rd ed. San Diego: Elsevier Academic Press; 2007. p. 279-96.
43. Owens GK, Kumar MS, Wamhoff BR. Molecular regulation of vascular smooth muscle cell

differentiation in development and disease. Physiol Rev 2004;84:767– 801.

44. Geiger B, Spatz JP, Bershadsky AD. Environmental sensing through focal adhesions. Nat Rev Mol Cell Bio 2009;10:21-33.
45. Parsons JT, Horwitz AR, Schwartz MA. Cell adhesion: integrating cytoskeletal dynamics and cellular tension. Nat Rev Mol Cell Bio 2011;11:633-43.
46. Zamir E, Geiger B. Molecular complexity and dynamics of cell-matrix adhesions. J Cell Sci 2001;114:3583-90.
47. Wozniak MA, Modzelewska K, Kwong L, Keely PJ. Focal adhesion regulation of cell behavior. Biochim Biophys Acta 2004;1692:103-19.
48. Giancotti FG, Ruoslahti E. Integrin Signaling. Science 1999;285(5430):1028-32.
49. Srivatsa SS, Fitzpatrick LA, Tsao PW, Reilly TM, Holmes DR Jr, Schwartz RS, Mousa SA. Selective alpha v beta 3 integrin blockade potently limits neointimal hyperplasia and lumen stenosis following deep coronary arterial stent injury: evidence for the functional importance of integrin alpha v beta 3 and osteopontin expression during neointima formation, Cardiovasc Res 1997;36:408-28.
50. Hynes RO. Integrins: bidirectional, allosteric signaling machines. Cell 2002;110:673-87.
51. Lin L, Wang Y, Huang XD, Xu ZK, Yao K. Modification of hydrophobic acrylic intraocular lens with poly(ethylene glycol) by atmospheric pressure glow discharge: A facile approach. Appl Surf Sci 2010;256:7354-64.
52. Nie FQ, Xu, Z, Ye P, Wu J, Seta P. Acrylonitrile-based copolymer membranes containing reactive groups: effects of surface-immobilized poly(ethylene glycol)s on anti-fouling properties and blood compatibility. Polymer 2004;45:399-407.
53. Jeon SI, Lee JH, Andrade JD, De Gennes PG. Protein surface interactions in the presence of polyethylene oxide: I simplified theory. J Colloid Interface Sci 1991;142:149-58.
54. Jeon SI, Andrade JD. Protein surface interactions in the presence of polyethylene oxide: II effect of protein size. J Colloid Interface Sci 1991;142:159-66.
55. Susan JS, Premnath V, Merrill EW. Poly(ethylene oxide) grafted to silicon surfaces: grafting density and protein adsorption. Macromolecules 1998;31:5059-70.
56. Chen X, Su Y, Shen F, Wan Y. Antifouling ultrafiltration membranes made from PAN-b-PEG copolymers: Effect of copolymer composition and PEG chain length. J Membr Sci

2011;384:44-51.

57. Jo S, Park K. Surface modification using silanated poly(ethylene glycol)s. Biomaterials 2000;21:605-16.

58. Lazos D, Franzka S, Ulbricht M. Size-selective protein adsorption to polystyrene surfaces by self-assembled grafted poly(ethylene glycols) with varied chain lengths. Langmuir 2005;21:8774-84.

59. Drumheller PD, Hubbell JA. Densely crosslinked polymer networks of poly(ethylene glycol) in trimethylolpropane triacrylate for cell-adhesion-resistant surfaces. J Biomed Mater Res. 1995;29(2):207-15.

60. Cai L, Lu J, Sheen V, Wang S. Lubricated biodegradable polymer networks for regulating nerve cell behavior and fabricating nerve conduits with a compositional gradient. Biomacromolecules 2012;12:358-68.

Chapter IX. Poly(ε-Caprolactone) Networks Tethered with Dangling Poly(L-Lysine) Chains for Promoting Smooth Muscle Cell Functions

Abstract

Extracellular microenvironments are critical for cell adhesion, phenotype, proliferation, differentiation, and gene/protein expression. The majority of the components in the microenvironments, such as adhesive proteins, growth factors, and cytokines, have diversified electronic properties. Poly(L-lysine) (PLL) is a type of cationic polypeptide often used for enhancing cell adhesion by providing positive charges. Here I developed a series of polymer networks with PLL dangling chains through photo-crosslinking PCLTA with a number-average molecular weight (M_w) of 7,020 g/mol with a photo-polymerizable PLL at different PLL compositions of 0.5%, 1.0%, 1.5%, and 3%. PCLTA networked grafted with dangling PLL chains were more hydrophilic and can adsorb more serum proteins from the cell culture media. Primary rat smooth muscle cells were cultured on these polymer networks and their attachment, spreading, proliferation, focal adhesions, expression of four contractile gene markers (SM-MHC, smoothlin, transgelin, and calponin) and one contractile protein, calponin, were characterized systematically. An optimal composition of PLL at 1% in the polymer networks was found to exist to promote the SMC performance best.

9.1 Introduction

Cardiovascular disease is the largest health threat in the United States, causing over 1 million deaths annually and accounting for tremendous health care costs [1]. Tissue engineering is a promising approach for cardiovascular disease treatment through developing biocompatible constructs that can support damaged cardiac tissue and supplement some functions for injured extracellular matrix (ECM) [2-6]. Biodegradable polymers are a popular category of biomaterials used in tissue engineering because of their tunable physicochemical and topographical properties and feasibility of being fabricated into numerous structures [7-19]. Inspired by the ECM components, numerous synthetic polymers have been developed for promoting cell adhesion, proliferation, and differentiation [20-22].

Surface characteristics such as chemical, mechanical and topographical properties of biomaterials are known factors in regulating cellular responses and tissue interactions when they are used in tissue engineering applications [12,23,24]. Among many chemical factors positive charges on the biomaterial surface can significantly influence cellular activities [25-29]. Cationic poly(L-lysine) (PLL) is a polypeptide that can provide positive charges to facilitate cell adhesion and strengthen cell functions through electrostatic interactions with anion sites on cytoplasmic membrane [29-32]. The typical methods used to incorporate PLL chains always involve the functionalization of amino groups, which causes a loss of charges due to less dissociation for secondary amine groups [30-32].

To address this issue, photo-polymerizable PLL (Fig. 9.1) was synthesized in our research laboratory through ring-opening polymerization of carbobenzyloxy-L-lysine-*N*-carboxyanhydride (Z-L-Lys NCA) using allylamine as the initiator [33,34]. The yielded PLL is end-capped with reactive an allyl group that has a double bond and thus can be covalently linked into polymeric networks, for example, hydrogels based on polyethylene glycol diacrylate (PEGDA) for promoting nerve cell functions [33,34]. Poly(ε-caprolactone acrylates) (PCLTAs, Fig. 9.1) are a series of photo-crosslinkable and biodegradable polymers also developed in our research laboratory and have been fabricated into different substrates and structures for regulating nerve cells, bone cells, and SMCs [11,35-39]. In particular, PCL acrylate networks were grafted with PEG chains to achieve better wettability, which improves adhesion and

proliferation of nerve cells and SMCs [39,40]. Here I incorporated PLL dangling chains into PCLTA networks (Fig. 9.1) to explore the influence of positive charges on SMC attachment, proliferation, and gene expression of phenotypic markers. . Four weight compositions of PLL (ϕ_{PLL}) of 0.5, 1, 1.5, and 3% in PCLTA networks were studied and compared with the neutral PCLTA network.

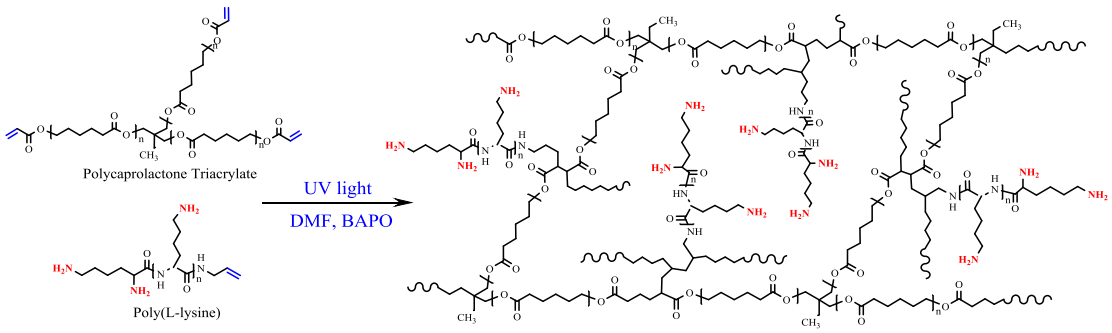

Figure 9.1 Photo-crosslinking of PCLTA with photo-polymerizable PLL.

9.2 Materials and methods

9.2.1 Photo-crosslinking of PCLTA/PLL and characterizations

PCLTA with a number-average molecular weight (M_n) of 7,020 g/mol and weight-average molecular weight (M_w) of 8130 g/mol and photo-polymerizable PLL (M_n = 1,990 g/mol, M_w = 2,120 g/mol) were synthesized according to previous reports from our laboratory [11,33,34]. All the other chemicals used in this study were purchased from Sigma-Aldrich (Milwaukee, WI) unless noted otherwise. PCLTA and PLL with desired weight ratios were dissolved in DMF at polymer:solvent weight ratios of 1:2. A high-intensity long-wave UV lamp (SB-100P, wavelength = 365 nm, Intensity = 4800 μw/cm^2) was used to photo-crosslink the blends of PCLTA and PLL. Phenyl bis(2,4,6-trimethyl benzoyl) phosphine oxide (BAPO, IRGACURE 819, Ciba Specialty Chemicals, Tarrytown, NY) was the photo-initiator (0.2 g BAPO for 1 ml PCLTA/PLL/BAPO/DMF solution). Homogeneous PCLTA/PLL/BAPO/DMF solution was filled in a silicon mold with round holes (10 mm × 0.5 mm, diameter × thickness) between two glass plates and crosslinked under the UV light for 20 min. The crosslinked polymer disks were dried completely in vacuum and then soaked in acetone for two days to remove BAPO and sol

fraction, followed by rinse with new acetone three times and complete drying in vacuum. Water contact angles on these polymer disks were determined using a Ramé-Hart NRC C. A. goniometer (Model 100-00-230, Mountain Lakes, NJ) with 20 μl droplets at 37 ℃ and repeated for 4 times. The amounts of serum proteins adsorbed on the polymer disks from the cell culture media (see Section 2.2) were analyzed using a MicroBCA protein assay kit (Pierce, Rockford, IL) and a micro-plate reader (SpectraMax Plus 384, Molecular Devices, Sunnyvale, CA), using the procedures reported by us previously [41].

9.2.2 In vitro cell studies

Prior to cell studies, the polymer disks were sterilized in 70% alcohol solution and dried in vacuum. Primary SMCs isolated from rat aorta stored in a liquid nitrogen tank were thawed and cultured in Dulbecco's modified eagle medium (DMEM) with 10% fetal bovine serum (FBS) in tissue culture polystyrene (TCPS) flasks. Cell culture was proceeded in an incubator with 5% CO_2 and saturated humidity (>90%) at 37 ℃ [42]. When SMCs were confluence, they were detached using trypsin-EDTA solution (Gibco) and collected using centrifuge at 1000 rpm for 3 min. SMCs were seeded onto the sterilized polymer disks at a density of ~20000 cells/cm^2 in a 48 well TCPS plates, using empty TCPS wells without samples as the positive control. The numbers of SMCs on the polymer disks and control sample at 4 h and days 1, 2, and 4 post-seeding were measured using MTS assay solutions (CellTiter 96 Aqueous One Solution, Promega, Madison, WI) and a micro-plate reader (SpectraMax Plus 384, Molecular Devices, Sunnyvale, CA) at the wavelength of 490 nm. For fluorescence imaging on an Axiovert 25 fluorescence microscope (Carl Zeiss, Germany), the cells on the polymer disks at 4 h and days 1, 2, and 4 post-seeding were fixed in 4% paraformaldehyde (PFA) solution for 10 min after washed twice in phosphate buffered saline (PBS) solution. Then SMCs were permeabilized in 0.2% Triton X-100 solution for 10 min at room temperature before incubation in rhodamine-phalloidin (RP) solution for 1 h at 37 ℃ and 4',6-diamidino-2-phenylindole (DAPI) for 5 min at room temperature to stain cytoplasm and cell nuclei, respectively. Cell area was determined and averaged from the fluorescence images of 20 non-overlapping cells using ImageJ software (National Institutes of Health, Bethesda).

9.2.3 Characterization of focal adhesions in the SMCs

SMCs at day 1 post-seeding were fixed and permeabilized using the same procedures described in Section 2.2. To block unspecific binding sites, the cells were incubated 1 h with 1% Bovine Serum Albumin (BSA) in PBS at 37 ℃, then washed three times to remove extra BSA from the cell membrane. Monoclonal vinculin primary antibody solution (1:1000 in PBS; Sigma) was used to target specific vinculin binding sites. After incubation with the primary antibody solution for 1 h at room temperature, the cells were further washed in PBS to remove unconjugated antibody. Goat anti-mouse IgG secondary antibody (1:200 in PBS; Sigma) solution was used to conjugate fluorescence groups onto the vinculin primary antibody to stain the focal adhesions (FAs) in the cells for 1 h at room temperature. Using the same procedures described in Section 2.2, SMCs were further stained with RP and DAPI to visualize cytoplasm and cell nulei, respectively. FAs were observed and photographed using a Leica DM6000B confocal fluorescent microscope. The density of FAs or the average number of FAs per cell was obtained as from five individual cells in the images. The average area of FAs was measured over 20 individual FAs using ImageJ. Based on the area and perimeter of a FA, its elongation was characterized using the inverse of its circularity calculated using the equation of $4\pi \times \text{area}/\text{perimeter}^2$ [43].

9.2.4 Gene expression analysis of contractile phenotypic markers

To characterize phenotypic conversion of SMCs on the polymer disks, the expression levels of typical contractile gene markers were analyzed. Primers used in gene analysis were designed using Oligoperfect software: smooth muscle myosin heavy chain (SM-MHC): forward 5'-AAGCAGCTCAAGAGGCAG-3', reverse 5'-AAGGAACAAATGAAGCCTCGTT-3'; calponin: forward 5'-AGTCTACTCTCTCTTGGCTCTGGCC-3', reverse 5'-CCTGCCTTCTCTCAGCTTCTCAGG-3'; transgelin (SM-22): forward 5'-GGCAGCTGAGGATTATGGAGTCACG-3', reverse 5'-TGGGATCTCCACGGTAGTGTCCA-3'; and house-keeping gene glyceraldehyde-3-phosphate dehydrogenase (GAPDH): forward 5'-TCTTCACCACCATGGAGAA-3', reverse 5'-ACTGTGGTCATGAGCCCTT-3'. SMCs cultured for three days on the polymer disks were collected for obtaining total RNA using an RNeasy Mini Kit (Qiagen, Valencia, CA). Total

cDNA was then reverse-transcripted from the RNA using a DyNAmo cDNA synthesis kit (Thermo Scientific) according to the manufacturer's instructions. For each sample, 20 μL reaction system was made by mixing 2.5 μL of total cDNA (5 ng/μL), 1 μL forward primer solution, 1 μL reverse primer solution, 5.5 μL DI water, and 10 μL of 2 × Power SYBR Green Polymerase Chain Reaction (PCR) Master Mix (Applied Biosystems, Warrington, UK). Real-time PCR amplification was performed on a Peltier Thermal Cycler fluorescence detection system (MJ Research PTC-200 Thermo Cycler), through a procedure set as 94 ℃ for 5 min and 40 cyclic steps of 94 ℃ for 30 s, 55 ℃ for 30 s, and 72 ℃ for 30 s. The relative expression levels of contractile gene markers were normalized to that of GAPDH. Reverse transcription PCR (RT-PCR) amplification was performed using the same primers except calponin and transgelin: calponin: forward 5'-ACAAAAGGAAACAAAGTCAAT-3', reverse 5'-GGGCAGCCCATACACCGTCAT-3'; transgelin (SM-22): forward 5'-TGTTCCAGACTGTTGACCTC-3', reverse 5'-GTGATACCTCAAAGCTGTCC-3'. The same thermal cycle steps were applied in the amplification process. After amplification, the products were stained with Gelgreen (Biotium, Hayward, CA) and proceeded for electrophoresis in 1.0% agarose gels. DNA bands were visualized and photographed using EpiChemi II darkroom imaging system (UVP, Upland, CA).

9.2.5 Calponin protein immunofluorescence staining

The expression level of key contractile marker calponin was analyzed to confirm the trend in gene expression. SMCs cultured on the polymer disks for two days were fixed with PFA and then stained at room temperature for 1 h with anti-rat calponin primary antibody produced in rabbit (sc-16604-R; Santa Cruz; 1;100 in PBS). After the cells were washed with PBS three times, they were incubated with anti-rabbit secondary IgG antibody produced in goat (F0382, Sigma; 1:80 in PBS) conjugated with fluorescein isothiocyanate (FITC). The same fluorescence microscope was used for photographing the fluorescence images of the cells.

9.2.6 Statistical analysis

Statistical analysis was performed using one-way analysis of variance (ANOVA). A *p*-value lower than 0.05 indicated significant difference.

9.3 Results

9.3.1 Hydrophilicity and protein adsorption of photo-crosslinked PCLTA/PLL networks

After hydrophilic PLL chains were tethered into the hydrophobic PCLTA networks, their hydrophilicity were improved and the improvement was more prominent when ϕ_{PLL} was higher, suggesting that PLL chains indeed appeared on the crosslinked PCLTA network surfaces. As indicated in Fig. 9.2a, the water contact angle decreased from 64.5 ±2.1 °on crosslinked PCLTA to 63.8 ±1.3 °, 59.5 ±2.4 °, 55.8 ±2.5 °, and 53.5 ±2.1 °for the networks grafted with 0.5%, 1%, 1.5%, and 3% PLL, respectively. Similar phenomena were observed PCLTA networks grafted with short mPEGA chains at ϕ_m of 0-20 %, as reported in our previous study [39]. Surface energy and the length of hydrophilic grafted chains can influence protein adsorption [44-48]. In contrast with the continuous decreased amount of adsorbed serum proteins in PCLTA networks grafted with PEG chains when the graft composition increased, the amount of adsorbed serum proteins increased continuously with increasing ϕ_{LL} in the PCLTA networks, as shown in Fig. 9.2b. These differences were believed to originate from nature essential of PEG chains and PLL chains. PEG chains were widely acknowledged as cell and protein repulsive thus frequently applied for construction of protein resistant surfaces [49,50]. Nevertheless, poly(L-lysine) (PLL) with positive charges were reported to facilitate protein attraction and cell adhesion through electrostatic interactions with anion sites on peptides or cytoplasmic membrane [29-32].

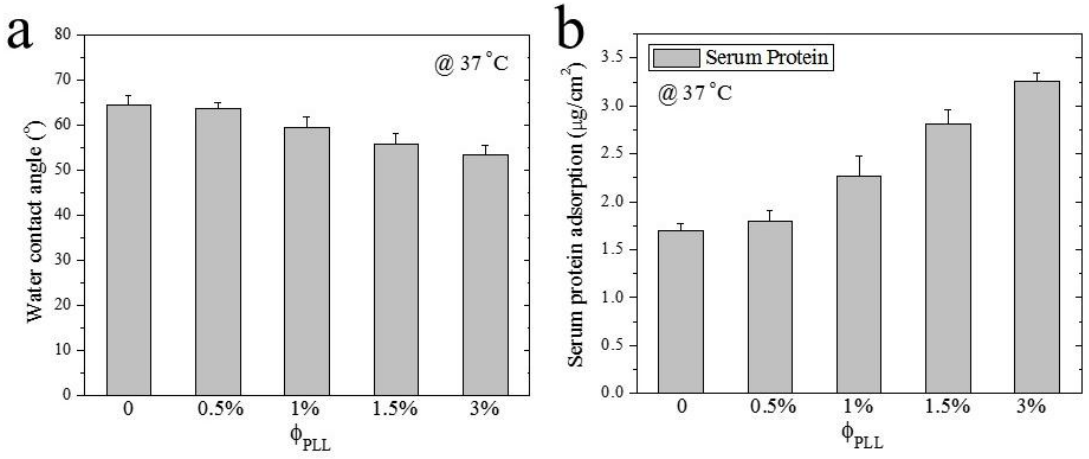

Figure 9.2 (a) Water contact angles on the PCLTA/PLL networks with ϕ_{PLL} of 0-3%. (b) Amount of serum proteins adsorbed on the PCLTA/PLL networks from cell culture media.

9.3.2 SMC attachment, spreading, and proliferation on the PCLTA/PLL networks

SMC attachment on PCLTA networks was achieved by normalizing the cell number to the value on TCPS at 4 h post-seeding. As shown in Fig. 9.3a, SMC attachment exhibited an asymptotic trend with increasing ϕ_{LL}. SMC attachment increased significantly from 0.30 ±0.11 to 0.53 ± 0.10 and 0.60 ± 0.10 when ϕ_{PLL} increased from 0 to 0.5% and 1%, respectively. However, with further increasing ϕ_{PLL} to 1.5% and 3%, SMC attachment varied little. Previously our research group reported there was an optimal composition of PLL grafted in PEG-hydrogels for neural progenitor cell attachment, proliferation, and differentiation because dense PLL chains with free amine groups could have cytotoxic effects and inhibit cell adhesion [30-34].

After attachment onto the polymer disks, SMCs started to spread. The capability of cell spreading is critical for later stages such as migration and proliferation [51]. To characterize SMC spreading, their spread areas on the polymer disks were quantified at day 1, as shown in Fig. 9.3b. The trend was similar to that in cell attachment. The average spread area of SMCs increased from ~2700 μm^2 on PCLTA network to ~3700 μm^2 for the PCLTA/PLL network with ϕ_{PLL} of 0.5% and further to ~4200 μm^2 asymptotically for ϕ_{PLL} of 1-3%.

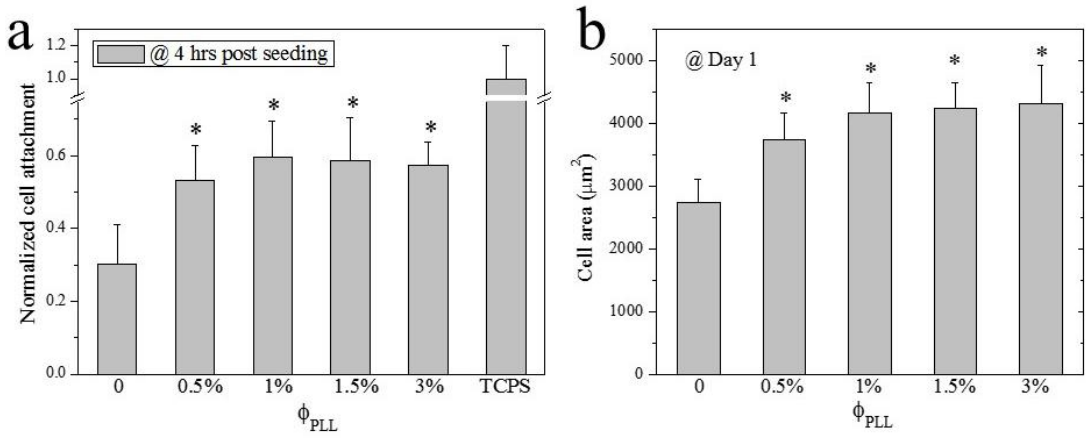

Figure 9.3 (a) SMC attachment at 4 h post-seeding on the PCLTA/PLL- networks normalized to the value on TCPS. (b) SMC spread area at day 1 post-seeding on the PCLTA/PLL networks. *: $p < 0.05$ relative to the PCLTA network ($\phi_{PLL} = 0$).

Although no apparent inhibition effect was observed in SMC attachment at 4 h and spreading at day 1, it was evident when the culture time was longer, i.e., 4 days for SMC proliferation. SMC numbers on the polymer disks at days 1, 2, and 4 are shown in Fig. 9.4a and

a non-monotonic dependence on ϕ_{PLL} was seen. The maximum cell number appeared at ϕ_{PLL} of 1% PLL before it decreased at ϕ_{PLL} of 1.5% and 3% for days 1, 2, and 4. The proliferation index (PI) of SMCs were calculated by dividing the cell number at 1 day by that at 4 h or the cell number at day 2 by that at day 1, or the number at day 4 by that at day 2. As shown in Fig. 9.4b, the PI of SMCs decreased with increasing ϕ_{PLL}. The growth rate (GR) of the SMCs on the polymer disks, determined by dividing ln(PI) by the time for calculating the PI, showed the same trend (Fig. 9.4b). The fluorescence images of SMCs on the polymer disks (Fig. 9.4c) showed consistent cell densities with those obtained using the MTS method in Fig. 9.4a. SMCs proliferated well on all the disks over a period of 4 days and the largest cell population with the best spreading was seen on the PCLTA/PLL network with ϕ_{PLL} of 1%.

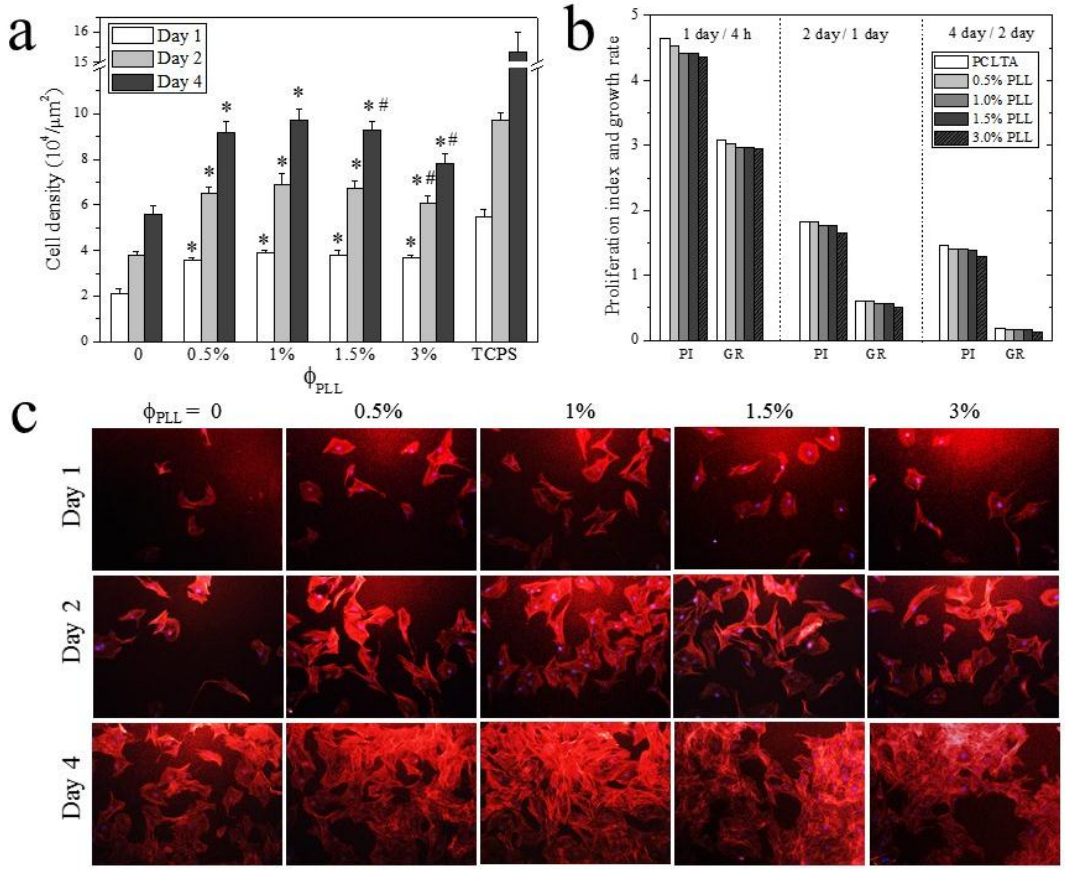

Figure 9.4 (a) SMC densities at days 1, 2, and 4 post-seeding on the PCLTA/PLL networks with TCPS as the positive control. (b) Proliferation indices and growth rates of SMCs on the PCLTA/PLL networks. (c) Fluorescence images of SMCs stained with RP and DAPI on the PCLTA/PLL networks at day 1, 2, and 4 post-seeding. *: significant higher ($p < 0.05$) than corresponding value on crosslinked PCLTA ($\phi_m = 0\%$) network. #: significant difference ($p < 0.05$) with PLL-PCLTAs ($\phi_m = 1\%$).

9.3.3 FAs in SMCs on the PCLTA/PLL substrates

FAs are dynamic complexes in cell membrane that can anchor ECM proteins and give responsive signals to the pathways of intracellular signaling [52,53]. FAs are composed of subunit proteins, e.g., paxillin and vinculin, and are able to adjust their size and elongation to form super-mature adhesion subtypes by responding to intracellular tension [53,54]. As demonstrated in Fig. 9.5a as green punctate spots, stronger FAs were observed in the SMCs cultured for 1 day on PCLTA/PLL networks with ϕ_{LL} of 5%than those with ϕ_{PLL} of 0 or 3%. Quantification of FAs in SMCs on the polymer disks in Fig. 9.5b,c showed that the largest

average FA area and the highest FA density appeared when ϕ_{PLL} was 1%, among all the samples. Elongation of FAs was significantly higher when ϕ_{PLL} was 1% than when ϕ_{PLL} was 0 or 3%, indicating the strength of FAs was higher (Fig. 9.5c). The differences in the FAs of SMCs on the different polymer disks substantiated that FAs are able to sense external substrate properties and adjust their own characteristics accordingly.

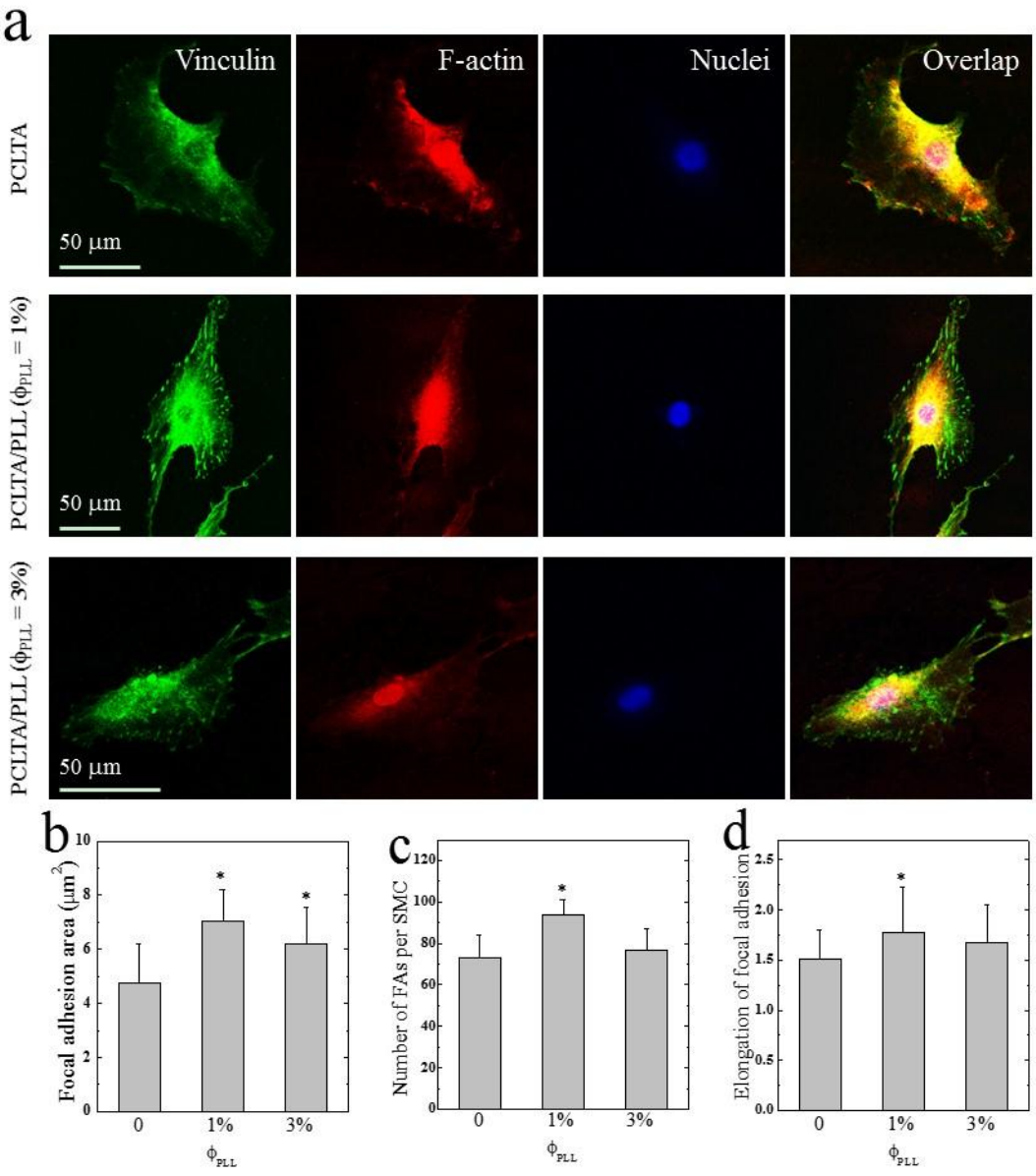

Figure 9.5 (a) Immunofluorescence images (b) average area, (c) density, and (d) elongation of FAs, cytoplasm, and nuclei in SMCs and on the networks of PCLTA, PCLTA/PLL (ϕ_{PLL} = 1%), and PCLTA/PLL (ϕ_{PLL} = 3%) at day 1 post-seeding. *: $p < 0.05$ relative to the PCLTA network.

9.3.4 SMC phenotypic expression on the PCLTA/PLL substrates

SMC has unique phenotypic conversion between the synthetic phenotype and the contractile phenotype and this conversion process is influenced by ECM properties including stiffness, surface proteins, growth factors, and chemical properties [55]. To evaluate the fraction of SMCs with the contractile phenotype, I analyzed the expression levels of four critical contractile gene markers in SMCs. As determined using real-time PCR and demonstrated in Fig. 9.6a, the expression levels of SM-MHC, smoothlin, transgelin and calponin normalized by the level of GAPDH were significantly higher in SMCs on the polymer disks with ϕ_{PLL} of 1% and 3% than those on the PCLTA network, suggesting that PLL dangling chains in the PCLTA networks could benefit the contractile phenotype. To confirm the results in Fig. 9.6a, I further analyzed the expression levels of these gene markers using semi-quantitative RT-PCR. As shown in Fig. 9.6b, brighter bands were observed for the four contractile markers in SMCs on the polymer disks with ϕ_{PLL} of 1% and 3% than those on the PCLTA network.

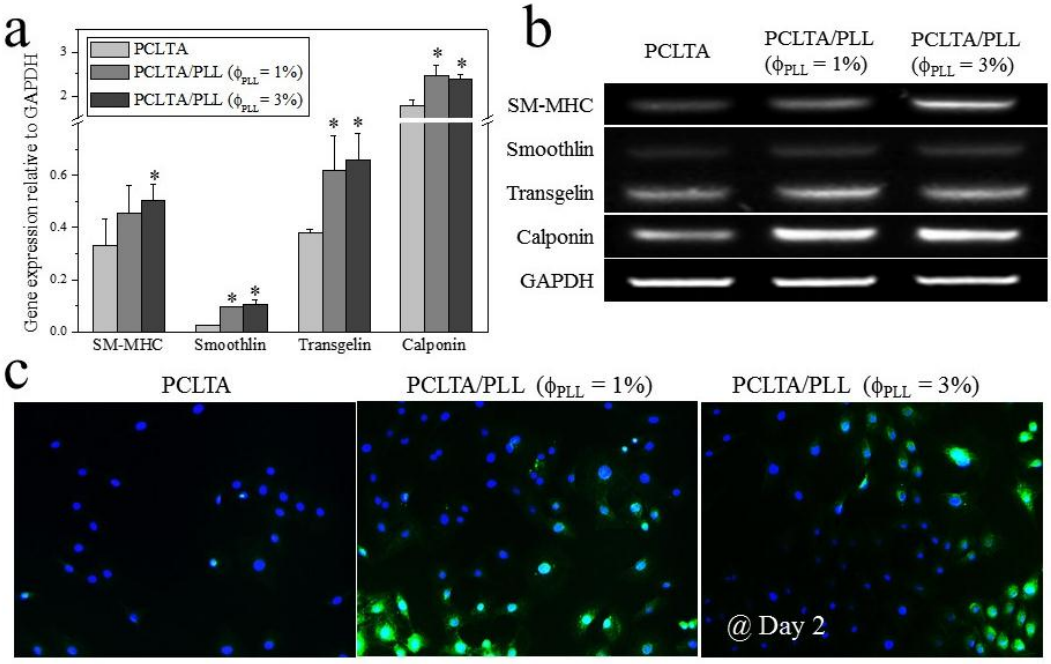

Figure 9.6 (a) Normalized expression levels of contractile gene markers, SM-MHC, smoothlin, transgelin, and calponin in SMCs on the PCLTA/PLL networks at day 3 post-seeding using real-time PCR. (b) Expression of the four gene markers analyzed using RT-PCR. (c) Immunofluorescence images of calponin, an important contractile marker protein, in SMCs on the PCLTA/PLL networks at day 2 post-seeding. *: $p < 0.05$ relative to the PCLTA network.

To demonstrate the correlation between gene expression and protein expression, I also characterized the level of an essential contractile phenotypic marker, calponin, using immunofluorescence staining. As shown in Fig. 9.6c, both the nuclei and calponin in SMCs at day 3 were stained using blue and green fluorescence, respectively. More cell nuclei were observed on the polymer disks containing PLL dangling chains than on the PCLTA network, consistent with the result on SMC proliferation in Section 3.2. As shown in Fig. 9.6c, stronger immunofluorescence indicated that a larger portion (>30%) of SMCs expressed calponin on the polymer disks with ϕ_{PLL} of 1% and 3% than on the PCLTA network. These results indicated that SMCs on the PCLTA/PLL networks with small ϕ_{PLL} of 1% and 3% upregulated the expression of contractile markers at both gene and protein levels. Therefore, modifying the PCLTA network with sparsely dangling cationic PLL chains is effective in facilitating SMC phenotypic conversion from proliferative synthetic phenotype to more functional contractile one.

9.4 Discussion

The PLL layer on a hyaluronic acid biomaterial surface was reported to be able to facilitate cell adhesion [56]. In this study, PLL chains were grafted into PCLTA networks as dangling chains to investigate the effect of the positive charges on SMC adhesion, proliferation and differentiation. The overall results demonstrated that the best cell performance occurred when the polymer networks contained 1% PLL dangling chains whereas higher ϕ_{PLL} could inhibit, suggesting that an optimal density of positive charges in the substrate existed for promoting SMCs.

Besides this study, there exist extensive reports that different cell types are affected by the amount of amine groups on the substrates, which is determined by the chain length and composition of PLL chains [57-60]. For example, red blood cells could adjust their spreading on substrates coated with PLL of different concentrations and molecular weights as the best cell spreading appeared when the concentration of PLL was 100, 10, and 0.1 mg/mL for when the molecular weight of PLL was 500, 3800, and 72000 g/mol, respectively [58]. Neither too low nor too high concentrations of PLL could result in better cell adhesion [58].

In addition, a series of poly(D-lysine) samples with molecular weights of 1000-4000 g/mol

were reported to improve foetal mouse cortical cells at an optimal composition of 0.5% when they were immobilized onto chitosan, whereas higher compositions inhibited neuronal proliferation and neurite lengths [59]. In another study, enhanced attachment, proliferation and chondrogenic differentiation of human mesenchymal stem cells (hMSCs) were observed when PLL samples with a series of molecular weights (M_n = 70000-150000 g/mol) were coated onto TCPS at a low concentration of 1 μg/mL [60]. When the concentration of coated PLL to 10 μg/mL, hMSCs were observed to detach from the substrates [60]. Adhesion of embryonic brain cells was also reported to be promoted on glass surfaces coated with 5 μg/mL of PLL (M_n ~ 400000 g/mol) [61]. The above results from previous studies were consistent with the present one by showing that PLL chains were beneficial for cell functions at an optimal density of PLL chains on the substrate surface, regardless of different cell types.

Although the coating methods of PLL mentioned above can be applied to improve cell adhesion, the coated layer is easy to detach from the substrates, causing inaccuracy for evaluation of surface density of PLL for regulating cell functions. Our present method by covalently incorporating PLL chains to polymer networks through photo-crosslinking has evident advantages for surface stability. In particular, the covalently tethered PLL chains inside polymer networks will appear continuously even after surface biodegradation and remain effective to supply positive charges in long run. Beside direct attraction with the negative charges on cell membrane, the cationic amine groups in PLL chains could attract cell adhesive peptides and in turn further facilitate cell attachment [62]. Our results provided guidance for enhancing vascular cell adhesion, proliferation, and differentiation on biodegradable substrates, aiming for cardiovascular tissue engineering applications. The enhanced cell proliferation and contractile conversion by grafting PLL into PCLTA networks can lead to better angiogenesis *in vivo* when the materials are used as blood vessel grafts.

9.5 Conclusions

I modified PCLTA networks by photo-crosslinking PCLTA withphoto-polymerizable poly(L-lysine) at ϕ_{PLL} of 0.5%, 1%, 1.5% and 3% . PCLTA networks modified with dangling PLL chains showed better surface hydrophilicity and capability in adsorbing serum proteins

from the cell culture media, especially when ϕ_{PLL} was higher. These PLL-modified PCLTA networks were also found to support better primary rat SMC attachment at 4 h post-seeding, spreading at day 1, proliferation over 4 days, and expression levels of four contractile gene markers, i.e., SM-MHC, smoothlin, transgelin, and calponin, and protein expression of calponin. Stronger, more elongated FAs with a larger average area and a higher density were observed on the PCLTA/PLL networks compared with the PCLTA network. Among all the studied compositions of 0.5-3%, PCLTA/PLL networks with ϕ_{PLL} of 1% could support best SMC performance whereas higher ϕ_{PLL} inhibited. All these properties are highly desirable in designing favorable replaceable grafts used in cardiovascular tissue engineering.

References

1. Go AS, Mozaffarian D, Roger VL, Benjamin EJ, Berry JD, Borden WB, et al.; on behalf of the American Heart Association Statistics Committee and Stroke Statistics Subcommittee. Heart disease and stroke statistics-2013 update: a report from the American Heart Association. Circulation 2013;127:e6-e245
2. Putnam AJ, Mooney DJ. Tissue engineering using synthetic extracellular matrices. Nat Med 1996;2(7):824-6.
3. Mooney DJ, Mikos AG. Growing new organs. Sci Am 1999;280(4): 60-5.
4. Nerem RM, Seliktar D. Vascular tissue engineering. Annu Rev Biomed Eng 2001;3:225-43.
5. Niklason LE. Functional arteries grown in vitro. Science 1999;284: 489–93.
6. Weber B, Emmert MY, Schoenauer R, Brokopp C, Baumgartner L, Hoerstrup SP. Tissue engineering on matrix: future of autologous tissue replacement. Semin Immunopathol 2011;33(3):307-15.
7. Gunatillake PA, Adhikari R. Biodegradable synthetic polymers for tissue engineering. Eur Cell Mater 2003;5:1-16; discussion 16.
8. Armentano I, Dottori M, Fortunati E, Mattioli S, Kenny JM. Biodegradable polymer matrix nanocomposites for tissue engineering: A review. Polym Deg Stability 2010;95(11):2126-2146.
9. Patel H, Bonde M, Srinivasan G. Biodegradable polymer scaffold for tissue engineering. Trends Biomater Artif Organs 2011;25(1): 20-29
10. Dhandayuthapani B, Yoshida Y, Maekawa T, Kumar DS. Polymeric scaffolds in tissue engineering application: a review. Int J Polym Sci 2011:290602.
11. Cai L, Wang S. Poly(ε-caprolactone) acrylates synthesized using a facile method for fabricating networks to achieve controllable physicochemical properties and tunable cell responses. Polymer 2010;51:164-77.
12. Benoit DS, Schwartz MP, Durney AR, Anseth KS. Small functional groups for controlled differentiation of hydrogel-encapsulated human mesenchymal stem cells. Nat Mater 2008;7(10):816-23.

13. Bouten CV, Dankers PY, Driessen-Mol A, Pedron S, Brizard AM, Baaijens FP. Substrates for cardiovascular tissue engineering. Adv Drug Deliv Rev 2011;63(4-5):221-41.
14. Ahmed M, Yildirimer L, Khademhosseini A, Seifalian AM. Nanostructured materials for cardiovascular tissue engineering. J Nanosci Nanotechnol 2012;12(6):4775-85.
15. Zhang B, Xiao Y, Hsieh A, Thavandiran N, Radisic M. Micro- and nanotechnology in cardiovascular tissue engineering. Nanotechnology 2011;22(49):494003.
16. Lutolf MP, Hubbell JA. Synthetic biomaterials as instructive extracellular microenvironments for morphogenesis in tissue engineering. Nat Biotechnol 2005;23(1):47-55.
17. Place ES, George JH, Williams CK, Stevens MM. Synthetic polymer scaffolds for tissue engineering. Chem Soc Rev 2009;38(4):1139-51.
18. Seunarine K, Gadegaard N, Tormen M, Meredith DO, Riehle MO, Wilkinson CD. 3D polymer scaffolds for tissue engineering. Nanomedicine 2006;1(3):281-96.
19. Ravichandran R, Sundarrajan S, Venugopal JR, Mukherjee S, Ramakrishna S. Advances in polymeric systems for tissue engineering and biomedical applications. Macromol Biosci 2012;12(3):286-311.
20. Ravi S, Qu Z, Chaikof EL. Polymeric materials for tissue engineering of arterial substitutes. Vascular 2009;17(S1):S45-54.
21. Venkatraman S, Boey F, Lao LL. Implanted cardiovascular polymers: natural, synthetic and bio-inspired. Prog Polym Sci 2008;33:853-874.
22. Dunn DA, Hodge AJ, Lipke EA. Biomimetic materials design for cardiac tissue regeneration. Wiley Interdiscip Rev Nanomed Nanobiotechnol 2014;6(1):15-39.
23. Wong JY, Leach JB, Brown XQ. Balance of chemistry, topography, and mechanics at the cell–biomaterial interface: Issues and challenges for assessing the role of substrate mechanics on cell response. Surface Sci 2004;570:119-133.
24. Wu X, Wang S. Regulating MC3T3-E1 cells on deformable poly(ε-caprolactone) honeycomb films prepared using a surfactant-free breath figure method in a water-miscible solvent. ACS Appl Mater Interfaces 2012;4(9):4966-75.
25. Dadsetan M, Knight AM, Lu L, Windebank AJ, Yaszemski MJ. Stimulation of neurite outgrowth using positively charged hydrogels. Biomaterials 2009;30(23-24):3874-81.

26. Peng H, Xiao Y, Mao X, Chen L, Crawford R, Whittaker AK. Amphiphilic triblock copolymers of methoxy-poly(ethylene glycol)-b-poly(L-lactide)-b-poly(L-lysine) for enhancement of osteoblast attachment and growth. Biomacromolecules 2009;10(1):95-104.
27. Wattendorf U, Koch MC, Walter E, V örös J, Textor M, Merkle HP. Phagocytosis of poly(L-lysine)-graft-poly(ethylene glycol) coated microspheres by antigen presenting cells: Impact of grafting ratio and poly(ethylene glycol) chain length on cellular recognition. Biointerphases 2006;1(4):123-33.
28. Schneider GB, English A, Abraham M, Zaharias R, Stanford C, Keller J. The effect of hydrogel charge density on cell attachment. Biomaterials 2004;25(15):3023-8.
29. Wang JH, Hung CH, Young TH. Proliferation and differentiation of neural stem cells on lysine-alanine sequential polymer substrates. Biomaterials 2006;27(18):3441-50.
30. Rao SS, Han N, Winter JO. Polylysine-modified PEG-based hydrogels to enhance the neuro-electrode interface. J Biomater Sci Polym Ed 2011;22(4-6):611-25.
31. Royce Hynes S, McGregor LM, Ford Rauch M, Lavik EB. Photopolymerized poly(ethylene glycol)/poly(L-lysine) hydrogels for the delivery of neural progenitor cells. J Biomater Sci Polym Ed 2007;18(8):1017-30.
32. Hynes SR, Rauch MF, Bertram JP, Lavik EB. A library of tunable poly(ethylene glycol)/poly(L-lysine) hydrogels to investigate the material cues that influence neural stem cell differentiation. J Biomed Mater Res A 2009;89(2):499-509.
33. Cai L, Lu J, Sheen V, Wang S. Promoting nerve cell functions on hydrogels grafted with poly(L-lysine). Biomacromolecules 2012;13(2):342-9.
34. Cai L, Lu J, Sheen V, Wang S. Optimal poly(L-lysine) grafting density in hydrogels for promoting neural progenitor cell functions. Biomacromolecules 2012;13(5):1663-74.
35. Cai L, Foster CJ, Liu X, Wang S. Enhanced bone cell functions on poly(ε-caprolactone) triacrylate networks grafted with polyhedral oligomeric silsesquioxane nanocages. Polymer 2014. DOI: 10.1016/j.polymer.2014.06.057
36. Wang K, Cai L, Zhang L, Dong JY, Wang SF. Biodegradable Photo-Crosslinked Polymer Substrates with Concentric Microgrooves for Regulating MC3T3-E1 Cell Behavior Adv Healthc Mater 2012;1:292-301.
37. Wu X, Wang S. Integration of photo-crosslinking and breath figures to fabricate

biodegradable polymer substrates with tunable pores that regulate cellular behavior. Polymer 2014;55:1756-62.

38. Liu X, Cai L, Hao F, Cui M, Wang S. Biodegradable elastomeric substrates with controllable stiffness for regulating smooth muscle cell behavior. Polym Mater Sci Eng 2011;242:260.
39. Liu X, Cai L, Wang S. Smooth muscle cell behavior on crosslinked poly(ε-caprolactone) triacrylate networks grafted with methoxy poly(ethylene glycol) monoacrylate of various composition and chain length. Abstracts of Papers of the American Chemical Society 2012;243.
40. Cai L, Lu J, Sheen V, Wang SF. Lubricated biodegradable polymer networks for regulating nerve cell behavior and fabricating nerve conduits with a compositional gradient. Biomacromolecules 2012;13:358-68.
41. Cai L, Wang K, Wang S. Poly(ethylene glycol)-grafted poly(propylene fumarate) networks and parabolic dependence of MC3T3 cell behavior on the network composition. Biomaterials 2010;31:4457-66.
42. Wang K, Cai L, Hao F, Xu X, Cui M, Wang S. Distinct cell responses to substrates consisting of poly(ε-caprolactone) and poly(propylene fumarate) in the presence or absence of cross-links. Biomacromolecules 2010;11:2748-59.
43. Peyton SR, Raub CB, Keschrumrus VP, Putnam AJ. The use of poly(ethylene glycol) hydrogels to investigate the impact of ECM chemistry and mechanics on smooth muscle cells. Biomaterials 2006;27:4881-93.
44. Santos L, Rodrigues D, Lira M, Oliveira ME, Oliveira R, Vilar EY, Azeredo J. The influence of surface treatment on hydrophobicity, protein adsorption and microbial colonisation of silicon hydrogel contact lenses. Cont Lens Anterior Eye 2007;30(3):183-8.
45. Carpenter J, Khang D, Webster TJ. Nanometer polymer surface features: the influence on surface energy, protein adsorption and endothelial cell adhesion. Nanotechnology. 2008;19(50):505103.
46. Addesso A, Lund DB. Influence of solid surface energy on protein adsorption. J Food Process Pres 1997;21: 319-333.
47. Sefton MV, Gemmell CH. Nonthrombogenic treatments and strategies. In: Ratner BD,

Hoffman AS, Schoen FJ, Lemons JE, editors. Biomaterials science. 2nd ed. Amsterdam: Elsevier Academic Press; 2002. p. 456-60.

48. Kingshott P, Griesser HJ. Surfaces that resist bioadhesion. Curr Opin Solid State Mater Sci 1999;4:403-12.
49. Mougin K, Lawrence MB, Fernandez EJ, Hillier AC. Construction of cell-resistant surfaces by immobilization of poly(ethylene glycol) on gold. Langmuir 2004;20:4302-5.
50. Blummel J, Perschmann N, Aydin D, Drinjakovic J, Surrey T, Lopez-Garcia M, et al. Protein repellent properties of covalently attached PEG coatings on nanostructured SiO2-based interfaces. Biomaterials 2007;28:4739-47.
51. Saltzman WM, Kyriakides TR. Cell interactions with polymers. In: Lanza R, Langer R, Vacanti J, editors. Principles of tissue engineering. 3rd ed. San Diego: Elsevier Academic Press; 2007. p. 279-96.
52. Geiger B, Spatz JP, Bershadsky AD. Environmental sensing through focal adhesions. Nat Rev Mol Cell Bio 2009;10:21-33.
53. Zamir E, Geiger B. Molecular complexity and dynamics of cell-matrix adhesions. J Cell Sci 2001;114:3583-90.
54. Parsons JT, Horwitz AR, Schwartz MA. Cell adhesion: integrating cytoskeletal dynamics and cellular tension. Nat Rev Mol Cell Bio 2011;11:633-43.
55. Owens GK, Kumar MS, Wamhoff BR. Molecular regulation of vascular smooth muscle cell differentiation in development and disease. Physiol Rev 2004;84:767– 801.
56. Khademhosseini A, Suh KY, Yang JM, Eng G, Yeh J, Levenberg S, Langer R. Layer-by-layer deposition of hyaluronic acid and poly-L-lysine for patterned cell co-cultures. Biomaterials 2004;25(17):3583-92.
57. Fischer D, Li Y, Ahlemeyer B, Krieglstein J, Kissel T. In vitro cytotoxicity testing of polycations: influence of polymer structure on cell viability and hemolysis. Biomaterials 2003;24(7):1121-31.
58. Hategan A, Sengupta K, Kahn S, Sackmann E, Discher DE. Topographical pattern dynamics in passive adhesion of cell membranes. Biophys J 2004;87(5):3547-60.
59. Crompton KE, Goud JD, Bellamkonda RV, Gengenbach TR, Finkelstein DI, Horne MK, Forsythe JS. Polylysine-functionalised thermoresponsive chitosan hydrogel for neural

tissue engineering. Biomaterials 2007;28(3):441-9.

60. Lu H, Guo L, Kawazoe N, Tateishi T, Chen G. Effects of poly(L-lysine), poly(acrylic acid) and poly(ethylene glycol) on the adhesion, proliferation and chondrogenic differentiation of human mesenchymal stem cells. J Biomater Sci Polym Ed 2009;20(5-6):577-89.
61. Rao SS, Winter JO. Adhesion molecule-modified biomaterials for neural tissue engineering. Front Neuroeng 2009;2:6.
62. Cook AD, Hrkach JS, Gao NN, Johnson IM, Pajvani UB, Cannizzaro SM, Langer R. Characterization and development of RGD-peptide-modified poly(lactic acid-co-lysine) as an interactive, resorbable biomaterial. J Biomed Mater Res 1997;35(4):513-23.

Chapter X. Conclusion

Substrates with controllable stiffness have emerged as important models in investigating cell-biomaterial interactions. Most substrates studied are hydrogels with a limited range of stiffness. Here in this thesis, I developed a series of biodegradable substrates using photo-crosslinked poly(ε-caprolactone) triacrylates (PCLTAs) with controllable stiffness by varying the crosslinking density and crystallinity, simultaneously. Further, I evaluated the surface characteristics of these crosslinked PCLTAs including roughness, hydrophilicity, and capability of adsorbing proteins from cell culture media for regulation of primary rat SMC behavior.

I found that stiffer crystalline crosslinked PCLTAs induced stronger stress fibers, larger spreading area, faster growth and motility, better supported conversion from synthetic phenotype to functional contractile phenotype and stronger focal adhesion both in size and density. Gene and protein expression has been performed to confirm that SMCs had higher levels of contractile gene markers and integrin subunits on semi-crystalline substrates of crosslinked PCLTA. Because of the controllability of physicochemical properties and possibility of being modified with other functional moieties, the crosslinked PCLTAs have great potentials for regulating cell behaviors and diverse tissue-engineering applications.

Cardiovascular tissues bear constant blood shear and dynamic hardening under diseased conditions, which causes the tissue stiffness varies all the time. To mimic the dynamic changing environment in the vessel tissues and investigate the influence of dynamically changing substrate mechanical properties on the cell behaviors, I fabricated a model polymer network from poly(ε-caprolactone) triacrylate that can gradually stiffen in 24 h through impeded crystallization at body temperature (37 ℃). Rat primary SMCs were cultured on both static and dynamic substrates and distinct SMC attachment, proliferation and spreading were found. Quantification of contractile gene expression and protein content showed that the dynamic substrates could facilitate the contractile conversion process of SMCs. The analysis of focal adhesions and integrin expression indicated that the cellular abilities to sensing and adhering to the substrate surface were enhanced by the dynamic stiffening stimulation. These results extend the knowledge about SMC mechanosensing to dynamic substrates with increasing stiffness, and demonstrate a new method of regulating SMC adhesion, growth, and functional conversion on substrates.

To evaluate the influence of stiffness in SMCs migration, a series of stiffness-gradient

substrates along the longitudinal direction by photo-crosslinking PCLTA binary homo-blends made from two samples with different molecular weights and crystallinities were developed. These gradient substrates with the stiffness range of 2-200 MPa and gradient strengths of 4.3-48.0 kPa/μm were used to exam primary rat vascular SMC adhesion, spreading, and migration on them. The findings indicated that the stiffness gradient patterns of the underlying substrates were important for SMC adhesion, spreading, and accumulation. SMCs exhibited different spreading areas at different locations along the gradient on the substrates and they accumulated in the stiff regions of the substrates. Real-time observation of SMC motility showed that a large portion of cells migrated distinctly toward the stiff region of the substrate, especially when the gradient strength was higher.

Vascular SMCs are sensitive to the topographical features of the extracellular matrix (ECM) through the sensing molecules in cell membrane. The desirable landscape of ECM at the micron, submicron, or even nanometer scales attracts vascular cell adhesion to the surface, promotes cell proliferation and differentiation, and supports formation of functional blood vessels. Here I fabricated cylindrical pillars with three different heights of 3.4, 7.4, and 15.1 μm by photo-crosslinking PCLTA in silicon molds with predesigned micropatterns. Then I studied SMC adhesion, spreading, elongation, proliferation, and differentiation on these substrates with micro-pillar arrays. The micro-pillars were found to facilitate the cellular attachment and elongation whereas they inhibited cellular spreading and proliferation. Cell nuclei were smaller on the micro-pillar arrays than those on the flat substrates. Immuno-fluorescence imaging demonstrated that cellular filaments and punctate focal adhesions were intensely distributed around the micro-pillars. SMCs on the micro-pillar arrays had higher contractile marker expression levels, implying that the topography facilitated the phenotypic conversion from the proliferating synthetic one to the more functional contractile one.

Based on these findings on micro-scale topography, I further investigated the SMCs responses to nanoscale features by fabricating photo-crosslinked PCLTA nanowire arrays with diameters of 20, 100 and 200 nm were prepared using inorganic nanoporous aluminum oxide (AAO) templates. The lengths and morphologies of the nanowires can be controlled by adjusting the PCLTA solution concentration. The surface morphology, hydrophilicity and serum protein adsorption of crosslinked PCLTA nanowire arrays were characterized. I investigated

SMC attachment, proliferation, spreading and differentiation as well as cellular sensing components as focal adhesions and integrins on these nanowire arrays. Nanowire arrays could adsorb more proteins and support SMC attachment, proliferation, spreading, and differentiation better than the smooth crosslinked PCLTA substrate, especially on nanowires with smaller diameters. Further analysis of cellular sensing components indicated that smaller nanowires triggered stronger focal adhesion dots and higher expression of integrins subunits.

Polymer crystallinity influences the morphological and mechanical properties, thus it is of interest to use it as a factor to regulate cell behavior in tissue engineering applications of semi-crystalline polymers. Here I reported a series of novel photo-crosslinkable poly(L-lactic acid) triacrylates (PLLATAs) that were synthesized and photo-crosslinked under UV light to achieve network substrates. With increasing the annealing time from 0 to 5, 7, 10, and 20 h at 70 ℃, both crystallinity and surface roughness increased for PLLATA networks without variance in chemical composition. Both water contact angle and the capability of adsorbing serum proteins from the culture media on the crystallized PLLATA networks were lower compared with the amorphous one. Primary rat smooth muscle cells (SMC) were found to respond to the substrate crystallinity by exhibiting reduced attachment, proliferation, and differentiation on the crystalline, rough surfaces of the PLLATA networks than on the amorphous, and smooth one. Down-regulated integrin expression and weakened focal adhesions (FAs) in terms of size, elongation, and density in SMCs were also observed on the crystalline networks. After removal of surface roughness through compression, SMCs exhibited no differences among compressed PLLATA networks regardless of the difference in bulk crystallinity.

For semi-crystalline crosslinked PCLTA, the high surface hydrophobicity may limit its potential tissue engineering applications. I found that the hydrophobic nature of crosslinked PCLTA can be greatly relieved when PCLTA was photo-crosslinked with hydrophilic methoxy poly(ethylene glycol) monoacrylate (mPEGA). To further clarify the role of mPEGA in modification of crosslinked PCLTA, I utilized a series of photo-crosslinked mPEGA/PCLTA samples with various ϕ_m of 0 to 50% and different mPEGA number-average molecular weights of 350, 2000, and 10000 g/mol. Material properties such as surface hydrophilicity, friction coefficient, roughness, thermal and mechanical properties were characterized. Crosslinked mPEGA/PCLTA samples with modified surface physicochemical characteristics were further

used to modulate primary rat SMC attachment, spreading, proliferation, and gene/protein expression. Our results showed that sparsely tethered short PEG chains were found to significantly enhance SMC attachment, proliferation, and gene/protein expression by reducing the substrate hydrophobicity. Nevertheless, densely tethered PEG chains diminished SMC attachment and proliferation due to their strong repulsion to proteins and cells.

Extracellular microenvironments are critical for cell adhesion, phenotype, proliferation, differentiation, and gene/protein expression. The majority of the components in the microenvironments, such as adhesive proteins, growth factors, and cytokines, have diversified electronic properties. Poly(L-lysine) (PLL) is a type of cationic polypeptide often used for enhancing cell adhesion by providing positive charges. Here I developed a series of polymer networks with PLL dangling chains through photo-crosslinking PCLTA with a weight-average molecular weight (M_w) of 7020 g/mol with a photo-polymerizable PLL at different PLL compositions of 0.5%, 1.0%, 1.5%, and 3%. PCLTA networked grafted with dangling PLL chains were more hydrophilic and can adsorb more serum proteins from the cell culture media. Primary rat smooth muscle cells were cultured on these polymer networks and their attachment, spreading, proliferation, focal adhesions, expression of four contractile gene markers (SM-MHC, smoothlin, transgelin, and calponin) and one contractile protein, calponin, were characterized systematically. An optimal composition of PLL at 1% in the polymer networks was found to exist to promote the SMC performance best.

In summary, I developed a series of biodegradable and photocurable polymer networks with tunable mechanical, chemical and topographical features. The influences of these properties were well correlated with cell behavior in terms of adhesion, proliferation and differentiation. Optimized groups of materials were demonstrated that could be served as candidate materials to fabricate injectable supports for cardiovascular tissue engineering applications. Further, these polymer networks owns great potential to find applications in various tissue engineering by achieving advanced functions or more complicated structures.

Vita

Xifeng Liu was born in Hunan Province, China. He attended Hunan University from 2004 to 2008, where he received a B.S. degree from College of Chemistry and Chemical Engineering. He enrolled in the doctoral program and joined Prof. Shanfeng Wang's group in the Department of Material Science and Engineering at the University of Tennessee Knoxville in the fall of 2010. He received a Doctor of Philosophy Degree in Material Science and Engineering from the University of Tennessee in August 2014.